DYNAMICS OF JBF ARCTIC DRILLING UNIT MOORED IN ICE

MASTER OF SCIENCE THESIS

CONFIDENTIAL

Chris Keijdener

2012-07-13

Faculty of Civil Engineering

Offshore Engineering

Dynamics of JBF Arctic drilling unit moored in ice

“Creation of an ice loading model and using it to design the mooring systems for a MODU”

MASTER OF SCIENCE THESIS

For obtaining the degree of Master of Science in Offshore Engineering at Delft University of Technology

Chris Keijdener
4034988
ckeijdener@gmail.com
Delft & Schiedam, the Netherlands

July 2012

Faculty of Civil Engineering - Delft University of Technology

Copyright ©
C. Keijdener & Huisman Equipment B.V., 2012
All rights reserved.

Cover image: ‘Snow crystals’
(http://en.wikipedia.org/wiki/File:Snow_crystals.jpg)

Delft University Of Technology
Department Of
Hydraulic Engineering

The undersigned hereby declare to have read this thesis report and recommend to the Faculty of Civil Engineering for acceptance this thesis entitled “Dynamics of JBF Arctic drilling unit moored in ice” by C. Keijdener in partial fulfillment of the requirements for the degree of Master of Science.

TU Delft: Prof. Dr. A. Metrikine

Dr. A. B. Cammaert

H. Hendrikse MSc

Huisman: Dr. A. Bereznitski

ABSTRACT

In light of the recent increasing interest in the oil and gas developments in the arctic region, Huisman Equipment B.V. started development of a drilling semi-submersible suited for arctic condition.

Model tests were performed by the Krylov Shipbuilding Research Institute to gain insight in the ice forces acting on the structure. Based upon the data gathered during these model tests a mooring system was designed using an ice loading model that was based on the means of the loads measured and assumed an ice-load independent of vessel motions. For a more accurate design of the mooring system and a better understanding of the dynamics, a dynamic model of the ice-loading and moored vessel motions is/was needed.

This thesis elaborates on a model that can model the dynamic interaction between the vessel motions and the ice-loads. Based upon this model, the mooring system is optimized for the highest possible ice conditions.

During the model tests the model of the JBF Arctic was retained in a fixed position while being towed through the ice. The main interest was in the interaction with level ice at operational draft. Three parameters were varied during these tests: the ice thickness, the ice velocity and the trim angle of the vessel.

To model the ice loads, the first step was to create a model for the mean part of the ice loading. A very simple ice model for the mean of the horizontal force had already been made by the Krylov Shipbuilding Research Institute. This ice model only depends on the ice thickness and the ice velocity and is only valid within a certain range. As part of this thesis the model was expanded so that it would be valid for the entire range of parameters which are required during the time domain simulations. Next the transition between bending and crushing was found to be dependent on the trim angle of the vessel. The mean loads in all other five DOF's were added based on correlations with the horizontal force or as separate entities. Several other ice phenomenon were also added to the model, such as the initial transient interaction between the approaching ice sheet and the vessel and a crude implementation of the interaction with ridges.

The second step to model the ice loads, was to add the fluctuating components of the ice loading. An extensive study was done to analyze the frequency characteristics of the data gathered. The frequency characteristics of the analyzed spectrums were random, and no correlation could be found with the variables that were varied during the tests. A flat or white noise spectrum with the correct energy density was used to model the dynamic part of the ice forces.

The moored vessel motions itself were modeled with AQWA DRIFT. The AQWA model was coupled with MATLAB to incorporate the mean and dynamic ice forces. Eventually a model was delivered that can be used to model the dynamics of a moored vessel in ice. This model was also used to do a comprehensive study to find the optimal mooring configuration (material type, grade and, the anchor radius, the number of lines and their layout etc.) for the JBF arctic.

The final mooring system can handle 3.1m thick ice moving at 0.5 m/s or 2.4m thick ice moving 1.5 m/s.

Keywords: ice model test, dynamics ice-structure interaction, ice loading model, mooring system optimization

PREFACE

The research presented in this report is performed as a final dissertation for the degree of Master of Science (MSc.) in Offshore Engineering at the Delft University of Technology. The research was carried out at Huisman Equipment B.V. from November 2011 to July 2012.

Arctic engineering encompasses a number of extreme challenges; this thesis focuses on the interaction between level ice and a mobile offshore semi-submersible. The foundation of this work is the creation of an ice loading model based on model test data done by the Krylov Shipbuilding Research Institute located in St. Petersburg and the integration of the ice model with time-domain software in order to investigate the impact of the dynamic ice-structure interaction on the choice of a mooring system.

The work done during this thesis will provide Huisman with a better understand of the process of deriving an ice loading model from model test data as well as an in depth analysis of the model test data itself and recommendations for future ice model tests. Finally it aims to increase the knowledge about the impact of the ice on the mooring system and how to optimize a mooring system for interaction with ice.

Throughout this report it is important to keep in mind that nearly every piece of data that is presented is based on the data from the model tests. As several things about the model tests are unknown, the most significant of which is how the scaling from model to full scale was done, the accuracy or confidence interval of the data received is unknown. Therefore the validity of the numbers presented here should not be interpreted as exact values but more as indications.

Delft University of Technology

The 13th of July, 2012

Chris Keijdener

C. Keijdener

ACKNOWLEDGEMENTS

I would like to express my gratitude towards the following people for providing help, ideas and support during the completion of this thesis:

From Delft University of Technology:

- Prof. Dr. A. Metrikine,
- Dr. A. B. Cammaert,
- H. Hendrikse MSc,
- Dr. R. Hendriks.

From Huisman B.V.:

- Dr. A. Bereznitski,
- E. Arens MSc.

I would like to thank my colleagues at Huisman B.V. for their help, support and interest during the couple of months I got to work alongside them at the Huisman B.V. office in Schiedam.

I would like to thank my family and my friends for their support and interest in my work.

TABLE OF CONTENTS

ABSTRACT ..... **VII**

PREFACE ..... **IX**

ACKNOWLEDGEMENTS ..... **XI**

TABLE OF CONTENTS ..... **XIII**

LIST OF FIGURES ..... **XIX**

LIST OF TABLES ..... **XXIII**

LIST OF TERMS AND DEFINITIONS ..... **XXV**

DEFINITIONS XXV

TERMS XXV

LIST OF ABREVIATIONS ..... **XXIX**

1 INTRODUCTION **1**

1.1 WHY GO TO ARCTIC 1

1.2 JBF ARCTIC 1

1.3 GOAL OF THIS THESIS 5

2 ANALYSIS OF MODEL TEST DATA **7**

2.1 TEST SETUP 7

2.2 PRE-PROCESSING OF THE DATA 8

2.3 QUALITATIVE ANALYSIS: VESSEL – ICE INTERACTIONS 10

2.3.1 Transit draft *11*

2.3.2 Operational draft *20*

2.3.3 Ice in the window *35*

2.3.4 Ice rubble accomulation properties *36*

2.4 QUICK COMPARISON WITH ISO 19906 37

2.5 CONCLUSION 38

3 CREATION OF THE VESSEL-ICE INTERACTION MODEL **39**

3.1 VESSEL DYNAMICS – EQUATION OF MOTION 40

3.1.1 Inertia: mass of the vessel *40*

3.1.2 Inertia: added mass *41*

3.1.3 Damping: radiation damping 42

3.1.4 Damping: viscous damping 42

3.1.5 Springs: hydrostatics 43

3.1.6 Springs: mooring forces 43

3.1.7 Equation of motion 44

3.1.8 Solving the Equation of motion 44

3.2 THE ICE LOADING MODEL 44

3.2.1 Px_mean 44

3.2.2 Px_fluc 60

3.2.3 Py_fluc 68

3.2.4 Pz_mean 69

3.2.5 Pz_fluc 73

3.2.6 Mx_fluc 75

3.2.7 My_mean 75

3.2.8 My_fluc 78

3.2.9 Mz_fluc 79

3.3 CONCLUSION 80

4 OPTIMISATION OF THE MOORING SYSTEM 81

4.1 DESIGN CRITERIA 82

4.1.1 Dynamic versus static approach 83

4.2 PRELIMINARY ANALYSES OF THE MOORING SYSTEM 85

4.3 DESIGNING FOR ICE 86

4.4 IMPROVING THE MOORING SYSTEM 87

4.4.1 The layout 88

4.4.2 The number of cables 93

4.4.3 The pretension 94

4.4.4 The anchor radius & The length of the bottom chain 96

4.4.5 Line makeup 98

4.4.6 Optimization for a specific ice load 100

4.4.7 Polyester seabed clearance 100

4.4.8 Final choice 100

4.5 INSTABILITY 103

4.6 CONCLUSION 104

5 CONCLUSION AND RECOMMENDATIONS 105

5.1 CONCLUSIONS 105

5.2 RECOMMENDATIONS 106

5.2.1 Recommendations for future model tests 106

5.2.2 Recommendations to improve the design of the mooring system 107

5.2.3 Recommendations for follow-up research for the JBF Arctic 107

6 REFERENCES 109

APPENDIX A OVERVIEW OF THE MODEL TEST SETUP 111

A.1 THE BASIN 111

A.2 THE MODEL OF THE JBF ARTIC 111

A.3 THE ICE 112

A.4 MEASUREMENT OF PHYSICAL PROPERTIES 115

A.5 ACCURACY OF INSTRUMENTATION 116

A.6 EXPERIMENT LAYOUT 117

A.7 THE TEST PROGRAM 117

A.8 SCALING FROM MODEL TO FULL-SCALE CONDITIONS 119

APPENDIX B DIVISION OF THE PROJECTED VESSEL-ICE INTERFACE AREA 121

B.1 GEOMETRY 121

B.2 STEP 1: THE DEPTH OF THE INTERFACE 123

B.3 STEP 2: FINDING THE BOUNDARIES 124

B.4 STEP 3: PROJECTING THE 3D SHAPE TO 2D 125

B.5 STEP 4: THE INTEGRAL 125

B.6 STEP 5: RESULTS 126

B.7 STEP 6: VERIFICATION 127

APPENDIX C DERIVATION OF THE COMPLEX MOORING SYSTEM 129

C.1 INDIVIDUAL MOORING LINES 130

C.2 THE COMBINED EFFECT OF ALL THE MOORING LINES 132

C.3 VERIFICATION 133

APPENDIX D ALLOWING THE ICE TO COME FROM ALL DIRECTIONS 135

D.1 RELATIVE VELOCITY 135

D.2 ICE FORCE AND MOMENTS 136

D.3 INCORPORATION OF THE MOMENTS 136

D.4 TRIM ANGLE 136

APPENDIX E SOLVING THE EQUATION OF MOTION 141

E.1 ANALYTICAL SOLUTION 141

E.2 NUMERICAL SOLUTION USING SIMULINK – 1DOF 141

E.3 NUMERICAL SOLUTION USING SIMULINK – 6DOF 144

APPENDIX F SIGNAL CREATION 147

F.1 SPECTRUMS 147

F.1.1 Background information 147

***F.1.2 Original data** 148*

F.1.3 Long data 149

F.1.4 Window functions 150

F.1.5 Autocorrelation 152

F.1.6 Interpolating the data 153

F.1.7 Conclusions 154

F.2 AUTOREGRESSIVE MODELS 155

APPENDIX G PRELIMINARY ANALYSES OF THE MOORING SYSTEM 157

G.1 CABLE DYNAMICS 158

G.2 WIND AND CURRENT LOADING 160

G.3 ASSUMPTION OF THE FLAT SPECTRUM 162

G.3.1 Impact on the offset of the vessel 162

G.3.2 Impact on the line tension 164

G.3.3 Conclusion 164

G.4 DYNAMIC VERSUS STATIC APPROACH 164

G.4.1 Comparison with the static case 166

APPENDIX H MOST PROBABLE MAXIMUM 170

H.1 STATIONARY GAUSSIAN PROCESS 170

H.2 EXTREME VALUE STATISTICS 171

H.3 STORM DURATION 172

H.4 MOORING LINE TENSION 172

LIST OF FIGURES

Figure 0-1: Radial and circumferential cracking. ... xxvi
Figure 0-2: Ice action sized of a circumferential crack. ... xxvi
Figure 0-3: The overshoot here is about 15.5 / 10 = 55%. ... xxvii
Figure 1-1: The JBF Arctic at its two drafts. ... 2
Figure 2-1: Coordinated system used for the load data, also reproduced in the top right corner. ... 10
Figure 2-2: Location of transit draft (blue arrow), 0.3 m below the top of the pontoon. ... 11
Figure 2-3: Hull geometry at transit draft. Draft is the pontoon. Light grey are the windows. ... 12
Figure 2-4: 1m thick level ice. Left: Initially rubble accumulation above and below the ice sheet. Right: Then resulting in a circumferential crack due to failing in buckling. ... 13
Figure 2-5: 1m thick level ice. Left: 0.75 m/s. Right: 1.50 m/s. Notice the difference in extent of the submerged ice. ... 13
Figure 2-6: Level ice at 0.75 m/s. Left: 1m thick. Right: 2m thick. The pictures show the different failure mechanisms occurring at the different ice thicknesses. The red arrow corresponds to the red stars. The blue lines show the deformed state of the sheet due to the force acting on it. ... 14
Figure 2-7: Both pictures show 1m thick with a 40m wide channel moving at 0.75 m/s. Notice not much has changed in the timespan between the two pictures. ... 15
Figure 2-8: Both pictures show 2m thick with a 80m wide channel moving at 0.75 m/s: Notice the rubble is slightly more mobile over time then in 40 m wide channel. ... 15
Figure 2-9: 1m thick 30m broken ice at 0.75 m/s. Time lapse series with a time interval of 76 s. Notice the ice rubble directly in front of the vessel is stable while the approach ice moves to the sides. ... 17
Figure 2-10: 1m thick 100 m broken ice at 0.75 m/s. Time lapse series clearly showing rafting. Time interval is 152 s. ... 18
Figure 2-11: 2m thick 100 broken ice at 0.75 m/s. Time lapse series. Notice the rafting of the ice. Time interval is 76 s. ... 19
Figure 2-12: Both figures show 100 m broken ice, but would they result in the same vessel-ice interaction? ... 19
Figure 2-13: Location of operational draft. ... 20
Figure 2-14: The vessel-ice interface for various trim angles and an ice thickness of 3 m. The thick solid line is the sea level. The cross-section was made over the center-line of the vessel. ... 21
Figure 2-15: Vessel-ice interface area as seen from the ice's point-of-view showing the influence of the location. ... 21
Figure 2-16: Vessel-ice interface area as seen from the ice's point-of-view showing the influence of the ice thickness. A trim angle of 5.0 degrees was used to create all four images within the figure. ... 22
Figure 2-17: 1.5m thick 100 broken ice. Time lapse series showing rafting and buildup of ice. Time interval is 114 s. ... 23
Figure 2-18: 100m broken ice. The arrows show the radial crack which split the ice floe. ... 24
Figure 2-19: Left: a large crack prior to arrival of model, its length is roughly 100 meters. Right: the rubble in the gap that behaves rather weak. ... 25
Figure 2-20: The keel of the hummock can be seen through the consolidated layer. ... 25
Figure 2-21: Graphical representation of group 1. ... 26
Figure 2-22: Graphical representation of group 2. ... 26
Figure 2-23: Left: normal situation. Right: one of the larger visible circumferential cracks. When estimating the ice action size it is easy to compare them to the hull of the vessel since it is not fully circular but rather 24-sided polygon, resulting in flat planes 15° apart. ... 27
Figure 2-24: The various stages of the ice fragmentation process can be observed in this picture taken after the test after the model has been pulled back. At the edge of the ice sheet the larger circumferential cracks can be seen. A little more inwards are the long slender pieces (up to 25 m) and finally the fairly regular, rectangular pieces. ... 27
Figure 2-25: Left: Circumferential crack extend further outwards. Right: the resulting ice pieces are slightly larger. ... 28
Figure 2-26: The largest circumferential crack observed in the test footage, extending over 150° of the vessel. ... 29
Figure 2-27: The full extent of the largest simultaneous ice action can be seen once the ice pieces start to rotate upwards as they get pushed against the hull and move down, below the approaching ice sheet. ... 29
Figure 2-28: 0.5 m/s ice velocity. The base case. ... 30
Figure 2-29: 1.0 m/s ice velocity. Left: the ice rubble moves further away from the hull. Right: increase in ice concentration. ... 30
Figure 2-30: 1.5 m/s ice velocity. Left: the ice rubble moves even further away from the hull. Right: an even larger increase in the ice concentration. ... 31
Figure 2-31: Left: 0.5 m/s. Right: 1.0 m/s. Notice that the ice penetrates deeper. ... 31
Figure 2-32: 2.5° trim angle. Crushing around the center line (the green line). ... 32
Figure 2-33: 2.0m thick 5.0° trim angle. Top: Larger rubble caused by the increased thickness. Bottom: Large pieces due to buckling. ... 33
Figure 2-34: Buckling of ice sheet followed by the distant ice sheet rolling over at 5.0° trim angle. ... 34
Figure 2-35: 3.0 m thick ice at 5.0 trim angle. Note that there is more rubble. ... 35
Figure 2-36: The vessel-ice interface clearly shows that crushing took place after the model had been pulled back. ... 35
Figure 3-1: The final five mooring configurations. ... 43
Figure 3-2: The data used by KSRI when curve-fitting the regression model (the nine dots) and the final model (the three lines). ... 46
Figure 3-3: The jump of the 3 meter thick ice at the 5.0° trim angle is clearly visible. ... 47

Figure 3-4: An example of the interaction with the three regions for 3 m thick ice as the trim angle increases. 47
Figure 3-5: An example of the three regions at a trim angle of 5.0° as the ice thickness increases. 47
Figure 3-6: The model test data (the large dots) and the results from model for the mean of Px. The black dotted line shows the onset of the interaction with the red area. One can see that the forces start increasing quickly after this. 48
Figure 3-7: Extreme trim angles. 49
Figure 3-8: The impact of the trim angle dependency. The blue lines at the bottom of both figures are the same. The dashed lines and the colored arrows indicate when interaction with that particular region starts for the purple lines. From left to right it is grey, red, orange, yellow and deck box. 49
Figure 3-9: The transient phase of the vessel-ice interaction for test 31. The red line is a moving average in order to make it easier to find the appropriate values for the black curve-fitting line. The green section is the steady-state solution. The vertical axis has been rescaled so 1 is equal to the mean of the steady-state solution. 50
Figure 3-10: Left: No scaling of the mean, showing an overshoot of about 50%. Right: Including the scaling of the mean, showing an overshoot of just a few per cent. (t = 1.0m, v_ice = 1.0 m/s, v_0 = 0 m/s) 51
Figure 3-11: Left: Overshoot as a function of the duration of the transient phase. Note that the natural frequency in this case was 108 seconds, exactly the distance between the minimums. Right: Vessel's offset is minimal at n*nat_period and maximum at (n-0.5)*nat_period. 52
Figure 3-12: Overshoot for the mooring system the longest natural period, 152 seconds. If the duration of the transient phase is longer than the natural period of 152 seconds, the overshoot will always be lower than about 5%. 52
Figure 3-13: Left: An example of the transient factor changing over time, where the vessel loses contact with the ice 4 times (the builddown to buildup ratio was 1 here). Right: Using several different initial velocities the overshoot is plotted for a variety of ratios. The maximum overshoot is achieved for an initial velocity of -.45 m/s. (t = 1.0m, v_ice = 0.5 m/s, v_0 = -0.45 m/s) 53
Figure 3-14: The original model by KSRI; predicting a horizontal load of 23 MN when the ice is bobbing next to the vessel. 54
Figure 3-15: Normally there is a peak at low velocities (red line); however this trend is not used during this thesis (blue line). 55
Figure 3-16: Left: Linear shape. Right: Quadratic shape. Transition velocity is 0.5 m/s for both sides. Note that by increasing the transition velocity from 0.5 m/s to 0.75 m/s (from the solid to the dashed line in the left figure) the overall loading will become lower since the area under the curve becomes smaller. 55
Figure 3-17: The force generated, 100 seconds between the two vertical gridline and the size of the drop is about 0.5 MN. Left: The linear transition shape was used. Right: The quadratic transition shape was used. 56
Figure 3-18: The response of the vessel for several different transition velocities. The red line standing out from the rest is the original model without the zero velocity correction. 56
Figure 3-19: Interaction with a small ridge, 3m consolidated layer and 10 m keel depth. The red line is a 10 second moving average and the green line is the resulting multiplication function for the small ridge. 57
Figure 3-20: Interaction with a large ridge, 3m consolidated layer and 18 m keel depth. 58
Figure 3-21: Half the cross-section failing in bending and the other half in crushing? Not likely... 59
Figure 3-22: Size of the failed ice. The picture was taken after test 3-1: 1.5 m thick ice at 0.5 m/s and a zero degree trim angle. 61
Figure 3-23: Smooth shapes due to the large D/t ratio of the vessel. 62
Figure 3-24: The DAF of the vessel for the five different mooring systems around zero meters offset. The natural periods are shown in the legend. The linearized drag at 0.4 m/s was used for the damping. 63
Figure 3-25: The restoring force of the mooring system as a function of offset and the transition point beyond which the natural period starts changing. 64
Figure 3-26: The SD of Px. Note the similar shape as was seen with Px_mean. 65
Figure 3-27: The SD as a ratio to the mean of Px. The trim angle is varied and the ice velocity is fixed. 65
Figure 3-28: The SD as a ratio to the mean of Px. The ice velocity is varied and the trim angle is fixed. 66
Figure 3-29: The fluctuating component starts at maximum magnitude while the mean value first has to grow. 67
Figure 3-30: Discretizing the spectrum, e.g. splitting the spectrum into waves. This turns the variance density spectrum into a variance spectrum. The height of each line is equal to the area stored in each frequency band. 67
Figure 3-31: The standard deviation of Py to Px_mean ratio plotted for all tests. The ice velocity is varied and the trim angle is fixed. 68
Figure 3-32: The standard deviation of Py to Px_mean ratio plotted for all tests. The trim angle is varied and the ice velocity is fixed. 69
Figure 3-33: Pz plotted against Px for every time step of every test. The smaller line on the right is from test 65 (the test with 3.0m thick ice failing in crushing). 70
Figure 3-34: Very strange fluctuations prior and during the interaction with the ice. 71
Figure 3-35: Pz is downward sloping even though the model is only being pulled through water. 71
Figure 3-36: Pz unaffected by the ice, even the fluctuating component shows very little change. 72
Figure 3-37: The different areas. The ice thickness is 1.5m. 73
Figure 3-38: Pz vs trim angle. 73
Figure 3-39: The standard deviation of Pz. The trim angle is varied and the ice velocity is fixed. 74
Figure 3-40: The standard deviation of Pz. The ice velocity is varied and the trim angle is fixed. 74
Figure 3-41: The curve-fitted SD of Pz. 74
Figure 3-42: The SD of Mx to Px_mean ratio. The trim angle is varied and the ice velocity is fixed. 75
Figure 3-43: The SD of Mx to Px_mean ratio. The ice velocity is varied and the trim angle is fixed. 75

Figure 3-44: Relation between Px and My (left) and Pz and My (right) at the same time instance. Each color is a different test. Note that the values in the right graph are not correct as they are not scaled properly. ... 76

Figure 3-45: The remaining My moment plotted against Pz. The data-cloud shows a weak correlation. The red line is the regression line. ... 77

Figure 3-46: The remaining My-moment after removing the components correlated with Px and Pz! ... 78

Figure 3-47: The SD of remaining part of My. ... 78

Figure 3-48: The standard deviation of Mz to Px_mean ratio plotted for all tests. ... 79

Figure 4-1: The layout and properties of the original mooring system designed for 350 m water depth from the static mooring report. ... 81

Figure 4-2: The layout of the mooring systems used in the static mooring report, 4 bundles of 5 lines each. ... 88

Figure 4-3: The impact of the direction on the stiffness of the vessel. The maximum global restoring force (MGRF) for a certain direction is defined as the global restoring force achieved at the maximum offset (red line). The directionally dependent stiffness results in a minimum MGRF of 37.2 MN and a maximum MGRF of 51.1 MN. ... 89

Figure 4-4: A cross-section of the JBF Arctic just below the deck box. The purple circles are the fairleads / chain lockers. ... 91

Figure 4-5: The impact of the location of the fairleads on the mooring systems with 10 and 20 bundle. ... 91

Figure 4-6: The required safety margin around the mooring lines are shown. A 100 meter margin was used while in reality a different one might be used, however this does not change the conflicts the margin creates. ... 92

Figure 4-7: The global restoring force as a function of the number of cables for the normal and broken-line case. ... 93

Figure 4-8: Left: the static response curves of the mooring system for the minimum and maximum direction. Right: the maximum line tension for different directions (the required safety factors by DNV are included). ... 95

Figure 4-9: The two different kinds of chain. ... 99

Figure 4-10: The relation between the trim angle and the horizontal ice load. ... 104

Figure A-1: The final model. ... 112

Figure A-2: A channel in level ice. ... 113

Figure A-3: Broken ice with dimensions of 30 m x 30 m and a concentration of 8/10. ... 113

Figure A-4: Broken ice with dimensions of 100 m x 100 m and a concentration of 8/10. ... 114

Figure A-5: A channel being created in a hummock using an icebreaker model. ... 114

Figure A-6: Ice bending strength measurements being performed ... 115

Figure A-7: Measuring the dynamic friction factor ... 116

Figure A-8: The coordinate system used during the tests ... 117

Figure B-1: One equation that calculates the percentage each colored areas takes up is coming right up! ... 121

Figure B-2: Geometry in side plane. Note that the actual COG is located below the mean water line, but this does not influence the derivation. ... 121

Figure B-3: Geometry in top-down plane ... 122

Figure B-4: External circular and 24-sided polygon. Not that when looking at the vessel from the top, the vessel is slightly thinner than the external circle. ... 123

Figure B-5: Integral. Note that the figures aspect ratio is not 1:1. ... 125

Figure B-6: %YELLOW. Ice thickness varies from 0 to 4.0 m. ... 126

Figure B-7: %ORANGE. Ice thickness varies from 0 to 4.0 m. ... 127

Figure B-8: %RED. Ice thickness varies from 0 to 4.0 m. ... 127

Figure C-1: The coordinate system of the vessel used in the rest of the report, (x,y), and the coordinate system used for the mooring lines, (q,d). Note that the q-axis is defined differently for every mooring line, as the axis is always parallel to the mooring line when viewed from the top. The starting point for the q-axis is always at the anchor point. The azimuth angle is defined as above and is 135 degrees for the red mooring line. ... 129

Figure C-2: Coordinate system used for the mooring system. The origin is at the anchor point. The ending points is located at $\boldsymbol{qe}, \boldsymbol{de}$. By looking up this location in the table from AQWA the quasi-static forces for this line can be determined. ... 130

Figure C-3: Checking if the correct area if used or not. ... 131

Figure C-4: Interpolating within the green area. ... 132

Figure C-5: A yaw-angle resulting in a different azimuth angle. The red line represents the mooring line. ... 132

Figure C-6: Comparison between the implementation explained in this appendix and the original data from the static mooring line report. ... 134

Figure D-1: Original situation where the pitch angle equals the trim angle. ... 137

Figure D-2: The new situation where the ice can come from any direction. Note that the ice direction (azimuth) does not have to coincide with omega, which is the maximum trim angle. ... 138

Figure E-1: 1DOF Simulink model. ... 142

Figure E-2: Decay in the peaks of the motions. Also somewhat visible is that the vessel will stabilize at an offset of 10 meters, given the correct offset as the force corresponding to 10 meter was entered. The natural frequency is 108 second, exactly like the period between the peaks. ... 144

Figure E-3: This main level of the final Simulink model. Grey boxes are subsystem, blue boxes are interfaces with Matlab and red boxes are used to show the output of the connection line. ... 145

Figure F-1: An example of a discrete spectrum (from Wikipedia). ... 148

Figure F-2: Two spectrum of the same time history. The top one has a large error but a high spectral resolution. The bottom one has a smaller error but this came at a loss in spectral resolution. ... 148

Figure F-3: Two sin waves superimposed result in beating. The red wave is the carrier wave and its frequency is equal to the beating frequency and thus to length of the signal that can be generated. 149
Figure F-4: Blue: original signal. Green: the segment selected by the algorithm. Red: the segment selected by KSRI. Note that this figure shows one of the better improvements in term of length, not all of the tests improved this much. 150
Figure F-5: The rectangular window and its spectrum (from Wikipedia). 151
Figure F-6: The Hamming window and its spectrum (from Wikipedia). 151
Figure F-7: Comparing the spectrums created when using different windows. Data is from Test 31, Px. 1.5 m, 0.5 m/s. 0 dgr. 152
Figure F-8: Window comparison for test 32, Px. 1.5 m, 1.5 m/s. 0 dgr. 152
Figure F-9: Window comparison for test 65, Px. 3.0 m, 0.5 m/s. 5 dgr. 152
Figure F-10: Spectrum from the autocorrelation. 153
Figure F-11: Although some groups of spectrums show some relation, most are very different. 154
Figure F-12: Blue: original signal and periodogram. Red: AR model's prediction (use Yule-Walker) 155
Figure G-1: MS3 (350m, semi-taut). The MPM offset of the vessel. The left graph has CD off, the right one on. The percentages in the figure show the changes between the two cases. 158
Figure G-2: MS3 (350m, semi-taut). The MPM line tension of the vessel. The left graph has CD off, the right on. 159
Figure G-3: MS3 (350m, semi-taut). The mpm offset of the vessel. The percentages in the figure show the changes between the default case and the test case. 160
Figure G-4: MS3 (350m, semi-taut). The mpm line tension. 161
Figure G-5: MS3 (350m, semi-taut). The mpm offset and line tension of the vessel. The standard deviations are multiplied by 1.25 [-]. The percentages in the figure show the changes between the default case and the test case. 163
Figure G-6: The results from the static case. Mooring systems for other water depths are also shown, however only the 350 m water depth one will be used further on. 165
Figure G-7: MS3 (350m, semi-taut). The mean of each test is plotted so they can be compared with the static case to validate the AQWA calculations. The left figure shows the offset and the right figure shows the line tension. 166
Figure H-1: For the four different simulations above a normal shape seems to give a very good fit for the data. All data is for an ice direction of zero degrees (moving towards the positive x-axis). Each graph contain almost 3 hours of data. 170
Figure H-2: A non-Gaussian distribution occurs when the ice is operating in the non-linear range of the mooring system. 171
Figure H-3: A series of histograms for the line tension. Each graph contain almost 3 hours of data. 173

LIST OF TABLES

TABLE 1: OVERVIEW OF TESTS PERFORMED AT OPERATIONAL DRAFT. THE NUMBERS IN THE TABLE MEAN THE FOLLOWING: X_Y, THEN X IS THE NUMBER OF THE ICE SHEET AND Y IS THE NUMBER OF THE TEST WITH THAT ICE SHEET. 26

TABLE 2: OVERVIEW OF RUBBLE PROPERTIES FOR THE TESTS PERFORMED AT OPERATIONAL DRAFT AND LEVEL ICE. TABLE COPIED FROM KSRI'S REPORT. 36

TABLE 3: IMPACT OF THE ADDED MASS ON THE MOTIONS OF THE VESSEL. 41

TABLE 4: THE MAXIMUM GLOBAL RESTORING FORCE FOR SEVERAL DIFFERENT LAYOUTS IS SHOWN. ALL FOUR SYSTEMS COMPRISE OF 20 LINES BUT HAVE A DIFFERENT AMOUNT OF BUNDLES. THE SPACE BETWEEN LINES WITHIN A SINGLE BUNDLE IS FIVE DEGREES. ... 90

TABLE 5: AT A PRETENSION OF 2.2 MN, THE PRETENSION TURNS OUT TO BE TOO HIGH. THE MOORING SYSTEM IS VERY STIFF WHICH RESULTS IN A HIGH MAXIMUM ALLOWABLE LOAD AT THE MAXIMUM OFFSET OF 28 M. HOWEVER THIS WILL QUICKLY EXHAUST THE LINE TENSION SO THE OFFSET AT WHICH THE MBL HAS BEEN REACHED IS 26.735 M; THIS IS BELOW THE DESIRED 28 METERS. THE OPTIMAL PRETENSION IS THIS CASE IS SOMEWHERE AROUND 2.03 MN AS BOTH LIMIT STATES ARE USED TO THEIR FULL EXTENT AT THIS OFFSET. WITH THIS PRETENSION, AT AN OFFSET EQUAL TO THE MAXIMUM OFFSET OF 28 METERS, THE MAXIMUM LINE TENSION IS EQUAL TO THE MBL. 95

TABLE 6: THE MAXIMUM GLOBAL RESTORING FORCE IS SHOWS FOR DIFFERENT ANCHOR RADII AND BOTTOM SECTION LENGTHS. THE PRETENSION WAS OPTIMIZED FOR EXTREME ICE LOAD (3 M THICK ICE). 96

TABLE 7: THE MAXIMUM GLOBAL RESTORING FORCE IS SHOWS IN CASE OF A BROKEN LINE. 96

TABLE 8: THE VERTICAL FORCE (WEIGHT) AT AN OFFSET OF ZERO METERS. 97

TABLE 9: THE OPTIMAL PRETENSION AT 350 M WATER DEPTH FOR EXTREME ICE LOAD (3+ M). 97

TABLE 10: MAXIMUM GLOBAL RESTORING FORCE AS A FUNCTION OF THE DIAMETERS. THE OPTIMAL SETS WHERE THE MBL OF BOTH MATERIAL ARE ALMOST EQUAL ARE HIGHLIGHTED IN GREEN. 98

TABLE 11: THE PROPERTIES OF THE SYNTHETIC MATERIALS 99

TABLE 12: ACCURACY OF MEASURING INSTRUMENTATION 117

TABLE 13: THE TEST PROGRAM 119

TABLE 14: MODEL TO FULL-SCALE EXTRAPOLATION RULES. WHERE: λ IS THE SCALE FACTOR AND EQUAL TO 58 INDEX M APPLIES TO MODEL AND F TO FULL-SCALE 119

TABLE 15: THE IMPACT OF THE INCREASED STANDARD DEVIATION ON THE OFFSET. 163

TABLE 16: THE IMPACT OF THE INCREASED STANDARD DEVIATION ON THE LINE TENSION. 164

TABLE 17: THIS TABLE SHOWS ALL THE RESULTS FOR THE FIVE MOORING SYSTEMS FROM THE STATIC REPORT. A DETAILED DESCRIPTION CAN BE FOUND ON THE NEXT PAGE 167

LIST OF TERMS AND DEFINITIONS

DEFINITIONS

Naming policy for the breakdown of the ice loads:

Ice loading refers to all the loads applied to the vessel due to ice.

The ice loading is split into **six components**, three forces and three moments (Fx, Fy, Fz, Mx, My, Mz); one for each of the three directions (X,Y,Z) and one for each of the three rotations (rx, ry, rz).

Each component is then split into **two parts**; a mean and a fluctuating part.

Coordinate system

Below is a figure of the coordinate system used throughout this thesis. During the model tests the model was pulled in the negative X-direction.

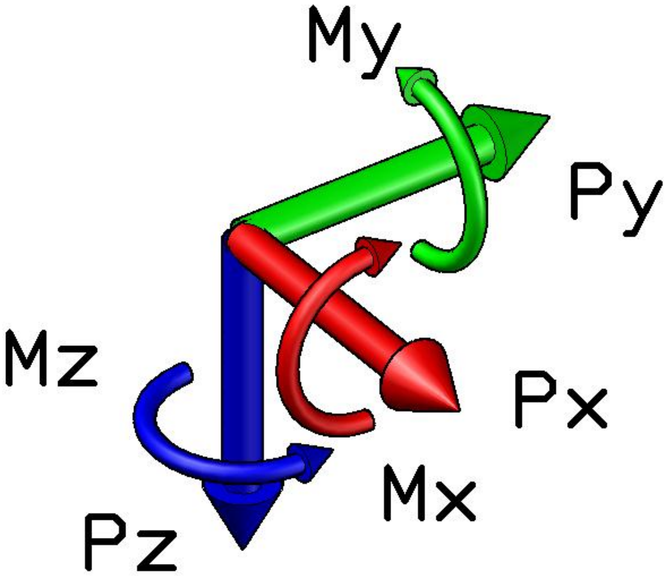

TERMS

Impact angle: The angle between the approaching ice and the hull of the vessel in the X-Z plane. 0 degrees is tangential, so that would results in no interaction. 90 degrees is perpendicular so that would result in crushing.

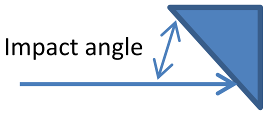

Trim angle: The rotation of the vessel around the y-axis, also known as the pitch angle.

Inner area: The area between the legs of the hull.

Radial cracking: Cracks that start perpendicular to the hull and then spread radially from the hull; see Figure 0-1.

Circumferential cracking:

Circumferential cracks are cracks that form a circular shape around the hull, following the general shape of the hull. See Figure 0-1.

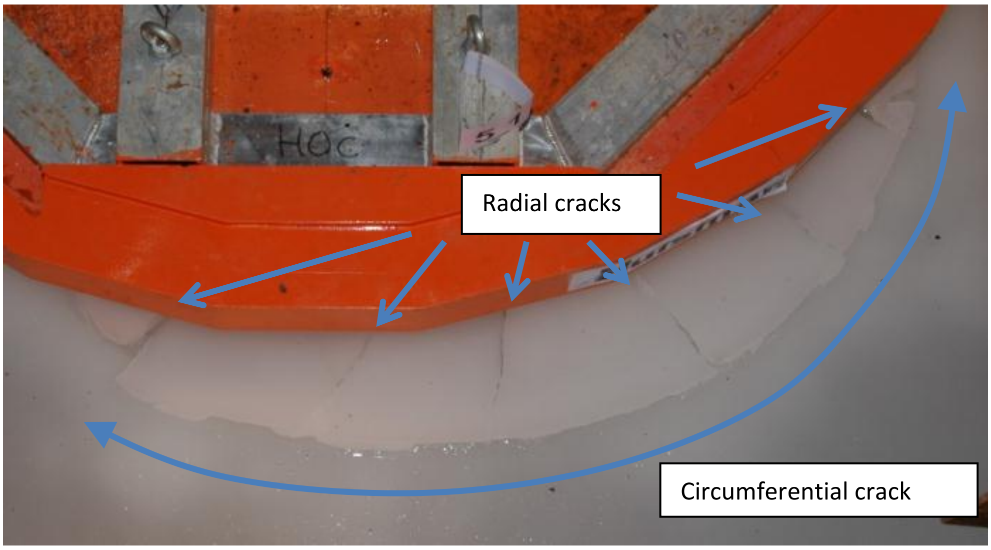

Figure 0-1: Radial and circumferential cracking.

Ice action size: The ice action size is the size of a circumferential crack expressed in degrees. See Figure 0-2.

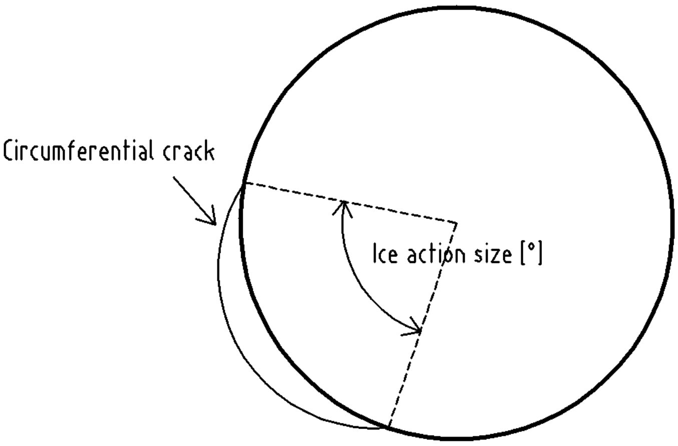

Figure 0-2: Ice action sized of a circumferential crack.

Overshoot: When applying a constant load to a system, overshoot is defined as the maximum displacement divided by the stationary displacement.

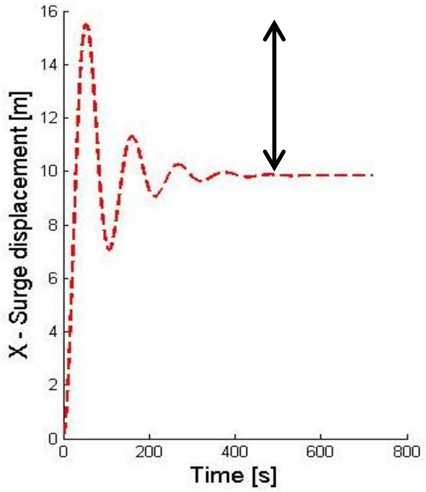

Figure 0-3: The overshoot here is about 15.5 / 10 = 55%.

LIST OF ABREVIATIONS

ALS	Accidental limit state
CD	cable dynamics
DAF	dynamic amplification factor
DOF	degree of freedom
FLS	Fatigue limit state
MBL	maximum breaking load (of a material used in a mooring line)
MGRF	maximum global restoring force (of a mooring system)
MODU	mobile offshore drilling unit
MPM	most probable maximum
MWL	mean water level
KSRI	Krylov Shipbuilding Research Institute
SD	standard deviation
ULS	Ultimate limit state

1 INTRODUCTION

In this introduction some background information is given on the arctic, how the JBF Arctic fits in the arctic picture then a description of the JBF Arctic and finally what the goal of this thesis is.

1.1 WHY GO TO ARCTIC

I would like to start with a famous quote from Mister Ger Tol: “The arctic is very sexy”. The very simple reason for this is that there are still vast quantities of untapped natural resources stored in the rock formations below the arctic. Another reason is at the moment there is still little experience on how to design offshore vessels and equipment for arctic operations, making it a challenging area to work in.

According to the United States Geological Survey the arctic region contains an estimated 30 % of the world’s undiscovered gas and about 13 % of the world’s undiscovered oil reserves. Because conventional hydrocarbons in easy to reach locations have already been depleted or are currently being depleted, the energy sector is now being faced with the problem of exploring new frontiers.

As the oil price increases and more money becomes available for the extraction of oil new options have become viable in the last few decades. Using new technologies, shale gas has become increasing popular in the United States and is also slowly gaining ground in Europe. The tar sands in Canada are also a new source of hydrocarbons. The offshore sector is now moving of the continental shelf to deeper and deeper water in order to exploit untapped hydrocarbon reservoir and also slowly moving into the arctic regions.

Huisman saw the growing interest in the arctic region and, after the recent success of designing its own drilling vessels, decided to start a research project to design an arctic drilling vessel. Their solution is the JBF Arctic.

1.2 JBF ARCTIC

The JBF Arctic is designed to combine a high resistance to ice with good motion characteristics in waves. Other vessels such as the MOSS CS50 MkII or the JBF 10000 W, which are winterized semi-subs, can only resist ice with a thickness of about 0.5 meter. Vessels with a cylindrical shape similar to the Kulluk have great resistance against ice but bad motion characteristics.

The way the JBF Arctic achieves this optimal performance in both ice and waves is by being able to operate at two different drafts; one for operating in ice infested waters and one for operating in waves, see Figure 1-1. At ice draft the vessel has a downward sloping shape, thus breaking the ice in the most efficient way. Its semi-submersible shape gives it great motion characteristics at wave draft.

On the next few pages a series of figures are shown to give an introduction of the geometry and overall dimensions of the vessel.

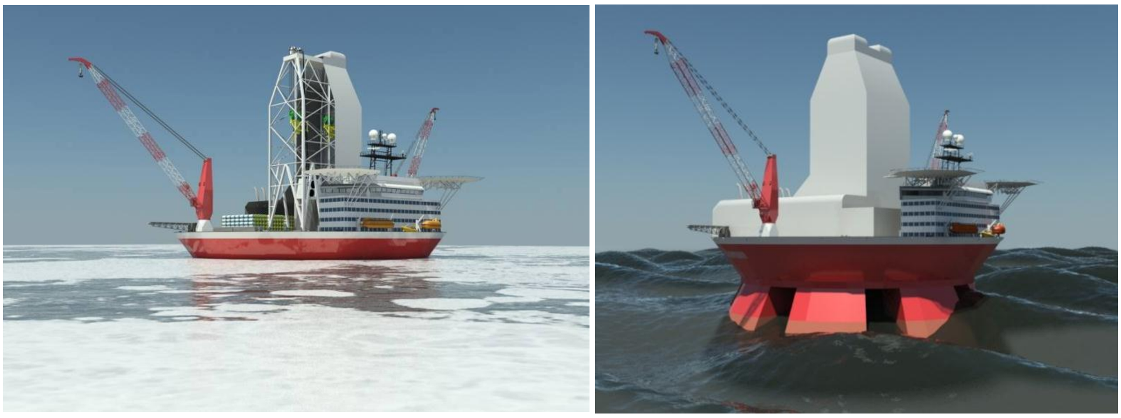

Figure 1-1: The JBF Arctic at its two drafts.

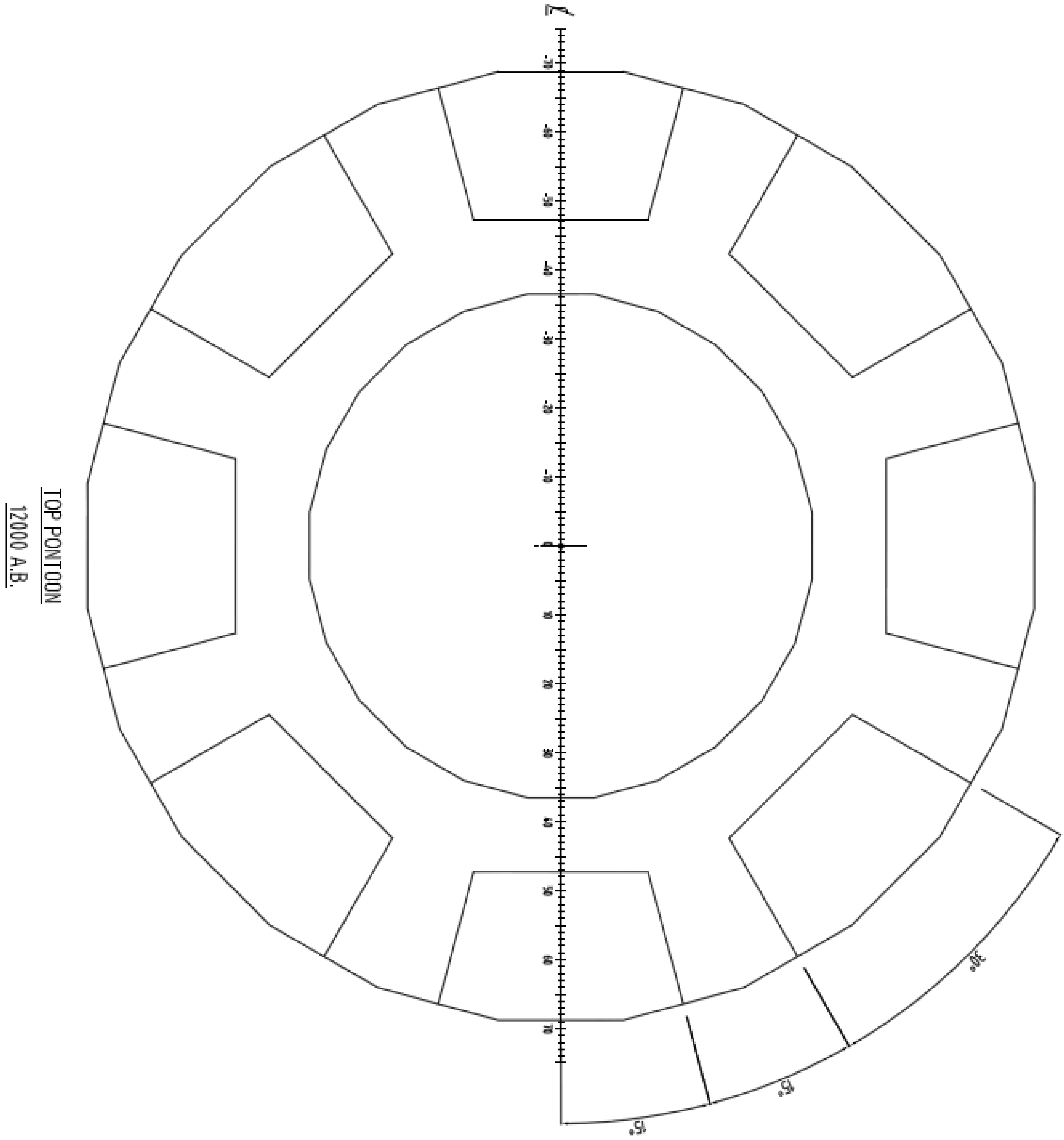
TOP PONTOON
12000 A.B.
-70
-60
-50
-40
-30
-20
-10
0
10
20
30
40
50
60
70
15°
15°
30°

Figure 1-2: A horizontal cross-section of the JBF Arctic just above the pontoon. The vessel has 8 legs.

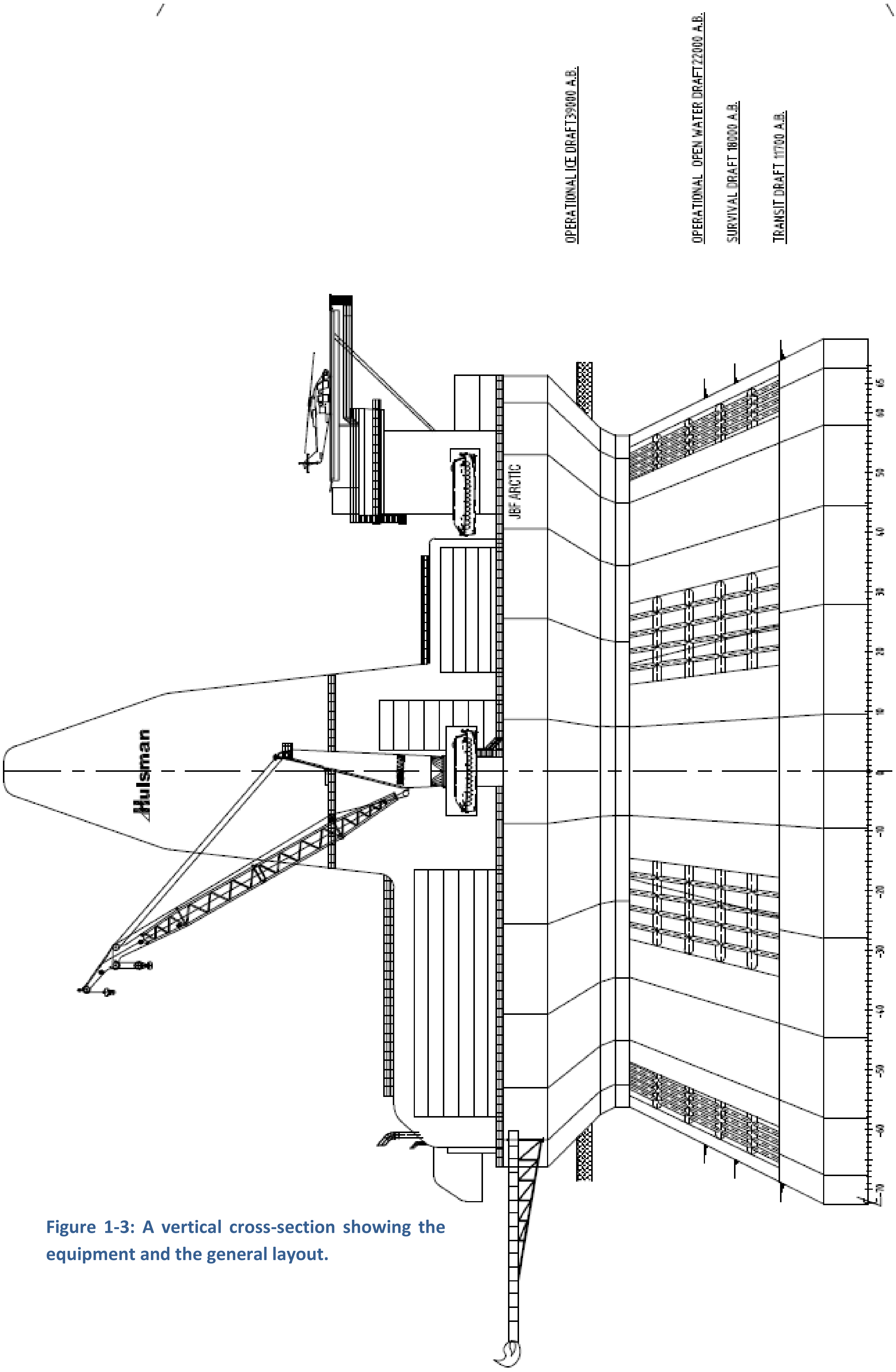
OPERATIONAL ICE DRAFT 39000 A.B.
OPERATIONAL OPEN WATER DRAFT 22000 A.B.
SURVIVAL DRAFT 18000 A.B.
TRANSIT DRAFT 11700 A.B.
JBF ARCTIC
Hulsman
70
60
50
40
30
20
10
0
-10
-20
-30
-40
-50
-60
-70

Figure 1-3: A vertical cross-section showing the equipment and the general layout.

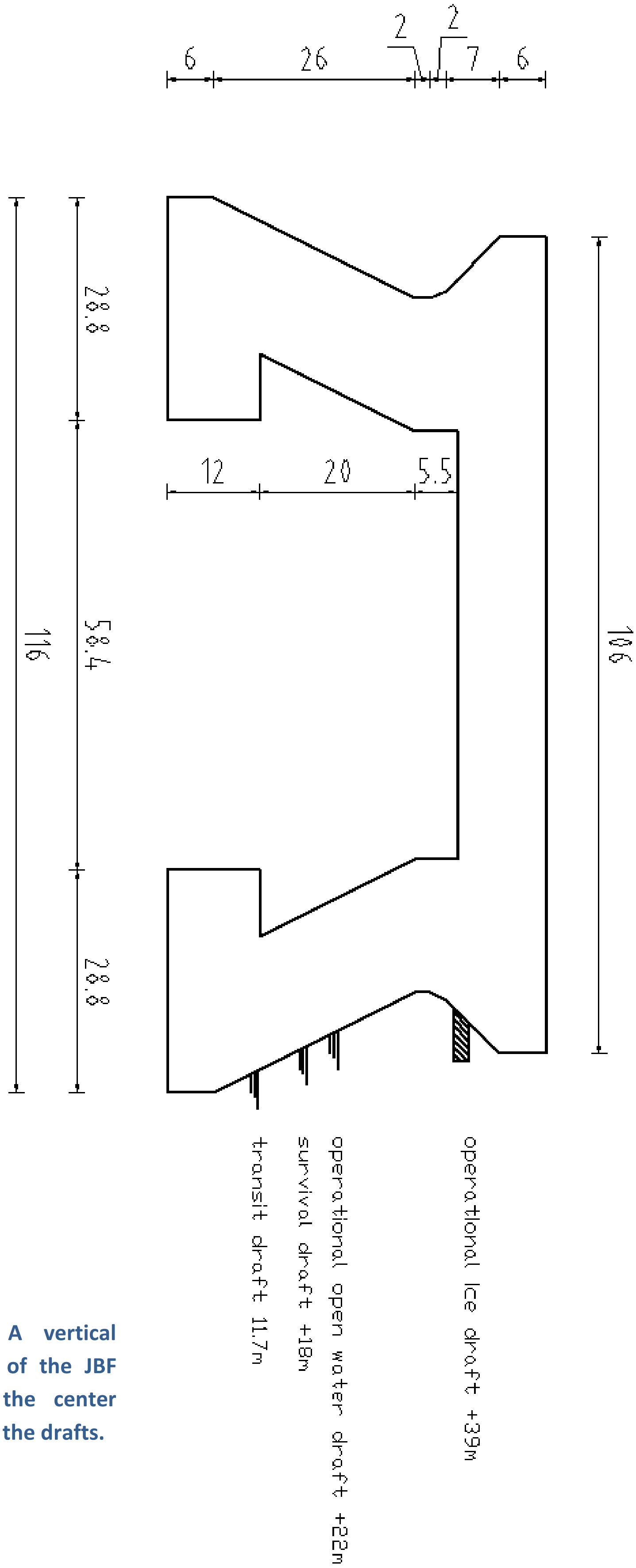
6
26
2
2
7
6
28.8
58.4
28.8
116
106
12
20
5.5
transit draft 11.7m
survival draft +18m
operational open water draft +22m
operational ice draft +39m

Figure 1-4: A vertical cross-section of the JBF Arctic over the center line including the drafts.

Station keeping of the vessel is facilitated by using a 20 point mooring system. The mooring system has to be able to withstand both loads from waves and from the ice. For this reason model tests were done in both an ice tank and a sea keeping tank in order to investigate the environmental loads on the JBF Arctic.

1.3 GOAL OF THIS THESIS

During the model tests in the ice tank, the model of the JBF Arctic was fixed in position and then pulled through an ice sheet. This was done for several thicknesses of the ice sheets, for several different ice velocities and for several different trim angles of the vessel.

The ultimate goal of this thesis is to design a mooring system that can resist the ice loads. In order to achieve this goal several steps have to be taken:

- Analysis of the model test data.
- Creation of an ice model that can create several hour long none-repeating loads in all 6 DOF of the vessel for any combination of ice properties and vessel velocity / rotation for level ice.
- Optimize the mooring systems to be used for operations in the arctic.
- Check the dynamic behavior of the vessel when interacting with ice to see if some set of ice properties can lead to instability.

The analysis of the model test data is described in chapter 2. The creation of the ice model is described in chapter 3. The optimization of the mooring systems is described in chapter 4. Finally chapter 0 gives the conclusions and recommendations.

2 ANALYSIS OF MODEL TEST DATA

From the start of the JBF Arctic project it was felt within Huisman that it was essential to do tests in an ice tank in order to get the best possible understanding of the vessel – ice interaction and the resulting behavior. So towards the end of 2010 Huisman contracted the Krylov Shipbuilding Research Institute (KSRI) to perform a series of model tests in their ice model basin located in St. Petersburg.

After a theoretical study by a previous graduating student (Alec van Nes: Dynamics of a mobile offshore drilling unit caused by ice loads, 2011) *to estimate and model the ice loading on the JBF Artic, the ice model test were completed and several studies were done by Huisman employees using only the static calculations in combination with only the static part of the load* (IVR, 08-04-2011) *and also using time domain simulation with both the static and the dynamic part* (BDA, 2011) *in order to design a mooring system for the JBF Arctic.*

The main objective of the model test was to study the process of the semi-submersible vessel – ice interaction in both transit and operating conditions, and to evaluate the loads acting on the vessel from varies ice formations. The tested ice formations were level ice and ice hummocks. In addition broken ice fields as well as channels in level ice and in hummocks were considered in order to simulate the impact of ice management with icebreakers.

The tests were performed with the model fixed to the towing carriage in all 6 degrees of freedom. The model was then dragged through fixed ice with a constant velocity at a fixed draft and trim angle. KSRI gathered the following information during each test:

- *Description of physical phenomena during the vessel/ice interaction;*
- *Ice loads acting on the vessel from the specified ice features;*
- *Dimension and behavior of ice rubble pile-up.*

This section will analyze the data gathered above.

Layout of this chapter

In this chapter the model test data will be discussed and analyzed. In section 2.1 the test setup will be discussed. Then in section 2.2 the pre-processing of the data by KSRI is discussed. In section 2.3 a qualitative analysis is done of the video footage, describing the phenomenon that occurred and the reasons behind them. Section 2.4 contains a comparison with the loads predicted by the ISO code. Finally in section 2.5 some conclusions are drawn on how to proceed with the creation of the ice model.

2.1 TEST SETUP

This section is a short summary of the full overview given in Appendix A which covers the setup used during the model test done by the Krylov Shipbuilding Research Institute (version 3). Readers who already read the original report can safely skip to section 2.3.

- The model test was done at a scale of 1:58.
- During the tests the following ice conditions were tested (however not all combinations of the parameters were tested): ice thickness of 1.5 m, 2.0 m and 3.0 m, ice velocities of 0.5 m/s, 1 m/s and 1.5 m/s and a trim angles of 0°, 2.5° and 5°.
- The model tests were done by towing the model through the immovable ice sheet. The model was fixed to the towing carriage through a six-component dynamometer. The model was orientated in

such a way that the model faces the ice with one of its legs rather than with one of the gaps between the legs.
- The scaling of the model test's results to full-scale was done by KSRI. It was done in accordance with the guidelines applied in the ice towing tank of the Krylov Institute. The only available information on the scaling is that "the guidelines are based on principles of simulating physical processes that ensure compliance with criteria of geometry, kinematic and dynamic similarity".
- KSRI also made a regression model based on the model test results, creating multi-factor regress-dependencies between measured load components and experiment parameters. If generation of the regress-models is not possible, corrections for measured load component values are introduced based on expert estimations. After this, recalculation of the load components to full-scale conditions is carried out according to the simulation principles.
- In order to separate the ice loads from the water resistance loads open water test runs were performed to measure the water resistance load. These were then deducted from the measured total loads to get the ice load.

For a more detailed description refer to Appendix A or refer to the original report from KSRI.

2.2 PRE-PROCESSING OF THE DATA

Before handing over the data to Huisman, KSRI did some pre-processing of the data. The known steps that were undertaken are described in this section.

Signal filtering

During each test the three forces and moment on the model were measured, resulting in six load records. The time records were then carefully filtered to remove influence caused by:

- Vibration of the towing carriage;
- Vibration of the model;
- The fact that the track the carriage was rolling on was not completely straight;
- By doing a cross-analysis between the load records and the video footage, unrealistic ice loading was removed.

Further processing of the data

The quality of the ice loading records was then further improved by removing the contributions due to the hydrodynamic loading. After this, the records were corrected in order to account for fluctuations in flexural strength and thickness based on measurements done. After this process was completed, KSRI carefully examined the loading records and then selected a segment out of each full-length time history during which they felt the loading was stationary. Based on these segments KSRI calculated the values they used in their report.

Unknown discrepancy

The segments selected by KRSI are very short. This presented problems when having to calculate spectrums from the spectrums. Longer segments give better spectrums so the full-length version of the data had to be used. The problem that presents itself now is that the full-length segments which were made available to Huisman are slightly different as their mean and maximum values calculated are not the same as the values given in KSRI's report (version 3). The reason for this difference is unknown but a possibly explanation could be that one of the corrections / modifications had not yet been applied before the full-length segments were send to Huisman. In order to somewhat correct for this mistake, the data from Huisman is scaled in order to give the same mean and standard deviation as KSRI published in their report. The way this is done is as follows:

$$P_{scaled} = (P_{hm} - Mean_{hm}) * \frac{Max_{KRSI} - SD_{KRSI}}{Max_{hm} - SD_{hm}} + Mean_{KRSI}$$

In words the following happens:

- The mean value of the Huisman record is subtracted from all time steps in order to get the fluctuating component.
- This fluctuating component is then scaled with the ratio between KSRI's and Huisman's fluctuating component. This scaling of the fluctuating component ensures that the standard deviations are equal.
- Next KSRI's mean is added to the fluctuating component. This ensures the mean components are equal.

This scaling has to be done for each of the six components of each loading record. However the second problem is that the mean and standard deviation required to perform the scaling are not available for all tests. For some sets of tests only the mean and standard deviation of Px are available. Based on symmetry three additional mean values are known (see below). This means that for the trim angle tests there are still seven values missing (6 components * (1mean + 1max) – (Px_mean – Px_max) – (Mx_mean – Mz_mean – Py_mean)). These seven values thus cannot be scaled and the original values from the Huisman data will be used.

All in all, not having KSRI's final loading records and then the lack of values required to perform the scaling, resulted in an unknown error on the data. However this does not mean that using the data at a later stage will results in an invalid model because:

- The biggest and therefore the most important force component when it comes to the design of the mooring system is Px. The mean and maximum of Px has been scaled for all tests, thus making it more reliable.
- The difference between Huisman's and KSRI values is fairly small in general. When looking at Px in the tests with level ice, the difference for both the mean and maximum is about 5% on average, with a single peak at 21.5% (test 3_1). Most other components have a similarly small difference.

Possible simplification for the ice model

Based on the geometry of the vessel (repeated in Figure A-2), several things can already be noted:

- Due to symmetry around the x-axis, the mean value of Mx should be zero;
- Due to symmetry around the z-axis, the mean value of Mz should be zero;
- Due to symmetry over the xz-plane, the mean value of Py should be zero;

It is important to note that during the model test the ice was fairly isotropic. This justifies the assumption of symmetrical loading, and therefore vessel response, but only when considering the model test data. In reality the vessel will not face such isotropic ice due to ridges, local increases in thickness, cracks or variance in other ice properties. This could results in a mean that is not zero for the three load discussed above for short periods of time.

However it is important to note that one would expect a zero mean based on the geometry and that therefore any non-zero mean would be a results of variance in the ice properties. As these properties are random one would not expect them to results in a constant mean for an extended period of time. Especially given that a non-zero mean in any of the three components would be the results of the same phenomenon: a non-symmetrical distribution of the load over the Y-Z plane. This would always results in a force in the Y-direction which will push the vessel out the ice feature which is causing the non-zero mean. This behavior prevents a non-zero mean over an extended period of time, but could still results in swaying of the vessel.

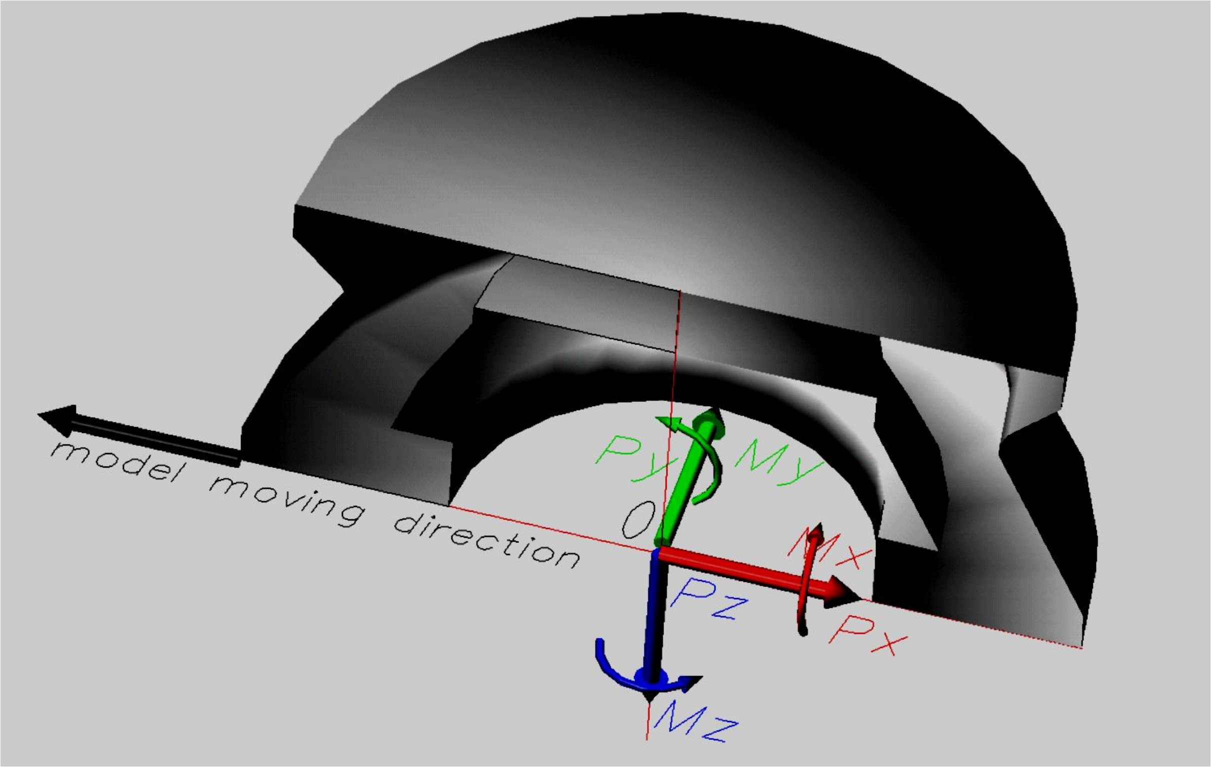

Figure 2-1: Coordinated system used for the load data, also reproduced in the top right corner.

This concludes the discussion of the pre-processing and the problems faced when handling the data from KRSI. Next the data itself will be analyzed to get a better understanding of the ice-vessel interaction.

2.3 QUALITATIVE ANALYSIS: VESSEL – ICE INTERACTIONS

During the model tests a lot of data was gathered. In this section this data will be analyzed.

The data comes in several forms. Of each test the following data is available:

- A time history of all 6 components of the load at an interval of 150 Hz (in model scale). This is equal to 150 Hz / sqrt(58) = 19.696 Hz or a period of 0.05077 seconds in full-scale time.
- A set of pictures
- A set of movies of the whole test shot from four different angles: one from the front, one from the side, one from the front but shot from below the ice used to investigate the rubble and a fourth underwater camera which captures the inner area. It should be noted that both underwater cameras have rather poor image quality.

Because up to eight tests were performed with the same ice sheet the order of the tests has an influence on the results. For instance when looking at two tests which were performed after each other in level ice with a 40 m channel made by an icebreaker. Let say the ice sheet is fresh prior to these tests. When doing the first test no ice rubble has accumulated yet in front of the model. During the first test ice rubble will accumulate there. After test one is over, the rubble is not removed. So the second test immediately starts with a lot of ice rubble in front of it. All tests were continued until a stationary situation was reached so one could argue that by not removing the rubble between tests, the only thing that changes is the build-up time until a stationary situation is reached.

14 out of the total 34 test were done using the transit draft. Since this data will not be used to design the mooring system, these data sets will only be qualitatively analyzed because analyzing the phenomenon that occur at this draft might help to better understand the phenomenon that occur at the operational draft.

Unless otherwise specified, all data in this chapter is for full-scale.

The layout of this section is as follows: first the tests at transit draft are discussed in section **Error! Reference source not found.** followed by the tests at operational draft in section 2.3.2. The flow of ice into the windows of the vessel is discussed separately in section 2.3.3 as this phenomenon occurs in most of the tests. Also the penetration depth of ice rubble is discussed separately in section 2.3.4 as this is also a general phenomenon.

Before continuing it should be noted that KSRI filtered some events because they were deemed unrealistic. Because it is not known which ones were filtered out, some of the events described below might not be realistic at full scale.

2.3.1 TRANSIT DRAFT

When moving between drilling sites the JBF Artic will be floating at its transit draft. At this draft the top of the pontoon is just above the waterline in order to lower the hydraulic resistance on the vessel, increasing its velocity. The transit draft is displayed in Figure 2-2.

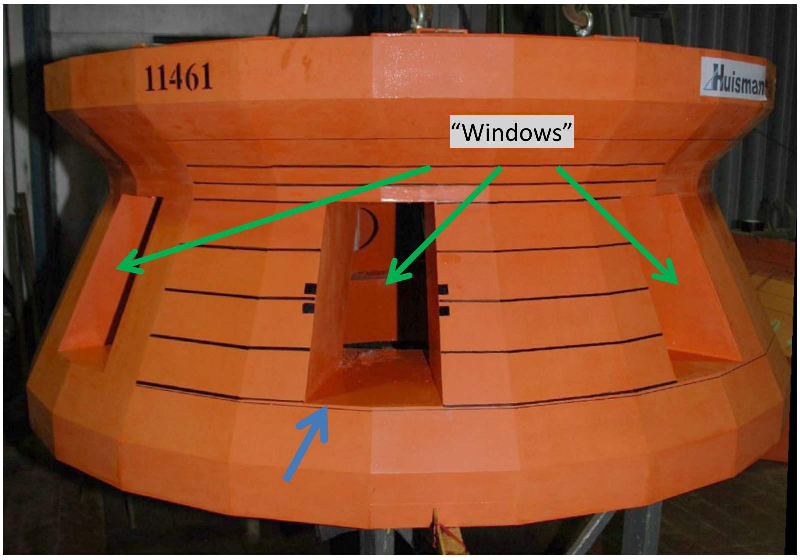

Figure 2-2: Location of transit draft (blue arrow), 0.3 m below the top of the pontoon

The layout of this section is as follows. First the impact of the hull geometry at the transit draft will be discussed in 2.3.1.1. Then, in turn, the different ice features are discussed: first level ice in 2.3.1.2, then level ice with a channel in it created by an icebreaker in 2.3.1.3 and finally broken ice in 2.3.1.4.

2.3.1.1 IMPACT OF HULL GEOMETRY ON VESSEL-ICE INTERACTION AT TRANSIT DRAFT

At the transit draft the hull is very regular in that the impact angle does not change dramatically (which is the case at the operational draft). This can be seen in Figure 2-3. High trim angles which could rotate the vessel to such much that the ice would interact with the tangential face of the pontoon were not considered during the transit draft tests.

The ice will generally interact with the top of the pontoon. The transit draft is located 0.3 m below the top of the pontoon (the pontoon is the dark grey area in Figure 2-3). The impact angle of the ice is 116.6 degrees, thus the ice will fail in upward bending.

The transit draft is close to the bottom of the hull. Therefore ice might flow underneath the hull and get into the inner area.

The presence of the windows is discussed separately in section 2.3.3.

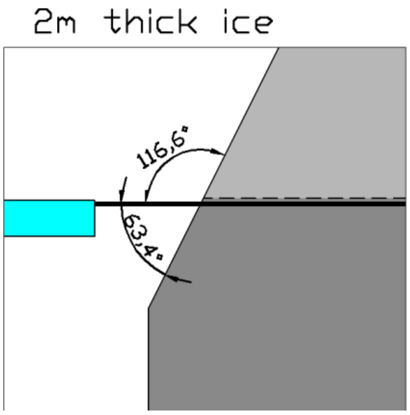

Figure 2-3: Hull geometry at transit draft. Draft is the pontoon. Light grey are the windows.

2.3.1.2 LEVEL ICE

For the transit draft three different tests were done with level ice:

- 1 m thick ice at 0.75 m/s
- 1 m thick ice at 1.50 m/s
- 2 m thick ice at 0.75 m/s

1 m thick ice

By analyzing the video footage of the 0.75 m/s ice velocity the following vessel-ice interaction can be observed:

- Ice breaks in upward bending in fragments of about 3 m – 6 m wide;
- The ice rubble accumulates on top and below the approaching ice sheet;
- After a certain amount of rubble has been reached, circumferential cracking occurs. The cracks seem to occur at about the same distance as the submerged rubble extends. The ice pieces that break off due to a circumferential crack are rather large, 30 m wide (perpendicular distance to the hull) and lengths varying from 50 m to 100 m long, which then almost immediately brake in smaller pieces.
- The ice pushes itself through the rubble again, in the process removing a lot of it. It then starts failing in upward bending again until another circumferential crack occurs;
- Repeat the cycle.

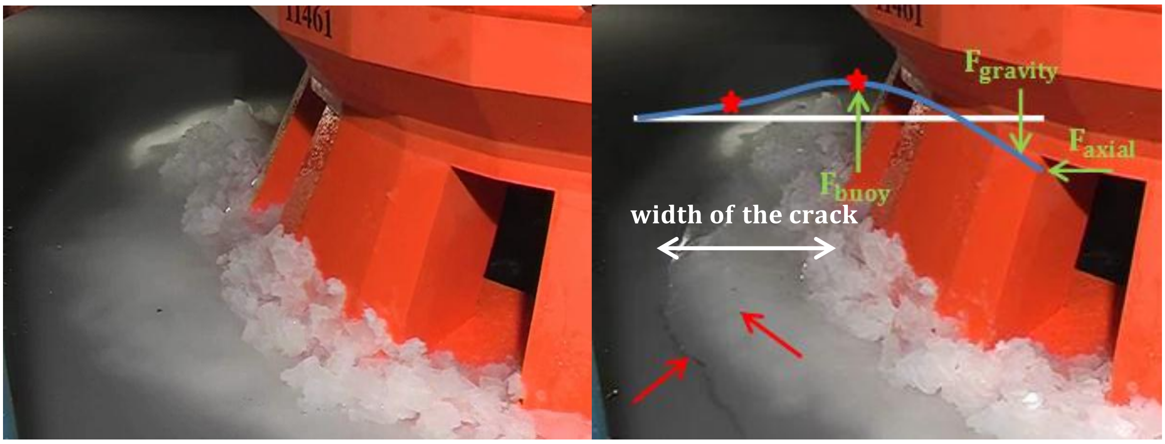

Figure 2-4: 1m thick level ice. Left: Initially rubble accumulation above and below the ice sheet. Right: Then resulting in a circumferential crack due to failing in buckling.

An explanation for the buckling / circumferential cracking cycle could be that as the rubble accumulates three things happen. First it becomes harder for the ice to move upwards in order to fail in pure bending due to the mass of the overlaying rubble. The second reason could be that it becomes harder for the ice to move forward through the rubble due to extra friction, increasing the axial load. Last the submerged rubble pushes against the ice sheet from below due to its buoyancy.

A possible result of the first two phenomenon described above is a higher axial loading in the sheet which could buckle the ice sheet and cause it bend. In combination with the upward buoyancy force of the submerged rubble and the downward force of the rubble laying on top of the ice sheet, the ice sheet can then fail in buckling, resulting in a circumferential crack. The failure state is described on the left in Figure 2-6. After the crack a lot of the rubble which was lying on the ice sheet is removed again, it takes some time for the axial load to build up again, resulting in the cycle. A very rough estimate for the cycle time is about 30 s – 60 s.

When analyzing the level ice with a 1.5 m/s ice velocity a similar vessel-ice interaction occurs. However there are a few differences. Due to the higher velocity the circumferential cracks occur more often and closer to the hull. A possible explanation could be that the submerged ruble more quickly flows around the structure than at the lower velocity, thus bringing the buoyancy force closer to the hull and reducing the width of the circumferential cracks. The higher frequency of the cracks is off course due to the higher velocity of the ice.

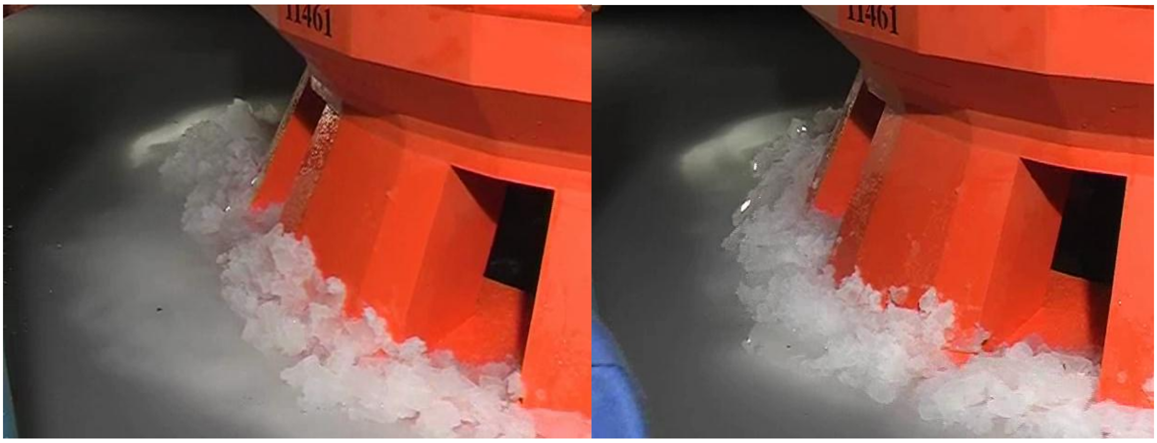

Figure 2-5: 1m thick level ice. Left: 0.75 m/s. Right: 1.50 m/s. Notice the difference in extent of the submerged ice.

2 m thick ice

The observations from this test are very similar to the 1m thick level ice. The differences:

- The ice sheet can handle a larger vertical load due to the increased bending stiffness of the ice; e.g. more rubble can accumulate on top of the ice sheet;
- The ice now fails in pure bending (no more buckling), resulting in a different failure mechanism.

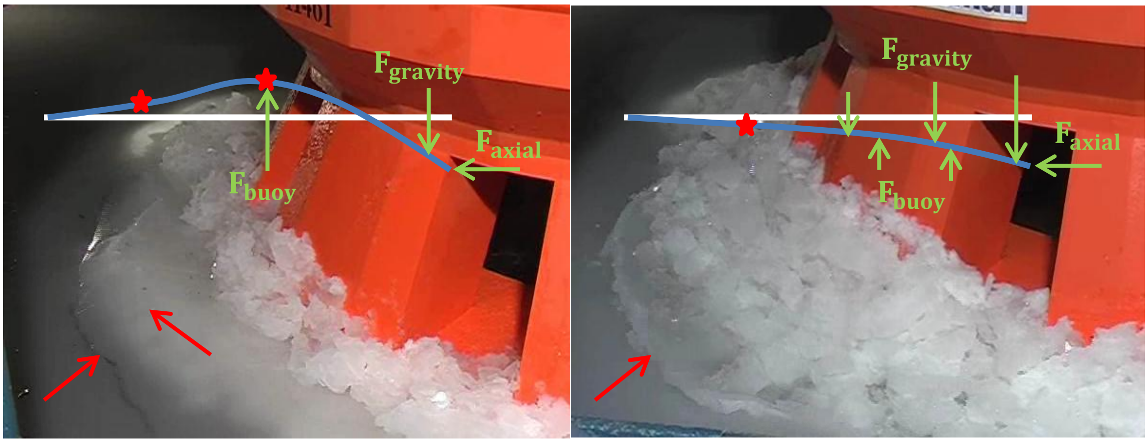

Figure 2-6: Level ice at 0.75 m/s. Left: 1m thick. Right: 2m thick. The pictures show the different failure mechanisms occurring at the different ice thicknesses. The red arrow corresponds to the red stars. The blue lines show the deformed state of the sheet due to the force acting on it.

When comparing the two failure mechanisms, the 2m thick ice only has one fracture line whereas the 1m thick ice has two fracture lines. Figure 2-6 shows the differences. A possible explanation could be that there is much more ruble on top of the ice which results in more downward force cancelling the upward buoyancy force. The ice will then fail in bending rather than buckling.

This concludes the analysis of the tests with level ice.

2.3.1.3 LEVEL ICE WITH ICE MANAGEMENT

For the transit draft four different tests were done with level ice with a channel in it, representing ice management with an ice breaker. The setup of the four tests was:

- 1 m thick ice with a 40 m wide channel at 0.75 m/s
- 1 m thick ice with a 40 m wide channel at 1.50 m/s
- 2 m thick ice with a 80 m wide channel at 0.75 m/s
- 2 m thick ice with a 80 m wide channel at 1.50 m/s

1 m thick level ice with a 40 m wide channel

For this test an icebreaker model was dragged through the ice to create a 40 m wide channel. By analyzing the video footage of the 0.75 m/s and 1.5 m/s ice velocity the following vessel-ice interaction can be observed:

- On either side of the channel the ice fails only in upward bending for the full duration of the test, so no circumferential cracking like in the tests without the channel;
- The ice rubble in the channel accumulates over time in front of the vessel by sliding over each other. The rubble group remains very stable for the full duration of the test. Some ice sheets are pushed under the edges of the channel.

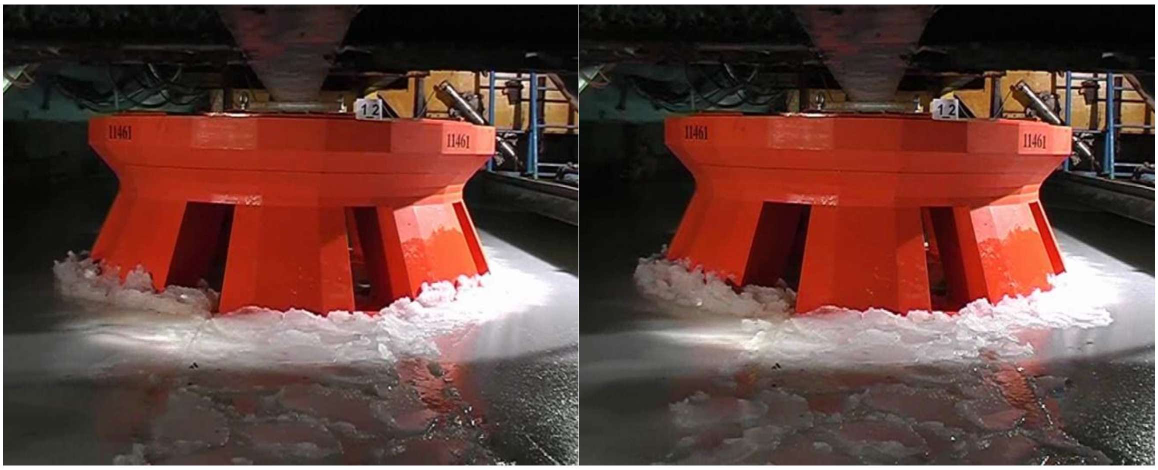

Figure 2-7: Both pictures show 1m thick with a 40m wide channel moving at 0.75 m/s. Notice not much has changed in the timespan between the two pictures.

It is hard to see what exactly happens in the channel with the rubble that is pushed against the rear of the stable ruble group because the interaction occurs outside of the area captured by the camera. It can be seen that some ice is pushed under the edges of the channel, however it cannot be seen whether all ice is pushed underneath or only a fraction. If the stable group keeps growing in time, the ice at the vessel-ice interface might start crushing or fail in some other way.

When comparing the different velocities (0.75 m/s and 1.5 m/s) the same vessel-ice interaction occurs with no notable differences.

2m thick level ice with an 80 m wide channel

The results of this test are very similar to the 1m thick level ice with a 40 m wide channel.

- Again there is failure due to upward bending towards the edges of the model but now on a smaller area due to the wider channel;
- Again there is accumulation of rubble in the channel over time, however due to the wider channel the rubble is more mobile when compared to the 40 m channel.

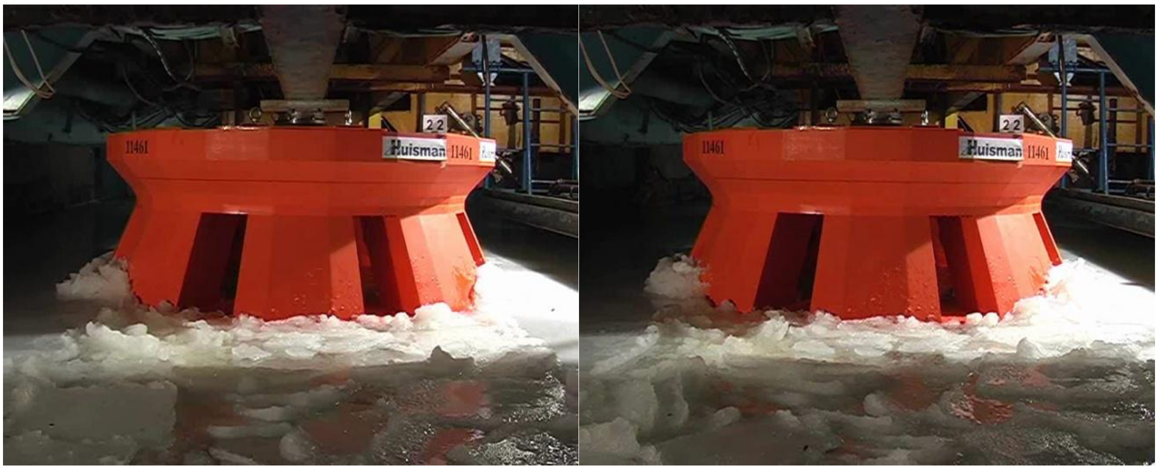

Figure 2-8: Both pictures show 2m thick with a 80m wide channel moving at 0.75 m/s: Notice the rubble is slightly more mobile over time then in 40 m wide channel.

When comparing the different velocities (0.75 m/s and 1.5 m/s) the same vessel-ice interaction occurs with no notable differences.

This concludes the analysis of the test with ice management.

2.3.1.4 BROKEN ICE

For the transit draft eight different tests were done with broken ice:

- 1 m thick broken ice with a dimension of 30 m x 30 m at 0.75 m/s
- 1 m thick broken ice with a dimension of 30 m x 30 m at 1.50 m/s
- 1 m thick broken ice with a dimension of 100 m x 100 m at 0.75 m/s
- 1 m thick broken ice with a dimension of 100 m x 100 m at 1.50 m/s
- 2 m thick broken ice with a dimension of 30 m x 30 m at 0.75 m/s
- 2 m thick broken ice with a dimension of 30 m x 30 m at 1.50 m/s
- 2 m thick broken ice with a dimension of 100 m x 100 m at 0.75 m/s
- 2 m thick broken ice with a dimension of 100 m x 100 m at 1.50 m/s

1m thick broken ice with dimensions of 30 m x 30 m

For this test the ice was cut into rectangular plates with a length of about 30 meters. A concentration of about 8/10 was used. By analyzing the video footage of the 0.75 m/s and 1.5 m/s ice velocities the following vessel-ice interaction can be observed:

- Initially the ice floes bump into the model and then slowly flow around it;
- After some time more and more ice floes accumulates in front of the model, taking on a wedge shape. The shape remains fairly stable over time, but the individual pieces within the shape get slowly replaced by new ice floes because the older ice sheets move aside and brake over time because they are so thin;
- The effects of upward bending are pretty much negligible and only impact the ice floes to the extent that some corners are broken off. The two important effects that occur are that the wedge shape pushes the approaching ice floes aside and that within the stable wedge shape, ice floes starts to raft;
- Eventually movement of the flow becomes hampered by the limited width of the ice basin, influencing the vessel-ice interaction.

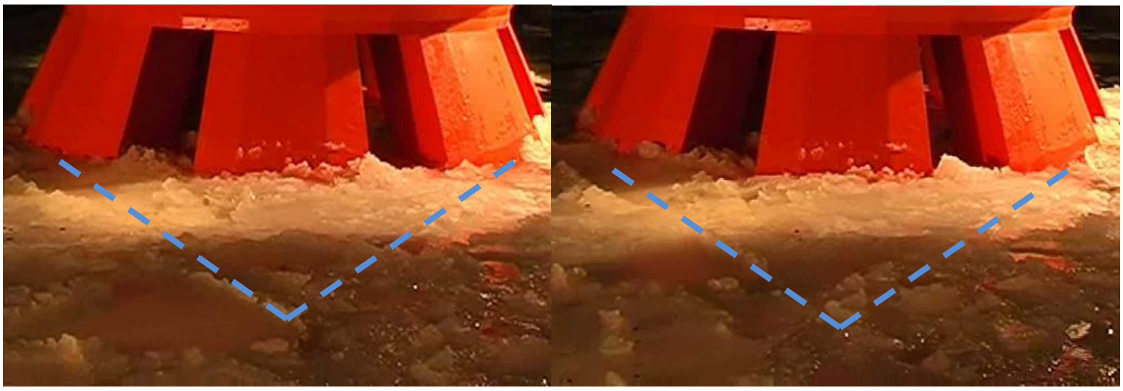

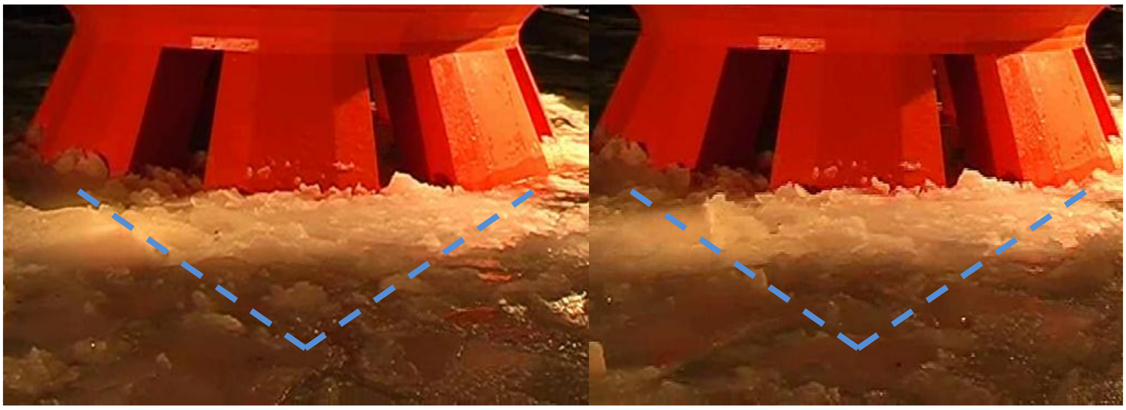

Figure 2-9: 1m thick 30m broken ice at 0.75 m/s. Time lapse series with a time interval of 76 s. Notice the ice rubble directly in front of the vessel is stable while the approach ice moves to the sides.

The vessel-ice interaction is similar to that of the channel in level ice. Ice floes accumulate in front of the vessel. However due to the absence of the channel's edges in the broken ice scenario, the ice floes are free to move around the vessel. The wedge that forms in front of the vessel is helping in pushing the incoming ice floes aside.

Towards the end of the test the ice floes moving around the structure start to interact with the walls of the basin due to the limit size of the ice basin. Eventually this clogs up the areas surrounding the model and starts to influence the test. For this reason the data gathered after this process started to occur are neglected when processing the data.

When comparing the different velocities (0.75 m/s and 1.5 m/s) the same vessel-ice interaction occurs with no notable differences.

1m thick broken ice with dimensions of 100 m x 100 m

For the broken ice of 100 m the vessel-ice interaction is very similar to the 30 m broken ice. However there are a couple of differences:

- Local failure due to upward bending is more prominent now at the vessel-ice interface causing the ice floes in contact with the vessel to slowly get smaller over time;
- Splitting of ice floes now happens (radial cracking);
- Rafting of whole floes on top of each other happens, especially at high velocities;
- The ice accumulated in front of the model is less stable. The stable wedge shaped rubble that occurred during the 30 meter broken ice could not be seen with 100 m broken ice.

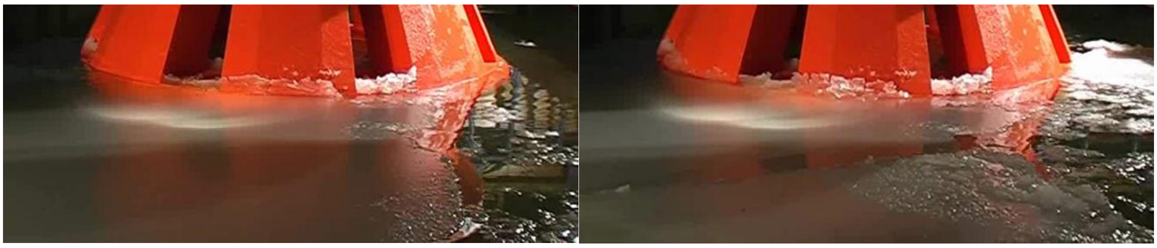

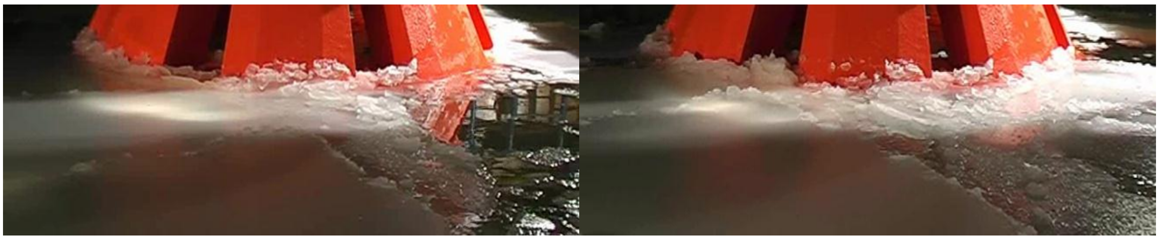

Figure 2-10: 1m thick 100 m broken ice at 0.75 m/s. Time lapse series clearly showing rafting. Time interval is 152 s.

When comparing the different velocities (0.75 m/s and 1.5 m/s) the same vessel-ice interaction occurs. The only difference is that the ice breaks / dents a bit more due to the higher levels of energy involved in the collisions and interactions.

2m thick broken ice with dimensions of 30 m x 30 m

For the 2 m thick broken ice of 30 m the vessel-ice interaction is very similar to the 1 m thick 30 m broken ice. However there are a couple of differences:

- Again a wedge forms over time which pushed approaching ice floes a side. However compared to the 1 m thick broken ice of 30 m the tip of the wedge is located a bit further away from the vessel.

This difference could be explained by the increased strength of the 2 m thick ice, resulting in a stronger and more stable wedge formation.

When comparing the different velocities (0.75 m/s and 1.5 m/s) the same vessel-ice interaction occurs with no notable differences.

2m thick broken ice with dimensions of 100 m x 100 m

For the 2 m thick broken ice of 100 m the vessel-ice interaction is very similar to the 1 m thick 30 m broken ice. However there are a couple of differences:

- Much more ice accumulates and more layers of rafting of the ice (up to 4 layers thick);
- The ice group in front of the vessel is more stable, resulting in a wedge shape. This was not present for the 1 m thick 100 m wide broken ice but was for the 1 and 2 m thick 30 m wide broken ice.

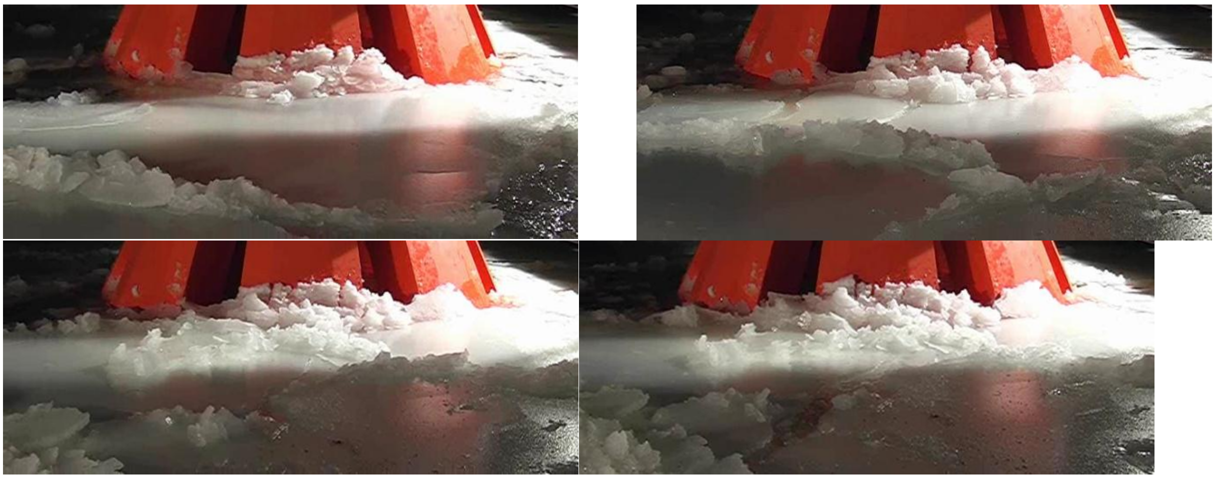

Figure 2-11: 2m thick 100 broken ice at 0.75 m/s. Time lapse series. Notice the rafting of the ice. Time interval is 76 s.

Because the ice now has a higher flexural strength the ice floes do not brake as easily when compared with the 1 m thick ice floes. This explains both differences.

When comparing the different velocities (0.75 m/s and 1.5 m/s) the same vessel-ice interaction occurs with no notable differences.

Commentary on the test setup of the 100 m broken ice

The way the broken ice was modeled was by cutting the original ice sheet into three lanes of 100 m wide and then cutting the lanes in to sections of about 100 m long. This resulted in a very regular ice pattern as can be seen in Figure 2-12. Since the structure is a 98.6 m wide at the operational draft, it can pass through the central path while leaving the two outer lanes of ice floes pretty much unscathed. Because of this some effects that would occur under different circumstances do not occur now because due to the layout of the sheets, the sheets are inclined to start rafting in the central lane.

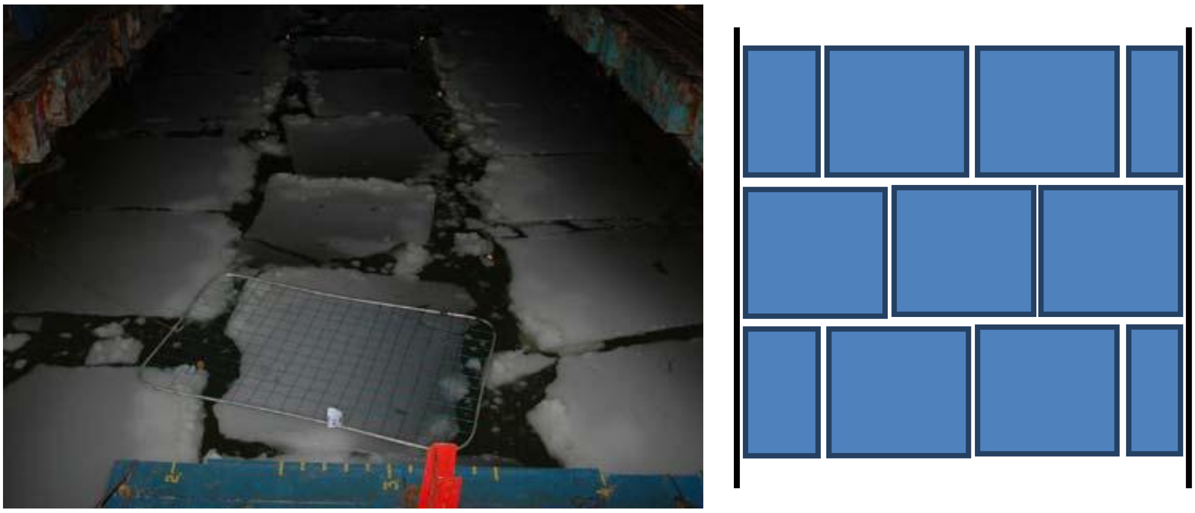

Figure 2-12: Both figures show 100 m broken ice, but would they result in the same vessel-ice interaction?

If the ice had been laid out as depicted in the right side of Figure 2-12, or even completely random with random orientation, then the results and phenomenon occurring could quite possibly be different. For 30 m broken ice this effect is not notable because the small pieces will acquire a random orientation during cutting since they are not so influenced by the limited dimension of the basin.

All the tests at the transit draft have now been discussed. Next up are the tests at the operational draft.

2.3.2 OPERATIONAL DRAFT

When drilling in ice conditions the JBF Artic will be floating at the operational draft. At this draft the hull is downwards sloping at a 45 degree angle in order to make incoming ice fail in bending rather than crushing thereby reducing the ice load on the vessel. In Figure 2-13 the location of the operational draft can be seen.

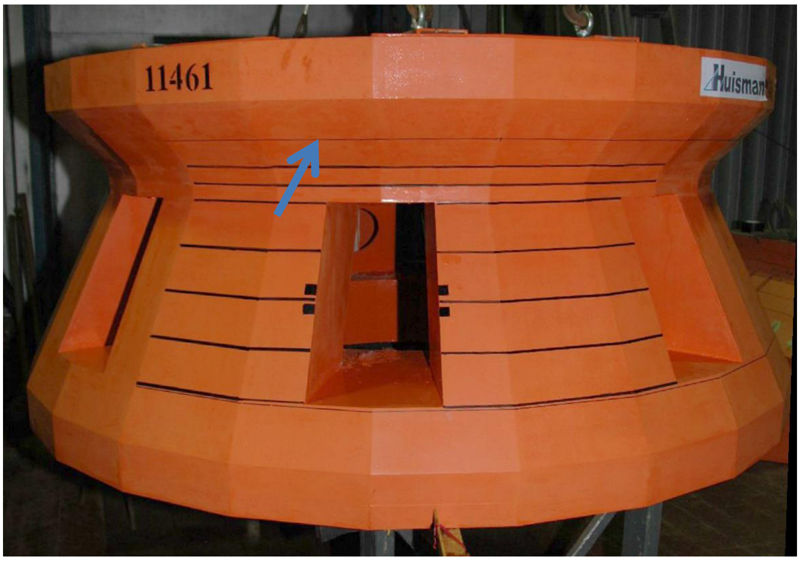

Figure 2-13: Location of operational draft.

The layout of this section is as follows. First the impact of the hull geometry at the operational draft will be discussed in 2.3.2.1. Then, in turn, the different ice features are discussed: broken ice in section 2.3.2.2, then hummocks with a channel in it created by an icebreaker in section 2.3.2.3 and finally broken ice in section 2.3.2.4.

2.3.2.1 IMPACT OF HULL GEOMETRY ON VESSEL-ICE INTERACTION AT OPERATIONAL DRAFT

At the operational draft, the properties of the interface between the ice and the vessel depend on three parameters: the trim angle of the vessel, where on the circumference of the vessel you look and on the ice thickness. These three parameters change vessel-ice interface but more importantly the impact angle and its distribution over the interface area. The reasons behind this are explained next.

Dependence on trim angle

The trim angle (a negative rotation of the vessel around the y-axis) has a very big effect on the impact angle of the ice. This is better explained in Figure 2-14. In this figure the colors represent the different impact angles of the vessel.

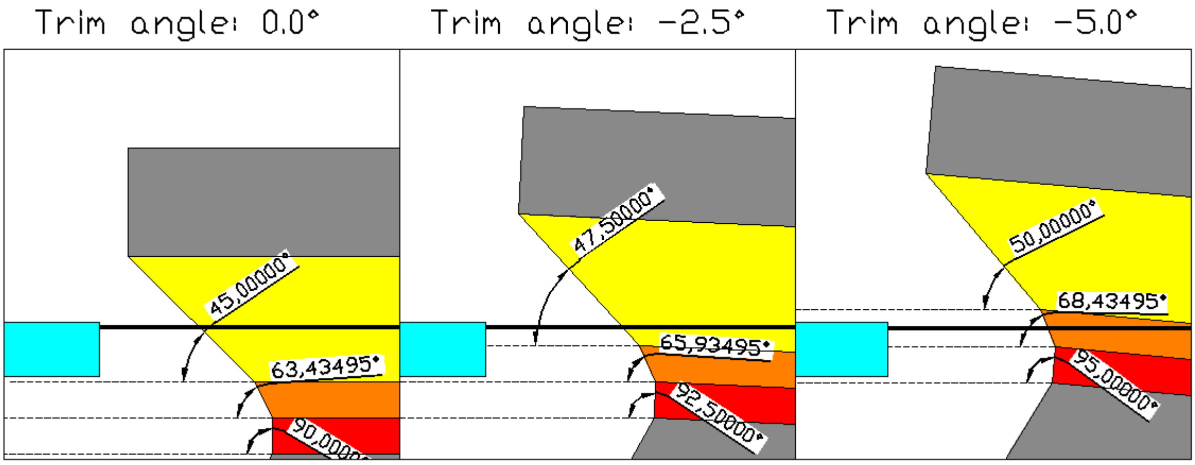

Figure 2-14: The vessel-ice interface for various trim angles and an ice thickness of 3 m. The thick solid line is the sea level. The cross-section was made over the center-line of the vessel.

For a trim angle of zero degrees the ice interacts with the yellow section of the hull over the full thickness of the ice, having an impact angle of 45 degrees. At this impact angle the ice will fail in downward bending.

However as the vessel acquires a trim angle of 2.5 degrees, as can be seen in the middle picture, the ice now interacts for only 59% with the yellow area (having an impact angle of 47.5 degrees) and for 41% with the orange area (having an impact angle of 65.9 degrees). Because the orange area has significantly higher impact angle (65.9 degrees compared to 47.5 degrees), this could have a notable impact on the vessel-ice interaction. At this angle it is harder to predict how the ice will fail, but it will most likely be due to downward bending again. The ice might also fail in crushing but in order to do so; the ice would first have to bend downwards quite considerably in order to get a vertical offset that is large enough for it to interact with the red section of the hull (where the impact angle is 92.5 degrees and one would expect crushing).

Finally at a trim angle of 5.0 degrees the division between the three colors is: yellow (16%), orange (51%) and red area (31%). As the impact area of the red area is 95 degrees one would expect some of the ice to fail in crushing at this trim angle in addition to failing in downward bending.

Dependence on location

In Figure 2-14 the cross-section was taken at the center line (the center of the interface areas displayed in Figure 2-15). Because of the cylindrical shape of the vessel the effect of the trim angle is the largest at the center line because this point is removed the furthest from the center-of-gravity of the vessel, thus rotation has the largest effect there. In Figure 2-15 one can see that towards the edges of the interaction area the effect reduces again, resulting in lower impact angles, as depicted by the colors.

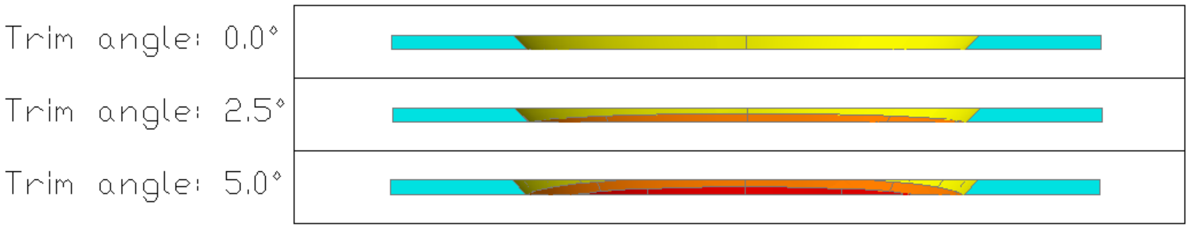

Figure 2-15: Vessel-ice interface area as seen from the ice's point-of-view showing the influence of the location.

Dependence on ice thickness

In Figure 2-14 an ice thickness of 3.0 m was used. The ice thickness has an important influence in that it changes the height over which the ice and structure interact. The thicker the ice, the deeper it reaches and thus increasing the interaction with the orange and red section. This effect is shown in Figure 2-16.

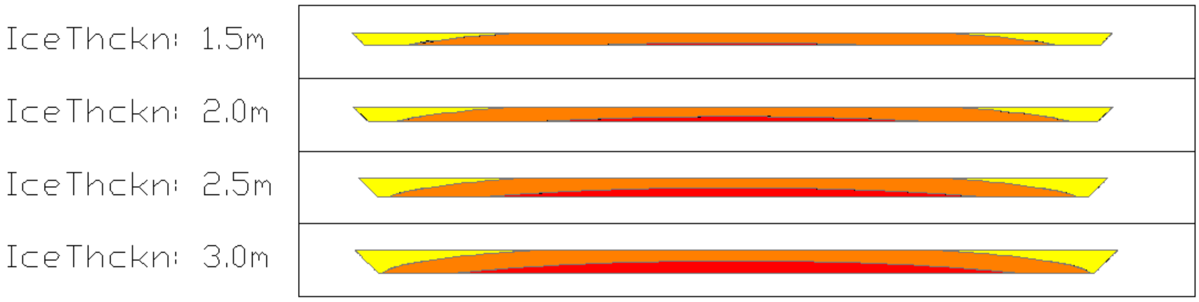

Figure 2-16: Vessel-ice interface area as seen from the ice's point-of-view showing the influence of the ice thickness. A trim angle of 5.0 degrees was used to create all four images within the figure.

In addition there is another small effect related to the ice thickness. As it becomes thicker a larger part of the ice will float above the water line due to buoyancy. When using the density of 920 kg/m^3, which was the average of model tests, 10.2539% of the ice sheet will be above the water line.

Now that all the influences of the hull have been discussed the analysis of the vessel-ice interaction can begin.

2.3.2.2 BROKEN ICE

For the operational draft all but 5 of the in total 20 tests were done with level ice. 3 tests were done with broken ice and 2 tests were done with hummocks. First broken ice and the hummocks will be analyzed and then ending with level ice.

For the operational draft three different tests were done with broken ice:

- 1.5 m thick broken ice with a dimension of 100 m x 100 m at 0.5 m/s
- 2.0 m thick broken ice with a dimension of 100 m x 100 m at 0.5 m/s
- 3.0 m thick broken ice with a dimension of 100 m x 100 m at 0.5 m/s

1.5 m thick broken ice with dimensions of 100 m x 100 m

For this test the ice was cut into rectangular plates with a length of about 100 m. A concentration of about 8/10 was used. The following can be observed from the footage:

- The ice floes bump into vessel and remain stable there;
- As more floes approach, they start rafting on top of the stable ones and/or bumping into the stable ones, the ice floe in contact with the vessel starts to fail in downward bending;
- Over time the plates very slowly get smaller due to the edges failing in bending and smaller pieces float out to the side where they are pickup up by the passing sheets and moved away;
- Lots of sheet end up rafting on top of each other (4 – 5 sheets thick, depending on whether the first ones are still there or they have already been crushed and flown away).

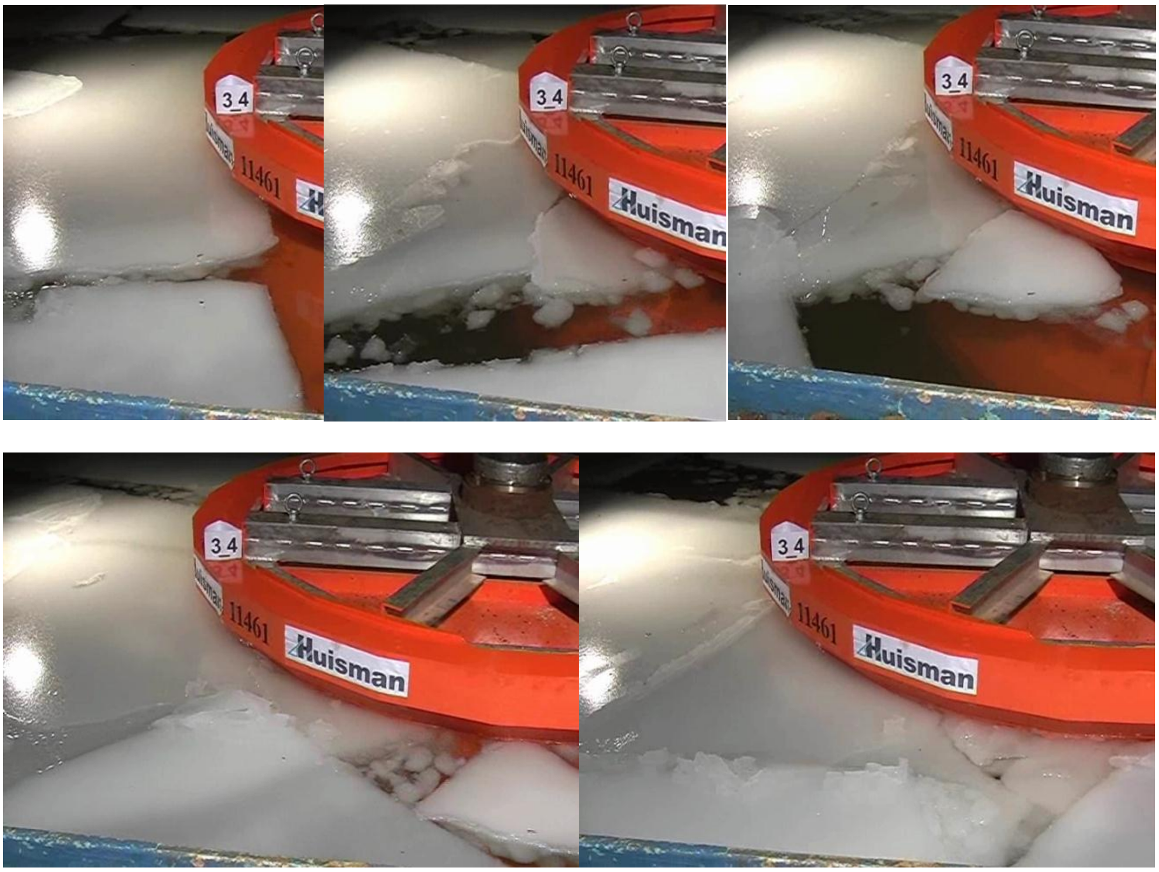

Figure 2-17: 1.5m thick 100 broken ice. Time lapse series showing rafting and buildup of ice. Time interval is 114 s.

Due to the low velocity, the forces on the ice floes are fairly small. Because of this the sheets remain intact for a fairly long time resulting in lots of rafting.

All in all the vessel-ice interaction is very similar to the broken ice at transit draft.

2.0m thick broken ice with dimensions of 100 m x 100 m

For the 2.0 m thick broken ice the vessel-ice interaction is very similar to the 1.0 m thick broken ice. However there are a couple of differences:

- Failure in downward bending occurs more easily and even some circumferential cracks occur;
- Ice floes also split now due to radial cracking (see Figure 2-18);

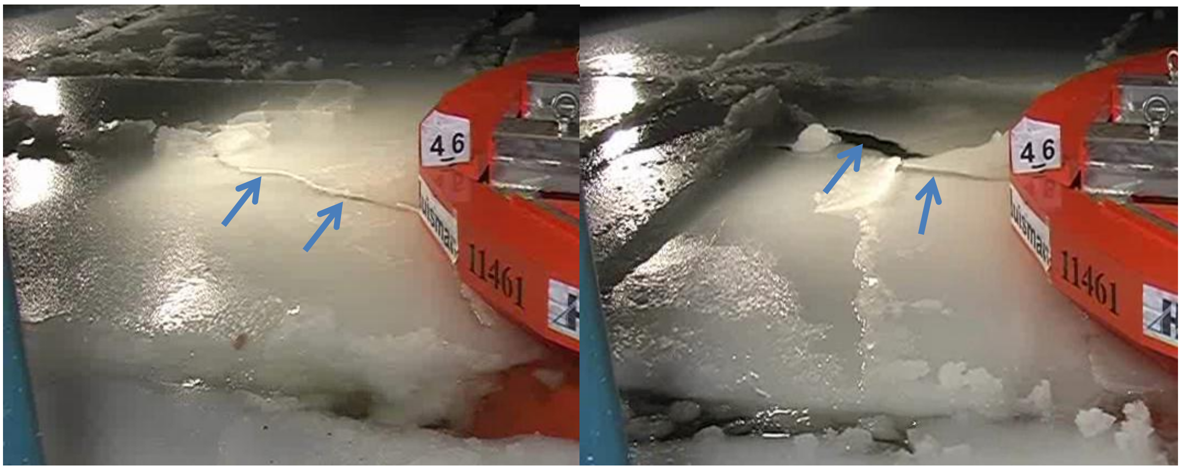

Figure 2-18: 100m broken ice. The arrows show the radial crack which split the ice floe.

3.0m thick broken ice with dimensions of 100 m x 100 m

For the 3.0 m thick broken ice the vessel-ice interaction is very similar to the 1.0 m thick broken ice. However there are a couple of differences:

- Due to the higher strength of the ice floes entire floes remain intact even when pushed down to considerable depths;
- Splitting of ice floes caused by radial cracking happens more frequently;
- Rafting up to 2 – 3 layers thick;

2.3.2.3 HUMMOCKS

At the operational draft two different tests were done with hummocks in level ice through which a 40 m wide channel was made with an icebreaker model:

- A hummock with a 3.0 m thick consolidated layer and a 10 m keel depth at 0.5 m/s
- A hummock with a 3.0 m thick consolidated layer and a 18 m keel depth at 0.5 m/s

A hummock with a 3.0 m thick consolidated layer and a 10 m / 18 m keel depth at 0.5 m/s

The following observation can be made when looking at the interaction between the hummock and the vessel:

- Radials cracks run from the hull towards the hummock through the consolidated layer, the ice floe created is then easily pushed aside;
- The remaining consolidated layer generally fails in downward bending.

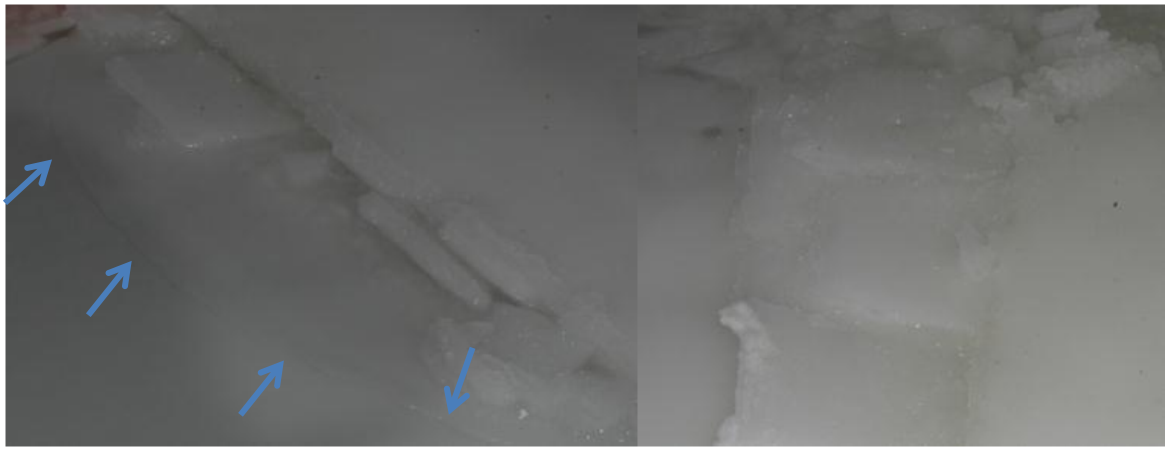

Figure 2-19: Left: a large crack prior to arrival of model, its length is roughly 100 meters. Right: the rubble in the gap that behaves rather weak.

The above water part of the ridge (of which good video footage is available) behaves somewhat strange. At the hummock's location a transverse cut has been made into the level ice, probably used to push the rubble below the consolidated layer to create the keel. From the photographs and also from the video footage it feels as though the water in the gap has not completely frozen again, but rather filled with lose rubble and weak ice slush (Figure 2-19 right side). Also there are already large fractures present prior to the arrival of the ice breaker (Figure 2-19 left side).

However the hummock's keel does seem to be made up of a lot of rubble. It is unclear to what extend the interaction with the consolidated layer is relevant for the overall loading created by the hummock. Therefore it is hard to evaluate the quality of the hummocks.

As a side note, during the ide ridge tests emphasize was put on the quality of the ridge itself and not on the level ice before or after the ridge. This might explain why the consolidated layer behaved somewhat strange.

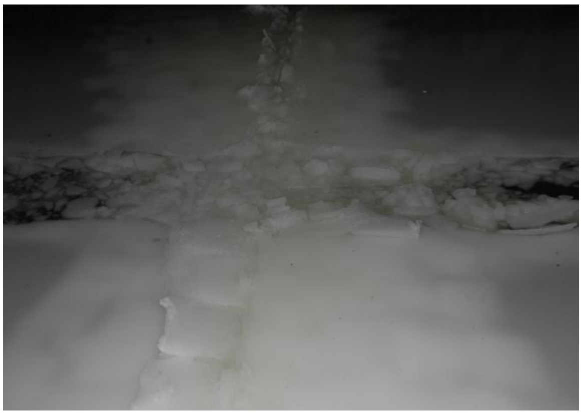

Figure 2-20: The keel of the hummock can be seen through the consolidated layer.

2.3.2.4 LEVEL ICE

The level ice data will be the main source of information for the ice model that will be created at a later stage, and thus the data from these tests is the most important for the rest of this report. The influence on the loading was tested for three parameters; the ice thickness, the ice velocity and the trim angle of the vessel.

At the operational draft 15 different tests were performed with level ice. Table 1 gives an overview of all the tests.

Overview of tests performed at operational draft									
	Level Ice – 1.5m			**Level Ice – 2.0m**			**Level Ice – 3.0m**		
	Ice velocity [m/s]			Ice velocity [m/s]			Ice velocity [m/s]		
Trim Angle [°]	0.5	1	1.5	0.5	1	1.5	0.5	1	1.5
0	3_1/5_1	3_3	3_2	4_5	4_4	4_3	6_1	6_3	6_2
2.5	3_6			4_1			6_4		
5	3_5			4_2			6_5		

Table 1: Overview of tests performed at operational draft. The numbers in the table mean the following: x_y, then x is the number of the ice sheet and y is the number of the test with that ice sheet.

There are basically two groups of nine tests each, which both keep one of the three parameters fixed and vary the other two:

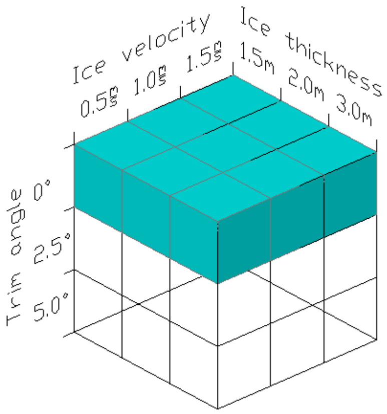

Figure 2-21: Graphical representation of group 1.

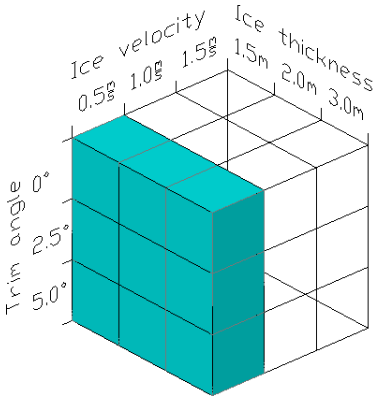

Figure 2-22: Graphical representation of group 2.

Group 1 – Thickness/Velocity (Figure 2-21)

Fixed parameter: trim angle fixed at 0°
Variable parameters: 1.5 m – 3.0 m ice thickness
0.5 m/s – 1.5 m/s ice velocity

Group 2 – Thickness/Trim Angle (Figure 2-22)

Fixed parameter: ice velocity fixed at 0.5 m/s

Variable parameters: 1.5 m – 3.0 m ice thickness
0° - 5° trim angle

The approach for analyzing the data is as follows.

- First the base case will be analyzed (1.5m, 0.5 m/s, 0°)
- Then group 1 – thickness / velocity
- Finally group 2 – thickness / trim angle

2.3.2.4.1 Base case

The base case consists of 1.5 m thick level ice at 0.5 m/s under a 0° trim angle. When looking at the footage of the base case the following can be observed:

- All ice fails in downward bending
- The circumferential cracks occur so close to the hull that they are almost impossible to see
- No rubble ends up on top of the ice sheet

- The ice actions are fairly small. The average ice action size (a measure of how many degrees around the hull the circumferential cracks spread) is about 5° to 15° (>95% of all the action). Large action, 25°+ happen very infrequently (<5% of the time) and the maximum size seen is about 45°.

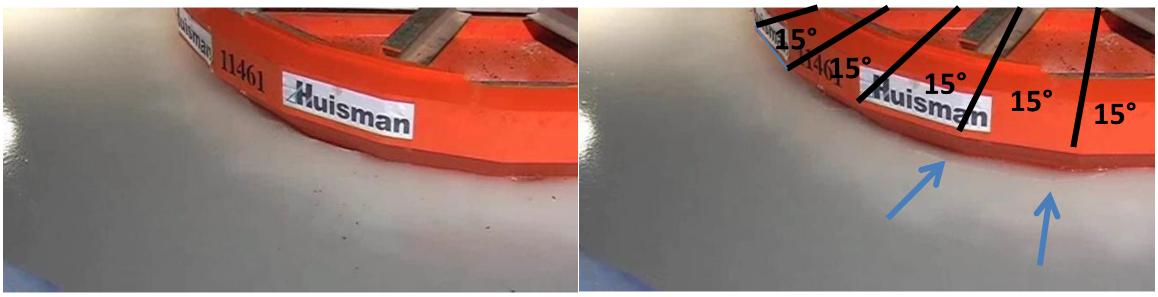

Figure 2-23: Left: normal situation. Right: one of the larger visible circumferential cracks. When estimating the ice action size it is easy to compare them to the hull of the vessel since it is not fully circular but rather 24-sided polygon, resulting in flat planes 15° apart.

Compared to all other tests discussed before at the transit draft, the vessel-ice interaction is almost completely stationary for this test. It is a continuous process of circumferential cracks breaking the sheet down into slender pieces of ice (10 - 25 m long, 2 - 4 m wide). As these slender pieces are squashed between the approaching ice sheet and the hull they are broken again in to smaller, fairly regular, rectangular pieces (2 m – 4 m long and wide). All of this can be seen in Figure 2-24.

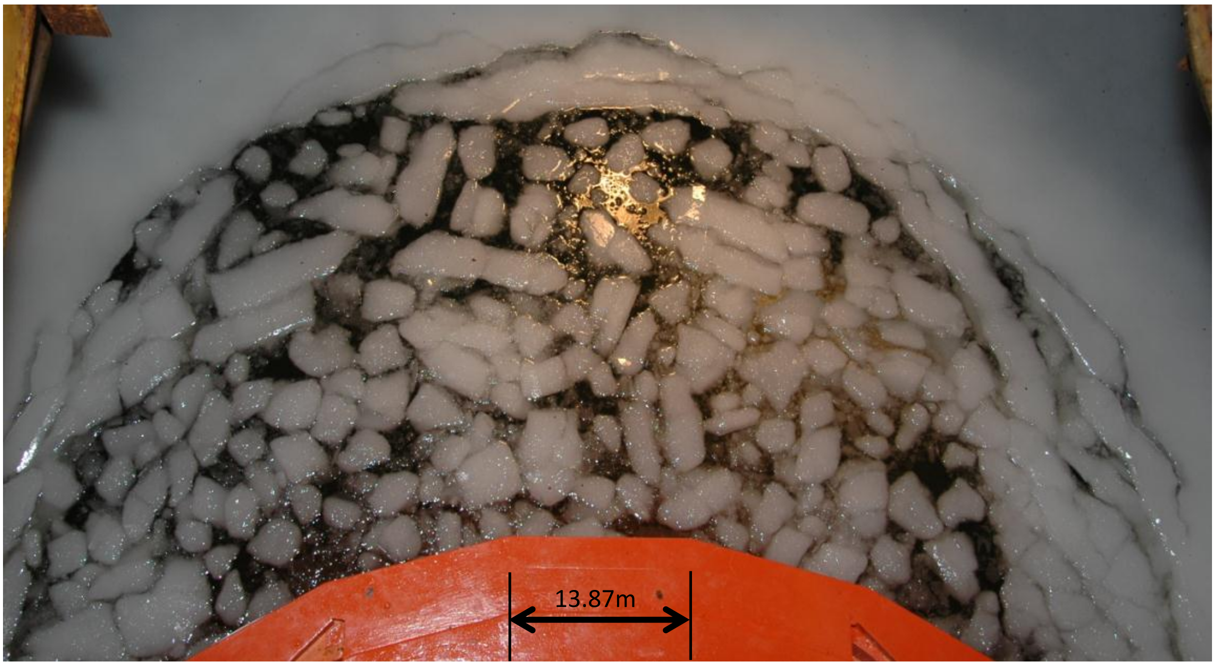

Figure 2-24: The various stages of the ice fragmentation process can be observed in this picture taken after the test after the model has been pulled back. At the edge of the ice sheet the larger circumferential cracks can be seen. A little more inwards are the long slender pieces (up to 25 m) and finally the fairly regular, rectangular pieces.

2.3.2.4.2 IMPACT OF ICE THICKNESS

Starting from the base case the ice thickness is increase to see what the impact is on the vessel-ice interaction.

2.0 m thick ice

When increasing the ice thickness from 1.0 m to 2.0 m the following changes are observed:

- All the ice still fails in downward bending and no rubble ends up on top of the ice sheet;
- The circumferential cracks now extend even further outwards from the hull, due to the increased bending stiffness. The average ice action size is still about 5° to 15° (about 90% of all the ice action). Larger ice actions, 30°+ now happens more frequently (about 10% of the time) and also the maximum ice action size is about 60° (compared to 45° before). Thus failure of the ice sheet becomes slightly more simultaneous over the circumference of the vessel;
- The resulting ice pieces are slightly larger in general (2 m – 5 m long and wide compared to 2 m – 4 m long and wide)

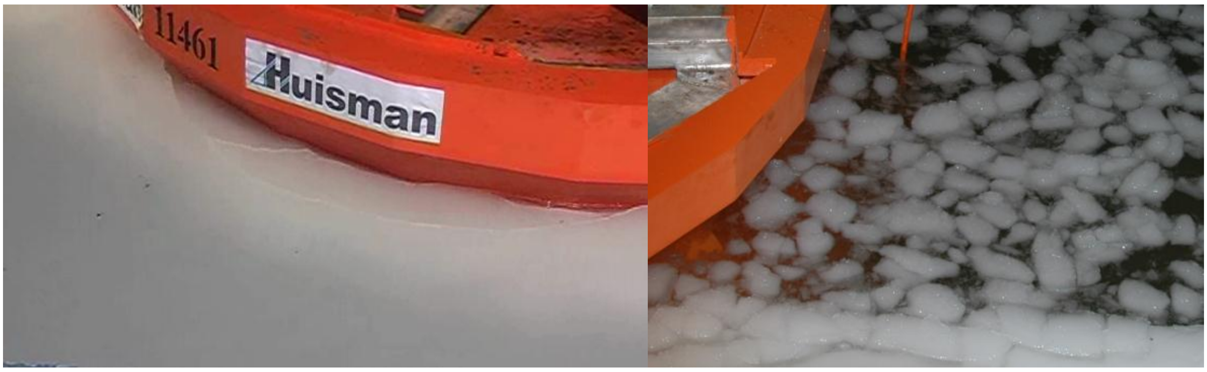

Figure 2-25: Left: Circumferential crack extend further outwards. Right: the resulting ice pieces are slightly larger.

3.0 m thick ice

When increasing the ice thickness from 2.0 m to 3.0 m the following changes are observed:

- All the ice still fails in downward bending and no rubble ends up on top of the ice sheet;
- Again even larger pieces are broken off by the circumferential cracks. About 40% of the ice action now has a size of about 30° to 60° with the other 60% being taken up by very large ice actions with a very large size, 90° to 120°. Maximums can go as high as 150° and ice actions with a size of 5° - 15° are pretty much absent.
- The Ice actions are very simultaneous over the circumference of the vessel.

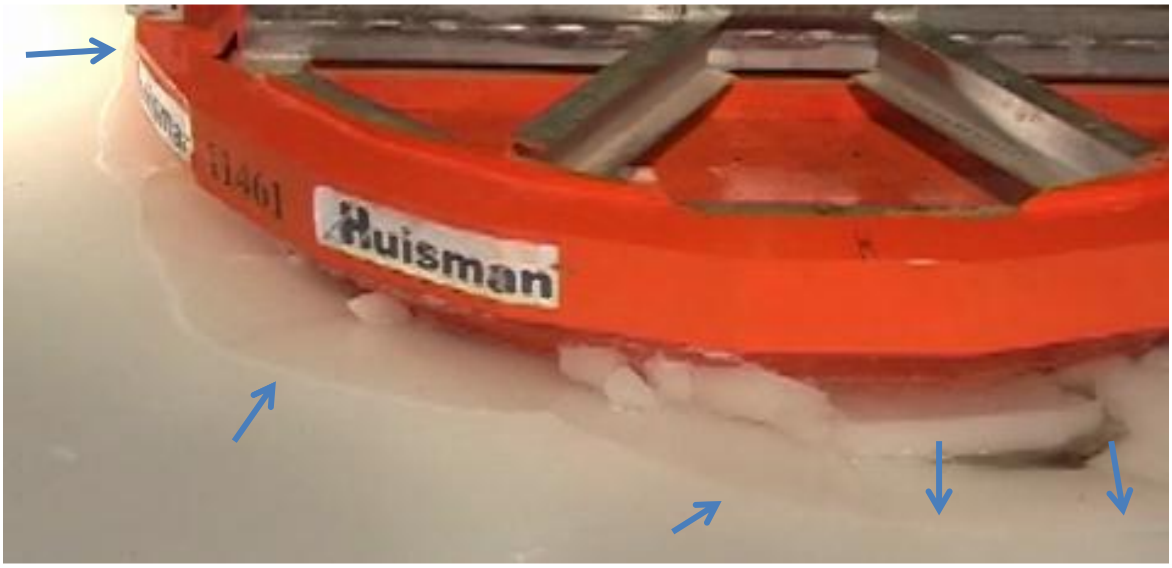

Figure 2-26: The largest circumferential crack observed in the test footage, extending over 150° of the vessel.

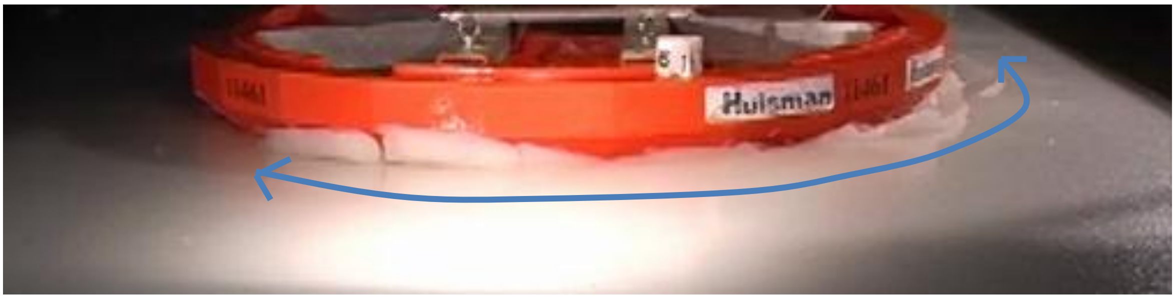

Figure 2-27: The full extent of the largest simultaneous ice action can be seen once the ice pieces start to rotate upwards as they get pushed against the hull and move down, below the approaching ice sheet.

Discussion of the impact of the ice thickness

The failure mode remains the same regardless of ice thickness, downward bending.

The very important effect of the increase in ice thickness is that the ice action goes from being a local phenomenon to being a more global phenomenon where whole sections of the vessel are affected by the same ice action at the same time.

The increase from 1.0 m to 2.0 m thickness increased the simultaneousness of the ice action, but when further increasing to 3.0 m thickness a much larger increase was seen.

Now that the impact of the ice thickness is clear, the impact of the ice velocity will be analyzed.

2.3.2.4.3 IMPACT OF ICE VELOCITY

Starting from the base case the ice velocity is increase to see what the impact is on the vessel-ice interaction.

1.0 m/s and 1.5 m/s ice velocity

When increasing the ice velocity from 0.5 m to 1.0 m/s and again when increasing from 1.0 m to 1.5 m/s, the following changes are observed:

- The ice action size keeps roughly the same distribution (mostly small sized). The circumferential cracks are located a bit further outwards from the hull.
- The ice rubble in front of the vessel moves more and so sticks less close to the hull.
- The biggest change can be seen when comparing the ice pieces behind the model. The size of the ice pieces does not seem to be influence by the increasing velocity. But when looking at the concentration of the ice, there is a rapid increase as the ice velocity increases.

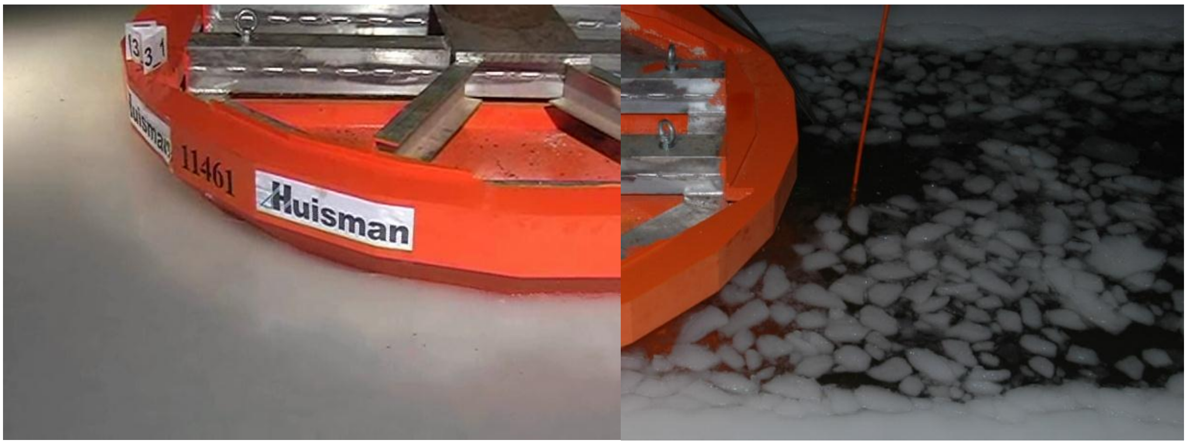

Figure 2-28: 0.5 m/s ice velocity. The base case.

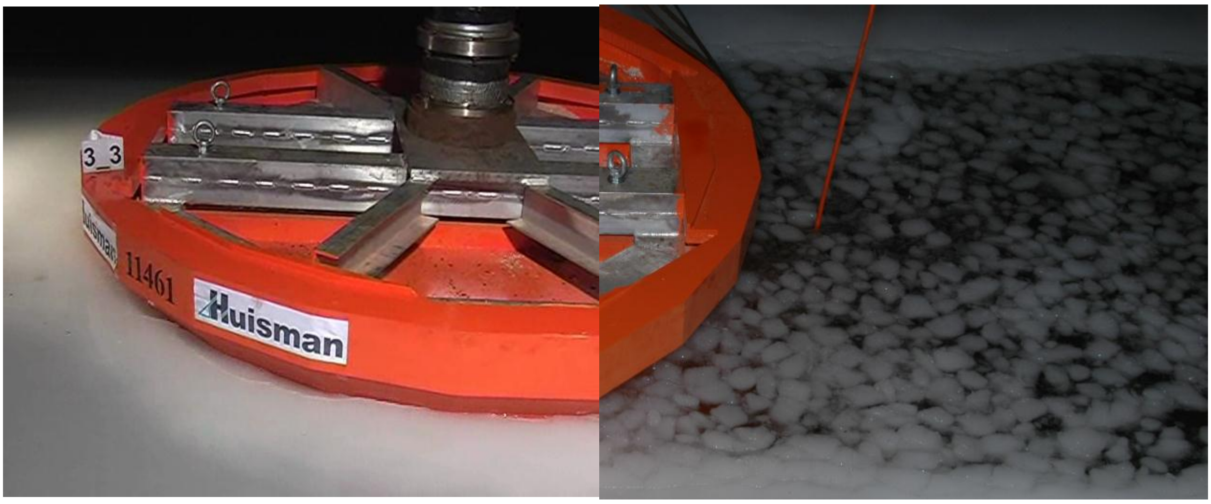

Figure 2-29: 1.0 m/s ice velocity. Left: the ice rubble moves further away from the hull. Right: increase in ice concentration.

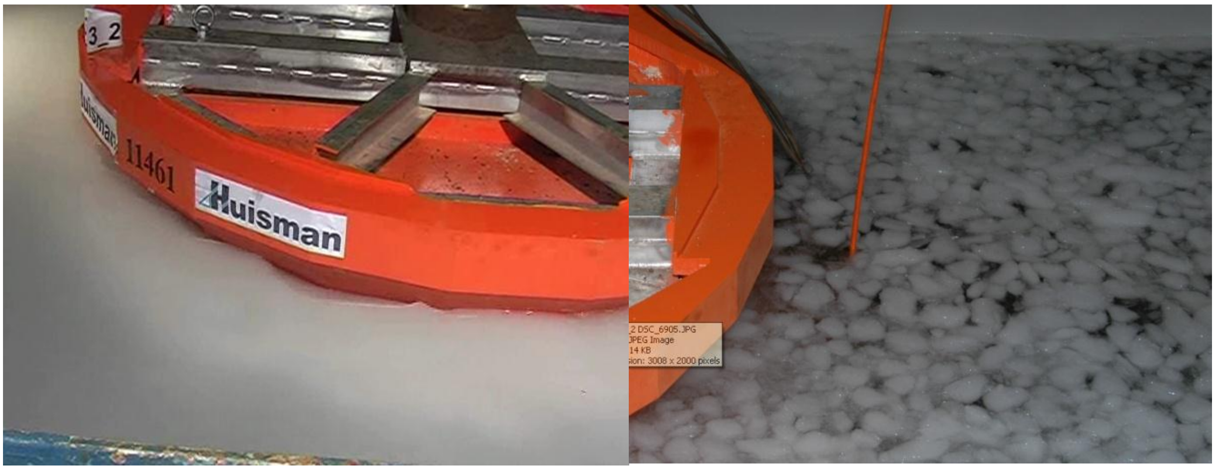

Figure 2-30: 1.5 m/s ice velocity. Left: the ice rubble moves even further away from the hull. Right: an even larger increase in the ice concentration.

As the size of the rubble pieces is not changed by the increasing velocity, the increase in concentration behind the vessel can only be explained if less ice is pushed under the edges of the channel created by the model. The reason could be that the ice has more energy and the flow around the hull is more turbulent. In Figure 2-31 the underwater footage confirms the deeper ice penetration. What is hard to capture in a figure is that the flow of the 1.5 m/s ice is far more turbulent underwater.

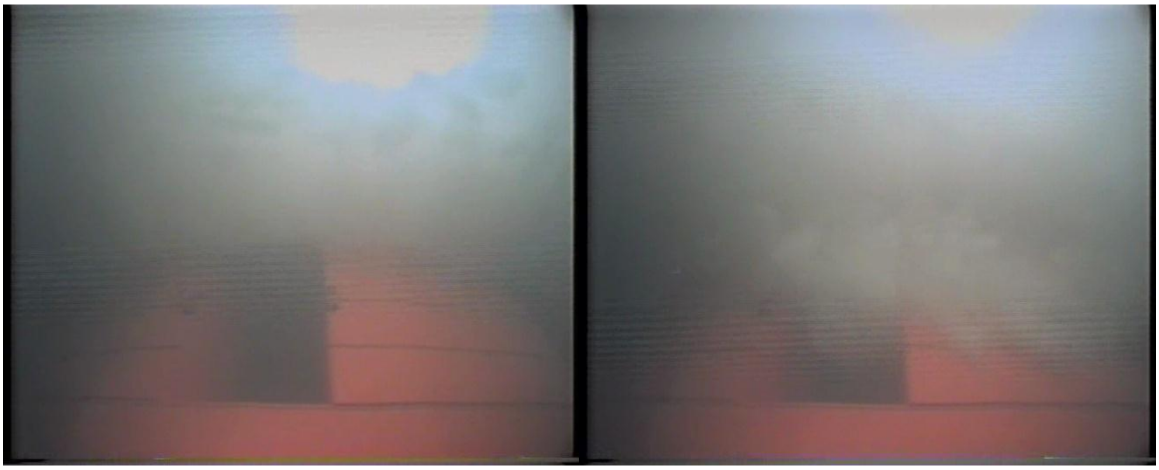

Figure 2-31: Left: 0.5 m/s. Right: 1.0 m/s. Notice that the ice penetrates deeper.

Velocity effect – lacking data

It is very important to note that two sets of velocity dependent data are missing.

First up, no tests were done that combine higher velocities with a trim angle. (Loset, 2006) suggests that higher velocities leads to a higher chance of crushing, even against sloped structures. Even though no crushing was seen at a trim angle of 0.0° this does not exclude the possibility that perhaps at a trim angle of 2.5° there would be a transition to crushing when increasing the ice velocity.

The second set of missing data is test at very low velocities. At low velocities the ice behaves ductile and has its higher strength, (Loset, 2006) page 63, 169. Therefore maximum loading and offset of the vessel might be caused by very low moving ice (less than about 0.1 m/s). Additional searching will be done when making the ice model to see whether the loading at low velocities can exceed the loading at high velocities.

2.3.2.4.4 IMPACT OF VESSEL TRIM ANGLE

The effect of the trim angle was explained in section 2.3.2.1. There it is explained that a change in trim angle can have a large impact on the impact angle of the ice. As a summary, the impact angle is a function of: trim angle, ice thickness and the location on the hull. The most important thing to check for is occurrence of crushing instead of bending.

Starting from the base case the vessel trim angle is increased to see what the impact is on the vessel-ice interaction. All tests that vary the trim angle have a constant ice velocity. In total 9 tests were done, since three trim angles were tested at three ice thicknesses. The effect of the trim angle will be checked for each ice thickness.

1.5 m thick level ice at a 2.5° trim angle

When increasing the trim angle from 0.0° to 2.5° m the following changes are observed:

- No notable differences. No crushing happens.

1.5 m thick level ice at a 5.0° trim angle

When increasing the trim angle from 2.5° to 5.0° m the following changes are observed:

- The hull can now be split into two sections: a section where all the ice fails in bending and a section where the ice fails in both bending and crushing. The crushing is located near the center line and is limited to an offset of about ±22.5° from the center line (3 panels of the hull).
- Crushing does not occur constantly, even at the center line, but alternates between crushing and bending. It is very hard to see from the video footage what exactly triggers crushing rather than bend. What can be seen is that when crushing occurs there is a notable warping of the ice sheet (possibly due to buckling). Unfortunately it cannot be seen in which direction the ice sheet bends when the crushing occurs.

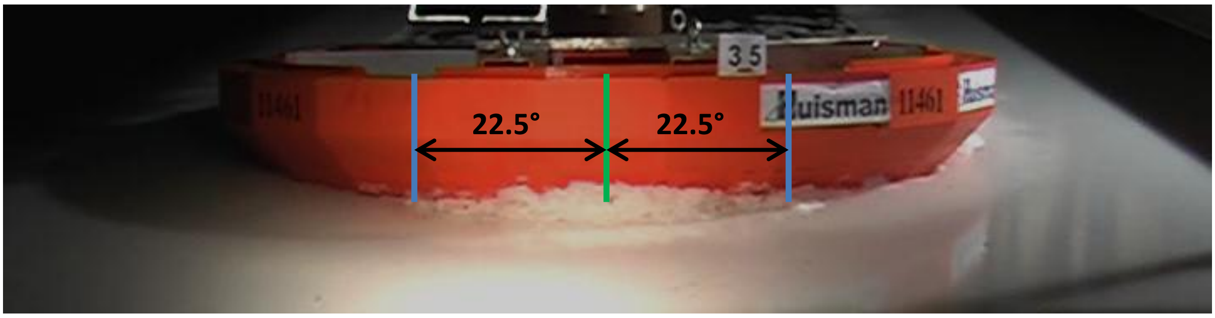

Figure 2-32: 2.5° trim angle. Crushing around the center line (the green line).

2.0 m thick level ice at a 2.5° trim angle

When increasing the trim angle from 0.0° to 2.5° the following changes are observed:

- Circumferential cracks with a large action size seem to appear a bit less frequent compared to the 0.0° situation. No crushing happens.

2.0 m thick level ice at a 5.0° trim angle

When increasing the trim angle from 2.5° to 5.0° the following changes are observed:

- The vessel-ice interactions are very similar to those observed with 1.5 m thick ice at a 5.0° trim angle. Again the hull can be split into two section; one section where the ice fails in crushing (this section now covers about 75° of the hull, 5 panels of the hull) and one section where it fails in bending. A difference is that now the ice fragment that are created by the crushing process are bigger and also the rubble pile up on top of the approaching sheet is bigger and higher. See the top photograph of Figure 2-33.
- Besides crushing there also seems to be a small amount of failure caused by buckling. As the ice sheet is pushed against the hull, it can be seen deflecting downward and is then wedged between the orange and red section. As the ice sheet keeps moving the axial force builds up, eventually buckling the sheet. See bottom photograph of Figure 2-33.

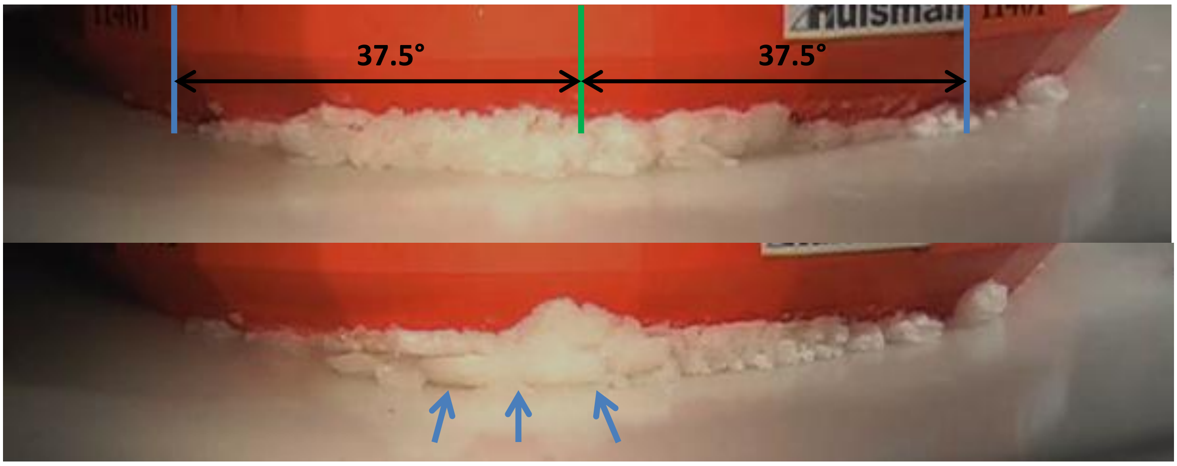

Figure 2-33: 2.0m thick 5.0° trim angle. Top: Larger rubble caused by the increased thickness. Bottom: Large pieces due to buckling.

3.0 m thick level ice at a 2.5° trim angle

When increasing the trim angle from 0.0° to 2.5° the following changes are observed:

- When compared with the 2.0 m thick level ice at a 2.5° trim angle, the drop in action size observed there is not present here. An additional special phenomenon that was observed (occurred only once during the video) was the upward buckling of the approaching ice sheet. This effect is illustrated in Figure 2-34. The upward buckling ice floe came as high as the deck box, showing the extent to which ice reinforcement would be needed. Whether this effect would occur at full scale is unsure.
- When compared with the 3.0 m thick level ice at a 2.5° trim angle, there is no notable change.

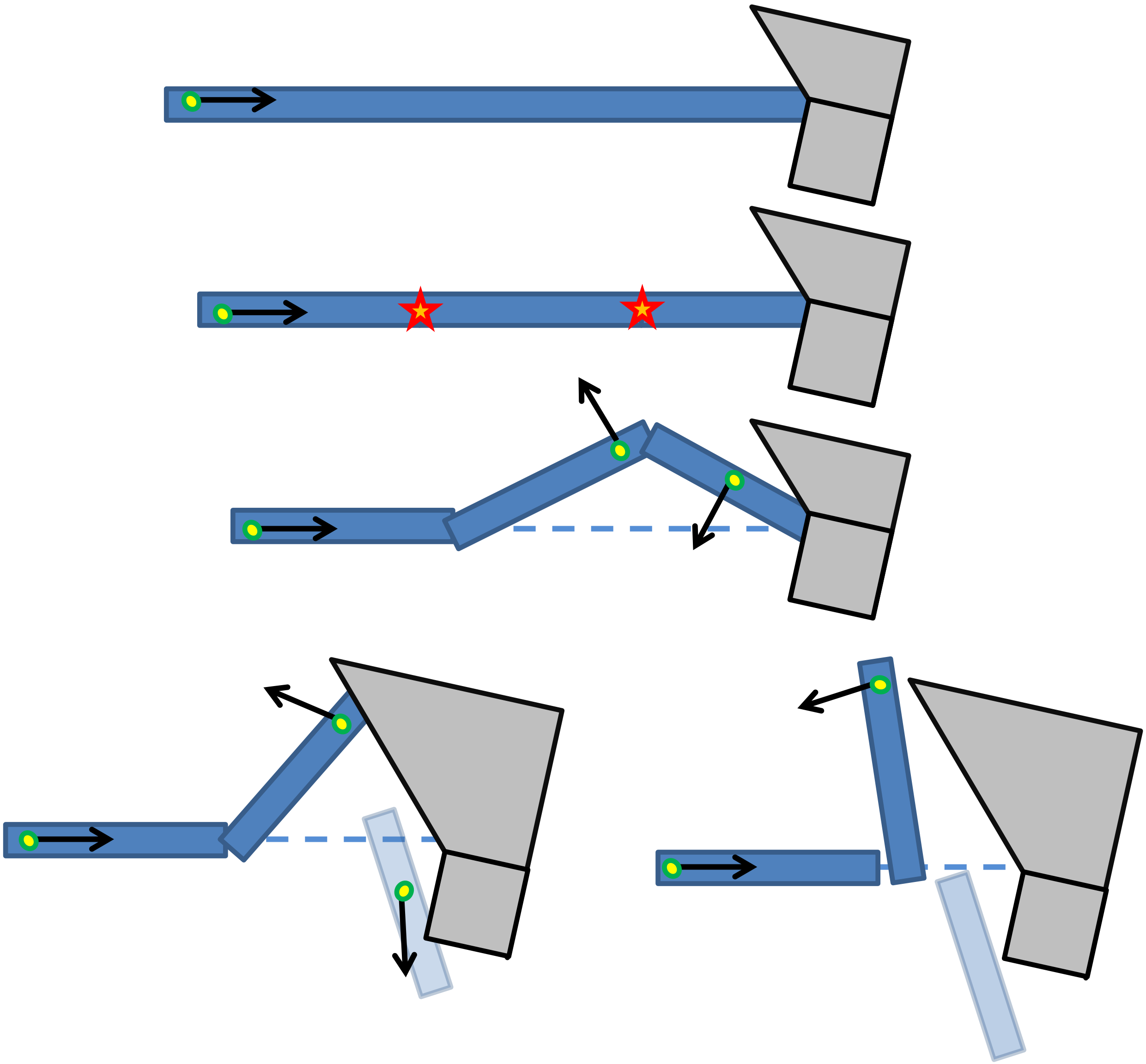

Figure 2-34: Buckling of ice sheet followed by the distant ice sheet rolling over at 5.0° trim angle.

3.0 m thick level ice at a 5.0° trim angle

When increasing the trim angle from 2.5° to 5.0° the following changes are observed:

- The behavior is very similar to both the 1.5 m and 2.0 m thick ice at a 5.0° trim angle; at the central section of the hull the ice is failing in crushing and towards the edges it is failing in bending. Compared to 2.5° there is more rubble on top of the approaching ice sheet.
- The range over which crushing occurs is slightly wider now, about 75° (5 panels of the hull).

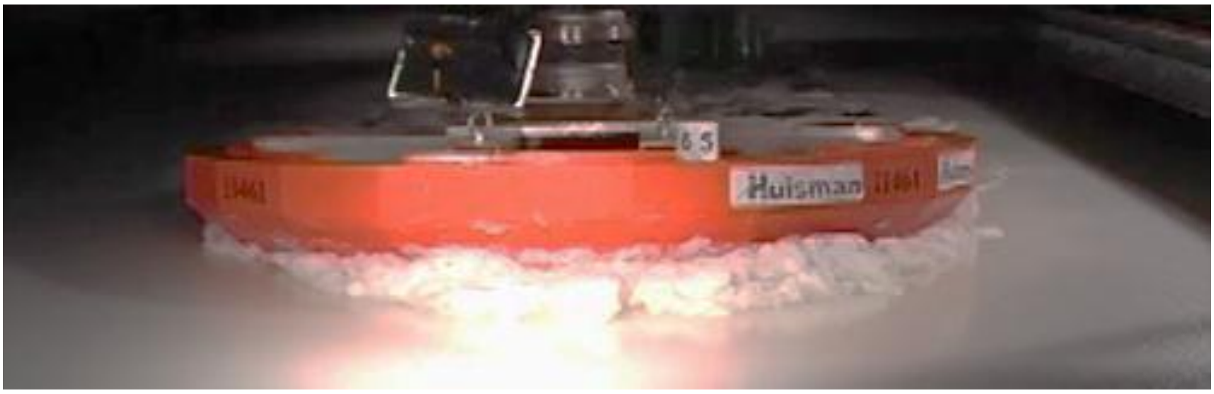

Figure 2-35: 3.0 m thick ice at 5.0 trim angle. Note that there is more rubble.

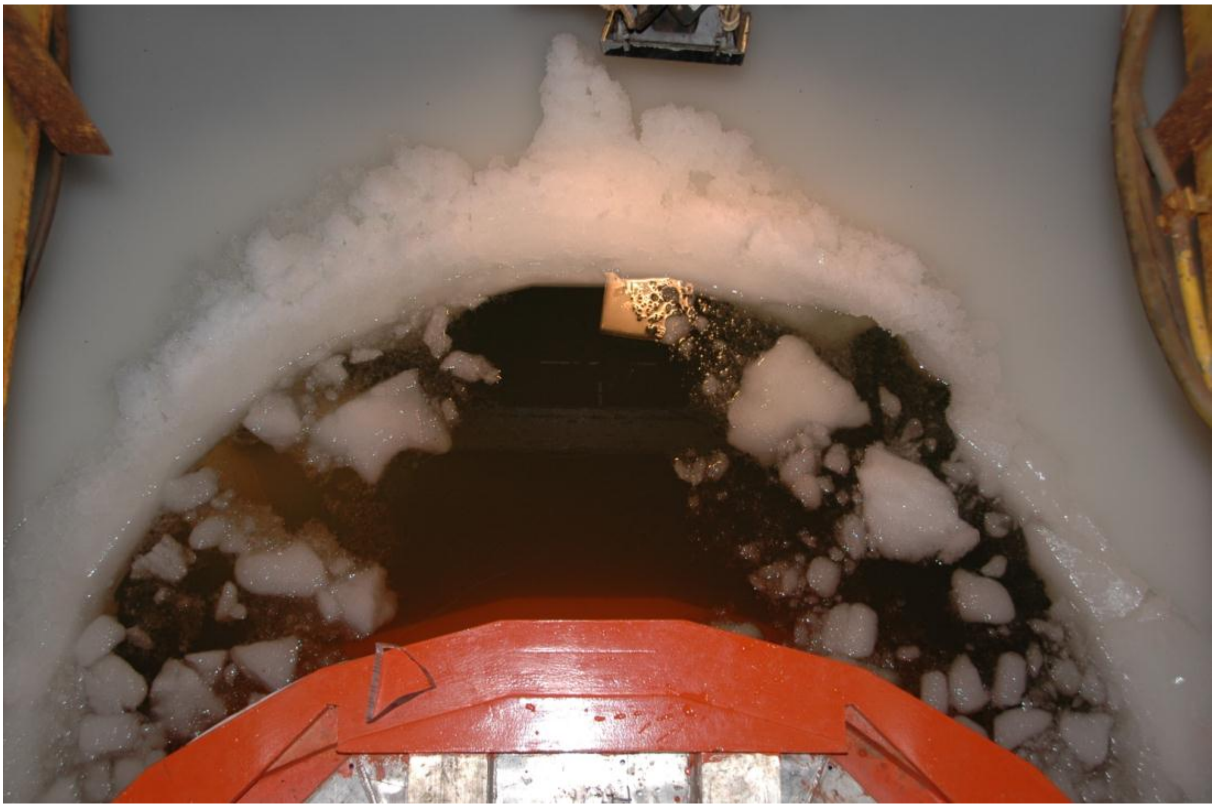

Figure 2-36: The vessel-ice interface clearly shows that crushing took place after the model had been pulled back.

2.3.3 ICE IN THE WINDOW

A common phenomenon that happened during nearly all test was that ice was going through the windows in the hull. Two different cases can be distinguished, at transit and at operational draft.

What happens at the transit draft is that the ice is pushed up by the upward sloping hull and then end up inside the windows. During several tests quite substantial quantities accumulated on top of the pontoon.

At the operational draft the downward deflected ice can float into the inner area by flowing through the windows. Here the ice can possibly interfere with the risers and other piping that is present there.

In order to fix both problems the design of the JBF Arctic has been adjust by adding grating between the legs. The grating will prevent ice from accumulating on top of the pontoon and more importantly from entering the inner area between the legs where the ice might damage the risers and mooring lines.

Possible side effects of this grating could be:

- Increased hydrodynamic loading;
- Some ice might still get through; balance between damage to riser/mooring lines and hydrodynamic loading;
- Ice could grow between the gratings, resulting in an ice wall which no longer lets any ice through.
- Fish can get stuck in the grating, possibly providing fresh food for all personal on the vessel. As fish is a good source of omega 3 fats, this will certainly boost health and morale onboard the vessel.

2.3.4 ICE RUBBLE ACCOMULATION PROPERTIES

In Table 2 several properties of the created ice rubble are noted that had been observed during the test. The table shows a direct relation between the ice thickness and the size of the blocks in the channel behind the model and also between the ice thickness and the rubble penetration depths.

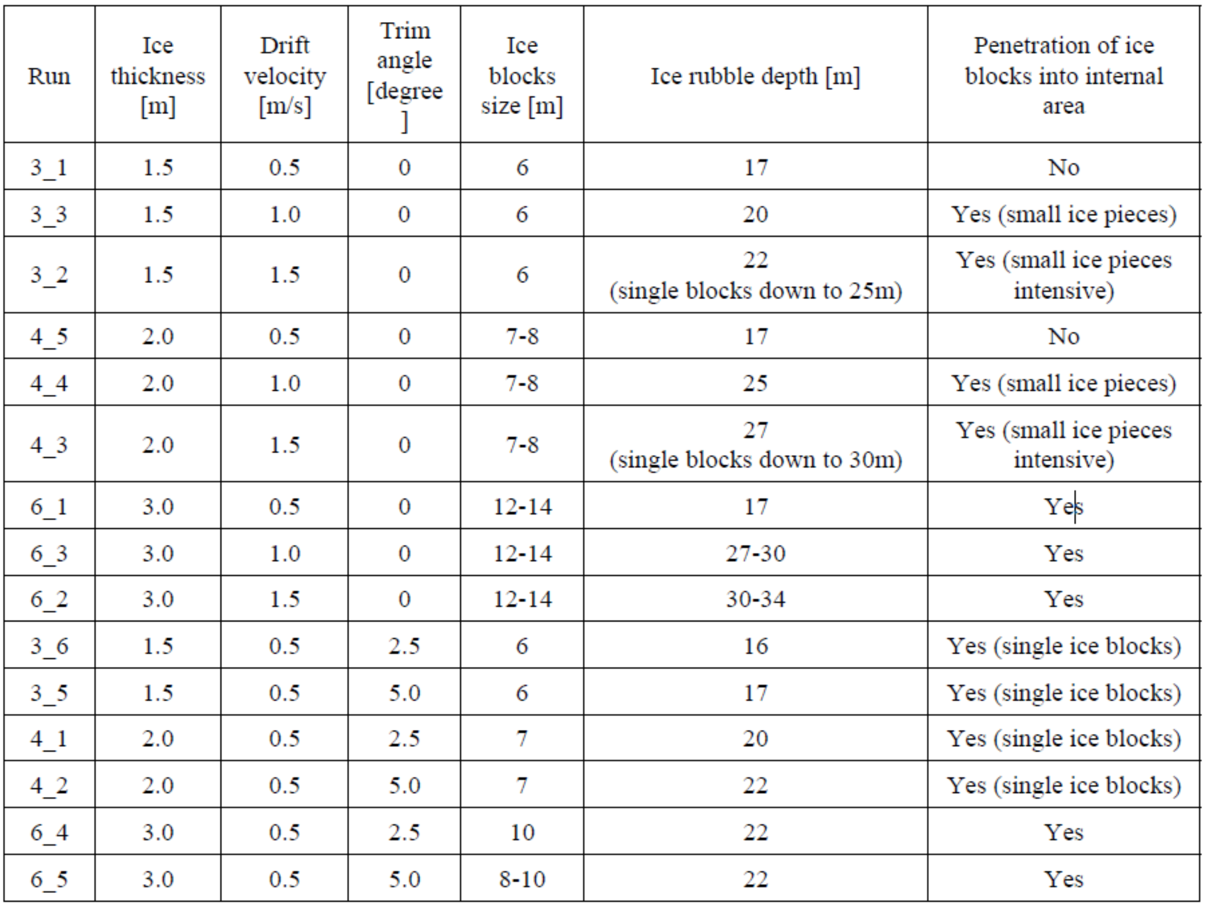

Run	Ice thickness [m]	Drift velocity [m/s]	Trim angle [degree]	Ice blocks size [m]	Ice rubble depth [m]	Penetration of ice blocks into internal area
3_1	1.5	0.5	0	6	17	No
3_3	1.5	1.0	0	6	20	Yes (small ice pieces)
3_2	1.5	1.5	0	6	22 (single blocks down to 25m)	Yes (small ice pieces intensive)
4_5	2.0	0.5	0	7-8	17	No
4_4	2.0	1.0	0	7-8	25	Yes (small ice pieces)
4_3	2.0	1.5	0	7-8	27 (single blocks down to 30m)	Yes (small ice pieces intensive)
6_1	3.0	0.5	0	12-14	17	Yes
6_3	3.0	1.0	0	12-14	27-30	Yes
6_2	3.0	1.5	0	12-14	30-34	Yes
3_6	1.5	0.5	2.5	6	16	Yes (single ice blocks)
3_5	1.5	0.5	5.0	6	17	Yes (single ice blocks)
4_1	2.0	0.5	2.5	7	20	Yes (single ice blocks)
4_2	2.0	0.5	5.0	7	22	Yes (single ice blocks)
6_4	3.0	0.5	2.5	10	22	Yes
6_5	3.0	0.5	5.0	8-10	22	Yes

Table 2: Overview of rubble properties for the tests performed at operational draft and level ice. Table copied from KSRI's report.

This concludes the analysis of the vessel-ice interaction at operational draft.

2.4 QUICK COMPARISON WITH ISO 19906

A quick comparison was done with the loads predicted by the ISO 19906-2010. The code gives two methods for calculating ice loads on a downward sloping conical structure; a method based on plastic theory and a method based on elastic bending beam theory. Calculations were done with both methods and the results are shown below.

An important thing to note is that the geometry of the JBF has a special feature that is not incorporated in the ISO calculations. Although at the water surface the vessel is downward sloping, the below water section with the columns is upward sloping. The ice rubble colliding with this section causes a vertical force in the opposite direction as the force generated in the downward breaking section. Therefore the vertical forces predicted by the ISO codes will be wrong. Also the equations are independent of the relative velocity which does have a significant impact on the ice loading.

The following parameters were used:

- Ice thickness	3 m
- Slope angle	45 degree
- Ice-hull friction coefficient	.16
- Ice density	820 kg/m^3
- Ice ride-up thickness	2 - 3 times the ice thickness
- Waterline diameter vessel	98 m
- Top diameter vessel	92 m
- Flexural strength	500 kPa
- Poisson ratio	.33
- Elasticity modules	5*10^9 N/m^2
- Ice-ice friction coefficient	0.1
- Porosity of the ice	0.35
- Rubble angle	70 degrees
- Friction angle rubble	15 degrees
- Cohesion	5.37*10^6 Pa

Quite a few parameters required by the methods are unknown (the red ones). As the accuracy of this section does not have to be very high as it only serves as a crude evaluation of the model test data not much time will be spend on finding their exact values. The estimate for the porosity comes from numerical calculations done by (Liferob, 2004) and is around 35%. The ice-ice friction coefficients come from (Serway, 1999) and are 0.1 for static friction and 0.03 for the kinetic friction. A value of 0.1 is taken.

The internal friction coefficient is from (Cold Region Reseach). They show that it is dependent on the temperature of the ice and the strain rate. At 0 degrees and a low strain rate the angle of internal friction is about 3%. During the ice-breaking process the strain rate will be higher so a higher angle of 15% is assumed. The impact of the coefficient on the resulting forces is not that large so its exact value is not that important. The cohesion comes from the same source and is 5.37 MPa.

For the final two parameters no good estimates could be found. In some sources where ice was crashing into bridge pillars the rubble reached an angle of up to 80 degrees. For a drilling vessel which is not stationary it is less likely that the rubble will achieve such high angles, so an angle of 70 degrees will be used.

For the bridge pillars the ice ride-up thickness has a quadratic dependence on the thickness, and a maximum of about 8 meters. For the JBF it is very hard to estimate the thickness of the rubble pile up as it submerged and the geometry of the vessel changes quite rapidly with depth. To get some results the ice ride up thickness is set to 2*t and 3*t where “t” is the ice thickness.

Results

The global horizontal loads estimated by the elastic bending beam method are on average about 40 to 60% lower than the ice forces that were estimated based on the model tests, depending on which thickness for the rubble ride up is used. On average the loads from the plastic method are about 50% lower than the loads from the elastic beam method.

Conclusion

Due to the complex geometry of the JBF the methods from the ISO codes are not suited to estimate the loads on the vessel (assuming that the loads from the model tests are correct). The methods do predict forces of the same order of magnitude.

2.5 CONCLUSION

Now that all video footage and photographs have been analyzed a good general understanding of the vessel-ice interaction has been created. The footage from the transit draft was interesting to review but will be neglected for the rest of the report. For this reason it is not included in the summary. The focus of the report will be on modeling the interaction with level ice at operational draft (a requirement from Huisman) so the interaction with broken ice will also be neglected for the rest of the report.

For level ice at the operational draft the following summary can be made for the failure mechanic. An important thing to note is that all are due to limit stress:

- The most common failure mechanic is downward bending;
- The second most common failure mechanic is buckling, due to rubble and the geometry of the vessel axial forces can build up resulting in buckling. The main reason for this is the jump in impact angle and the force required to push through the rubble.
- Crushing occurs situational; it is highly dependent on the trim angle and the ice thickness.

General observations:

- The ice action becomes more simultaneous as the ice becomes thicker (larger ice action size);
- The velocity has a negligible impact on the vessel-ice interaction phenomenon observed;

When making the ice model a few things might need to be further investigated:

- As the trim angle increases what exactly triggers the transition from bending to crushing failure, and at what angle does it happen?
- How does the interaction between vessel and ice change as the ice thickness increases?
- How does the increasing ice action size influence the loading on the vessel?

This concludes the analysis of the model test data. In the next chapter the obtained knowledge will be used to create a model for the loading caused by level ice at operational draft.

3 CREATION OF THE VESSEL-ICE INTERACTION MODEL

Now that all the test data has been analyzed the time has come to start using the data to create a model for the vessel-ice interaction. In this section the construction of two models are discussed: the ice loading model and the dynamic model of the vessel.

Ice loading model.

The approach that will be used for the ice loading model is to base it completely on the model test data, thus creating an empirical model which will only be applicable to the JBF arctic. This also means that any parameter not varied during the test will not be part of the model. No effort will be taken to create mechanical or phenomenological models to overcome these shortcomings. The reason for this is that it will only bring more uncertainty into the final model due to all the assumptions required. Therefore the goal is to try and create the best possible model based on the model test data.

To principal behind the ice model is that the six components of the ice loading are all split into two parts, a mean part and a fluctuating part. Both parts can have some dependency on both the ice properties (thickness, velocity, flexural strength) and vessel motions (heave of the vessel, roll angle φ and the pitch angle ϑ). This means that in total 12 models have to be created which can each depend on several variables. To avoid overly complex models simplifications will be used where possible although never up to the point where they would jeopardize the integrity of the final model (sensitivity analysis will be done where needed). As already mentioned before the mean components of Px, Mx and Mz are assumed to be zero due to symmetry and also some of the other loads might not depend on all 6 of the variables but this will be investigated for each individual case later on in this chapter.

It quickly becomes apparent that the final vessel-ice interaction model will be a complex system with a lot of interconnectedness. In order to minimize the possibility of error or bugs in the code, the ice model will be built up one step at a time. Next a brief description is given of each of these steps to give a feel for the rest of the chapter and the layout of the model.

1DOF: X-component

The first step to be taken will be to model the most important component, the inline component Px. In addition to the creating of the model for Px_mean and Px_fluc, one more important step has to be completed. In order to test the ice model a test environment has to be created in which the ice model can be checked. So parallel to the development of the ice model a dynamic model of the vessel will to be created. The model will be a mass-spring-dashpot system and allow for time-domain simulation of the motions of the vessel (excluding dynamics of the mooring).

3DOF: X,Z,ϑ-components

Once the 1DOF model has been finished and thoroughly tested the next step towards a 6DOF model can be taken; 3DOF. Similar steps have to be taken as with the 1DOF model. First the 1DOF dynamic Matlab model will be expanded to 3DOF and then the ice model has to be upgraded to allow for 3DOF loading. Then a series of test will be done to eliminate bugs.

6DOF / AQWA

The final step for the dynamic model in Matlab is to go from 3DOF to 6DOF thereby finishing model. 6DOF will be the last step taken in Matlab and allow the results from AQWA to be checked. The last step of the ice model is to couple the 6DOF ice model to AQWA in order to run time-domain simulation with dynamics of the mooring system included. Everything related to AQWA and the design of the mooring systems will be discussed separately in chapter 4.

Starting

Now that the layout is clear we can take the first step in our epic journey where the fearsome 6DOF coupled time-domain simulation of the moored JBF-arctic takes on the dreaded 3m thick ice of the arctic! Can the JBF withstand the ferocious conditions and unrelenting forces put forth by the arctic or will its mooring lines snap one by one only for its frozen remains to drift off into the desolate waters of the arctic never to be heard of again? We are about to find out.

3.1 VESSEL DYNAMICS – EQUATION OF MOTION

After the thrilling introduction I can only imagine you must be thrilled to move on, so let us start with the first step of modeling the vessel dynamics; the equation of motion. As the vessel is modeled as a rigid body the equation of motion that will be used is a mass-spring-dashpot system with six degrees of freedom. The equation of motion will include the following items:

- Inertia
  - Mass / Inertia of the vessel
  - Added mass
- Damping
  - Viscous damping
  - Radiation damping
- Springs
  - Hydrostatics
  - Mooring forces
- External forces
  - Ice
  - Current
  - Wind

When looking at the three forces terms, the ice loading term is by far the largest of the three. In order to simplify the Matlab model only the ice loading is considered for the Matlab model.

3.1.1 INERTIA: MASS OF THE VESSEL

The mass and moment of inertia were estimated by Huisman based on a weight calculation. The 6x6 mass matrix looks as follows:

$$\boldsymbol{M} = \begin{bmatrix} m & 0 & 0 & 0 & 0 & 0 \\ 0 & m & 0 & 0 & 0 & 0 \\ 0 & 0 & m & 0 & 0 & 0 \\ 0 & 0 & 0 & I_{xx} & 0 & 0 \\ 0 & 0 & 0 & 0 & I_{yy} & 0 \\ 0 & 0 & 0 & 0 & 0 & I_{zz} \end{bmatrix}$$

Here m, the mass of the vessel, has a value of 183.3 * 10^6 kg or 183,300 metric ton (at the ice draft).

3.1.2 INERTIA: ADDED MASS

The added mass that has to be used for calculations with level ice are a bit of a problem. Normally the added mass is calculated using AQWA which is part of the Ansys software package. AQWA calculates the added mass as a function of wave frequency using potential theory. However when ice is present no free-surface waves will be present.

The initial idea was to approach the water covered with level ice by taking the high frequency limit of the waves as this will start to approach a flat water surface. However this idea was shot down by Metrikine because the vessel will cause low frequency vibrations in the ice, so this approach would results in mismatched frequencies.

So what added mass should be used for the calculations? A suggestion by Metrikine is to model the ice sheet with a spring foundations on the water in order to add the extra resistance against free-surface waves caused by the ice. However this kind of calculation is not possible in AQWA and requires specialized software.

A sensitivity analysis was done in order to determine the impact of the added mass on the moored behavior of the vessel. As the base case the added mass resulting from the faulty high-frequency limit calculations is taken, see the matrix below.

$$\boldsymbol{A} = \begin{bmatrix} 9.342 \ast 10^{7} & 0 & 0 & 0 & -2.74 \ast 10^{9} & 0 \\ 0 & 93342 \ast 10^{7} & 0 & 2.738 \ast 10^{9} & 0 & 0 \\ 0 & 0 & 2.388 \ast 10^{8} & 0 & 0 & 0 \\ 0 & 2.725 \ast 10^{9} & 0 & 2.428 \ast 10^{11} & 0 & 0 \\ -2.73 \ast 10^{9} & 0 & 0 & 0 & 2.428 \ast 10^{11} & 0 \\ 0 & 0 & 0 & 0 & 0 & 4.698 \ast 10^{10} \end{bmatrix}$$

The added mass was increased and decreased by 50% and the impact on the motions was calculated. The results are in the table below:

Sensitivity of the added mass			
Change in added mass	Mean [m]	Std [m]	T_0 [s]
-50%	19.57	1.02	51.74
Base case	19.64	1.03	55.29
50%	19.66	1.04	59.07

Table 3: Impact of the added mass on the motions of the vessel.

The table shows that the impact of the added mass on the mean and standard deviation is very small. The impact on the zero-crossing period is slightly larger but still much less than the increase in the added mass. As the added mass does not have a significant impact on the statistics of the vessel, using the wrong added mass should not have a significant impact on the design of the mooring system later on so the base case will be used as this one had already been used in all previous calculations.

Implementation into AQWA

The implementation of this frequency independent added mass matrix into AQWA requires that the original added mass matrices calculated by AQWA are overwritten with this matrix. Unfortunately doing this does no longer allows AQWA to use convolution which, according to the manual, will increases calculation time and reduces the accuracy.

3.1.3 DAMPING: RADIATION DAMPING

As the water surface is covered with ice, radiation waves and as such radiation damping is limited due to the large mass and bending stiffness of the ice sheet floating on the water surface. Only in the wake behind the vessel where the broken ice is located can waves be created by the vessel. For simplicity the radiation damping is assumed to be zero however more detailed calculations should be done to get a more accurate estimate of the radiation damping in ice.

$$\boldsymbol{B_{rad}} = \begin{bmatrix} 0 & 0 & 0 & 0 & 0 & 0 \\ 0 & 0 & 0 & 0 & 0 & 0 \\ 0 & 0 & 0 & 0 & 0 & 0 \\ 0 & 0 & 0 & 0 & 0 & 0 \\ 0 & 0 & 0 & 0 & 0 & 0 \\ 0 & 0 & 0 & 0 & 0 & 0 \end{bmatrix}$$

3.1.4 DAMPING: VISCOUS DAMPING

Three terms of the viscous damping are based on free vibration test done during the hydrodynamic model tests. The 6x6 damping matrix is given below:

$$\boldsymbol{B_{visc}} = \begin{bmatrix} 0 & 0 & 0 & 0 & 0 & 0 \\ 0 & 0 & 0 & 0 & 0 & 0 \\ 0 & 0 & b_{33} & 0 & 0 & 0 \\ 0 & 0 & 0 & b_{44} & 0 & 0 \\ 0 & 0 & 0 & 0 & b_{55} & 0 \\ 0 & 0 & 0 & 0 & 0 & 0 \end{bmatrix}$$

Drag

For the other three directions a drag force equation is used. The drag force is calculated with the standard formula:

$$\boldsymbol{F_d} = \frac{1}{2}\rho v^2 \boldsymbol{C_d A}$$

Where:

- $\rho = 1025 \frac{kg}{m^3}$ $density\ of\ seawater$
- $v^2 = v_x^2 + v_y^2$ $velocity\ of\ the\ vessel$
- $\boldsymbol{C_d} = [C_{d,x} \quad C_{d,y} \quad C_{d,\phi}]$ $drag\ coefficients, dependend\ on\ the\ direction\ of\ the\ vessel$
- $\boldsymbol{A} = [A_x \quad A_y \quad A_\phi]$ $area\ of\ the\ vessel\ exposed\ to\ water\ at\ the\ ice\ draft$

The drag coefficients are taken from a current calculation (IVR, 08-04-2011) and are given every 10 degrees over the full 360 degrees. For the current calculation the zero-angle is in the positive X-direction. Because the coefficients come from a current calculation they cannot be directly used to calculate the vessel's drag. The reason for this is that if the vessel is moving in the positive X-direction it effectively will experience a current coming from the positive X-direction. Therefore in order to use the current drag coefficients, 180 degrees has to be added when looking up the value to be used for the platform (reversing the direction). The drag coefficients are also different for each of the load components so X, Y and yaw all have a different drag coefficient. The frontal area is the same for all directions but for the yaw moment it has to be multiplied by the width of the vessel to get moments.

$$F_{drag,x} = \frac{1}{2} 1025 * C_{d,x}(direction + 180°) * 2568 * \left(v_x^2 + v_y^2\right)$$

$$F_{drag,y} = \frac{1}{2} 1025 * C_{d,y}(direction + 180°) * 2568 * \left(v_x^2 + v_y^2\right)$$

$$F_{drag,\phi} = \frac{1}{2} 1025 * C_{d,\phi}(direction + 180°) * 2568 * 116 * \left(v_x^2 + v_y^2\right)$$

3.1.5 SPRINGS: HYDROSTATICS

All the hydrostatic spring terms were calculated in AQWA-line.

$$\boldsymbol{K_{hs}} = \begin{bmatrix} 0 & 0 & 0 & 0 & 0 & 0 \\ 0 & 0 & 0 & 0 & 0 & 0 \\ 0 & 0 & k_{33} & k_{34} & k_{35} & 0 \\ 0 & 0 & k_{43} & k_{44} & k_{45} & 0 \\ 0 & 0 & k_{53} & k_{54} & k_{55} & 0 \\ 0 & 0 & 0 & 0 & 0 & 0 \end{bmatrix}$$

3.1.6 SPRINGS: MOORING FORCES

During the first stage of the thesis a simple model will be used for the mooring system. This comprises of a lookup table which gives the global restoring force as a function of the horizontal offset. This simple method proved to be sufficient for the 1DOF models and the simpler 3DOF model. However for the later stage a better model was needed. First the simple model will be discussed and then the complex model.

3.1.6.1 SIMPLE MODEL FOR THE MOORING FORCES

The simple model is based on the static mooring forces calculated by Huisman and can be found in (IVR, 08-04-2011). In this static analysis of the mooring line system a total of 30 different setups were investigated at four different water depths (200m, 350m, 500m and 850m). For each water depth the optimal configuration was chosen and this resulted in 5 different configurations. In Figure 3-1 the original table is replicated.

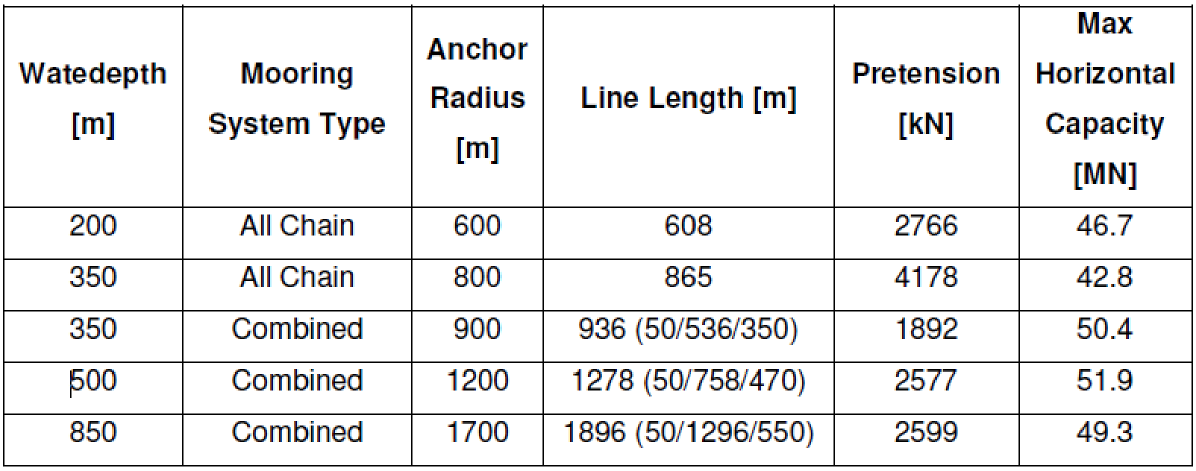

Watedepth [m]	Mooring System Type	Anchor Radius [m]	Line Length [m]	Pretension [kN]	Max Horizontal Capacity [MN]
200	All Chain	600	608	2766	46.7
350	All Chain	800	865	4178	42.8
350	Combined	900	936 (50/536/350)	1892	50.4
500	Combined	1200	1278 (50/758/470)	2577	51.9
850	Combined	1700	1896 (50/1296/550)	2599	49.3

Figure 3-1: The final five mooring configurations.

For each of these mooring systems the global horizontal restoring force (in the X direction) is given as a function of the offset. This means that based on this information the model can only move in the X-direction.

$$k_{11} = \boldsymbol{f}_{\boldsymbol{ms}}(x)$$

This method is sufficient for 1DOF model as they only require motions in the X-direction. Initially this method was also used for the 3DOF model but eventually the other five terms were needed and this required an upgrade of the mooring system's model.

3.1.6.2 COMPLEX MODEL FOR THE MOORING FORCES

The complex version of the mooring system's model is based on a table calculated by AQWA-LINE and as such this method aims to recreate the quasi-static mooring line calculation done by AQWA-drift during the time-domain simulations. These tables contain the quasi-static mooring forces for a single mooring line as a function of inline horizontal and vertical offset. Here inline means displacements in the 2D-plane between the starting and end point of the mooring line. As the derivation is a bit lengthy it can be found in Appendix 2. First the mooring force is calculated for each individual mooring line based on the position of the vessel. Then the complex model combines the mooring forces of all 20 lines in order to derive the 3 global forces and 3 global moments working on the vessel. For this reason it cannot be expressed as a simple matrix but only as a function:

$$\boldsymbol{f}_{ms}(x, y, z, \varphi, \theta, \phi) = see \text{ Appendix C}$$

3.1.7 EQUATION OF MOTION

Based on the data above the following equation of motion can be derived:

$$(\boldsymbol{M} + \boldsymbol{A})\ddot{\boldsymbol{u}} + (\boldsymbol{B}_{\boldsymbol{visc}} + \boldsymbol{B}_{\boldsymbol{rad}})\dot{\boldsymbol{u}} + \boldsymbol{B}_{\boldsymbol{drag}}\dot{\boldsymbol{u}}^2 + (\boldsymbol{K}_{\boldsymbol{hs}} + \boldsymbol{K}_{\boldsymbol{ms}})\boldsymbol{u} = \boldsymbol{f}_{ice}$$

Where **M**, **A**, **B** and **K** are 6x6 matrices and **u**, its derivatives and **f** are 6x1 vectors. Note that the drag and inertia of the mooring system itself are not included in the equation of motion as these will not be included in the Matlab model. These are included in the final AQWA model.

3.1.8 SOLVING THE EQUATION OF MOTION

A lot of time and effort was put into creating a dynamic model to solve the equation of motion in order to gradually build up to the AQWA model. This process is discussed in 0.

This concludes the section about the equation of motion.

3.2 THE ICE LOADING MODEL

Now that all the parameters for the equation of motion have been established and methods to solve it, it is time to start work on the ice loading model. As said before in the introduction, a total of 6 components need to be model. In order to simplify the modeling process, the load components are split into two parts: a part that is constant in time and a part that fluctuates in time. Each directional component of the load requires a model for both the mean and fluctuating part. The models created are discussed in this section.

3.2.1 PX_MEAN

Px is by far the largest component in terms of generating a response of the vessel. Px will result in a large offset and therefore is the most important component to stress the mooring system. Due to its importance the model for Px will be given the most attention of all the six components. The layout is as follows: first the parameters which were neglected will be discussed, next the model for Px_mean made by KSRI, then how the original KSRI model's capabilities was expanded, then some corrections made to the model and finally a discussion of the model and recommendations.

3.2.1.1 CHOOSING THE PARAMETERS

In the model described here, Px only depends on the following parameters: ice thickness, ice velocity, trim angle of the vessel and the flexural strength. Other parameters cannot be taken into account due to the absence of test data needed to curve fit a relation. The absence of these dependencies will have a negative impact on the quality of the model. In this section the severity of their absence is assessed and arguments are given why their absence does not have to detrimental to the overall quality of the model.

Many parameters influence the load generated by level ice, but the important parameters that will not be taken into account are:

- **Temperature**: the temperature of the ice influences whether the ice behaves brittle (at low temperatures) or ductile (close to thawing temperature) and also influences the strength of the ice.
- **Salinity**: the salinity of the ice is strongly related to the porosity of the ice, which is turn is related to the strength of the ice and crack propagation / growth.
- **Thick ice in combination with high velocities**: because no tests were done in this regime, no data is available. However in (Loset, 2006) it is said that crushing occurs more easily at high velocities.
- **Low velocities**: creep occurs at low velocities. Since no tests were done in this regime, it regretfully cannot be part of the model.

Next some arguments will be given why the ice model that will be created is still valid despite these shortcomings:

- Both **temperature** and **salinity** influence the strength of the ice. This has been taken into account to some extend by using the flexural strength as a parameter. However as the ice can also fail in crushing, the compressive strength is also important and this has been neglected.
- The influence of the ice **temperature** on the brittle or ductile behavior of the ice is also neglected. But as ice only behaves ductile at very slow velocities (<0.1 m/s), and all test were done at velocities well above that velocity, this problem automatically falls outside the scope of this model, as there is no data available to investigate the ductile (creeping) vessel-ice interaction.
- The influence of the salinity is taken into account to some extend in the flexural strength. However the porosity is also a critical item when it comes to the (statistical) **size effect**. The scaling process was handled by KSRI and no information is available on their process so it is unknown if salinity is part of their scaling process or not.
- The lack of data on **creep** is quite a big loss. As ice can behave ductile at very low velocities it can create a very large interaction area with the hull because local peaks in forces can be smoothed out due to the ductile behavior (Loset, 2006). This can results in very large forces. Some more tests would have to be done to confirm or deny this.

3.2.1.2 KSRI'S REGRESSION MODEL

The model for the mean of Px is based on a regression model made by KSRI. They made a model which is based on three parameters: flexural strength, ice thickness and ice velocity. The model is based on the following equation:

$$P_x = a_0 * \sigma_f * h_{ice} + a_1 * h_{ice}^{a_2} + a_3 * h_{ice} * v^{a_4}$$

Where P_x is the horizontal component of the load in MN, σ_f is the flexural strength in kPa, h_{ice} is the ice thickness in meter, v_{ice} is the ice drift velocity in m/s and all the a's are unknowns. Curve fitting the equation to the data shown in Figure 3-2, KSRI obtained the following final equation:

$$P_x = 0.0068308 * \sigma_f * h_{ice} + 4.0815508 * h_{ice}^{1.9885986} + 3.7404579 * h_{ice} * v^{2.0710474}$$

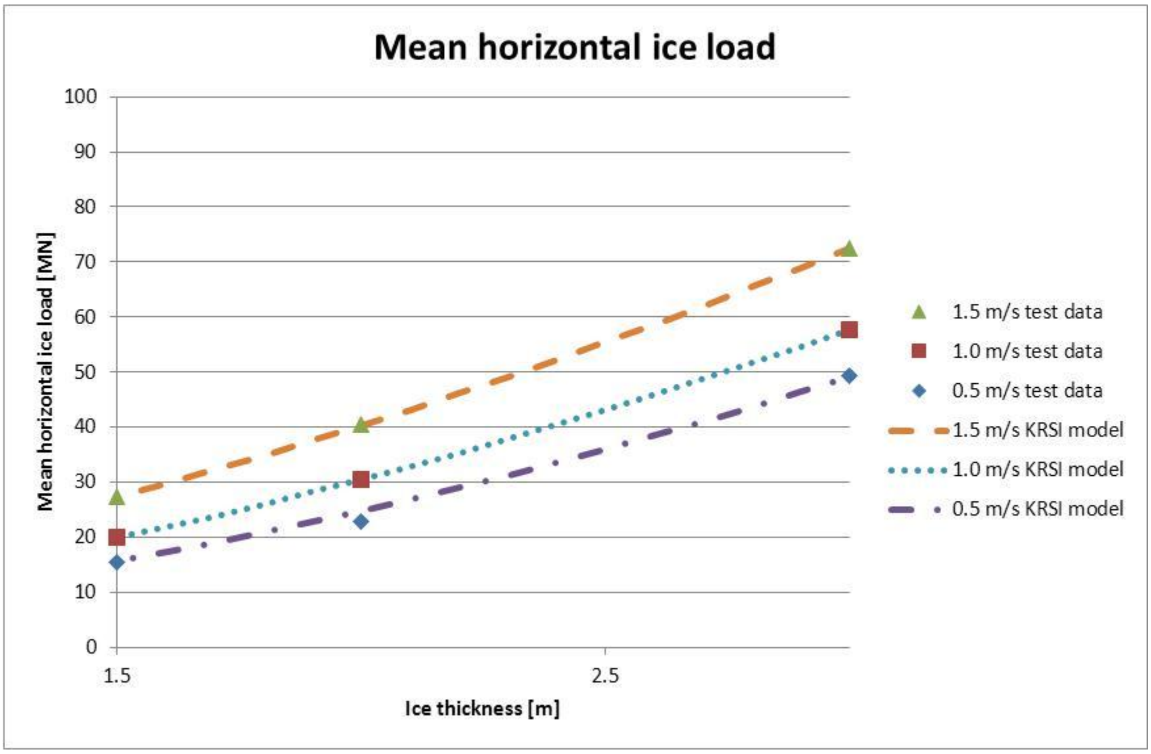

Figure 3-2: The data used by KSRI when curve-fitting the regression model (the nine dots) and the final model (the three lines).

There is one big problem with the model they created and that is that there it comes with no documentation what so ever. Several questions can be raised about the model:

- Why is only the first term dependent on the flexural strength? This means that when the flexural stiffness is zero, there are still some forces left.
- Why does the first term scale linear with the thickness and the second term quadratic?
- Keeping the first two items in mind, what aspect of the ice loading do the first and second term represent?
- Why are the first two terms independent of the velocity? This means that even when the ice is standing still it is still exerting forces on the vessel.

Especially the fact that the force is not zero at a velocity of zero is very unrealistic. But trying with both one dimensional and two dimensional curve-fits and all sorts of combination and types of different equation did not result in a better fit so eventually KSRI's model was used. However in order to overcome some of the problems presented above some attempts will be made to make the model more realistic.

The first problem of the regression model is that it is independent of the trim angle. In the next section its functionality is expanded by adding a dependency on the trim angle of the vessel.

3.2.1.3 TRIM ANGLE DEPENDENCY

The dependency on the thickness and velocity is fairly straightforward as can be seen in Figure 3-2 above, there are no abnormalities and all nine points follow a nice and smooth path. However when looking at the data from the trim angle the relation between the points is not so smooth, as can be seen in Figure 3-3 below. All three lines make a jump at the trim angle of 5.0° and in particular the 3 meter thick ice.

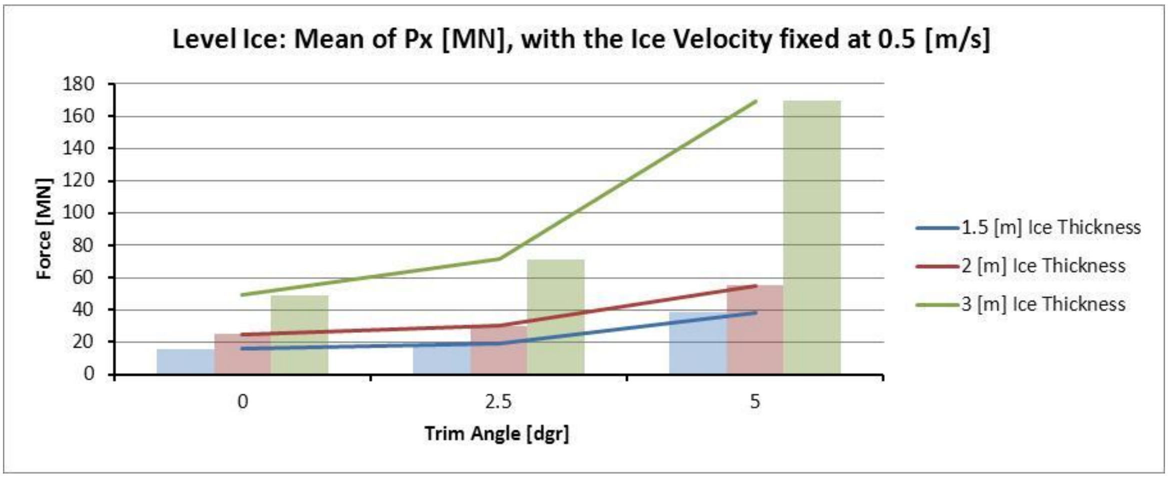

Figure 3-3: The jump of the 3 meter thick ice at the 5.0° trim angle is clearly visible.

The initial explanation for the 2.5°->5.0° jump was the transition from failing in bending to failing in crushing. When the trim angle changes, what effectively happens (as explained in section 2.3.2.1) is that the impact angle of the ice changes, see Figure 3-4. At a 0° trim angle the ice interacts with the yellow section of the hull where the ice has an impact angle of 45°. As the trim angle increases the ice eventually is interacting with the red section where the ice has an impact angle of more than 90°. This transition in impact angle in turn causes the ice to fail in crushing rather than bending.

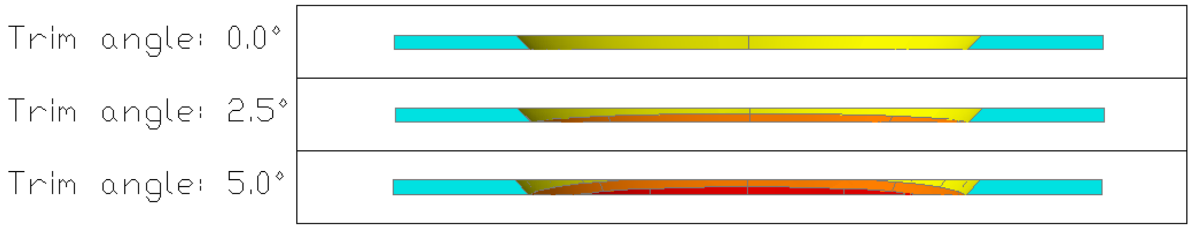

Figure 3-4: An example of the interaction with the three regions for 3 m thick ice as the trim angle increases.

The explanation for the 2.0 m -> 3.0 m jump is that the increased thickness makes the ice reach deeper below the water line, thus allowing for more interaction with the red section (and thus more crushing), see Figure 3-5.

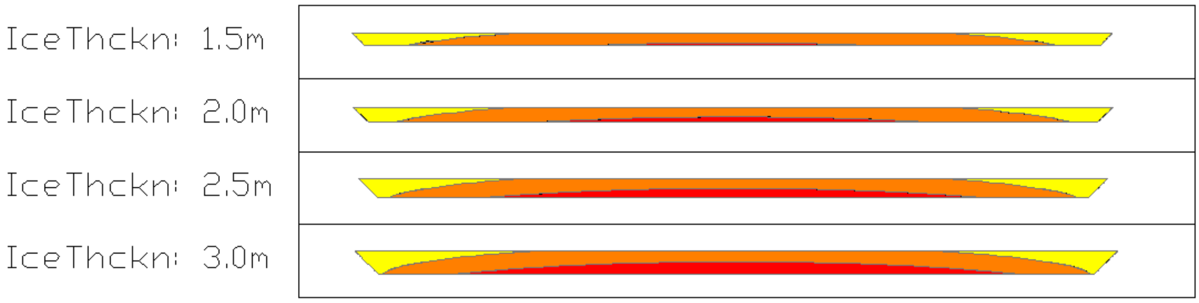

Figure 3-5: An example of the three regions at a trim angle of 5.0° as the ice thickness increases.

Based on these two ideas an AutoCAD model of the vessel was made to check the interaction of the ice with the three sections of the hull (given the pictures above). After varies tests using the data from the AutoCAD model confidence grew that the ratio of interaction with the three different sections of the hull could explain a different kind of ice action. So it was decided to derive an analytical equation which calculates the division of the total vessel-ice interaction area over the three different sections (yellow, orange and red). The derivation of the equation and more information can be found in Appendix B.

Using these ratios KSRI's model was expanded to look as follows (the "a" variables are shown below instead of their numerical values to reduce the length), where the green part is new:

$$P_x = \left[a_0 \sigma_f h_{ice} + a_1 h_{ice}^{a_2} + a_3 h_{ice} v^{a_4}\right] * \left[\%_{yellow} + b_1 * \%_{orange} + b_2 * \%_{red}\right]$$

Where $\%_{yellow}$, $\%_{orange}$ and $\%_{red}$ are the respective percentage of the total vessel-ice interaction area and b_1 and b_2 are unknowns.

Curve-fitting this relation to the data the following values for b_1 and b_2 were obtained:

$$P_x = \left[a_0 \sigma_f h_{ice} + a_1 h_{ice}^{a_2} + a_3 h_{ice} v^{a_4}\right] * \left[\%_{yellow} + 2.1 * \%_{orange} + 7.25 * \%_{red}\right]$$

The predictions made by the new model for the mean of Px are shown in Figure 3-6.

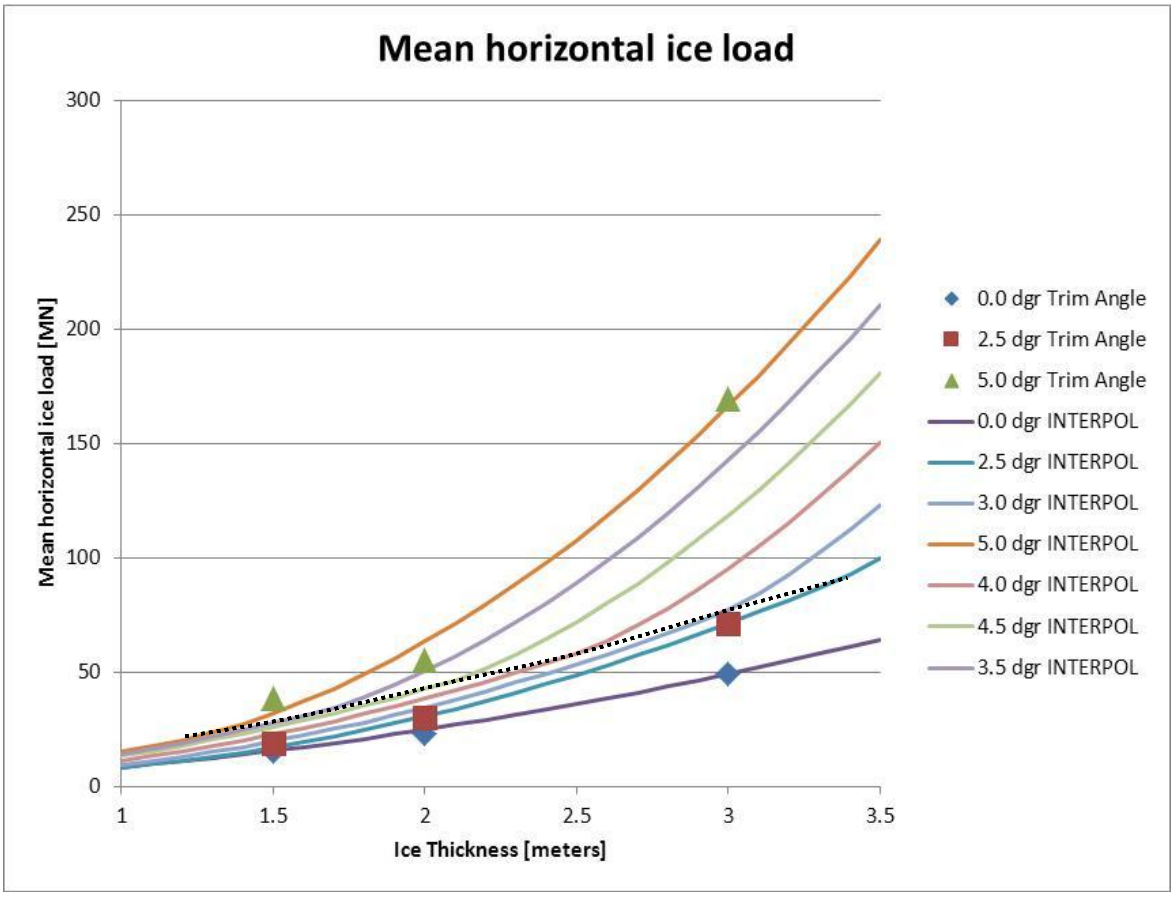

Figure 3-6: The model test data (the large dots) and the results from model for the mean of Px. The black dotted line shows the onset of the interaction with the red area. One can see that the forces start increasing quickly after this.

The basic idea behind the model is that when the ice interacts with the orange and red area the loading will be higher due to the different impact angle and the ice failing in crushing rather than bending. Therefore the section of the hull where the ice interacts with the red section should weigh heavier than the section where the ice fails in bending. Also when interacting with the orange section the horizontal component of the load is larger than when interacting with the yellow section (due to the slightly higher impact angle) which also explains why there is an increase when the interaction switches from the yellow to the orange section.

Extreme values of the trim angle

In order to let the model cope with extreme values for the trim angle it needs to be expanded a bit. In Figure 3-7 the cross-section at the level of the ice is shown. If the trim angle were to become very large in the negative positive direction the ice could be interacting with the area below the red section, which from now on will be called the grey section. If the trim angle were to become very large in the positive direction the ice could be interacting with the deck box above the yellow section. In order to incorporate them in the model they need to be assigned a value for the trim angle dependency. Because the deck box also has a 90 degree impact angle it is given the same value as the red section. The grey section has pretty much the same impact angle as the orange section. However instead of downward breaking it is upwards breaking. As no model test data is available on upwards breaking section, the grey section is given the same value as the orange section.

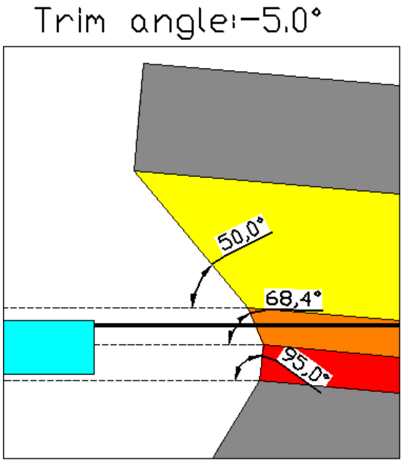

Figure 3-7: Extreme trim angles.

Results

Below the results of the trim angle dependency can be seen.

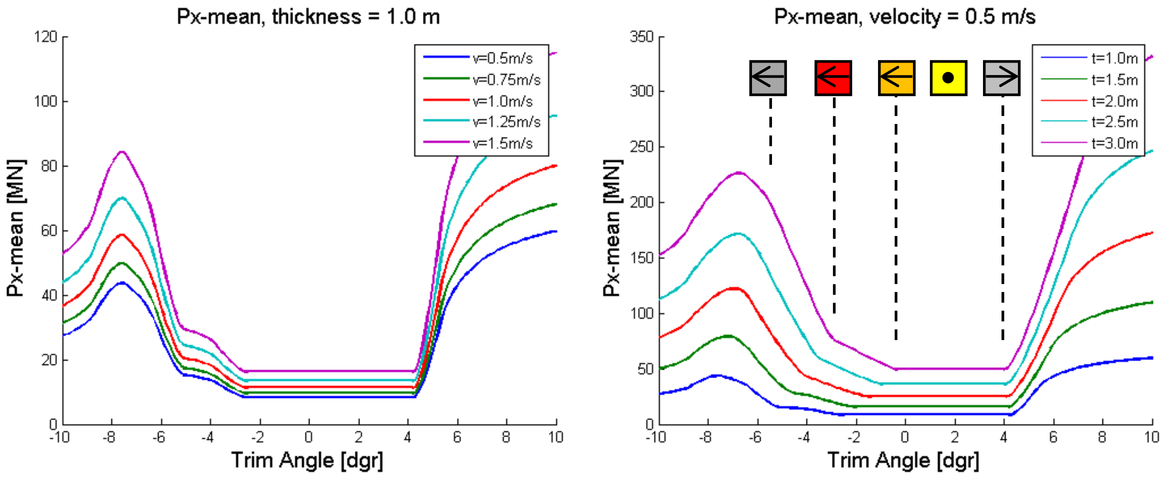

Figure 3-8: The impact of the trim angle dependency. The blue lines at the bottom of both figures are the same. The dashed lines and the colored arrows indicate when interaction with that particular region starts for the purple lines. From left to right it is grey, red, orange, yellow and deck box.

When comparing the two graphs we can see that when increasing the velocity (the left figure) the shape of the graph does not change. This is because the calculation for the ratios is independent of the relative velocity.

In terms of increase in loads, going from 0.5 m/s to 1.5 m/s has about the same effect as increasing the ice thickness from 1.0 m to 1.5 m. Increasing the ice thickness has a much bigger effect on the loading then increasing the velocity.

When looking at how the shape of the curve changes as the thickness increases several things can be noted:

- The thicker the ice, the quicker the forces start to increase around -4 to 0 degrees. This is because as the ice becomes thicker it reaches deeper and thus will start interacting with the orange section of the hull faster. When interaction with the orange area starts the force start increasing.
- The same can be seen when going further negative. Around -3 to -5 degrees there is a second kink. This is when the interaction with the red section starts again accompanied by a sharp increase in the force.
- Around -6 degrees the increase starts to slow down. This is because interaction with the grey area is starting here. The grey area has a lower impact angle as the red area (which results in upper bending instead of crushing) and thus the force starts to decrease again,
- If we go back to 0 degrees and start increasing the trim angle we can see a very sharp increase around 4 degrees as the ice starts interacting with the deck box. The impact angle of the deck box also results in crushing and thus in very large forces. After a while the forces reach a maximum as the whole vessel-ice interaction area is eventually interacting with the deck box. Eventually the deck itself would hit the water (at 10.6 degrees) but this extreme effect is not included in the model.

The basic framework for the model for Px_mean has now been completed. Next there are two special cases that require more attention and these are discussed in the next two sections.

3.2.1.4 TRANSIENT INTERACTION

The first problem with the model derived in the sections above is that it is only valid for the steady-state mean force. During the initial impact the mean value shows a very different behavior. The reason for this is that during the transient phase of the interaction the rubble in front of the vessel is still building up.

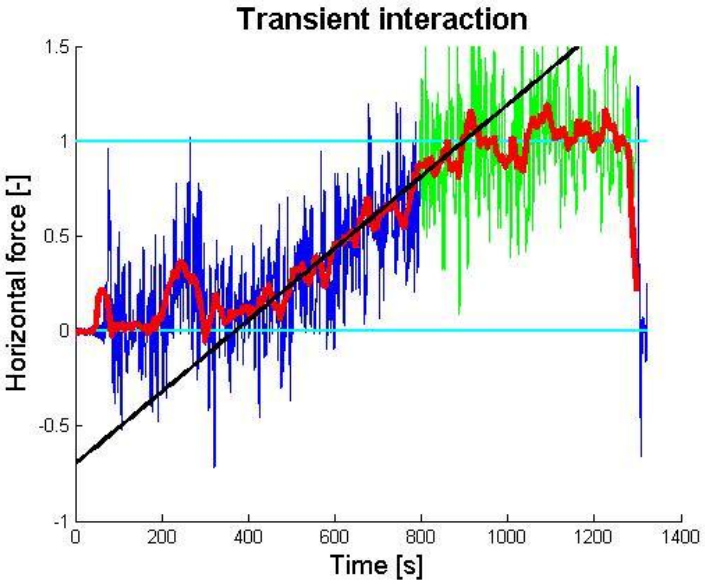

Figure 3-9: The transient phase of the vessel-ice interaction for test 31. The red line is a moving average in order to make it easier to find the appropriate values for the black curve-fitting line. The green section is the

steady-state solution. The vertical axis has been rescaled so 1 is equal to the mean of the steady-state solution.

When looking at Figure 3-9 it is clear that there is a linear buildup for the mean value of Px_mean during the transient phase. The transient effect can therefore be quite easily incorporated in the model for Px_mean but including a linear scaling between 0 and 1. The time over which this scale-factor grows from 0 to 1 was estimated by using graphs like Figure 3-9. In total only three tests were done where the transient interaction was measured because this phase of the interaction is only visible when there is no rubble present yet and that is only for the first test in each test series (test number 3_1, 4_1 and 6_1).

The duration is calculated by curve-fitting the black line to the data and then calculating the time difference between the two intersections of the black line with the two cyan lines. This gave the following results:

- 1.5 m ice, 0.5 m/s, 0 degree trim angle:	421 seconds
- 2.0 m ice, 0.5 m/s, 0 degree trim angle:	303 seconds
- 3.0 m ice, 0.5 m/s, 0 degree trim angle:	530 seconds

There does not appear to be a clear relation between the three values. Therefore the conservative approach is taken by using the minimum value of 300 seconds. The implementation in the ice model resulting from this is that at time 0 s, the mean is multiplied by 0. Over the next 300 seconds the multiplication factor grows to 1. The results of including the transient phase can be seen below in Figure 3-10.

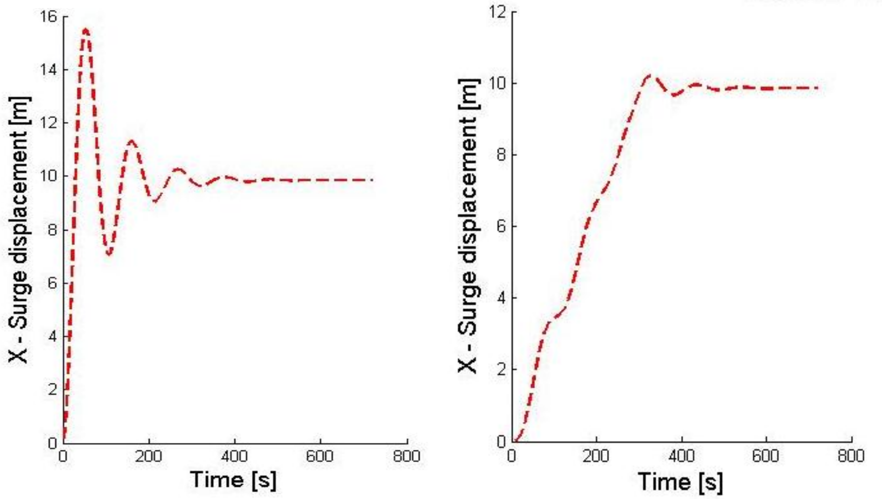

Figure 3-10: Left: No scaling of the mean, showing an overshoot of about 50%. Right: Including the scaling of the mean, showing an overshoot of just a few per cent. (t = 1.0m, v_ice = 1.0 m/s, v_0 = 0 m/s)

Sensitivity analysis: duration of the transient phase

In Figure 3-10 it can be seen that the impact of the transient phase addition is very big. Therefore it is very important to investigate the sensitivity of the response to the chosen duration. In order to investigate the influence, Figure 3-11 shows the overshoot (maximum offset / steady state offset) as a function of the duration of the transient phase.

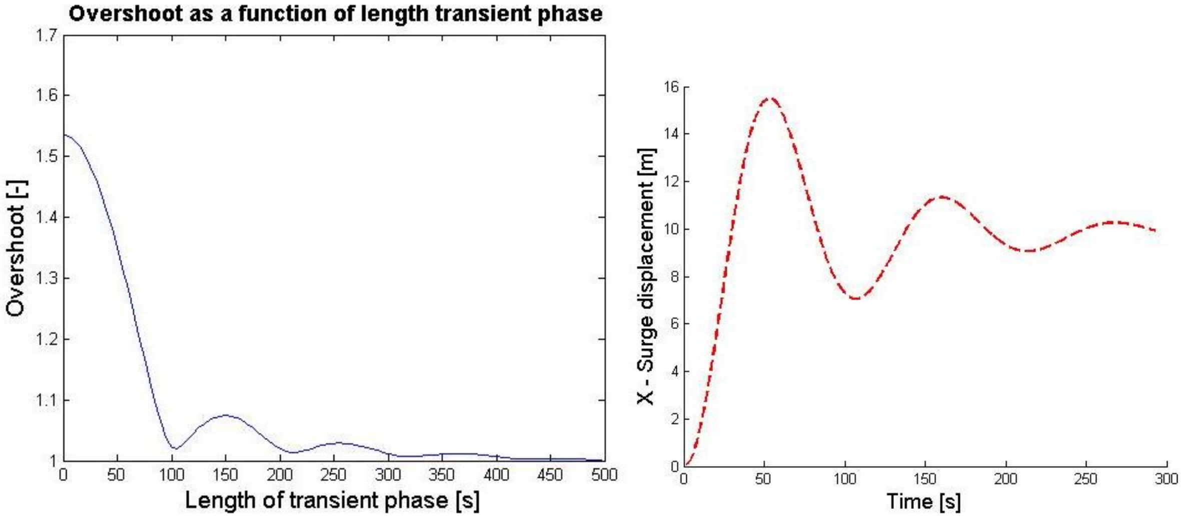

Figure 3-11: Left: Overshoot as a function of the duration of the transient phase. Note that the natural frequency in this case was 108 seconds, exactly the distance between the minimums. Right: Vessel's offset is minimal at n*nat_period and maximum at (n-0.5)*nat_period.

The relation has a very peculiar shape, with a minimum at each multiple of the natural period (108 seconds in this case). This is because if the duration of the transient phase is the same as the natural period, the load is approaching its maximum as the vessel is moving in the opposite direction as the ice, thus the increasing load is reducing the motions of the vessel.

However if the duration of the transient phase is equal to 1.5 times the natural period than the ice loading is approaching its maximum as the vessel is moving in the same direction as the ice, thus amplifying the motions of the vessel.

When the duration of the transient phase is lower than the natural period, the ice load and the motion of the vessel are in the same direction again thus amplifying the motions. The maximum displacement of the vessel increases as the duration becomes smaller because the earlier the force achieves its maximum, the more energy can be transferred to the vessel and resulting in the largest displacements.

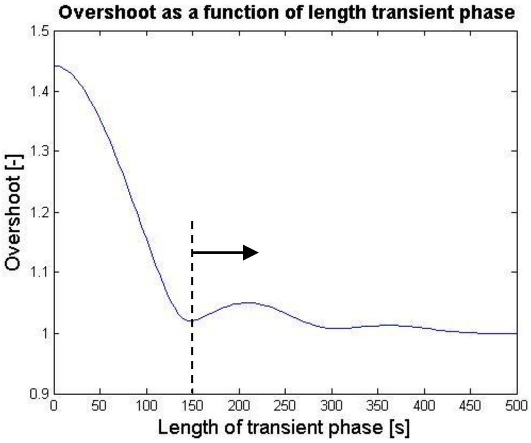

Figure 3-12: Overshoot for the mooring system the longest natural period, 152 seconds. If the duration of the transient phase is longer than the natural period of 152 seconds, the overshoot will always be lower than about 5%.

Sensitivity analysis: duration of the transient phase – Conclusion

Even with the conservative value of 300 seconds the overshoot is still in a very safe range. Even if the actual duration is much less (as long as it is above the natural period!) the vessel will always have an overshoot of less than 8%.

In the analysis before the mooring system with the shortest natural period was used. Just to be safe the longest natural period of 152 seconds is shown in Figure 3-12. The second peak is even smaller in this case, only 5% compared to 8% before, again showing that as long as the duration is above the natural period changing the duration only has a small influence.

Since the longest natural period is 152 seconds and the duration was 300 seconds this gives a sufficient safety margin for error, within which the results will not vary more than 5-8%.

Sensitivity analysis: Clearing of rubble

When the vessel is moving faster than the ice there is no interaction between the two. This means that rubble can clear away from the front of the vessel while no new rubble is created thus resulting in the removal of rubble and in the reduction of the transient phase's scaling factor. Since there is no model test data available where this phenomenon occurred, it is assumed that this process takes the same amount of time as the buildup process, so also 300 seconds. This gives a ratio between builddown and buildup of 1.

In order to test the sensitivity of the response to the ratio some tests are done. It is not very common for the vessel to move faster than the ice after the transient scaling factor was added. But a situation can still be created by given the vessel an initial velocity in the X-direction. The results of this can be seen in Figure 3-13.

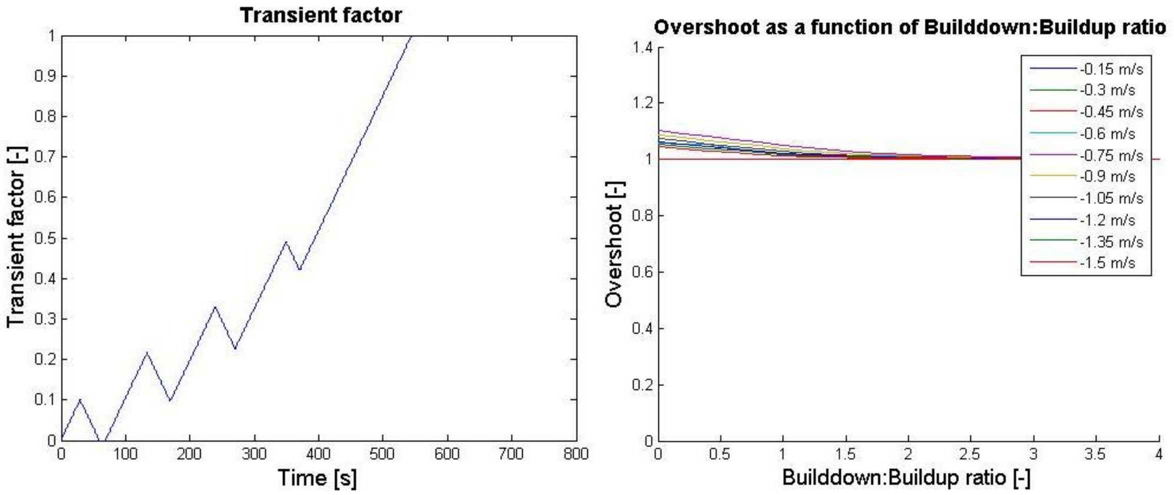

Figure 3-13: Left: An example of the transient factor changing over time, where the vessel loses contact with the ice 4 times (the builddown to buildup ratio was 1 here). Right: Using several different initial velocities the overshoot is plotted for a variety of ratios. The maximum overshoot is achieved for an initial velocity of -.45 m/s. (t = 1.0m, v_ice = 0.5 m/s, v_0 = -0.45 m/s)

Sensitivity analysis: Clearing of rubble – Conclusion

The builddown time basically creates a delay when the mean reaches it maximum, thus it creates a shift to the right in Figure 3-12. This could result in slightly larger forces as the overshoot moves away from one of the minimums in that figure.

The maximum overshoot for an instant builddown is only about 5% higher than the 1:1 ratio. All in all the influence of the "builddown to buildup"-ratio is not so big and it will be left at 1:1.

As the transient interaction has now been added to the model this fixes the first problem with KSRI's model. Next the second problem is discussed.

3.2.1.5 ZERO VELOCITY = ZERO FORCE

The second big shortcoming of the regression model made by KSRI is the way they included the dependency on the velocity. Although it is originally defined as the ice velocity it should be seen as the relative velocity between the vessel and the ice, because if the vessel is moving in the same direction and with the same velocity there is no interaction between the two. Below the original equation is shown again:

$$P_x = a_0 * \sigma_f * h_{ice} + a_1 * h_{ice}^{a_2} + a_3 * h_{ice} * v_{rel}^{a_4}$$

$$P_x|_{vrel=0} = a_0 * \sigma_f * h_{ice} + a_1 * h_{ice}^{a_2}$$

One can see that when the relative velocity is zero, there are still two components left. This means that even though the ice is not pushing against the vessel, it is still exerting forces on it (see Figure 3-14). This is off course extremely unrealistic.

After trying to replace KSRI's equation by trying to come up with a whole new velocity term, it became apparent that it is not so easy to do. So in order to fix this problem the whole equation will be multiplied by a new term that ensures the force is zero when the relative velocity is zero.

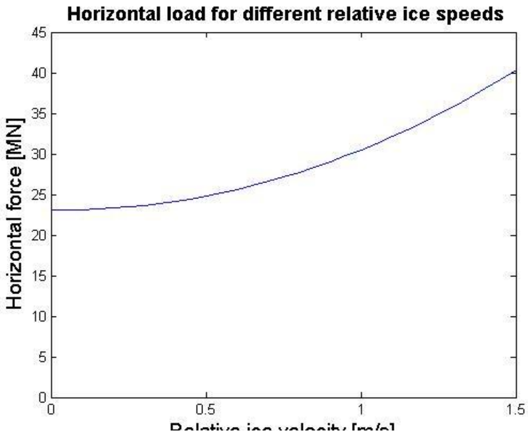

Figure 3-14: The original model by KSRI; predicting a horizontal load of 23 MN when the ice is bobbing next to the vessel.

Creep

It is commonly accepted that the ice loading shows at peak at low relative velocities (< 0.1 m/s), see Figure F-2. This peak will not be incorporated in the relative ice velocity relation used in this thesis. The reason for this is that the processes that cause the peak require the low velocities to be maintained for an extended period of time in order for ductile deformation of the ice to occur. The ice model in this report is only valid for ice velocities between 0.5 m/s and 1.5 m/s. This means that the velocities associated with the peak will only occur for very brief durations, durations not long enough for plastic deformation to start occurring. For this reason the low velocity peak is not taken into account.

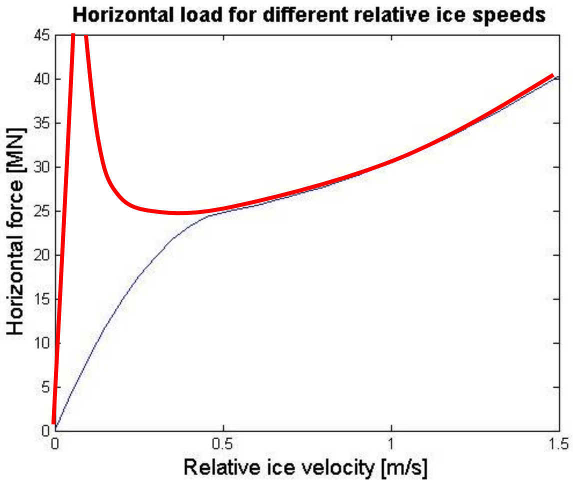

Figure 3-15: Normally there is a peak at low velocities (red line); however this trend is not used during this thesis (blue line).

Sensitivity analysis

The solution that was opted for was to create a transition function that scales the force between 0 and 1 when the velocity is between 0 m/s and some yet to be defined transition velocity. Two types of shapes for the transition function will be tested; a linear and a quadratic shape.

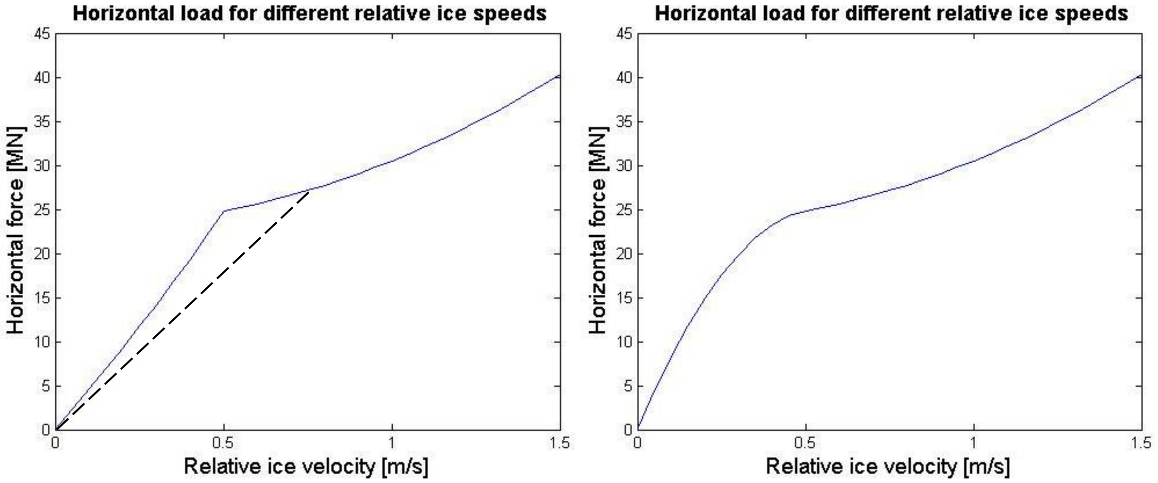

Figure 3-16: Left: Linear shape. Right: Quadratic shape. Transition velocity is 0.5 m/s for both sides. Note that by increasing the transition velocity from 0.5 m/s to 0.75 m/s (from the solid to the dashed line in the left figure) the overall loading will become lower since the area under the curve becomes smaller.

After doing some tests with several values for the transition velocity and also with both shapes several things can be noted:

- When comparing the linear versus the quadratic transition shape at the same transition velocity, the displacement of the quadratic shape is always slightly higher. This makes sense as the overall loading is higher for the quadratic shape (larger area under the curve).
- Below is a comparison between using the linear versus the quadratic transition shape when looking at the horizontal force generated. The quadratic shape results in a smoother activation of the transition term.

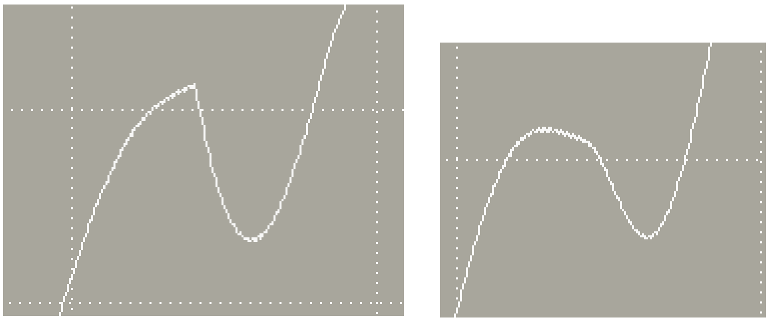

Figure 3-17: The force generated, 100 seconds between the two vertical gridline and the size of the drop is about 0.5 MN. Left: The linear transition shape was used. Right: The quadratic transition shape was used.

- The higher the transition velocity the earlier the steady-state response is reached. This is the correct behavior because as the transition velocity becomes higher, the overall loading on the vessel becomes smaller (smaller integral in Figure 3-16).

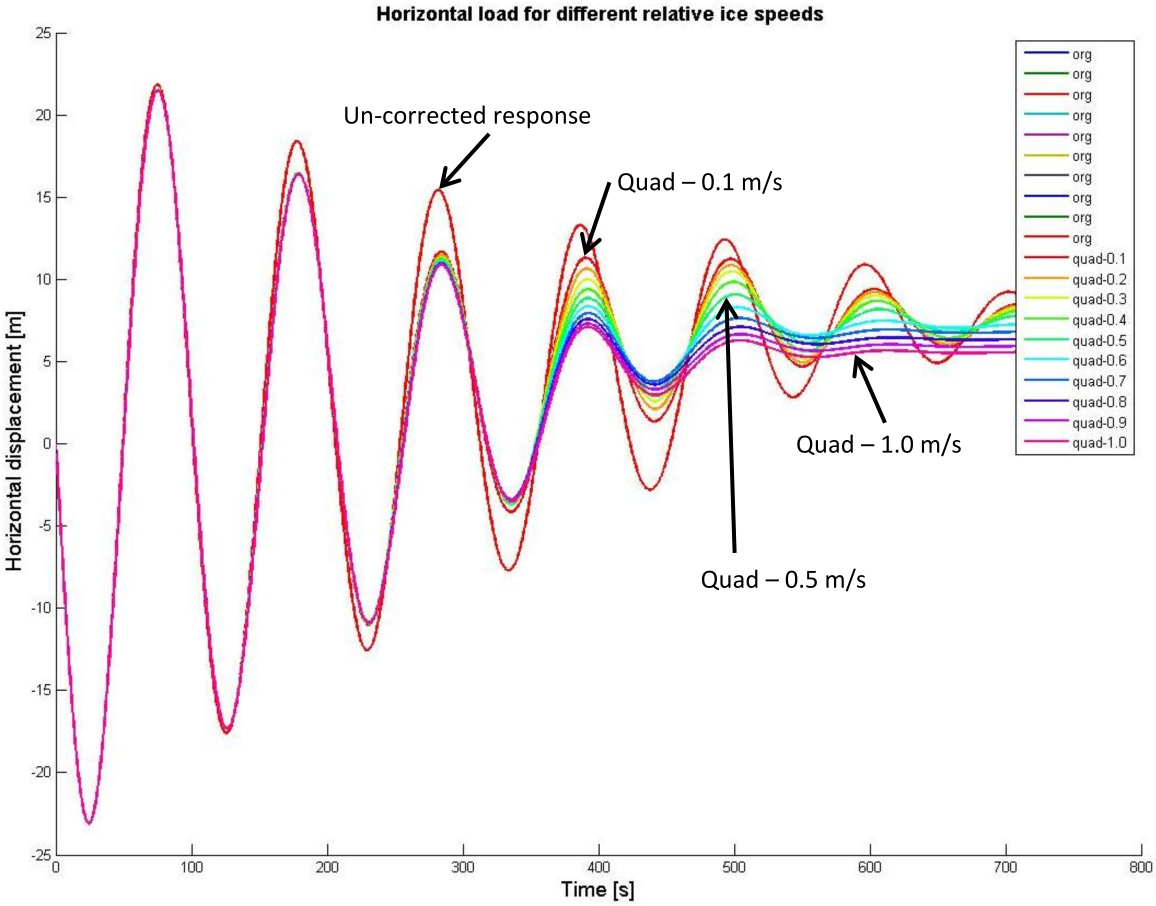

Figure 3-18: The response of the vessel for several different transition velocities. The red line standing out from the rest is the original model without the zero velocity correction.

Conclusion

The quadratic transition shape results in smoother shapes in the generated force due to the smoother transition shown in Figure 3-16. For this reason the quadratic shape is chosen.

A very high transition velocity creates very smooth transition but will lower the overall loading on the vessel. Because 0.5 m/s was the last value to be measured during the model tests, the transition velocity is assumed to be equal to this value.

With the implementation of this fix both major problems with KSRI's model are now fixed. The ice model is now working in a way that allows it to be used in time-domain simulations. In the next section interaction with ridges will be added.

3.2.1.6 RIDGES

In this section the two tests that were done with ridges will be analyzed and used to add the capability of ridges to the ice model. The resulting model is not very accurate and serves more as a rough indication than anything else.

A channel was made through the ridges to resemble the effect of an icebreaker. Both tests were done in an ice sheet with a consolidated layer of 3 meters thick but the depth of the keel was different; 10 and 18 meters.

Small ridge

Next the data from the ridges is examined. The idea is the express the ridge as an amplification of the mean forces. It is best explained by looking at Figure 3-19.

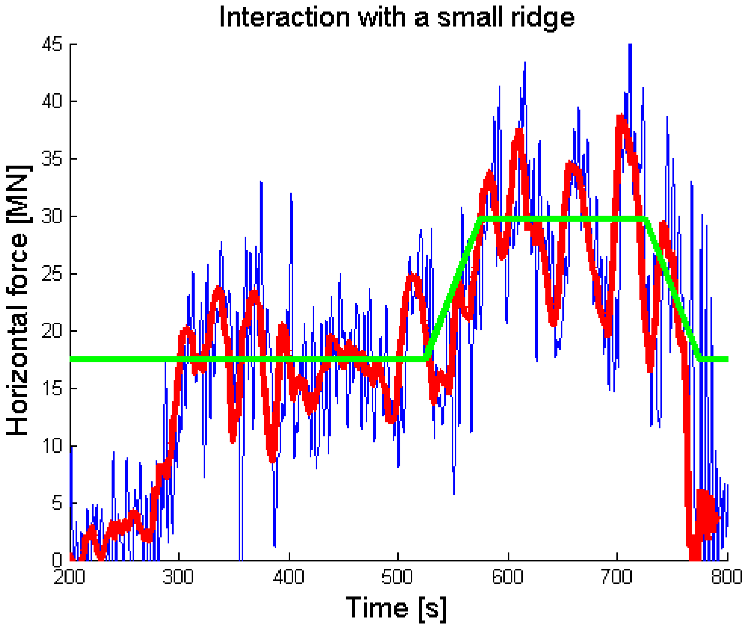

Figure 3-19: Interaction with a small ridge, 3m consolidated layer and 10 m keel depth. The red line is a 10 second moving average and the green line is the resulting multiplication function for the small ridge.

The mean force prior to the interaction with the ridge (about 17.5 MN) is used as a reference and thus the ridge multiplication function is 1 here. Next the green line gives the amplification of the mean due to the ridge over time. It is given by the following formula:

$$Small\ ridge\ factor = \begin{cases} 1, & t = 0\ s \\ 1.7, & t = 50\ s \\ 1.7, & t = 200\ s \\ 1, & t = 250\ s \end{cases}$$

So the interaction with the small ridge lasts 250 seconds.

For the implementation of ridges into the ice model it is assumed that the increase in forces due to ridges is independent of the thickness of the consolidated layer. By assuming this, the mean of any stationary load can be multiplied with the equation above to add the interaction with a ridge.

Big ridge

Finally the interaction with the big ridge is examined in Figure 3-20.

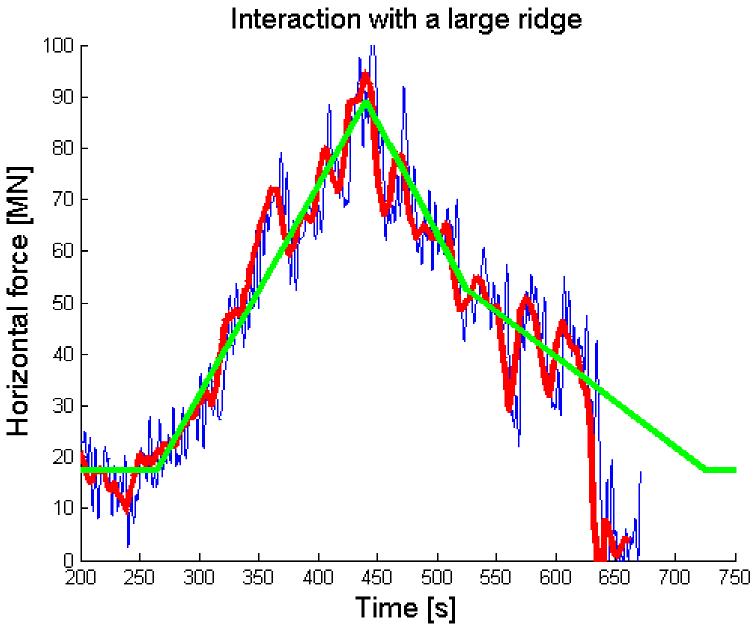

Figure 3-20: Interaction with a large ridge, 3m consolidated layer and 18 m keel depth.

The amplification formula for a large ridge is:

$$Large\ ridge\ factor = \begin{cases} 1, & t = 0\ s \\ 5.1, & t = 175\ s \\ 3, & t = 260\ s \\ 1, & t = 460\ s \end{cases}$$

Final notes

The current implementation of ridges only amplify the horizontal forces on the vessel, all other directions have been neglected for now.

3.2.1.7 DISCUSSION OF THE MODEL FOR PX_MEAN

The model has some limitation and some things were neglected. Some issues one might have and some comments:

"The model overestimates the loading for the 3m thick ice at 0.0 degree trim angle by 16% and underestimates the 3m thick ice at 2.5 degree trim angle by 15%."

Indeed, unlike the original KSRI regression model which gave a near perfect fit, the new model is less accurate. The main reason for this is that the new model is based on KSRI's model, which only has a second order dependency on the ice thickness. This is not a problem in itself but the three data points of the 3m thick ice do not lend themselves to be easily fit with a quadratic equation. A higher order equation might increase its accuracy; however several attempts to use a third order equation resulted in curves with very strange shapes. Even higher order fits are not possible due to the lack of data, so a second order fit is the best given the current data.

"Simply taken the ratio between the three sections implies that the top half of the ice will fail in bending and the bottom part will fail in crushing."

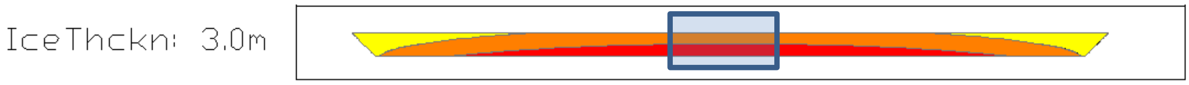

Figure 3-21: Half the cross-section failing in bending and the other half in crushing? Not likely...

Yes and no. Because the orange section also has a higher weighing factor than the yellow there is also an increase in the force due to interaction with the orange section. The orange area is a bit ambiguous in terms of what kind of failure will actually happen because at smaller trim angles it still results in bending failure but when combined with the red area at larger trim angles it results in crushing.

In reality the transition from bending to crushing is probably more complicated and intricate. However due to the limited test results there is no clear point where one can clearly say; this is the trim angle which signifies the onset of crushing.

In reality there will be some dependency on the bending depth of the ice which would increase the interaction with the orange/red section. Also due to the strength of the ice a certain level of simultaneousness of the ice failure mode is to be expected. For example this can cause the sides of the ice, which are generally interacting with the yellow/orange section (and as such are failing in bending) to drag down the center part of the ice, causing the center to also fail in bending, even though the center part might actually be interacting with the red section. And vice versa this is also possible; if a large section of the vessel-ice interaction area is failing in crushing, the crushing could extend beyond its normal reach.

However I am confident the mean of Px is dependent on the division between the three sections. Several other models were also tested but proved to be unsuitable for curve-fitting the data. These models used the ratio between the lengths (not area) of the three sections at MSL or some depth below MSL based on an estimate for the bending depth of the ice. I think because crushing is dependent on the area, the current model based on the ratio between the areas, and therefore based on the impact angle, gives a good approximation. Although it might not make 100% accurate, it does incorporate the same parameters which govern the ice failure modes.

"How do you know whether the model is correct at velocities higher than 0.5 m/s in combination with ice thicknesses higher than 1.5 m?"

Due to the lack of model tests in this region it is impossible to know exactly what kind of interaction will occur. Also as noted before, in (Loset, 2006) there is data that indicate that at higher velocities, crushing occurs more easily. Unfortunately currently these effects cannot be taken into account without a lot of assumptions. In the future more tests should be done to investigate this combination of ice parameters.

The current addition to KSRI's model does not distinguish between the three different components of the original regression model. Both the part depending on the ice thickness and the part depending on the relative velocity are scaled using the same factors (2.1 for the orange area and 7.5 for red).

Therefore it is assumed that the same amount of crushing will occur regardless of the velocity. This is the best that can be done without additional testing.

3.2.1.8 RECOMMENDATIONS

Some things that could be done to improve the quality of the Px_mean model:

- Do model tests at the higher velocities, but now for several ice thicknesses.
    - This will allow the effect of the extra crushing due to the higher velocities to be incorporated (which should occur according to the literature).
- Do model tests at very low velocities (<0.5 m/s) also in combination with very thick ice and possibly at temperatures around thawing.
    - This would give better insight into the horizontal force at low velocities.
    - (Loset, 2006) suggest that this combination of ice parameters results in the highest overall loading due to the ductile behavior of ice at very low velocities and temperatures around thawing in combination with ice to failing in creep.
- Do more model tests in general to allow for higher order interpolation (e.g. check more trim angles with the same ice thickness / velocity).
    - This would show when exactly the ice transitions from bending to crushing and allow for a better model.
- Do tests were other parameters are varied, such as temperature and salinity in order to test their impact on the loading.

This concludes the section about Px_mean. Next up is the fluctuating part, Px_fluc.

3.2.2 PX_FLUC

The fluctuating part of Px, Px_fluc for short, proved to be much more of a challenge to model than the mean part. The goal is to be able to generate a signal that has the same statistical properties but with increased length for any combination of ice and vessel properties.

The general approach that is commonly use is to get a spectrum of the signal. Based on this spectrum a statistically identical signal can be recreated, however each signal will be unique since it uses random phase angles for each individual wave that makes up the total signal. The attempts to apply this method are discussed in Appendix F.

Section 3.2.2.1 contains an analysis of the frequencies of the ice and the vessel and 3.2.2.2 contains the method used to create the fluctuating parts of the loads.

3.2.2.1 ANALYZING THE FREQUENCIES OF THE ICE AND THE VESSEL

Before starting with the actual frequencies contained in the data it is interesting to first do a rough estimate of the frequencies that can be expected by reexamining the footage taken during the model test. Also an investigation into the DAFs of the vessel will be done to see which frequencies of ice loading will generate a large response.

3.2.2.1.1 ANALYZING THE FREQUENCIES OF THE ICE LOAD

In order to see what the actual frequencies of the ice load are another look is taken at the footage made during the tests. The most important thing to analyze is a set of pictures taken after the model test had already been finished and the model was then pulled back. It shows the size of the ice rubble created by the interaction process.

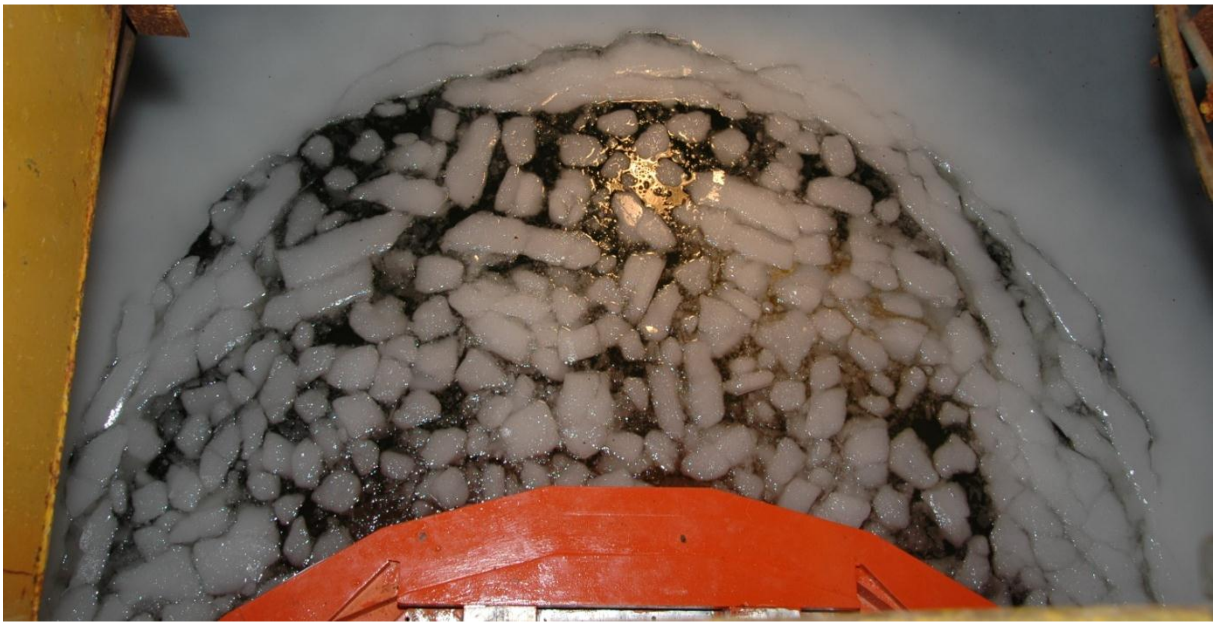

Figure 3-22: Size of the failed ice. The picture was taken after test 3-1: 1.5 m thick ice at 0.5 m/s and a zero degree trim angle.

By comparing the length of one of the sections that make up the polygonal circumference of the hull to the length of the broken off ice pieces, their length can be estimated. The length of a hull section is 13.84 meter. The width of an ice section is then about 2.422 to 3.46 meters (full scale). For test 3-1 the velocity at full scale was 0.5 m/s. So this gives an ice period of about 5 to 7 seconds.

- For test 4-1 (2.0 m thick ice. 0.5 m/s. 0 degree trim angle) the period of the ice failing is about 5.5 to 8 seconds.
- For test 4-3 (2.0 m thick ice. 1.5 m/s. 0 degree trim angle) the period of the ice failing is about 2 to 3 seconds.
- For test 4-4 (2.0 m thick ice. 1.0 m/s. 0 degree trim angle) the period of the ice failing is about 2.8 to 4.8 seconds. The picture from the test also shows a larger circumferential crack, which would have a frequency of about 12 seconds.
- For test 6_4 (3.0 m thick ice. 0.5 m/s. 2.5 degree trim angle) the period of the ice failing is a bit more varied; about 4 seconds for the thinnest circumferential cracks, 11 seconds for medium crack and 19 seconds for the largest crack.
- When analyzing the video footage the larger cracks in test 6_4 and the other 3.0 m thick ice tests seems to occur at a period of about 20 to 60 seconds. Sometimes there is a pause between consecutive cracks and sometimes they occur right after each other, it appears to be quite random.

In general it can be said that the frequencies of the ice cover a wide range. The periods associated with the final small rubble are quite small. Most are between 5 and 10 seconds. The periods associated with the large circumferential cracks can have a period of up to 60 seconds.

However it is very important to note that no correction has taken place for the bending stiffness of the ice and therefore in full scale the ice will by much stronger. This means that the periods at full scale will be a higher than those measured at model scale. This questionability of the frequencies contained in the model test data cannot be overcome.

3.2.2.1.2 FREQUENCIES OF THE VESSEL

In ice modeling the D/t ratio (diameter at the water line divided by the ice thickness) is one of the key dimensionless numbers to estimate what kind of platform-ice interactions will take place. For the JBF arctic the D/t ratio is very large. Depending on the ice thickness the ratio starts at 32.67 [-] for an ice thickness of 3.0m thick and goes to as high as 98 [-] for an ice thickness of 1.0 m. The large D/t ratio of the vessel has several consequences on the loading.

The most important one is that the global loading on the vessel is somewhat independent of what happens at a local scale. When we have wide structure, a contribution of ice failure into total ice load is less than in case of narrow structure interaction with ice. Significant portion of total ice load is due to ice rubble presence in front of the structure. When adding up all these forces the saw-tooth pattern that one normally expects fades away and makes place for a smooth shape. This is also in a large part due to the large mass of the vessel which makes it irresponsive to high-frequency forces. When looking at the time histories, an example is shown in Figure 3-22, they all have a very sinusoidal-looking shape. Similar results with a smooth shape were also obtained from model tests done for the Sevan which is also a downwards slooping floating structure with a similar D/t ratio.

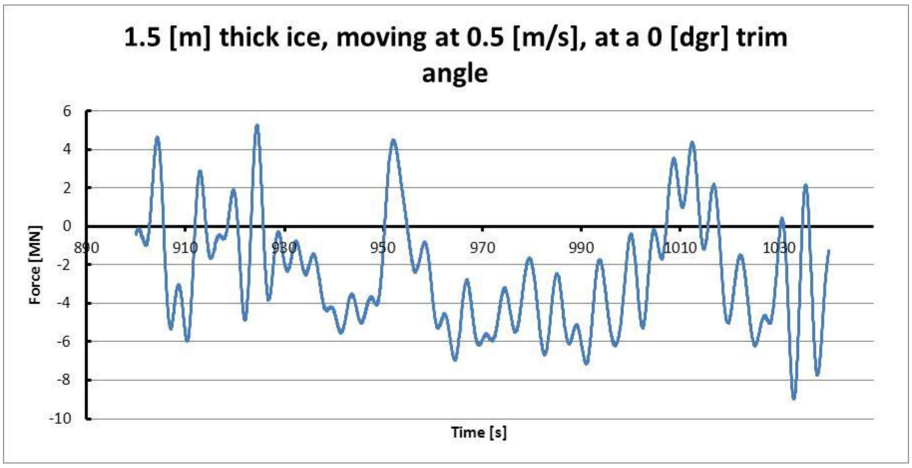

Figure 3-23: Smooth shapes due to the large D/t ratio of the vessel.

Dynamic amplification

Next the dynamic amplification factor (DAF) of the vessel will be calculated to check the frequencies of the vessel. The 1DOF DAF will be used as reference as this gives a very good indication of the actual response. The 1DOF DAF is given by the following equation:

$$DAF = \frac{1}{\sqrt{\left(1-\frac{\omega^2}{\omega_n^2}\right)^2 + \frac{\gamma^2}{\omega_n^2}}}, \qquad with\ n = \frac{c}{2m}, \qquad \omega_n^2 = \frac{k_{ms,lin}}{m}, \qquad \gamma = \frac{2n}{\omega_n}$$

The spring term here is the linearized mooring system force.

The mass term is the mass of the vessel plus added mass at the natural frequency of the vessel. When looking at the DAF in Figure 3-24 it can be seen that not much of the ice loading is important when it comes to generating motions in the vessel.

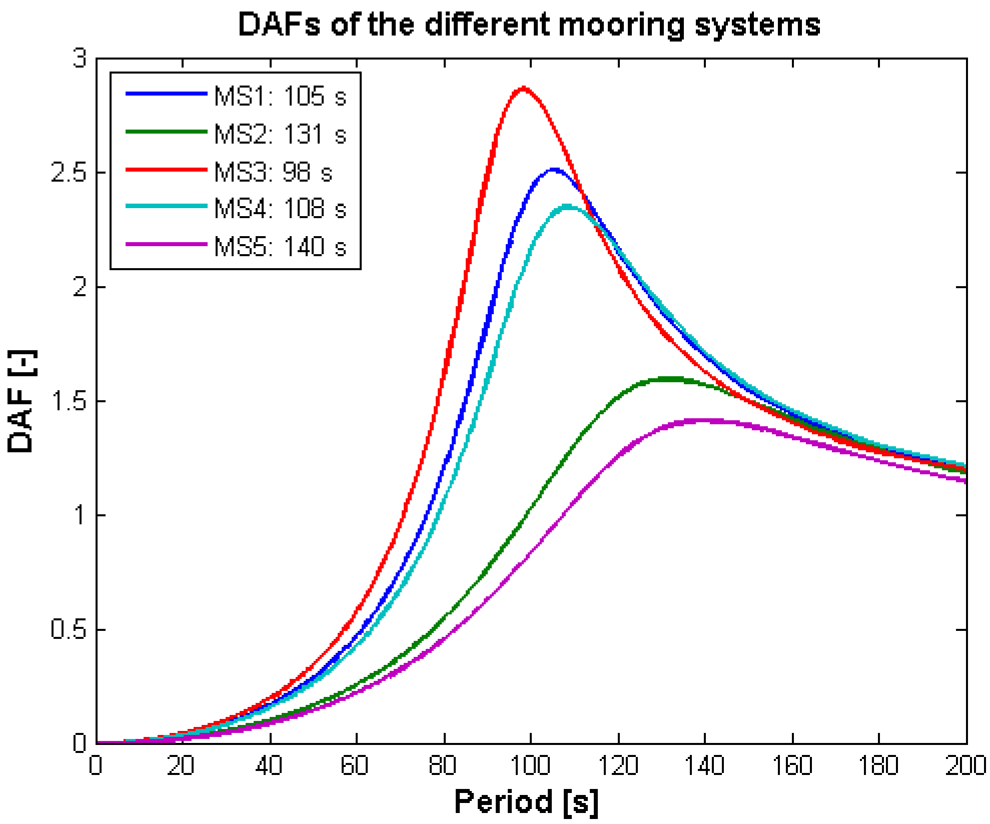

Figure 3-24: The DAF of the vessel for the five different mooring systems around zero meters offset. The natural periods are shown in the legend. The linearized drag at 0.4 m/s was used for the damping.

A couple observations and notes about the DAF:

- The periods of the ice (4 – 60 s) are all located within the lower end of the DAFs for all mooring systems so no large vessel motions are expected due to the ice loading at an offset of zero meters. However these low period motions might still be very important for the dynamics of the mooring lines.
- The damping used here is a linearization of the drag term. So in reality the height of the peaks will be different.
- The springs terms used here are the linearization of the mooring system at an offset of zero meters. At larger offsets the mooring system no longer behaves linear so then this linearization is invalid, see Figure 3-25. The stiffness of the system increases (up to three times higher) at larger offsets so the natural periods will go down quite considerably. This brings the natural period in the band of periods observed in the ice.

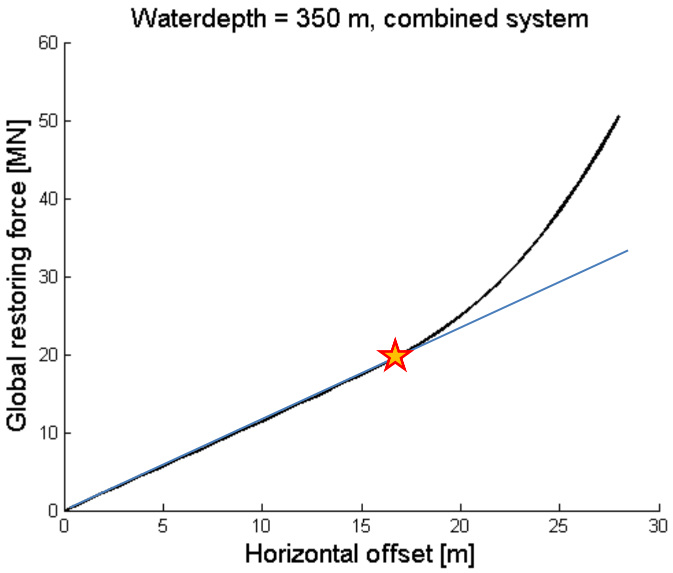

Figure 3-25: The restoring force of the mooring system as a function of offset and the transition point beyond which the natural period starts changing.

Conclusion

When looking at the DAFs of the vessel we can that only very high periods are important for the response of the vessel, this corresponds to (very) large circumferential cracks. If we now look at the frequencies calculated from the model test footage then resonance would not be expected to occur as the calculated ice frequencies are all much lower (<60 seconds) then the natural periods (~100-140 seconds).

When proceeding forward with the creating of spectrums it is thus very important to keep a close eye on the very high periods.

3.2.2.2 SIGNAL CREATION

Now that the periods of the ice and the vessel have been analyzed it is time to start with creating of the fluctuating ice loads. When trying to create a different but statically identical signal based on measured data it is common to create a spectrum and then use random phase angles to achieve this. This method was attempted but did not work for ice loads. The full analysis can be found in Appendix F and the conclusions are presented below:

- The length of the time histories varies between all the tests. This means that the resulting spectrums have different spectral resolutions and errors.
- The statistical properties of the full length data differ from the values in KSRI report and cannot be rescaled properly to give it the same values as in the report.
- There is no correction for the scaling of the bending stiffness, which results in inaccurate frequencies in the spectrums.
- The impact of the windows is unclear and it is not clear which one is the most appropriate one to use.
- Interpolating between the different spectrums proved to be impossible since their shapes are very irregular and chaotic.

Especially the interpolation problems made it impossible to use spectrum. In order to overcome this problem it was assumed to use flat spectrums instead of the shapes that were obtained from the model test data. Although it is bold assumption a wide range of frequencies was observed in the footage and in the spectrums.

The approach that will be used to create the fluctuating parts of the forces is to base them on the standard deviation (or variance) measured during the model tests. In section 3.5.4 of (Holthuijsen, 2007), the following equation can be found for a variance density spectrum:

$$Var = \int_0^\infty E(f)\ df = \int_0^\infty \lim_{\Delta f \to 0} \frac{1}{\Delta f} E\left\{\frac{1}{2}\underline{a_i^2}\right\} df,$$
$$where\ the\ \underline{underscore}\ indicates\ a\ stochastic\ parameter$$

Since the variance is equal to the integral of any spectrum, the variance can be used to scale any spectrum to give it the correct amount of "energy" if the shape of the spectrum is known. In combination with the assumed flat shape the artificial spectrums can be created.

3.2.2.2.1 STANDARD DEVIATION

The basis for this model is the standard deviation (SD), see Figure 3-26 and Figure 3-28. At first glance Figure 3-26 looks similar to Figure 3-3 (page 47, it shows the mean of Px for varies ice thicknesses / trim angles) making it likely that the same effects are dominating the mean and SD of Px. In order to able to investigate the relation between the mean and fluctuating parts of the loading, the SD is divided by the mean to give Figure 3-28.

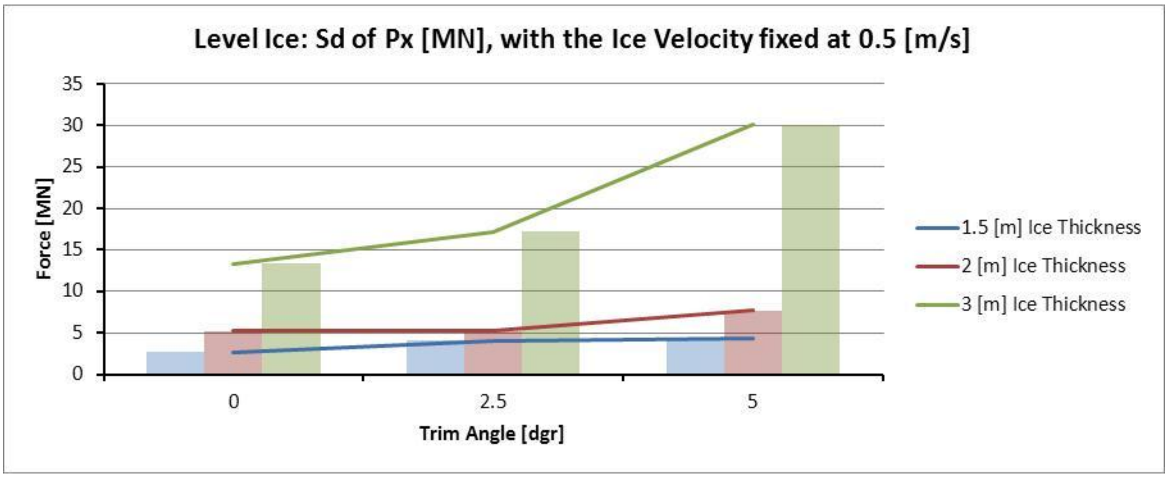

Figure 3-26: The SD of Px. Note the similar shape as was seen with Px_mean.

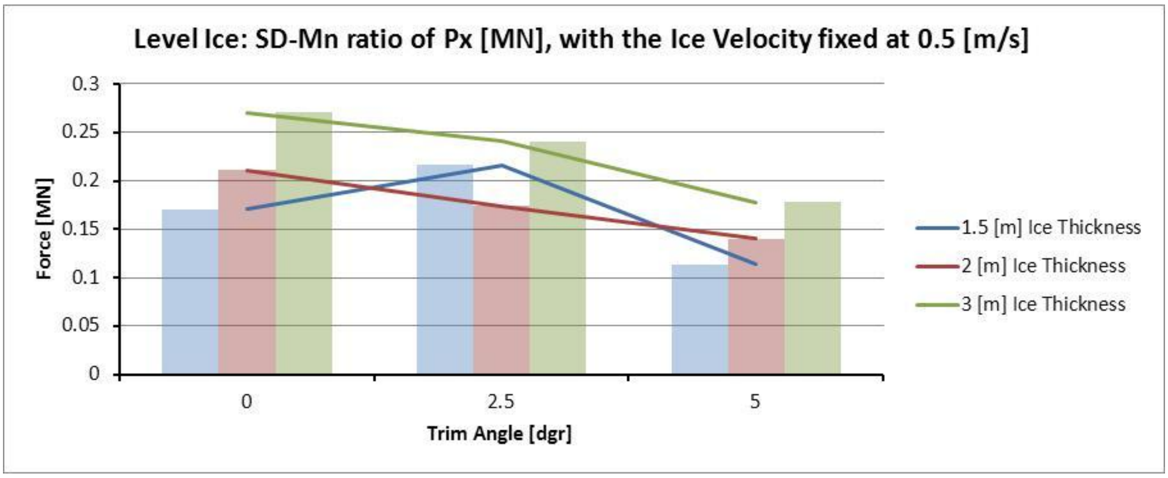

Figure 3-27: The SD as a ratio to the mean of Px. The trim angle is varied and the ice velocity is fixed.

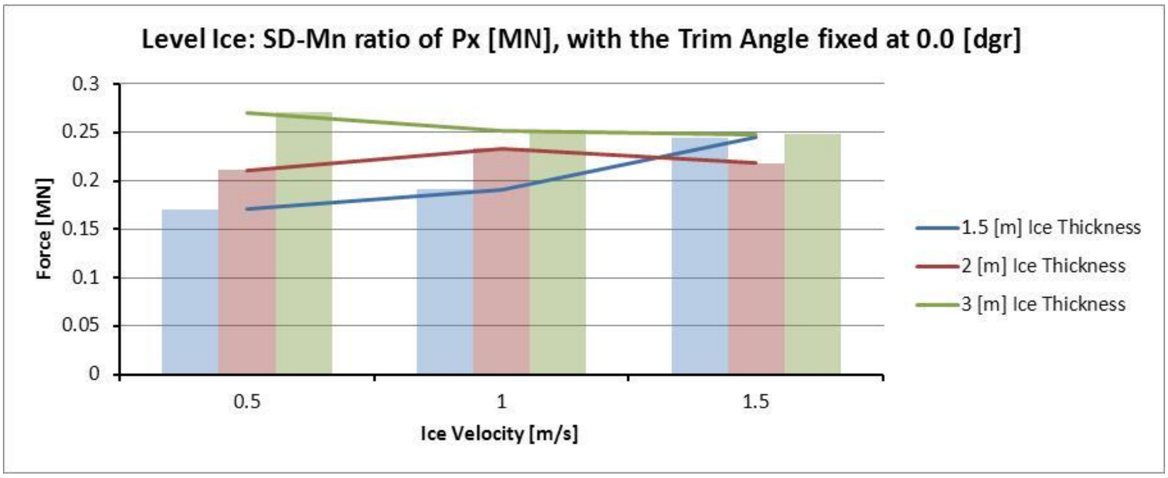

Figure 3-28: The SD as a ratio to the mean of Px. The ice velocity is varied and the trim angle is fixed.

When looking at the SD to mean ratio of Px a few things can be observed:

- The blue line in Figure 3-27 (1.5m thick ice) shows a value that appears to not be following the trend of the other two lines. When looking at the time series of the test which corresponds to the kink, there are two large spikes in it, which explains why the SD is higher. When looking at the video footage, nothing special can be seen that would explain the two spikes. Because of this the peak in the blue line shall be ignored.
- When increasing the ice thickness the SD-Mean ratio increases. A likely explanation for this could be that, when looking at the footage, the ice action size (simultaneousness of the ice action) becomes larger and also these larger action sizes occur much more frequently when increasing the ice thickness. Large action sizes results in larger load spikes which increase the SD-Mean ratio.
- When increasing the trim angle the SD-Mean ratio drops fairly constantly. The drop between 2.5° and 5.0° could be explained by the much small ice action size of crushing, resulting in more constant loading and a lower SD-Mean ratio.

Because the model Px_mean is of good quality, being able to relate the SD's model to it would greatly simplify the creation of the model for the SD. Since the SD to mean ratios are very regular the SD of Px will be modeled as a ratio of the mean of Px.

One can see in Figure 3-28 that the ratios are nearly constant at each ice velocity, so the SD to mean ratio is independent of the ice velocity. There is one data points which does not follow this trend; the last data point of the blue line (1.5m thick ice). When looking at the corresponding time histories and video footage no abnormal things can be seen that can explain why this test does not follow the trend. However, even though there is no good reason to ignore the peak, it is still ignored in order to simplify the model. Next the three (or two) values at each of the three velocities can be averaged to get three points only dependent on the ice thickness. These three points can be curve-fitted to get an equation for the SD at each ice thickness:

$$\sigma = Pxmean * (0.1144427857 \ + \ 0.0484867143 \ * \ t)$$

When looking at Figure 3-28 a downward sloping relation can be seen between the trim angle and the SD of the force (again the middle blue value is ignored for simplicity). Setting the values at a trim angle of zero degrees to unity and using three linear curve-fits which were then averaged the following relation was calculated:

$$\sigma = Px\_mean * (0.1144427857 \ + \ 0.0484867143 \ * \ t) * (1 - 0.0673 * a), \qquad where\ a\ is\ in\ radians$$

The last term in the equation, $(1 - 0.0673 * a)$, has a maximum value of 1. Because positive angles means that the vessel is interacting with the yellow section of the hull the SD should not change. At a trim angle of +4 degrees interaction with the deck box starts which is not accounted for by this model and neither is interaction with the grey area. This means that the model for the SD of Px is only valid between +4 and -5 degrees. During normal conditions this range is more than sufficient.

The value used for Px_mean is without the scaling factor for the transient interaction. In the time histories it can be seen that the fluctuation component does not grow in time but immediately starts with pretty much the maximum magnitude, see Figure 3-29.

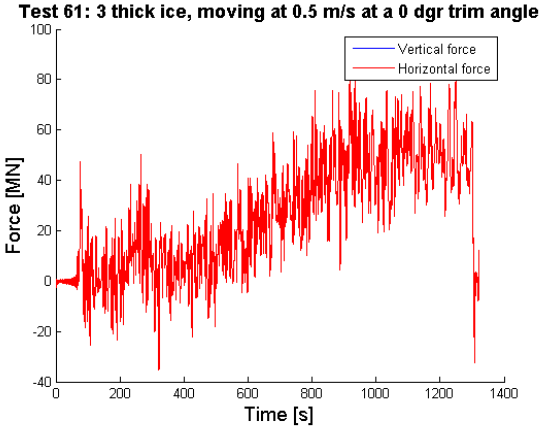

Figure 3-29: The fluctuating component starts at maximum magnitude while the mean value first has to grow.

Now that the SD is known, the total energy that the spectrum contains is set. The energy now has to be distributed over the different frequencies.

3.2.2.2.2 CREATING WAVES

As the total available energy is contained in the variance it has to be distributed over the different waves. The energy available for a single wave can be calculated from the shape-function as follows, where SF is the shape-function:

$$Ratio_i = \frac{SF(f_{i-1}) + SF(f_i)}{2} * \Delta f = \frac{SF(f_{i-1}) + SF(f_i)}{2} * (f_i - f_{i-1})$$

By integrating the spectrum between two frequencies one can calculate how much of the total variance is avialable for that frequency band. By calculating the integral the graph is turned from a variance density spectrum into a variance spectrum. Using the ratio and the formula for the variance spectrum the amplitudes can be calculated as follows:

$$Ratio_i * Var = E\left\{\frac{1}{2}\underline{a_i^2}\right\}$$

If we assume that the shape of the spectrum is deterministic then the equation can be simplified to the following:

$$Ratio_i * Var = \frac{1}{2} a_i^2 \rightarrow a_i = \sqrt{2 * Var * Ratio_i}$$

Next a shape is needed in order to turn the ampitudes into a time varying signal. As discussed before the motion of the vessel have a smooth shape due to the large D/t ratio so a sinussoidal shape is suitable to recreate this shape.

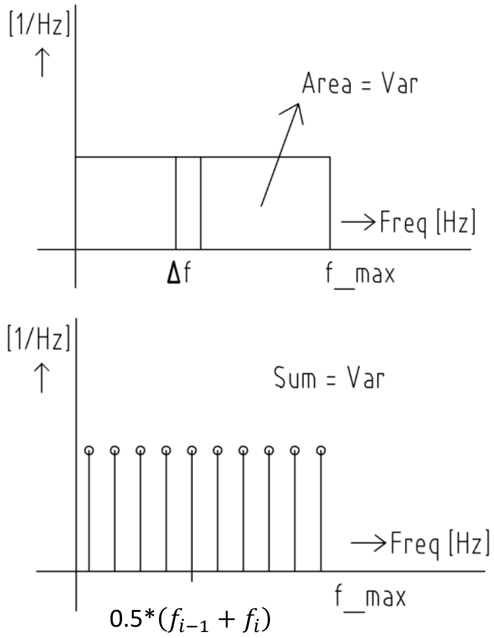

Figure 3-30: Discretizing the spectrum, e.g. splitting the spectrum into waves. This turns the variance density spectrum into a variance spectrum. The height of each line is equal to the area stored in each frequency band.

The next question is which frequency to use for each of the waves. For simplicity the frequencies half way each of the frequency bands are used. This results in the following equation, where f_max is equal to the maximum frequency from the model tests which is around 0.25 Hz (it varies between the tests):

$$Px\_fluc = \sum_{i=1}^{N} \sqrt{2 * Var * Ratio_i} * \sin\left(\frac{i - 0.5}{N} * f_{max} * t * 2\pi + \varphi_i\right)$$

No beating

The equation above gives the total fluctuating part of the force at any given time instance. Another issue that surfaced when discussing the creation of the spectrum was beating. When the period of the total generated signal is smaller than the simulation time beating occurs as the generated signal starts to repeat itself during the simulation.

In order to avoid this problem the frequency bands must have to correct width. The relation between the duration of the simulation and the frequency band it the following: $D = 1/\Delta f$. So if the desired simulation time is 1000 seconds, $\Delta f = 0.001\ Hz$. As KSRI filtered out every vibration with a frequency above about 0.25 Hz this maximum frequency is equal to 0.25 Hz. This means the amount of waves needed is 0.25 Hz / 0.001 Hz = 250 waves.

Fluctuating components

This concludes the section about the fluctuating component of Px. The method explained here will also be used to model the fluctuating parts of the other five components.

3.2.3 PY_FLUC

Px is one of the three load components whose mean is zero due to symmetry, therefore only the fluctuating part has to be modeled. Below the ratio of the SD of Py to Px_mean is shown.

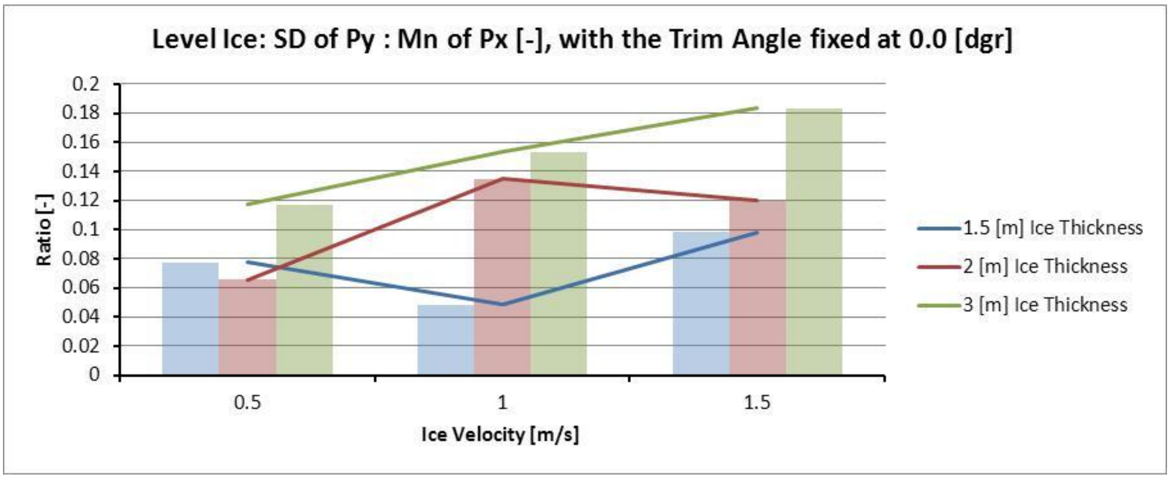

Figure 3-31: The standard deviation of Py to Px_mean ratio plotted for all tests. The ice velocity is varied and the trim angle is fixed.

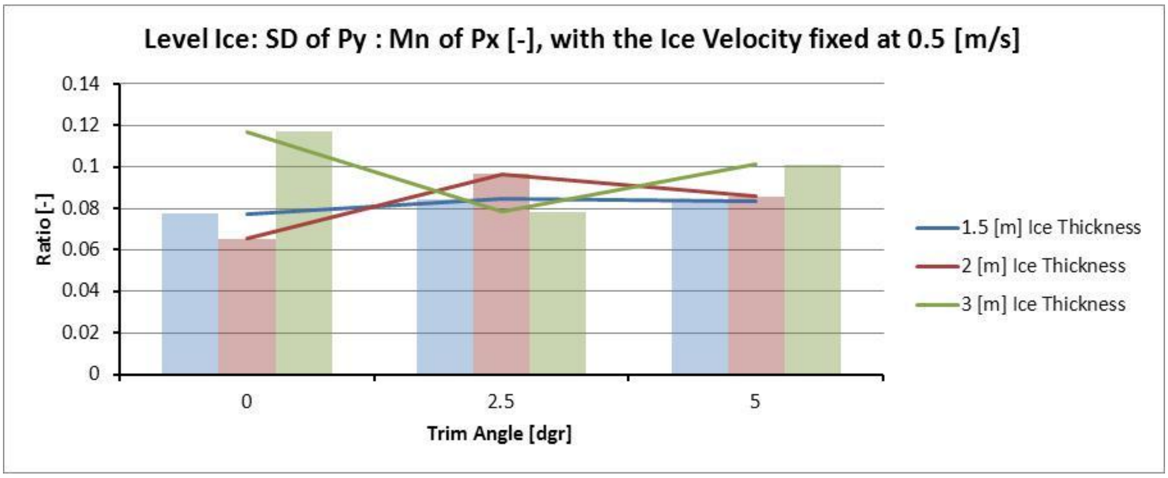

Figure 3-32: The standard deviation of Py to Px_mean ratio plotted for all tests. The trim angle is varied and the ice velocity is fixed.

First looking at Figure 3-32, the ratio is assumed to be independent of the ice thickness and trim angle. The slightly conservative value of 0.1 [-] is taken. Next the relation with the relative velocity is added based on Figure 3-21. The lines are generally upward sloping. The averaged slope is about 0.03 per 0.5 m/s increment. This results in the following equation for the SD of Py:

$$SD_Y = Pxmean_{transient} * \left(0.07 + 0.03\left(\frac{v}{0.5}\right)\right)$$

The value used here for Px_mean is including the transient factor. The reason for this is that the amplitude of Py grows during the transient phase.

3.2.4 PZ_MEAN

Pz is an important component of the force since the resulting heave motion will have a similar effect as the trim angle on the impact angle of the ice, but now uniformly over the whole circumference of the hull. It would be a logical thing to assume that due to the 45 degree impact angle (when interacting with the yellow area), Px and Pz would be about equally large and have 1:1 correlation at every time step. But due to the geometry of the vessel this did not turn out to be the case. Figure 3-33 shows the uncorrelated forces.

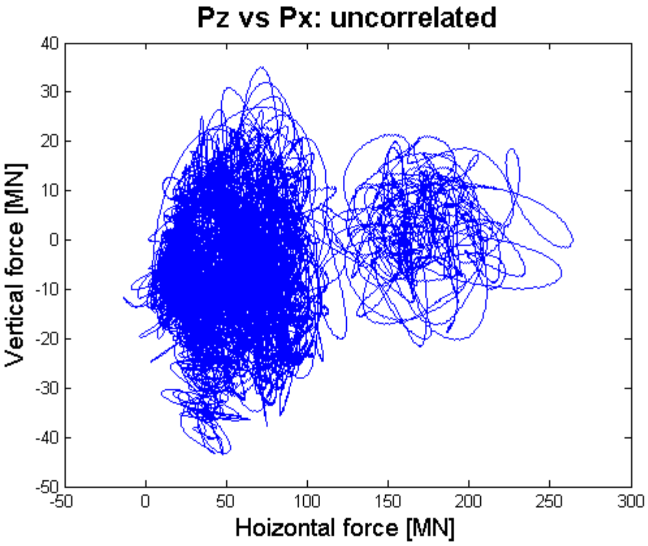

Figure 3-33: Pz plotted against Px for every time step of every test. The smaller line on the right is from test 65 (the test with 3.0m thick ice failing in crushing).

The two forces are not correlated because of the ice rubble. At the initial interaction the ice fails in bending is interacting with the downward sloping section of the hull, resulting in upward forces. After the ice is broken and gets pushed downwards, the rubble is pushed against the lower section of the hull. As the lower section of the hull is upward sloping, this results in downward forces.

The downward forces due to the rubble distort the correlation between the horizontal and vertical component of the force caused by the breaking of the ice. Because of this Pz does not have a simple relation to Px based on the geometrical relation between the two.

A second problem facing Pz is that due to the nature of the setup used during the model test it was very hard to measure Pz correctly. As the model was fixed to the rig any vertical motion of the rig will result in very large force due to the hydrostatic force. Corrections were done to the Pz data by KSRI but still the data remains rather chaotic.

The third problem with the Pz data is that when selecting the segments from the total time series KSRI paid most attention to Px (probably because they only had to make a regression model that component). The impact of this can be seen when looking at the Pz data. In most cases the segment of data they choose clearly does not represent a stationary situation for Pz. This creates problems with the statistical properties calculated from the data.

Keeping these three problems in mind, the time histories of Pz are more closely investigated.

3.2.4.1 TIME HISTORIES OF PZ

When looking at the time histories of Pz for the different tests there is no clear pattern over time. Where Px started at zero in each time history, then showing a linear growth and the finally reached a stable situation, there is not the case for the time histories of Pz. A few tests show a fairly stable growth of the vertical force due to the rubble build up, however many of them show very irregular behavior. Below are some examples:

- Pz shows very large and slow fluctuations, while Px is stable for the same period
- Pz shows very large and slow fluctuations while there is no interaction with the ice (so it should just be constant around zero)

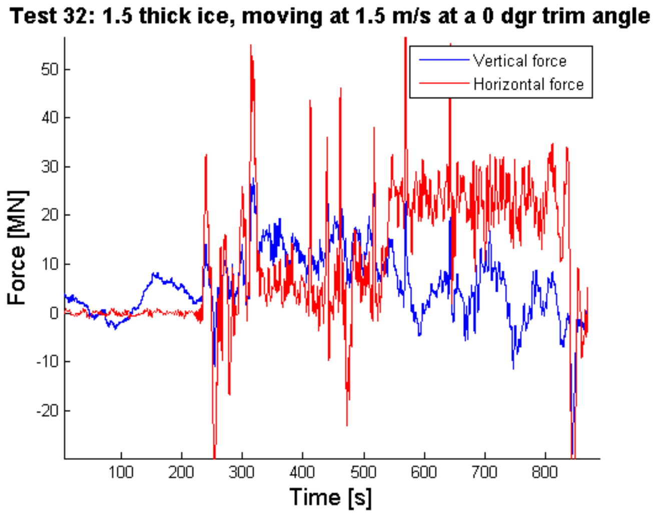

Figure 3-34: Very strange fluctuations prior and during the interaction with the ice.

- Most time series show a downward sloping trend over the full length of the test, even when there is no ice. An explanation could be that some motions of the rig were not removed.

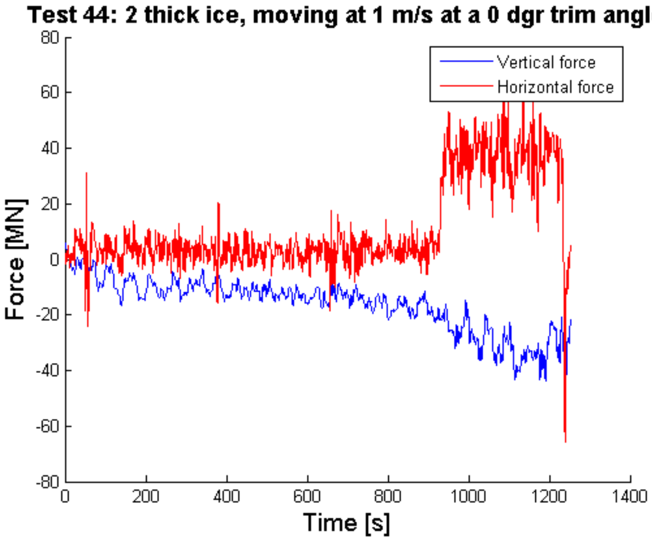

Figure 3-35: Pz is downward sloping even though the model is only being pulled through water.

- During some tests the vertical force is unaffected by the interaction with the ice.

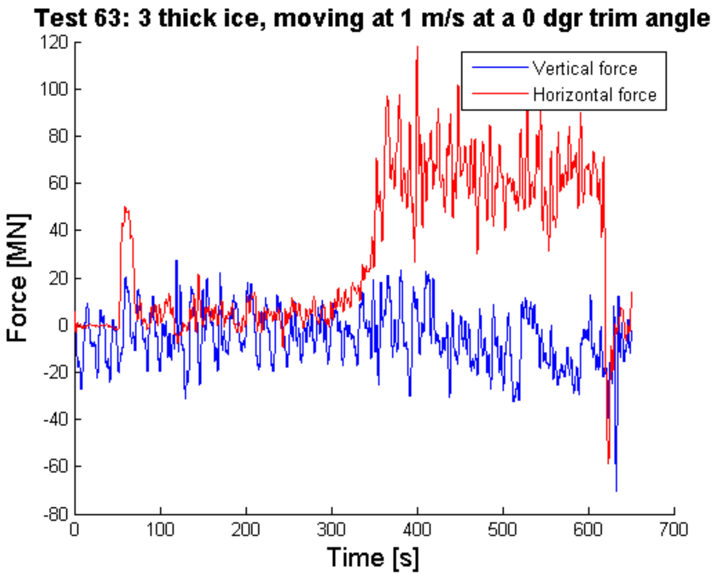

Figure 3-36: Pz unaffected by the ice, even the fluctuating component shows very little change.

For these reasons using the raw data from the tests is not a good idea. In order to see how important Pz actually is, a quick calculation is done to check what kind of offset results from a typical vertical force:

$$z_{mean} = \frac{10MN}{k_{3,3}} = \frac{10^7 N}{76283000\ N/m} = 0.131\ m$$

It is hard to see due to the downward sloping trend in all the Pz data, but the mean of most of the tests is between +10 MN and -10MN. This is equal to an offset of only +0.131 or -0.131 m. A vertical offset influences the calculation for Px_mean and the mooring forces. For the mooring forces this small offset is insignificant. The dependence of Px_mean on the vertical offset of the vessel is much more sensitive. An offset of +3 meters (so that is downwards) will result in a permanent interaction with the orange section of the hull, resulting in much larger horizontal ice forces. However an offset of 0.131 meter is only about 4.5% of this value so again the vertical offset is not that important.

All in all it can be said that the model for the vertical forces is not so important. For this reason a qualitative approach is used.

3.2.4.2 QUALITATIVE MODEL

When looking at the data of Pz, the only thing that really seems to influence the load is whether the ice is failing in bending or crushing. This means that the trim angle is the biggest parameter influencing Pz. Other parameters such as the ice thickness or the ice velocity do not show a clear correlation with Pz. A possible reason could be that even though the upward breaking forces increase with a higher thickness or velocity, so do the downward forces caused by the rubble. These two effects could cancel each other out resulting in mean value that is fairly independent of the ice thickness and velocity.

When looking at the trim angle the following angles are of interest:

- Around 4.0° (depends on the ice thickness) the deck box area starts interacting with the ice
- Around -2.5° (depends on the ice thickness) the orange area starts interacting with the ice
- Around -5.0° (depends on the ice thickness) the red area starts interacting with the ice
- Around -7.5° (depends on the ice thickness) the grey area starts interacting with the ice

Note that the exact angles where the interaction starts depend strongly on the ice thickness. But as the model for Pz is not that important a simplified approach will be used. An average ice thickness of 1.5 m thick ice was used to calculate the angles above.

Next values for the mean are required at each trim angle. By carefully looking at the data, a mean value of -10 MN was chosen when the ice is interacting with the yellow area (no crushing and downward sloping so upward/negative force). When interacting with the red area and the ice is failing in crushing and the resulting mean is about +10 MN.

No data is available for interactions with the grey area but since it is much more upward sloping than the red area, a value of + 20 MN is given to this area. The same reasoning applies to the deck box; it is much less downward sloping than the yellow section so it is given a value of -5 MN.

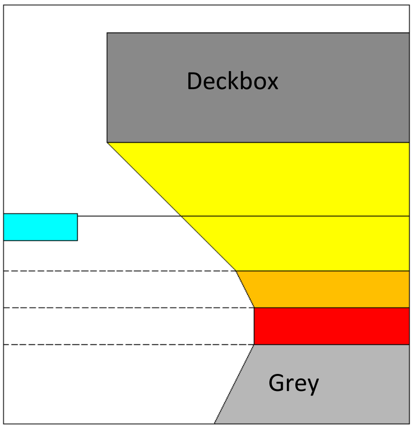

Figure 3-37: The different areas. The ice thickness is 1.5m.

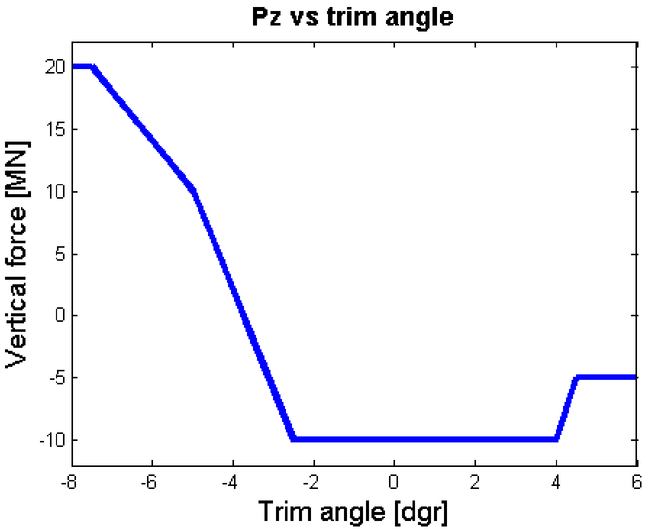

Figure 3-38: Pz versus trim angle.

The final formulation of Pz_mean can be seen in Figure 3-38.

3.2.5 PZ_FLUC

The standard deviation for Pz is shown below in Figure 3-40.

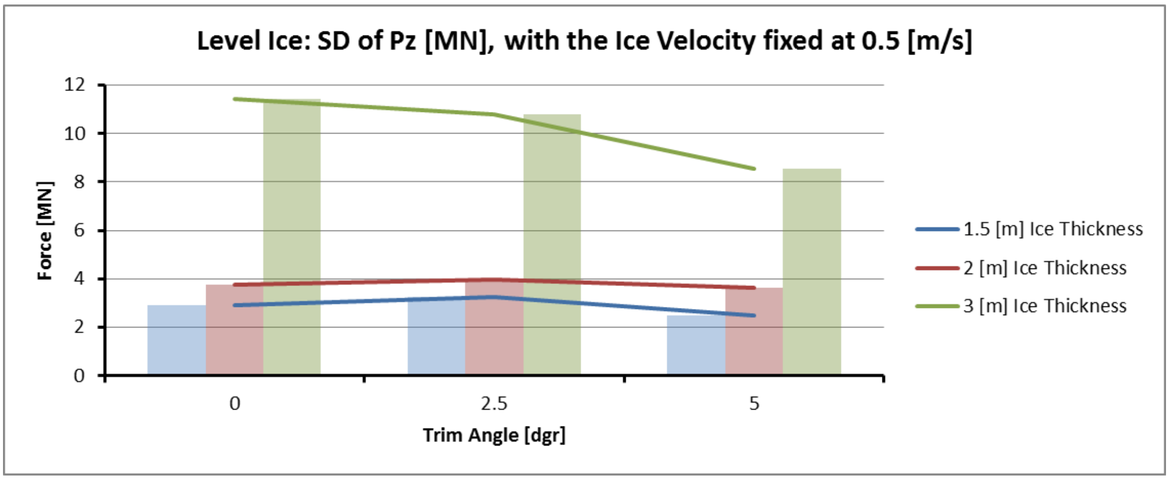

Figure 3-39: The standard deviation of Pz. The trim angle is varied and the ice velocity is fixed.

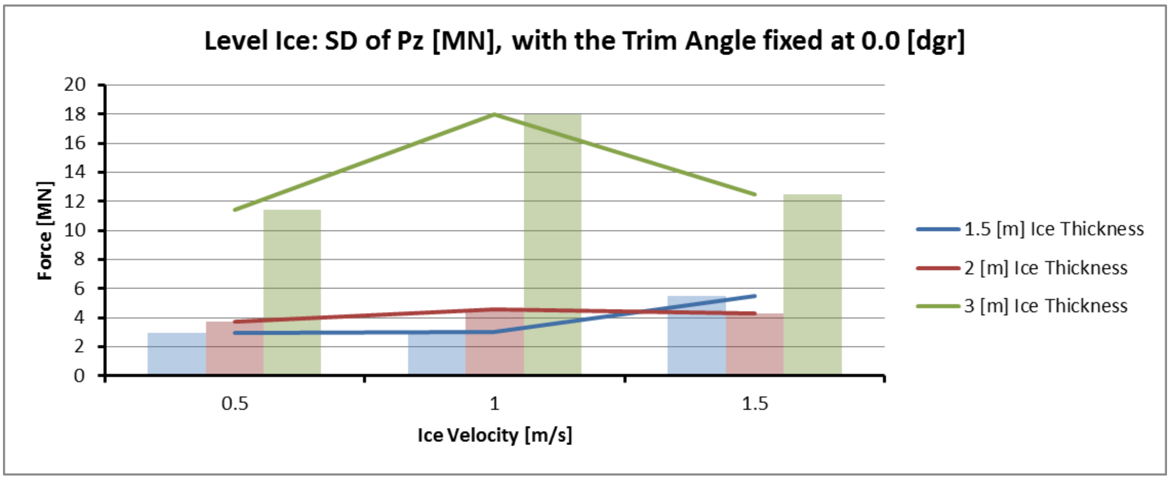

Figure 3-40: The standard deviation of Pz. The ice velocity is varied and the trim angle is fixed.

For the model the SD of Pz it is assumed that Pz is independent of both the ice velocity and the trim angle. This has the biggest impact on the 3.0 m thick ice as this one does not show very constant relations, but for simplicity this will be enforced. For 1.5 m thick ice a SD of 3 MN is used, for 2.0 m a SD of 4 MN and for 3.0 m a SD of 12 MN.

Adding the condition that at an ice thickness of zero the SD is also zero, the data can be curve-fitted. The following equation provided the most realistic looking fit, see Figure 3-41:

$$SD_z = \frac{14200 * t + 1331}{t^2 - 3294 * t + 13540} * 10^6$$

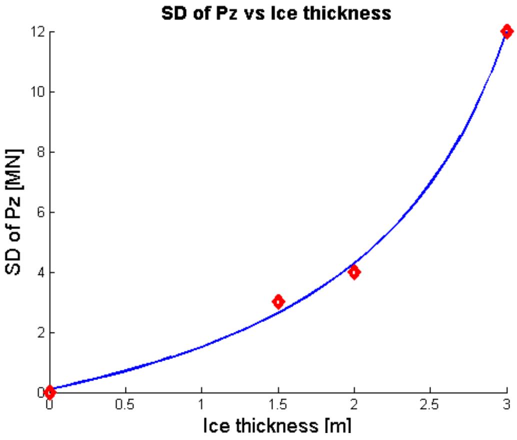

Figure 3-41: The curve-fitted SD of Pz.

The equation is not exactly zero at 0 m thickness, but the remaining term is so small that it is negligible.

3.2.6 MX_FLUC

Mx is one of the three load components whose mean is zero due to symmetry, therefore only the fluctuating component has to be looked at. Below the ratio of the SD of Mx to Px_mean is plotted.

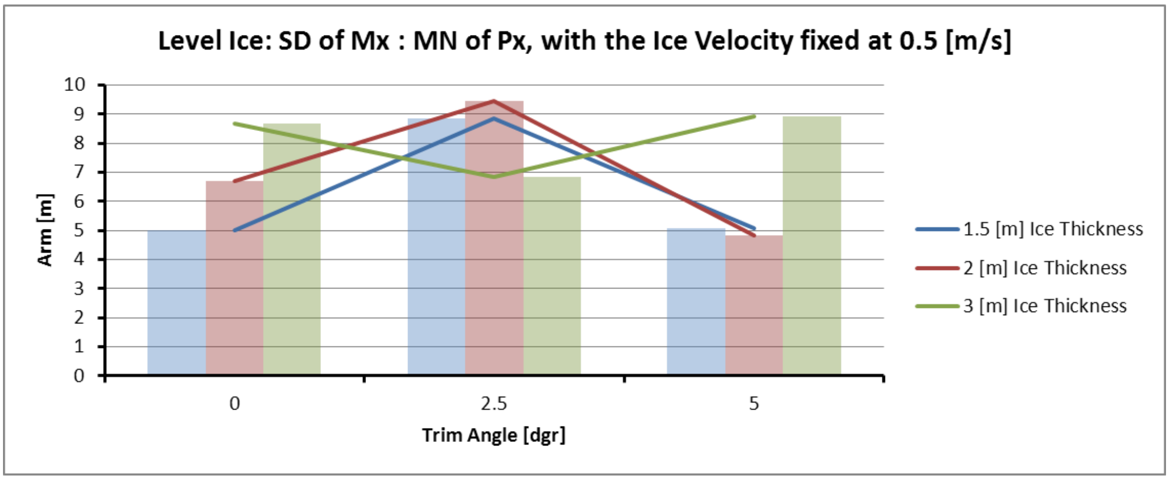

Figure 3-42: The SD of Mx to Px_mean ratio. The trim angle is varied and the ice velocity is fixed.

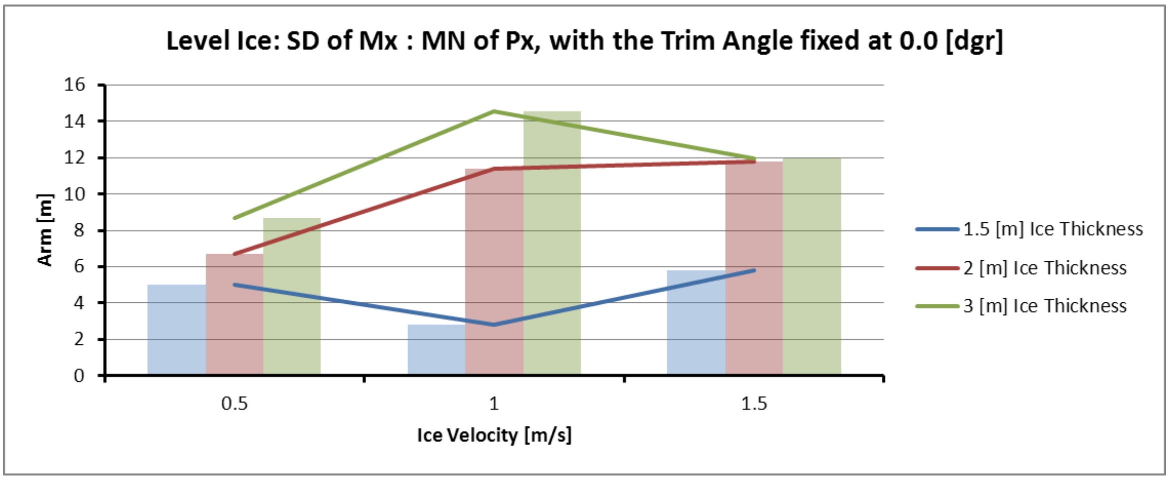

Figure 3-43: The SD of Mx to Px_mean ratio. The ice velocity is varied and the trim angle is fixed.

First looking at the top figure, the relation is not very clear. The SD of Mx is assumed to be independent of the trim angle and ice thickness and to be safe the conservative value of 9 m is taken for all trim angles. When looking at the relation with the relative velocity, the lines are all slightly increasing. Using the average slope the SD of Mx gets the following equation:

$$SD_{mx} = Pxmean * \left(6.75 + 9 * 0.25 * \left(\frac{v}{0.5}\right)\right)$$

The value used here for Px_mean is excluding the transient factor. The reason for this is that the amplitude of Mx does not grow during the transient phase but has its maximum value right away.

3.2.7 MY_MEAN

My is a moment and therefore a consequence of the forces working on the vessel and one would therefore expect a good correlation between My and Px, and Pz at any given moment in time. The correlation between the moment and the forces are equal to the arm of the force around the COG. The correlations which each of these two forces will be investigate in turn, starting with Px. Since Py does not cause a moment over the y-axis it is not checked.

3.2.7.1 CORRELATION WITH PX

As Px is the largest of the three forces one would expect it to give the largest contribution to My. When looking at Figure 3-44, one can see that there is a clear linear relation between My and Px at each time step, while there is no clear relation with Pz yet. This shows that My is mainly dependent on Px.

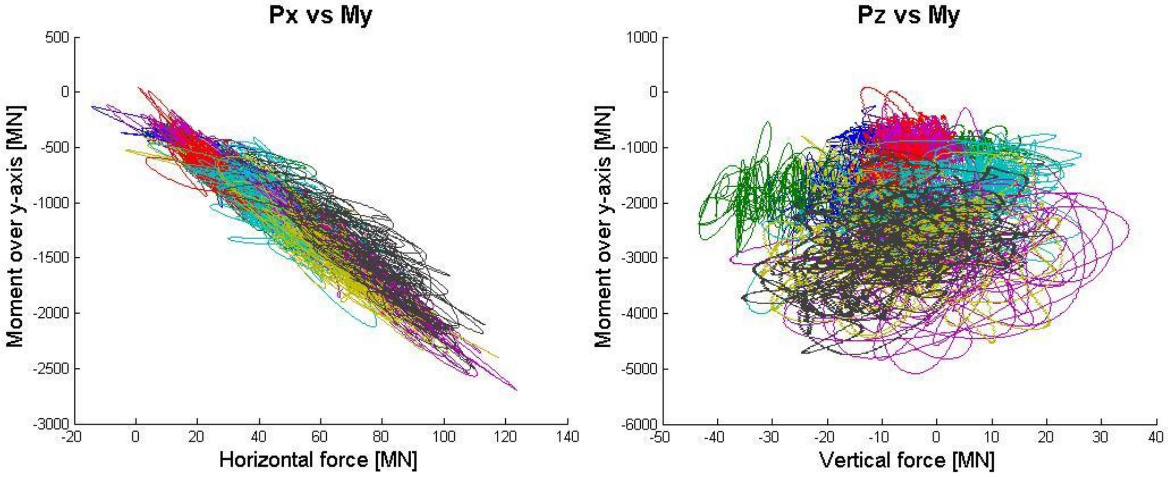

Figure 3-44: Relation between Px and My (left) and Pz and My (right) at the same time instance. Each color is a different test. Note that the values in the right graph are not correct as they are not scaled properly.

Prior to making the graph above, the data from the model test concerning the My-moments had to be scaled to the correct coordinate system. In the original data KSRI calculated the moments around the keel of the vessel. However in reality the vessel will rotate around its COG and thus the moments should be calculated around that point. The scaling of the moments was done as follows:

$$M_{y,px,scaled} = M_{y,krsi} * \frac{1}{distance(ice \rightarrow keel)} * distance(ice \rightarrow COG)$$

$$M_{y,px,scaled} = M_{y,krsi} * \frac{1}{39} * 18.308$$

After the scaling the next step was to curve-fit the relation shown on the left in Figure 3-44. Because My is a moment, the relation with Px would the arm around the COG. For this reason the following equation was used to curve-fit:

$$M_{y,px,scaled} = a * P_x = -18.289\ m * P_x$$

This shows that scaling factor is almost equal to the distance between the force and the COG or that the original KSRI data scaled pretty much exactly linear with the arm of the force. The negative sign is also correct. When a positive horizontal (X) force is acting on the vessel it does so above the COG. Therefore it creates a negative moment, thus verifying the minus sign.

3.2.7.2 CORRELATION WITH PZ

Next the part of My that was caused by Px can be removed from all the data. Then it can be checked whether there is any correlation with Pz. In Figure 3-45 this dataset is shown.

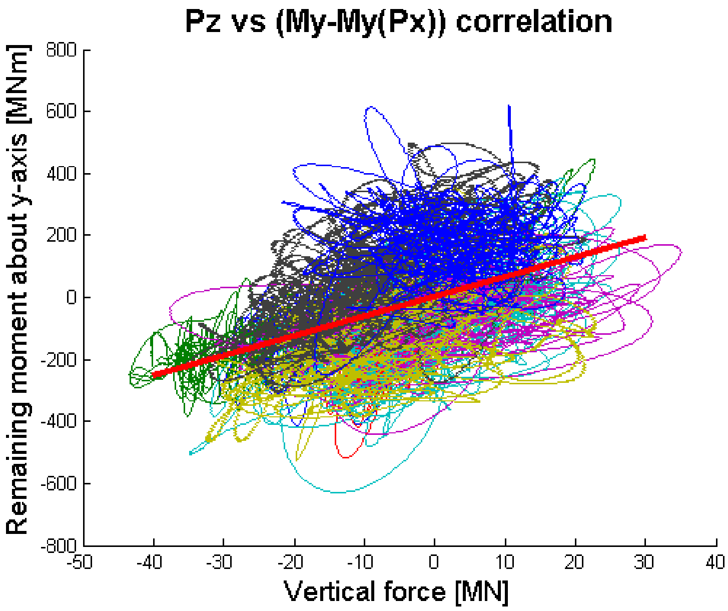

Figure 3-45: The remaining My moment plotted against Pz. The data-cloud shows a weak correlation. The red line is the regression line.

Next to dataset is curve-fitted in order to find the correlation (the arm of the force) between Pz and My.

$$M_{y,pz,scaled} = +6.356\, m * P_z$$

The positive sign is correct as the vertical force is acting on the vessel in a line that is in the negative x-domain. A positive Pz force should create a positive My moment, so the sign is correct. The value of the arm does not make much sense as it is not even close to the arm that one would expect when looking at the geometry of the vessel (49 meters). A possible reason could be that the measurements of Pz are not extremely reliable as explained before in section 3.2.4.

3.2.7.3 THE UNCORRELATED PART OF MY_MEAN

Figure 3-46 shows the remaining My-moments after removing the components correlated with Px and Pz. One can see that for all the tests the mean value is still not zero. Also there does not appear to be a clear relation between the values (when going from 1.5m to 2.0m the moments drop and when going to 3.0m they increased again).

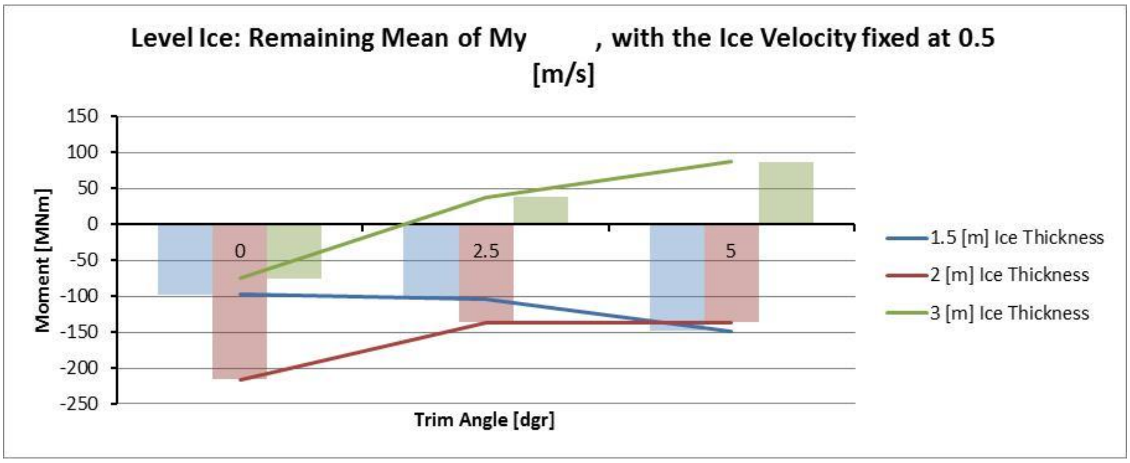

Figure 3-46: The remaining My-moment after removing the components correlated with Px and Pz!

The uncorrelated part will be ignored and not be incorporated in the ice model because the remaining part of the mean of My is only about 10% of the mean prior to removing the components correlated with Px and Pz and because there is no clear source to explain this component (no correlation with Py, the ice thickness/velocity or trim angle).

The final equation for My_mean is:

$$M_{y,mean} = -18.209\,m * P_x + 6.356\,m * P_z$$

3.2.8 MY_FLUC

After the components of My that were correlated with Px and Pz where removed the SD was calculated of the remaining signal.

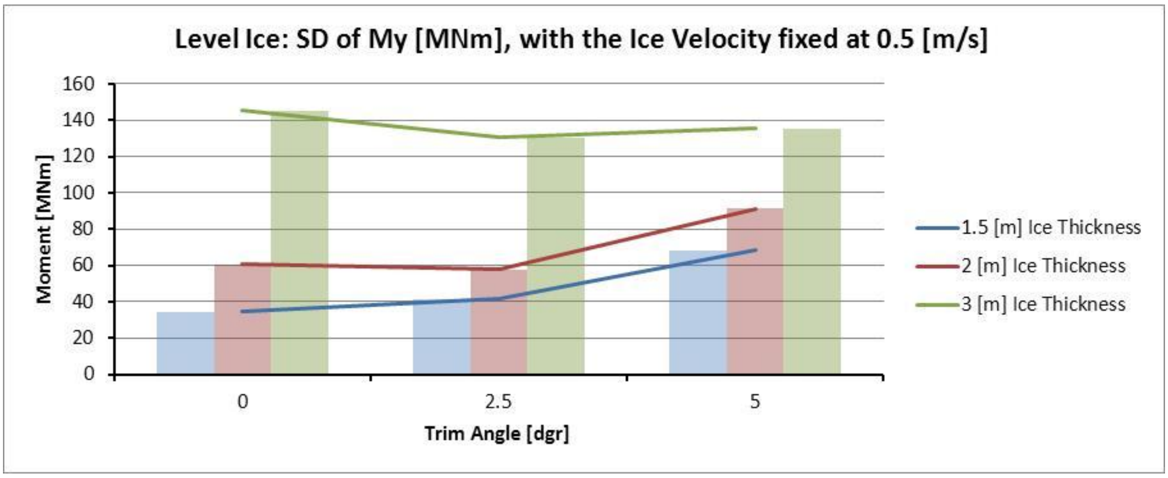

Figure 3-47: The SD of remaining part of My.

The SD of the remaining My component has no correlation with the trim angle or the ice velocity, only with the ice thickness. The three lines above are simplified to three values by averaging them:

$$\begin{aligned} 1.5\,m&: \quad 48\,MNm \\ 2.0\,m&: \quad 70\,MNm \\ 3.0\,m&: \quad 137\,MNm \end{aligned}$$

The three data points are then divided by the ice thickness to ensure that all terms in the equation are dependent on the ice thickness as this would results in an equation which is not zero at an ice thickness of zero. This gives the following values:

$$\begin{aligned} 1.5\,m&: \quad 32\,MNm \\ 2.0\,m&: \quad 35\,MNm \\ 3.0\,m&: \quad 46\,MNm \end{aligned}$$

These data points are then curve-fitted to give the following equation:

$$SD_{my} = 3.304 * t^3 - 5.805 * t^2 + 33.358 * t \qquad [MNm]$$

3.2.9 MZ_FLUC

Mz is one of the three load components whose mean is zero due to symmetry, therefore only the fluctuating component has to be looked at. Below the ratio of the SD of Mz to Px_mean is plotted.

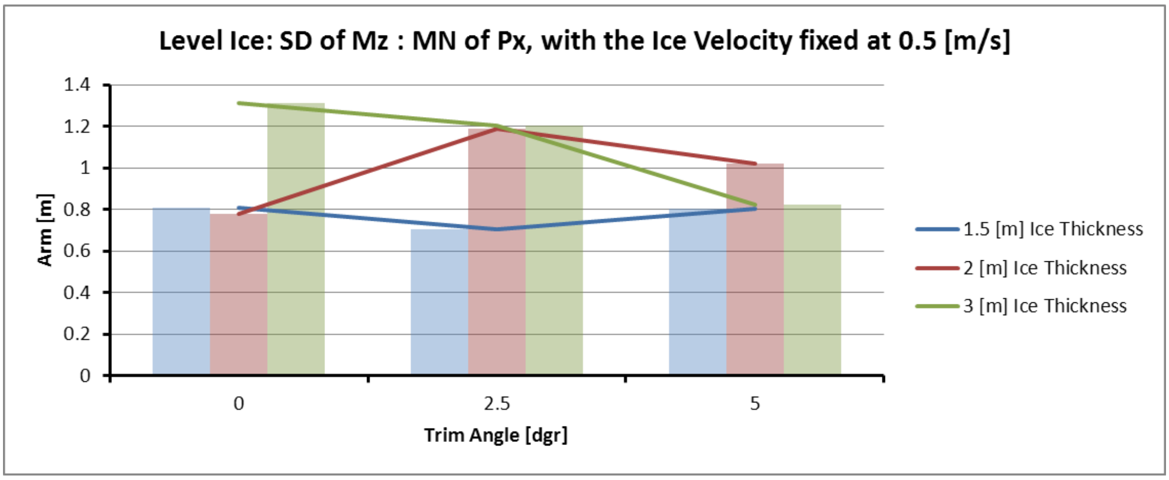

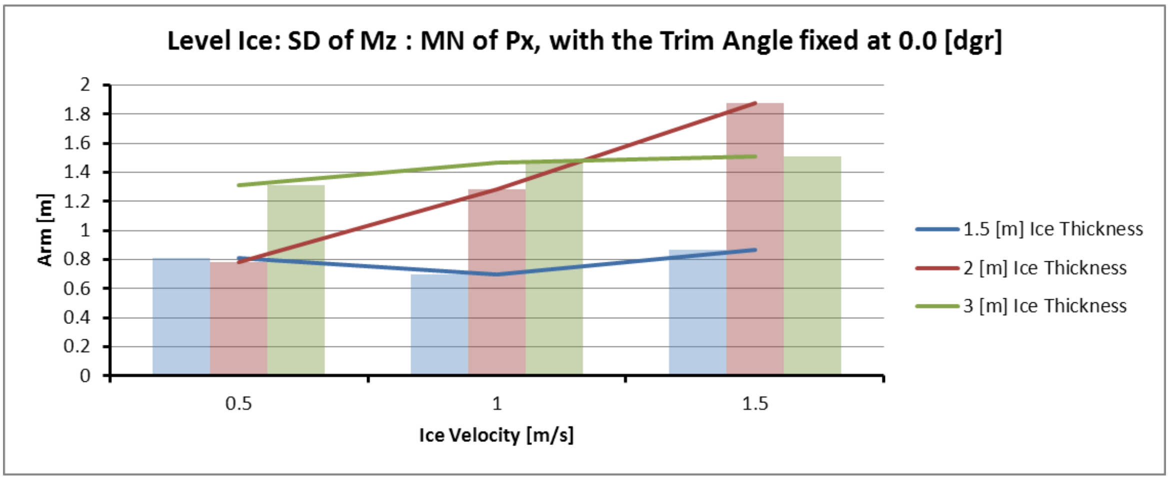

Figure 3-48: The standard deviation of Mz to Px_mean ratio plotted for all tests.

It was assumed that the SD of Mz is independent of both the trim angle and ice velocity. All the six values for each ice thickness can then be averaged and curve-fitted to get the following equation:

$$SD_{mz} = Pxmean * (-0.1013 * t^2 + 0.7384 * t)$$

The value used here for Px_mean is including the transient factor. The reason for this is that the amplitude of Mz grows during the transient phase.

3.3 CONCLUSION

As the subsections of this chapter already contain their own recommendation or conclusion they are not included in this final conclusion (see section 3.2.1.7 from recommendations related to Px and see section F.1.7 for the conclusion about spectrums).

A few more conclusions and recommendations not listed in the subsections:

- Do a more detailed calculation or model tests to determine the added mass of the JBF Arctic when it is surrounded by ice. This way of better understanding of the impact of the adjacent ice sheet and rubble can be obtained.
- Calculations or model tests should be done in order to determine the radiation damping caused by the propagation of waves through the ice sheet.
- The data of Pz was very poor. More attention should be paid to the other components next time model tests are done.

4 OPTIMISATION OF THE MOORING SYSTEM

The ice model has now been finished and can now be used in time-domain simulations. Before, the ice model was combined with the dynamic model of the vessel in Simulink. For the final phase of the thesis the dynamic model will be replaced with AQWA. AQWA is an extension of Ansys and is based on potential theory to solve the hydrodynamics. The advantage that AQWA offers above the Simulink model are:

- *The current and wind forces are already integrated*
- *It can calculate the dynamics of the mooring cables*

The downside is that the AQWA calculations take quite a bit more time due to the Matlab-AQWA interface.

In order to integrate the ice model with AQWA, the part of the Simulink model dealing with the generation of the ice loads had to be rebuilt in Matlab. After this the Matlab ice model integrated with AQWA as an external force using the interface programmed by employees of Huisman. Once this had been completed and tested the required time-domain simulations could be done in order to obtain the required data.

The basis for this chapter is a report written by a Huisman employee (IVR, 08-04-2011) *called the static mooring report. In this report a total of 30 different mooring systems are evaluated and finally 5 mooring systems are chosen each optimized for a different water depth (200, 350, 500 and 850 m, there are two for 350 m water depth). For the ice loading the regression model for the mean of Px made by KSRI was used.*

During this chapter one of the five final mooring systems from the static mooring report is chosen and used for the remainder of this report for comparison and optimization: the one design for a water depth of 350 meters. The maximum global restoring force (MGRF) that this system can handle is 51.1 MN if the ice is moving along the x or y-axis. If the ice moves along a diagonal then the MGRF is only 37.2 MN. See Figure 4-1 for details.

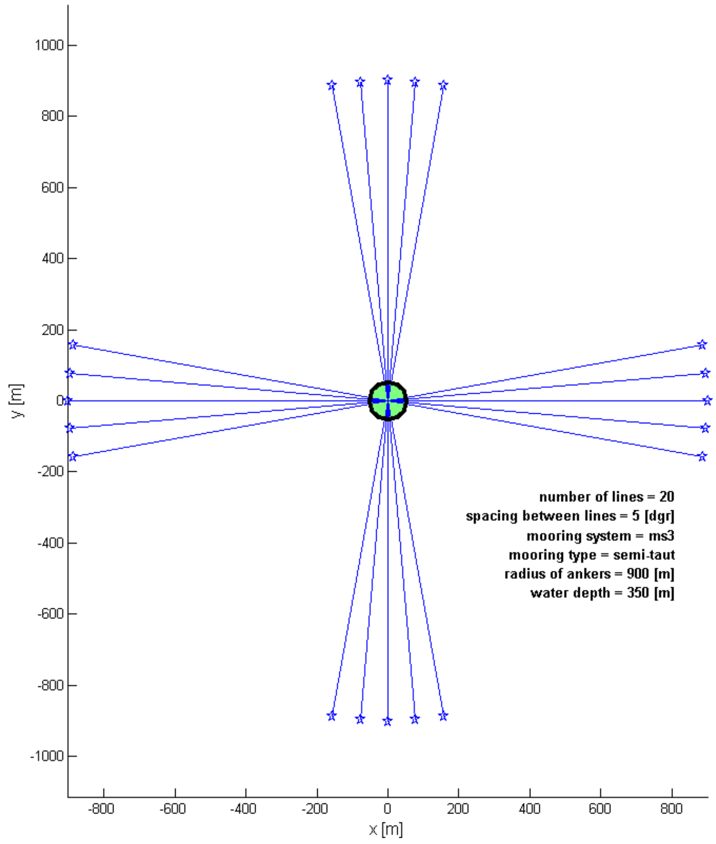

General properties:
Mooring type = semi-taut
Number of lines = 20
Bundles = 4
Spacing between lines = 5 degrees
Anchor radius = 900 m
Water depth = 350 m

Line makeup (starting at the hull):
50 m – R4 Chain – D = 162 mm
536 m – Polyester – D = 300 mm
350 m – R4 Chain – D = 162 mm

Figure 4-1: The layout and properties of the original mooring system designed for 350 m water depth from the static mooring report.

First the design criteria are listed in section 4.1. In section 4.2 preliminary analyses are done to check the influences of certain parameters on the performance of the mooring system and to find any flaws in the design.

In section 4.3 an analysis is done on how to design for ice. Based on this analysis and the improvements points from section 4.2 a new mooring system is designed in section 4.4. The conclusion of this chapter can be found in section 4.6.

4.1 DESIGN CRITERIA

The design will be done according to DNV-OS-E301 Position Mooring (October 2008). Although this code says that loading due to snow and ice should be taken into account, no design criteria are specified nor does it contain any information of how to design for ice. However as no other code is available at the moment for designing for interactions with ice the design will be done according to the code.

The code specifies three design criteria: ULS (ultimate limit state), ALS (accidental) and FLS (fatigue). In this report the ULS and ALS will be checked and operational limits, FLS is not checked.

ULS

In the ULS the vessel has to be able to withstand environmental loads with a 100 year return period. At the moment there is no clear definition yet for ice conditions with a 100 year return period. Therefor the goal of this thesis is to design a mooring system for level ice of about 3 meters thick. In the ULS there are two criteria: one for the offset of the vessel and one for the line tension. They are discussed below.

ULS - Offset

The requirements of the offset are not set by DNV but by the operator of the vessel. In this case we are dealing with a fictitious product and there is no client yet so the limit states were estimate by a Huisman employee based on experience. However as that person is no longer working for Huisman the reasons behind the exact values is not clear.

The maximum offsets are defined as a percentage of the water depth. The reason for this is that the limit is imposed by the riser-string spanning the water column. This is especially critical while drilling operations are going on so the maximum offset during operations is very low, around ~3-5% of the water depth. If the offset becomes larger than this, drilling has to be stopped and can be restarted once the vessel's offset is within the safe zone again.

While drilling has stopped another, higher, maximum offset applies. The riser-string can be seen as a fixed-fixed beam, so any horizontal offset of the vessel will result in forced deformations of the riser-string which can result in rupture or buckling of the riser-string. For this reason a maximum offset of the vessel is prescribed to guarantee the integrity of the riser-string. If the offset exceeds this maximum than the riser-string has to be disconnect in order to avoid damage to the string and the vessel. The criteria that will be used in this report are 12% of the water depth for catenary systems and 8% of the water depth for semi-taut systems.

Finally DNV-OS-E301 Ch2 Sec2 D702 (page 34) says the following:

"When the unit is connected to a rigid or vertical riser (e.g. drilling riser), the maximum horizontal offset is limited by the maximum allowable riser angle at the BOP flex joint. A safety margin of 2.5% of the water depth shall be included."

It is assumed that this safety factor is already included in the offset limit found in the static mooring report.

ULS – Line tension

The JBF Arctic is classified as a Class 2 vessel; this means that failure of the mooring system is likely to lead to unacceptable consequences such as loss of life or uncontrolled outflow of oil or gas. The following safety factors have to be used for the ULS of the mooring line tension:

$$MBL - T_{c,mean} * \gamma_{mean} - T_{c,dyn} * \gamma_{dyn} \geq 0$$

$$MBL - T_{c,mean} * 1.4 - T_{c,dyn} * 2.1 \geq 0$$

Where $T_{c,mean}$ is the mean part of the cable tension and $T_{c,dyn}$ is the dynamic part of the cable tension. γ_{mean} and γ_{dyn} are the corresponding safety factors.

ALS

For the ALS the same environmental conditions apply as the ULS, e.g. those with a 100 year return period. The only difference is, is that in the ALS one of the mooring line has failed. The same maximum offset applies and the following safety factors apply to the line tension:

$$MBL - T_{c,mean} * 1.0 - T_{c,dyn} * 1.25 \geq 0$$

General notes from the code

- C2-S2-B107; the visco-elastic properties of the synthetic fiber ropes are ignored and the material is assumed to be elastic so the elasticity modules does not change over time.
- C2-S2-B205; the duration of the ice is taken as three hours, even though there is no real good physical reason to choose this duration as ice does not come in storms like waves, its length is enough to provide adequate statistics.
- C2-S2-B206; the required extreme values shall be estimated as the MPM (most probable maximum) value of the extreme value distribution for the line tension.
- C2-S2-B209; time-domain simulations are required as the effect of the anchor line dynamics has to be included.

Special criteria for polyester

For polyester sections there is an additional criterion which says that the polyester section of the line can never come in contact with the seabed. The reason being that polyester has a weak resistance against abrasion which would be occur when the lines are repeatedly coming into contact with the seabed.

Uplift angle

An important design criterion for anchor is the uplift angle. This is the angle that the mooring line makes with the seabed at the anchor point. Normally this angle cannot become too large to avoid pulling the anchor out from the ground. However due to the large force on the anchors a special anchor will already be required. For this reason it was decided to ignore this rule and to do evaluate special types of anchors such as piles at a later stage.

4.1.1 DYNAMIC VERSUS STATIC SAFETY FACTORS

The static analysis was done by Huisman in 2011 right after the model test data was received from KSRI. In this report only the mean part of the ice loading was used. The ice model constructed during this thesis also takes the fluctuating part in to account in addition to the mean part. It is interesting to check when the dynamic approach will result in larger forces based on the different safety factors.

Safety factors

DNV requires a safety factor of 2.5 if you want to do a static calculation. However this high safety factor proved to be too high so a switch was made to the ABS rules which only require a safety factor of 2.0 for the static calculation. This results in the following equation for the line tension:

$$MBL - T_{c,mean} * 2.0 \geq 0$$

For the dynamic case DNV requires the following safety factors as shown before:

$$MBL - T_{c,mean} * 1.4 - T_{c,fluc} * 2.1 \geq 0$$

Because there are no safety factors for the offset, the limit-states related to the offset are not affected by the switch from static to dynamic.

When does the dynamic line tension become higher than the static one?

Depending on the ratio between the mean and fluctuating component of the line tension the dynamic case can either be lower of higher than the static case. For this calculation the ABS 2.0 safety factor for the static case is used.

$$Static: \quad 2.0 * F_{ice} \leq MBL \rightarrow F_{ice} = \frac{MBL}{2.0}$$

$$Dynamic: \quad 1.4 * F_{ice} + 2.1(\alpha - 1)F_{ice} \leq MBL, \quad where\ \alpha = \%\ increase\ in\ design\ load\ due\ to\ dynamics$$

$$F_{ice} = \frac{MBL}{1.4 + 2.1(\alpha - 1)}$$

The dynamic load is larger than static when:

$$\frac{MBL}{2.0} \leq \frac{MBL}{1.4 + 2.1(\alpha - 1)} \rightarrow 2.0 \geq 1.4 + 2.1(\alpha - 1) \rightarrow \alpha \geq 1.286\ [-]$$

So when the increase due to the fluctuating component is greater than 28.6 % the dynamic case has a lower maximum line tension than the static case.

This can be rewritten to give the percentage of the total load:

$$\frac{0.29}{1.29} = 0.225\ [-]$$

So if fluctuating component is larger than 22.5 % of the total load then the dynamic case has a lower maximum line tension than the static case.

With the DNV safety factor of 2.5

The same calculation can be done but now with the safety factor required by DNV for the static calculation which is 2.5. This gives the following results:

- When the increase due to the fluctuating component is greater than 52.4 % the dynamic case has a lower maximum line tension than the static case.
- If fluctuating component is larger than 34.4 % of the total load then the dynamic case has a lower maximum line tension than the static case.

This concludes the description of the limit states.

4.2 PRELIMINARY ANALYSES OF THE MOORING SYSTEM

Before designing the new mooring system it is interesting to investigate the impact of certain parameters so that their effects are known when doing the final design. Below is a list of the checked parameters:

- Cable dynamics
- Wind and current loading
- Assumption of the flat spectrum
- Dynamic versus static approach

The detailed analysis can be found in Appendix G. Below a summary is presented of the results.

Cable dynamics: As the usage of cable dynamics is required by DNV it will be used as the default case (since its effects are not negligible, otherwise it could be turned off to saved computation time as using cable dynamics doubles it), however it is still interesting to note the impact it has on the calculation:

- The vessel's MPM offsets are barely influenced by cable dynamics; it is reduced by about 1-3%.
- For the 0 degree ice direction cases cable dynamics on average reduces the MPM line tensions by about 10%. For the 45 degree cases the differences are about -1 to +1%.
- Cable dynamics has the same impact on both semi-taut and catenary mooring systems.

Wind and current loading

- The impact on the offset is quite small for the extreme ice cases and only results in an increase of about 3-5%.
- For the more modest ice cases the increase due to the wind and current is much more significant (increased by 10 to 60 %). However it should be noted that the values taken for the wind and current were the extreme values and thus under normal circumstances the loads would be less. But even then there will still be a significant impact on operability.
- The impact of wind and current on the fatigue limit state will probably be fairly significant and definitely should not be neglected.

Assumption of the flat spectrum

- When increasing the SD of the ice load the resulting increase in the SD of the fluctuating components was checked. The ratio between an increase in the SD of the load and an increase in the SD of the **offset** is **0.92 [-]** and **0.76 [-]** for the **line tension**.
- Because the fluctuating component of the offset is only a relatively small part of the total offset (fluctuating + mean), any increase in the fluctuating component of the offset only has a minor increase in the overall offset. This same applies to the line tension.

Dynamic versus static approach

- **General differences**

    - When directly comparing the maximum allowable ice thicknesses for the static and the dynamic case the dynamic case falls short be about 10 to 25 %.
- **Notes for the optimization**

  After this an optimization will be done of the layout of the mooring system. There are two points of weakness in the mooring system designs from the static report which will be improved upon during the optimization:

    - The most important result is that for all cases the maximum ice conditions are limited by the offset of the vessel. In general only 65-75% of the maximum allowable line tension is used when the offset has already reached the full 100% that is available (the last two columns in the table). During the optimization one of the main goals will be to rebalance the distribution between the two design criteria so that they will both be utilized around 100%.
    - The second most important result is that, with the mooring system from the static report, the mooring system can handle higher ice conditions in the 45 degree direction than in the 0 degree direction. On average the maximum allowable ice thickness in the 0 degree direction is 10-15% lower than in the 45 degree direction. As the JBF Arctic has to operate in many different areas it is very unlikely that all of these areas will have ice coming from one particular direction at all times. During the optimization the second goal will be to minimize the difference in strength between the different directions.

This concludes the preliminary analyses of the mooring systems from the static report. The results will be used in the when designing the improved version of the mooring system.

4.3 DESIGNING FOR ICE

This section was written based on several discussions with Andrei Metrikine and Gus Cammaert and the other committee members.

In section 4.1 the requirements from DNV-OS-E301 were discussed and one of them was that in the ULS and ALS the mooring system should be designed for an environmental load with an occurrence probability of once every 100 years. For waves (which the code based around) these survival conditions can be found by using long-term statistics to estimate the corresponding H_s (significant wave height) and T_0 (zero crossing period).

For ice no such method has been developed yet. Although there are many parameters which influence the loading caused by ice there are two which are very important: the ice thickness and the ice velocity. In addition to these parameters the ice differs from waves in that it can come in multiple physical forms, where each ice feature results in a different load on the vessel. As there is no method yet to determine the 100 year ice conditions the vessel will be designed for the highest possible ice conditions possible.

In this thesis the focus is on designing a vessel for interaction with level ice of a particular ice thickness and velocity. However in reality the ice will never have one specific ice thickness or velocity for an extended period of time because both parameters will vary over time. Due to the large mass the ice velocity will not change very rapidly in time. However the thickness can change dramatically over only a small distance and in addition ridges can occur which results in even larger forces.

Large ridges cannot be handled by the vessel due to the extremely large forces required to break them. This means that the vessel on its own can only handle very small ridges. However by using an ice breaker the ridges and level ice can be broken down into smaller pieces which induce a much lower force on the vessel.

In total three different kinds of ice scenarios have to be analyzed:

- Only level ice

- Level ice with a small ridge
- Broken ice due to an ice breaker

Only level ice

During the model tests most of the tests were done with level ice. The availability of the data allowed the ice model to be created which makes it relatively easy to find the maximum level ice conditions that the vessel can handle. Although this type of loading is not realistic it will be checked as it was requested by Huisman as it gives them a good indication of the allowable ice conditions.

The way this will be done is to do several time-domain simulations with level ice of a certain thickness and velocity. By increasing the thickness and velocity the maximum ice conditions can be found which results in a vessel offset and line tension which is just below the design criteria.

Level ice with a small ridge

This type of loading is more realistic in that it takes into account the occurrence of a ridge. In this case it would be possible for the JBF Arctic to operate on its own without the assistance of ice breakers. Two tests with ridges were done so this type of loading will be analyzed.

What will be done is to use the ridge multiplication functions determined in section 3.2.1.6 to add a ridge to level ice with a certain thickness and velocity. This way the maximum level ice conditions including a ridge (small and large) can be determined.

Broken ice due to an ice breaker

This is the most realistic kind of loading especially for the regions with more severe ice conditions and larger ridges where the JBF Arctic can no longer operate on its own and the assistance of an icebreaker is required in order to break down the ice features and reduce the loading. Although a few tests were done with broken ice much more information is needed before this kind of loading can be analyzed:

- Information is needed on the performance of ice breakers and the type of broken ice that they produce from a certain type of level ice or ridge.
- Based on this information more model tests need to be done so an ice model can be made to predict the loads from the broken ice.
- After this an extensive study should be done to determine what kind of ice breakers and other ice management features are needed in order to ensure and timely breakdown of approaching hazardous ice features and guarantee a safe operation of the JBF Arctic in a certain area.

Since the required data is not available this analysis should be done in future research.

Conclusion

The types of ice loading that will be checked are level ice and level ice in combination with a ridge.

4.4 IMPROVING THE MOORING SYSTEM

While comparing the results from the static and dynamic case two problems came forward with the original design of the mooring system:

- The non-uniform distribution of the mooring lines results in a large gap between the minimum and the maximum load. Because the minimum case limits the mooring system reducing the gap will increase the overall performance of the mooring system.

- The line tension capacity remains largely unused while the offset capacity is maxed out, e.g. the offset is proven to be the limiting factor for the designs from the static report. By rebalancing the distribution between the two design criteria a more optimized design can be achieved.

First the layout of the mooring system will be optimized to get a more uniform stiffness of the mooring system. After that the pre-tension will be optimized to get a better distribution between the usage of the line tension and the offset of the vessel. Finally the following other parameters are investigated to see if changing them can lead to improvements: anchor radius, laid length and the choice of materials for the lines.

Several times in this section the MPM of a certain parameters is shown. How this is calculated is explained in Appendix H.

4.4.1 THE LAYOUT

The base case for the layout comes from (IVR, 08-04-2011) and is shown in Figure 4-2.

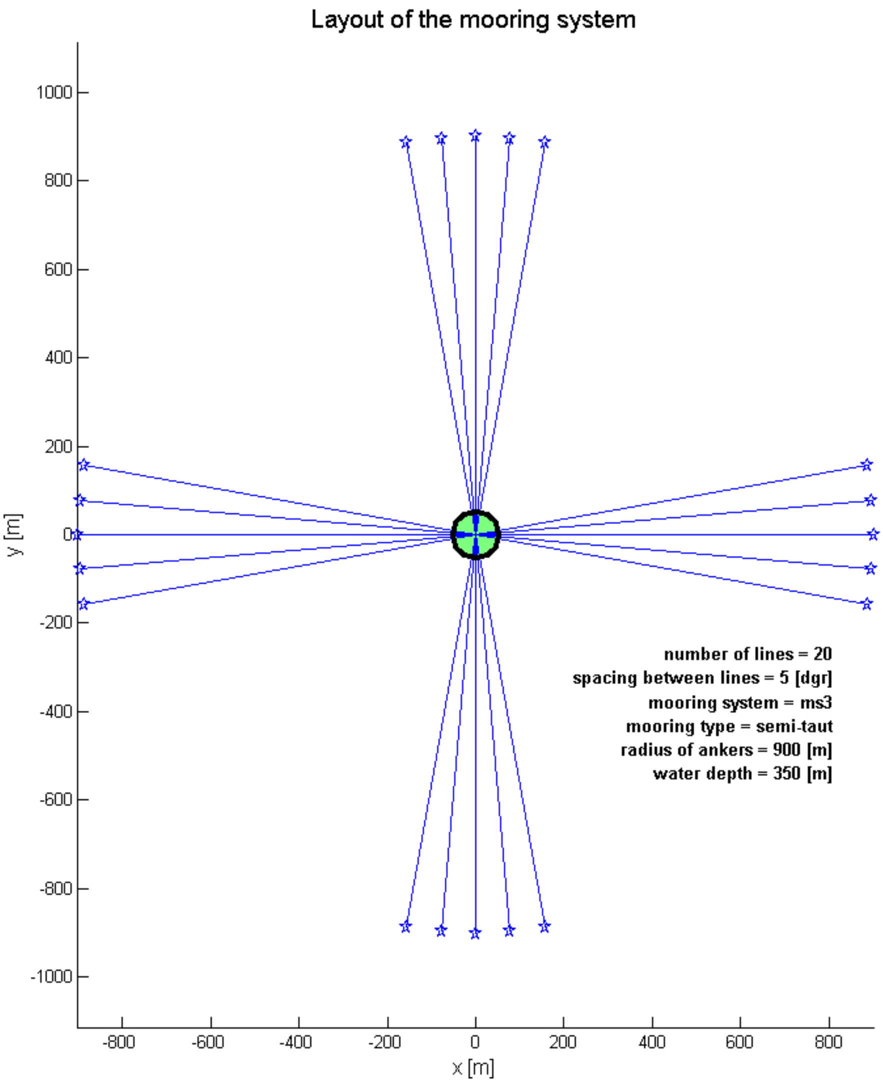
Layout of the mooring system
1000
800
600
400
200
0
-200
-400
-600
-800
-1000
y [m]
-800
-600
-400
-200
0
200
400
600
800
x [m]
number of lines = 20
spacing between lines = 5 [dgr]
mooring system = ms3
mooring type = semi-taut
radius of ankers = 900 [m]
water depth = 350 [m]

Figure 4-2: The layout of the mooring systems used in the static mooring report, 4 bundles of 5 lines each.

The problem with the layout above is that its stiffness is highly dependent on the direction of the motions. If the vessel moves along the X- or Y-axis then the stiffness is the highest. However along the diagonals the mooring system is much less stiff, see Figure 4-3.

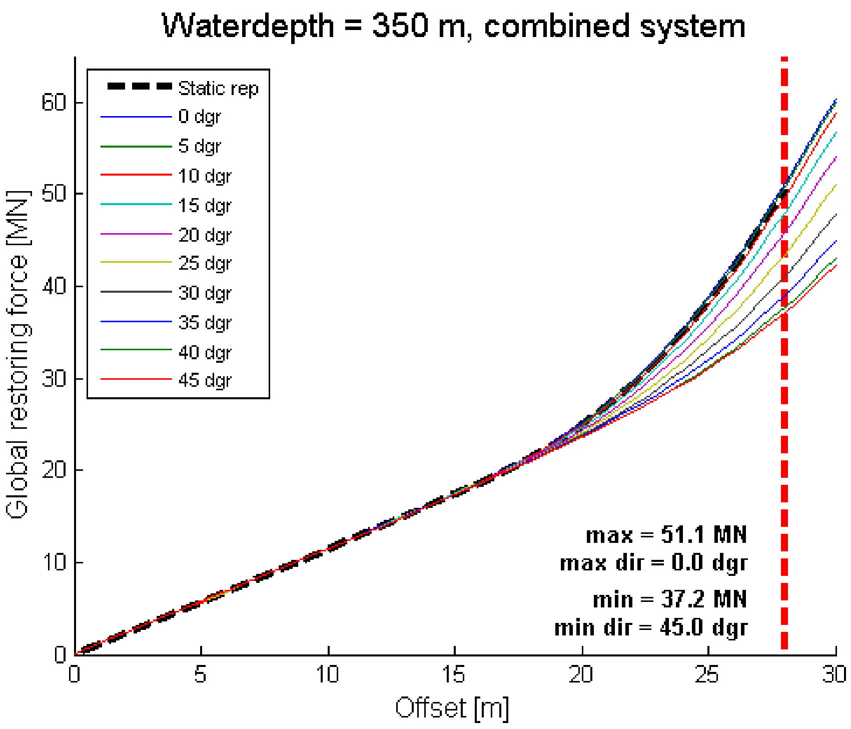

Figure 4-3: The impact of the direction on the stiffness of the vessel. The maximum global restoring force (MGRF) for a certain direction is defined as the global restoring force achieved at the maximum offset (red line). The directionally dependent stiffness results in a minimum MGRF of 37.2 MN and a maximum MGRF of 51.1 MN.

Due to the directionally dependent stiffness the maximum global restoring is 51.1 MN (in the X- and Y-direction) while the minimum is 37.2 MN (along the diagonals). As the ice can come from any direction this means that the maximum global restoring force (MGRF) is limited to 37.2 MN. This variation of the MGRF over the direction can be reduced by distributing the lines more uniformly.

An important thing to keep in mind is how a broken line influences the system capabilities of the system since this required by the ALS. Therefore the maximum global restoring force with a broken line is also included in

Global restoring force for 20 lines					
		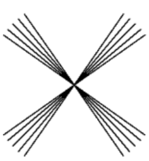	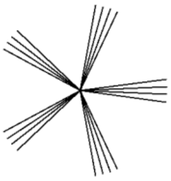	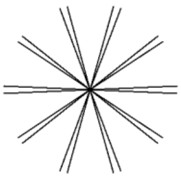	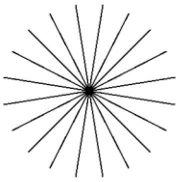
Bundles:	**[-]**	**4**	**5**	**10**	**20**
Lines/ bundle	[-]	5	4	2	1
Normal: Min MGRF	[MN]	37.2	41.1	44.3	44.3
Normal: Max MGRF	[MN]	51.1	47.6	44.5	44.4
Broken: Min MGRF	[MN]	31.2	33.4	33.9	33.9

.

Global restoring force for 20 lines				
	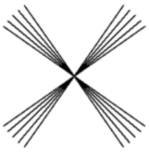	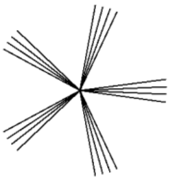	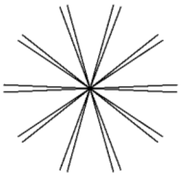	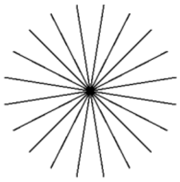
Bundles: [-]	**4**	**5**	**10**	**20**
Lines/ bundle [-]	5	4	2	1
Normal: Min MGRF [MN]	37.2	41.1	44.3	44.3
Normal: Max MGRF [MN]	51.1	47.6	44.5	44.4
Broken: Min MGRF [MN]	31.2	33.4	33.9	33.9

Table 4: The maximum global restoring force for several different layouts is shown. All four systems comprise of 20 lines but have a different amount of bundles. The space between lines within a single bundle is five degrees.

A couple of things can be seen; first, the minimum and maximum loads converge thus making the system's response more uniform. At 10 bundles the minimum and maximum MGRF have nearly converged so in this respect there is no difference between the 10 and 20 bundle system. In addition the 5, 10 and 20 bundle layouts have a higher minimum MGRF in the broken-line scenario than the 4 bundle layout. This means that for all cases the layouts with more than four bundles shows a better performance.

Position of the fairleads

The final thing to consider is the position of the fairleads. Inside the vessel winches have to be positioned that can reel in the chain during operation to shorting or lengthen the mooring lines. This allows the vessel to acquire a different mean offset which allows it to drill multiple wells from a single anchoring position. If the chain is reeled in the chain has to be stored within the vessel in a so called chain locker. The chain locker has to be vertical to avoid the chain forming a single pile and not taking up the full volume of the locker (this would require a crewmember to go into the locker and push the chain to make it fall over). As the chain lockers have to be vertical they have to be positioned inside one of the eight legs the JBF Arctic has. The legs also have to be used for other purposes so in the current design the winches and locker boxes were positioned in four of the eight legs, see Figure 4-4.

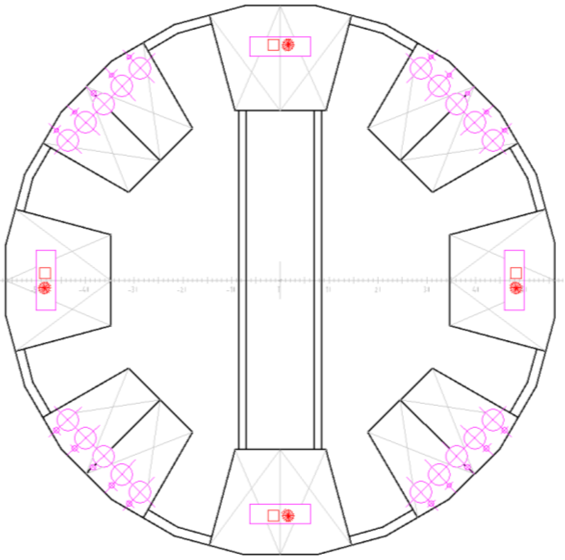

Figure 4-4: A cross-section of the JBF Arctic just below the deck box. The purple circles are the fairleads / chain lockers.

Figure 4-4 shows the position of the fairleads. As you can see the fairleads are positioned in four groups of five units each inside the orthogonal corners. As their position is fixed the switch from 4 to 10 or 20 bundles creates a minor problem. In the layout with 4 bundles the mooring lines extend radially outward from the center of the vessel, so if you draw a line from the center of the vessel to the fairlead and then to the anchor point you would get a straight line. For any other amount of bundles this is no longer possible, e.g. the position of the fairlead is no longer in line with the anchor and center of the vessel. This means that some of the lines have to be made a little bit longer. In

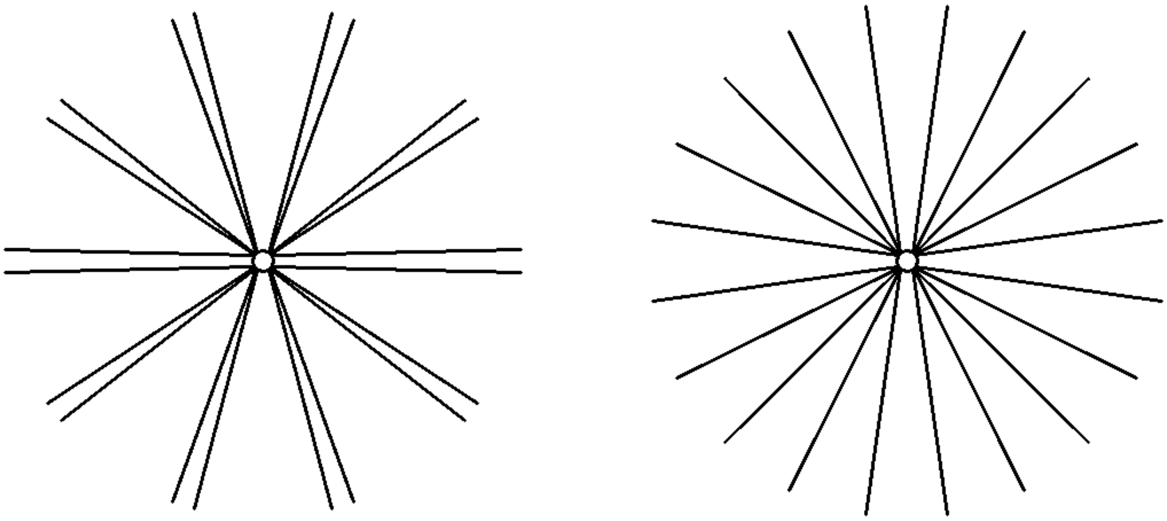

Figure 4-5: The impact of the location of the fairleads on the mooring systems with 10 and 20 bundle.

Now a decision has to be made between 10 and 20 bundles since they both have nearly the same MGRFs. The problem with the 10 bundle layout is that it is not possible to divide the lines between the four fairlead locations in a double symmetrical way. This would again results in different behavior for different directions. For this reason the 20 bundles layout is chosen. The only change that has to be made in order to accommodate the fixed location of the fairleads is to lengthen some of the lines because the fairleads are now slightly further away for some of the lines. If the lines would not be lengthened there would be a none-uniform pretension across all the lines which would results in some lines reaching the maximum allowable tension quicker than others.

The disadvantage of a 20 bundle mooring system

The 20 bundle mooring system has some disadvantages. When drilling near an existing platform, anchor lines of the drilling vessel are quite the nuisance. Normally, for safety reasons, a zone with an offset of about 100 – 200 meters is taken around the lines between the mooring lines of the drilling vessel and any possible nearby subsea equipment, pipelines or anchor lines of other vessels (which in turn have their own safety zone). This is shown in Figure 4-6.

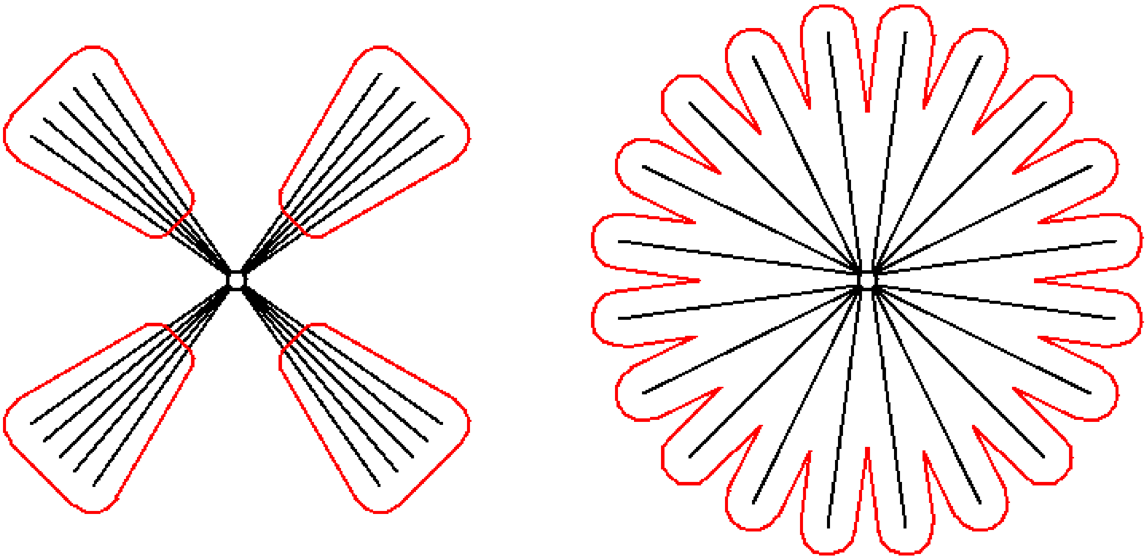

Figure 4-6: The required safety margin around the mooring lines are shown. A 100 meter margin was used while in reality a different one might be used, however this does not change the conflicts the margin creates.

The mooring lines are only in contact with the seabed towards the ends of the lines, so only there can there be no contact with subsea equipment. For the four bundle system pipelines and other lines can pass underneath the vessel through the four zones between the bundles. This is not possible for the 20 bundle system where the mooring lines completely block all approach angles thus making it impossible to drill within “anchor radius + safety margin” of any vessel or subsea items.

This means that when the JBF Arctic has to drill next to an existing platform a 4 or maybe 5 bundle system has to be used. This layout can be achieved with the same set of lines which are used in the 20 bundles system so no new system has to be bought and no parts have to be exchanged. The only downside is that this would again introduce a much stronger directional dependent responses of the mooring system, and thus lower the MGRF of the vessel. However as the arctic is an unexploited location for the offshore industry which does not contain any subsea equipment or platforms yet, for now the 20 bundle system can be used without any problems.

Summary

The 20 bundle system will be used because:

- It gives a minimum and maximum MGRF which are nearly identical.

- It gives a higher minimum MGRF for the broken line scenario (which is for the ALS).
- When the JBF Arctic has to operate near another vessel a 4 or 5 bundles layout could be used if needed.

4.4.2 THE NUMBER OF CABLES

The second parameter to look at is the number of cables to use in the mooring system. When trying to increase the strength of the mooring system an obvious thing to do is to increase the number of mooring lines. Figure 4-7 shows the increase in the minimum MGRF as a function of the number of lines. A uniform spacing between the lines was used (so the amount of bundles was equal to the amount of lines).

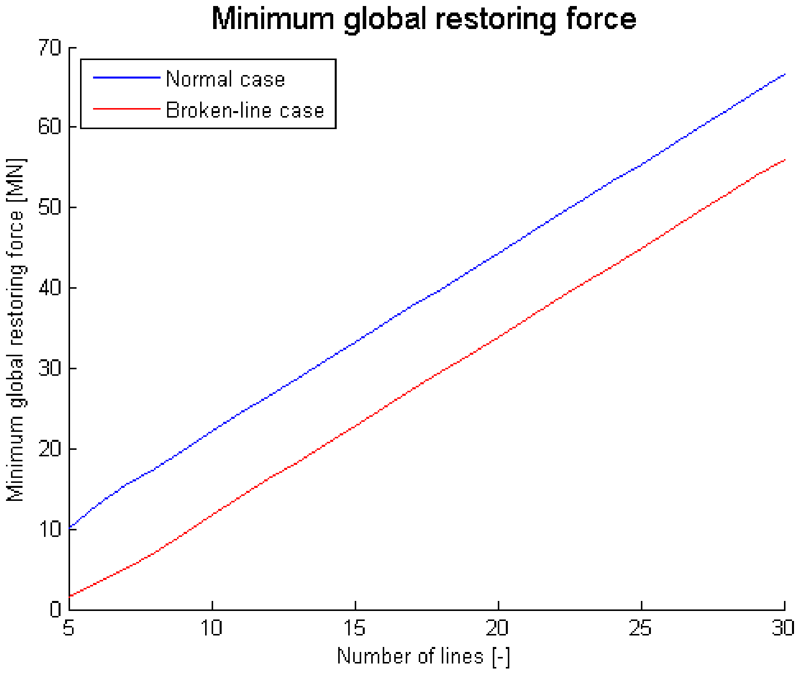

Figure 4-7: The global restoring force as a function of the number of cables for the normal and broken-line case.

When looking at the Figure 4-7 it certainly seems very appealing to increase the number of lines as it directly increases the MGRF. However there are several problems with changing the number of mooring lines:

- The weight capacity of a semi-sub is rather limited. This means that the weight of the semi-sub has to be carefully monitored during the design and that the allowable combined weight of the mooring system has already been pre-allocated during the concept design. Because of this it is not easy to increase the number of lines however there is some flexibility.
- As each line requires its own winch and chain locker, adding even more lines is very tricky because the available space is very limited.
- The fairleads need some room to allow them to move during operation but especially during the hookup-process of the mooring lines. While the lines are being installed their orientation is not fixed yet and so the lines can easy move and slam into each other. Because of this the lines cannot be too close to each other. As the available space for the fairleads is fixed adding more lines will put them closer to each other and cause problems.
- The engines that operate the winches are shared between each group (bundle) of mooring lines. By using a “switch” the engines can be connected to one or more of the winches to reel them in. The

total capacity for the engines is fixed so by adding more lines it will take longer to reeling in the lines if the vessel wants to move for instance. More engines could be added so this is only a minor problem.

Although increasing the number of mooring lines would allow the vessel to handle tougher ice conditions the number is limited by the space which is needed for all the support equipment. During the concept stage the number of lines was already gradually increased from 12 to 16 and finally to 20. At this point there is no more space available for additional lines.

4.4.3 THE PRETENSION

So far it has been established that 20 lines will be used, that they will be spread over 20 bundles, giving a uniform distribution and that due the fixed location of the fairleads some lines will have to be longer than others. In this section two more questions will be answered:

- How much longer do those lines have to be?
- Which pretension gives the highest minimum MGRF?

Setting different lengths for different lines

With the 20 bundles system and the fixed fairlead positions some lines need to have different lengths. A specific length should be chosen so that at an offset of 0 meters all lines have the same pretension. This ensures that at the maximum offset all the lines will have about the same line tension (they will differ slightly due to the different lengths). Because the location of the anchors and the fairleads are fixed, changing the length of the line changes the pretension in the line: the shorter the line the larger the pretension.

The length of the lines is calculated using a Matlab program written as part of this thesis. The lengths are determined iteratively by the program until it has converged to within the desired error from the target pretension which was specified by the user. During each iteration the length of the total line is changed by changing the length of the polyester section for the semi-taut systems. The chain systems only have one section so the length of that section is changed.

Finding the optimal pretension

After the pretension has been set and the program has found the lengths of the lines that result in the desired pretension, the response curves of the mooring system are shown, an example in shown in Figure 4-8.

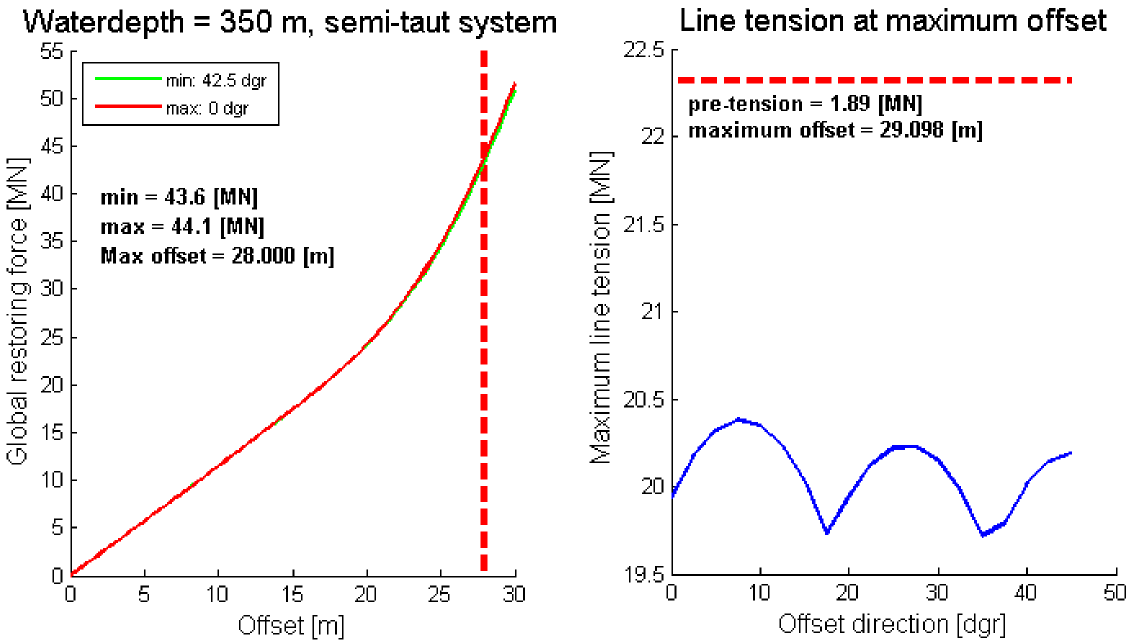

Figure 4-8: Left: the static response curves of the mooring system for the minimum and maximum direction. Right: the maximum line tension for different directions (the required safety factors by DNV are included).

The mooring system has two design criteria for the ULS: the maximum offset and the maximum line tension. For the semi-taut system the maximum offset is set at 8% of the water depth, this is equal to 28 m in the example shown in Figure 4-8.

The maximum allowable line tension is equal to the MBL (maximum breaking load) which is specified by the manufacturer of the material. In this example the MBL is equal to 22.32 MN. By checking at which offset the maximum line tension is equal to the MBL, the maximum allowable offset due to the line tension can be determined (shown in the right figure). When the offsets allowed by both criteria are the same then the pretension has reached its optimal level.

Below is a table which shows the impact of the changing pretension on the maximum allowable offsets due the line tensions when the vessel is at the offset criteria (28 meters).

Pretension [MN]	Max global restoring force at an offset of 28 m [MN]	Offset when max line tension = MBL [m]
2.2	53	26.735
2.1	49.8	27.498
2.03	**47.6**	**28.034**
2	46.7	28.272
1.9	43.8	29.044

Table 5: At a pretension of 2.2 MN, the pretension turns out to be too high. The mooring system is very stiff which results in a high maximum allowable load at the maximum offset of 28 m. However this will quickly exhaust the line tension so the offset at which the MBL has been reached is 26.735 m; this is below the desired 28 meters. The optimal pretension is this case is somewhere around 2.03 MN as both limit states are used to their full extent at this offset. With this pretension, at an offset equal to the maximum offset of 28 meters, the maximum line tension is equal to the MBL.

The process to find the optimal pretension for a certain mooring system for a certain ice condition has now been explained. Next the anchor radius will be looked at.

4.4.4 THE ANCHOR RADIUS & THE LENGTH OF THE BOTTOM CHAIN

By increasing the anchor radius a few properties of the mooring system are changed. Due to the increased length of the lines:

- The lines become more elastic.
- The laid length is longer which means that in general the uplift angle will be reduced.
- The angle at the fairlead becomes larger so the horizontal component of the restoring force becomes larger.
- The combined weight of the mooring system will become larger.

In the tables below the impact of the anchor radius and the length of the bottom section of chain is shown. It is important to note that each entry in the tables not only has a different anchor radius and bottom section length but also a different pretension. For each combination of parameters the pretension has been optimized as described in the previous section.

Anchor radius [m]	Maximum global restoring force [MN]				
	Length of bottom section [m]				
	350	400	450	500	550
900	47.6	47.6	-	-	-
950	48.8	49.3	48.9	-	-
1000	50	50.6	50.5	49.8	-
1050	50.7	51.6	51.9	51.7	50.7
1100	51.6	52.3	52.9	53.1	52.6

Table 6: The maximum global restoring force is shows for different anchor radii and bottom section lengths. The pretension was optimized for extreme ice load (3 m thick ice).

Anchor radius [m]	Maximum global restoring force - damaged case [MN]				
	Length of bottom section [m]				
	350	400	450	500	550
900	36.4	36.4			
950	37.5	38	37.6		
1000	38.6	39.1	39.2	38.5	
1050	39.2	40.1	40.5	40.3	39.3
1100	40	41	41.4	41.6	41.2

Table 7: The maximum global restoring force is shows in case of a broken line.

Anchor radius [m]	Vertical force [metric tonnes]				
	Length of bottom section [m]				
	350	400	450	500	550
900	2353	2884			
950	2144	2655	3169		

1000	1957	2429	2917	3415	
1050	1773	2219	2681	3153	3633
1100	1625	2019	2450	2897	3354

Table 8: The vertical force (weight) at an offset of zero meters.

Anchor radius [m]	Optimal pretension [MN] Length of bottom section [m] 350	400	450	500	550
900	2.03	2.53			
950	1.88	2.39	2.87		
1000	1.74	2.23	2.71	3.17	
1050	1.58	2.07	2.55	3.01	3.45
1100	1.45	1.9	2.37	2.83	3.27

Table 9: The optimal pretension at 350 m water depth for extreme ice load (3+ m).

The tables show a couple of interesting things:

- Increasing the anchor radius increases the maximum load. This is most likely due to the larger horizontal component of the restoring force at the fairleads.
- Increasing the length of the bottom section starts to reduce the maximum load if polyester section is removed in favor of a longer chain section (entries to the right/above the diagonal). This is probably due to the larger mass of chain compared to polyester.
- Increasing the anchor radius reduces the vertical load on the vessel (the weight of the mooring system at an offset of zero). This is probably due to the smaller pretension which reduces the tension force at the fairleads.

When choosing a set of parameters a few things need to be taken into account:

- When increasing the length of the chain section, the total weight of the mooring system quickly increases. Increasing the dry weight of the mooring lines will make installation more difficult and time consuming which will both add to the cost.
- Increasing the weight of the mooring system will also make it take up more of the weight carrying capacity.
- The material cost of increasing the length of the twenty lines is quite significant.

Conclusion

At this point it is hard to find out which combination of anchor radius and bottom section length is the most optimal one. The increase in MGRF is only a few percent while the increase in cost can be quite substantial; the increase in the amount of chain required is increased by 30-40% and the extra weight can make installation and handling of the lines much more difficult. The economic aspect plays an important role in the decision and as the required data is not readily available the optimization of these two parameters is not further investigated.

It is however important to note that an improvement of 11% is possible with the configurations investigated in this section. By checking other combinations with larger anchor radii even larger gains might be realized but probably at significant costs.

4.4.5 LINE MAKEUP

The last group of parameters to be investigated is related to the makeup of the lines themselves. In this section the impact of the following parameters are checked:

- Changing the diameters
- Using a different grade of steel
- Using different types of polyester
- Using either stud link or studless chain

4.4.5.1 DIAMETERS & STEEL GRADE

Increasing the diameter has the following impact:

- The MBL increases
- The mass of the system increases
- The hydrodynamic properties of the line changes (added mass and drag)

The change in MBL has a significant impact on the capabilities of the mooring system. The change in hydrodynamic properties has a negligible impact on the behavior, so its impact is further investigated.

For the semi-taut systems the lines are made up of two materials: chain and polyester. Both materials should have about the same MBL otherwise the chain will literally have a weakest link which will limit its performance.

R5 Diameter chain [mm]	Maximum global restoring force [MN]				
	Diameter polyester [mm]				
	274	281	286	291	296
142	45.2		45.5	45.3	45
147		47.3	48.6	48.4	47.9
152			49.6	51.7	51.2
157			49.7	51.7	53.7
162				52	53.9
167			50.3	52.1	54.2
172					54.5
177	46.8		50.5		54.6

Table 10: Maximum global restoring force as a function of the diameters. The optimal sets where the MBL of both materials are almost equal are highlighted in green.

When looking at Table 10 one can see that deviating from the optimal values has only a minor impact on the MGRF. Increasing the diameter of the polyester section above the optimal values actually reduces the MGRF while increase the diameter of the chain section results in only a minor increase which is insignificant compared to the extra costs and mass that also come with this change.

Steel grade

The grade of steel has a similar impact as increasing the diameter but it only increases the MBL and the other properties are unchanged. So by choosing a lower steel grade the diameter of the chain has to be increased to keep the same MBL. As a higher chain diameter has a lot disadvantages, the steel grade should be as high as possible. The only downside of the higher steel grade is the extra costs.

Conclusion

A set of diameters should be chosen where the MBL of both materials is the same. The maximum steel grade R5 will be used as this keeps the diameter of the chain as low as possible.

4.4.5.2 POLYESTER TYPES

During research of the available materials two different types of polyester were found; “normal” polyester and High Modules PolyEthylene or HMPE (also known as Dyneema, developed by DSM). The differences are best shown by comparing two different materials with diameters which results in a similar MBL:

	Polyester	HMPE
MBL [MN]	20.6	20.4
Diameter [mm]	274	171
Stiffness [MN]	576.8	1140

Table 11: The properties of the synthetic materials

Table 11 shows the two major differences between the two materials. As the name suggest HMPE has a much higher yield stress so its required diameter is significantly lower. Next HMPE’s stiffness, which is calculated by multiplying the elasticity modules times the area of the line, is significantly higher.

Next a similar mooring system is used to compare both types of material in action. When using HMPE the MGRF is reduced by about 5 MN or about 10% of the total MGRF, the reason is probably the much higher stiffness. The upside of the HMPE system is that the vertical load (mass of the mooring system) decreases by about 750 mt, which is about 34% of the total mass. However, because the MGRF is quite a bit lower, HMPE will be dropped as an option.

4.4.5.3 STUD LINK OR STUDLESS CHAIN

There are two types of chain available on the market, stud link and studless, see Figure 4-9.

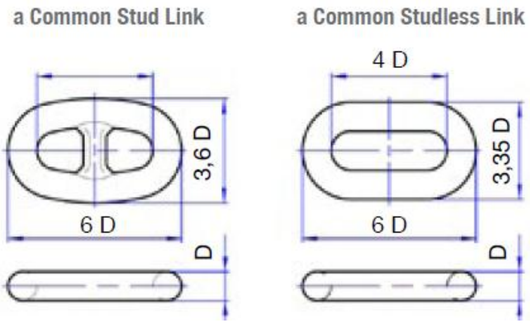

Figure 4-9: The two different kinds of chain.

When comparing several cases with both stud link and studless chains there is almost no difference in terms of MGRF. The increase in the vertical force at the fairlead is only around 6%. At maximum offset the relative increase in vertical force is even smaller.

Besides the calculation related items there are also some other aspect to consider:

- Stud-link chains have a slightly higher mass.
- Stud-link chains have up to 35% more fatigue resistance than studless chains, according to (Ramnas Offshore Safety), page 3.
- Stud-link chains are employed on rigs where the chain is often reeled in and out.

As the impact on the MGRF and vertical force is very low while the fatigue benefits are considerable, stud link chain is chosen.

4.4.6 OPTIMIZATION FOR A SPECIFIC ICE LOAD

During the design process of the mooring system used thus far the load on the system has been an arbitrary load and the MGRF of the mooring system is based on the static response of the system. As the focus of the thesis is on the dynamic interaction some extra steps are taken.

Because the dynamic part of the line tension has a different, higher safety factor then the static part, the ratio between the two is important as it determines how large the design line tension should be.

The design line tension is calculated as follows:

$$F_{design} = \%_{mean} * SF_{mean} + \%_{fluc} * SF_{fluc} = 1.4\left(1 - \%_{fluc}\right) F_{aqwa} + 2.1\ \%_{fluc}\ F_{aqwa}$$

$$F_{aqwa} = \frac{F_{design}}{1.4\left(1 - \%_{dyn}\right) + 2.1\ \%_{dyn}}$$

This means that the higher the percentage of dynamic load, the lower the force from AQWA can be and thus the lower the ice conditions that can be handled by the system. Based on preliminary calculations the ratio was estimated to be about 20% for the cases with extreme ice conditions (20% of the total line tension is due to the dynamic part) and drops down to around 15% for the lower ice conditions. As the system will be optimized for the extreme conditions the 20% will be used.

4.4.7 POLYESTER SEABED CLEARANCE

The polyester section cannot come in contact with the seabed at any time. This means that the bottom section of chain has to be long enough. As an example, for a certain mooring system with a bottom chain length of 350 meters there is still 50+ meters of chain floating above the seabed and it has MGRF of 65 MN. If the bottom chain section is reduced to 300 meters there should just be a few meters of clearance left at the maximum offset but 50 meters of chain has been saved. This has a sizable impact on the weight of the system and even increases the MGRF to 65.9 MN.

4.4.8 FINAL DESIGN

The resulting mooring system for a water depth of 350 m looks as follows:

- Semi-taut system
- 20 lines uniformly distributed
- An anchor radius of 900 meters
- The lines have the following lengths (from vessel to seabed): 50 m of chain, 676 – 680 m of polyester, 200 m of chain
- Chain:

  - Diameter: 157 mm
  - Steel grade: R5
  - Stud link
- Polyester:
  - Diameter: 296 mm
  - “Regular” polyester

The mooring system has the following properties:

- At the maximum offset of 28 meters (8% of the water depth) the MGRF is 66.9 MN and 52 MN with a broken line.
- The MBL is 24.52 MN (24.52 MN for the polyester section and 24.88 MN for the chain section)
- The pretension is 1.3 MN.
- The downwards force on the vessel at 0 m offset is 1511 mt. At the maximum offset of 28 meters the vertical force increases to 3782 mt due to the larger tension in the mooring lines resulting in a higher downward force on the vessel.

The mooring system is capable of handling the following environmental conditions:

ULS - Level ice

- 3.13 m thick ice moving at 0.5 m/s without wind and current
- 2.40 m thick ice moving at 1.5 m/s without wind and current
- 2.91 m thick ice moving at 0.5 m/s with wind (40 m/s) and current (1.3 m/s)
- 2.21 m thick ice moving at 1.5 m/s with wind (40 m/s) and current (1.3 m/s)

ULS – Ridges

- A small ridge in level ice of 1.79 meters thick moving at 0.5 m/s without wind and current
- A large ridge in level ice of 0.92 meters thick moving at 0.5 m/s without wind and current

ULS – Waves

- Johnswap spectrum, H_s = 15 m, T_0 = 15.3 s with wind (40 m/s) and current (1.3 m/s) results in:
  - MPM offset of 18.91 m out of the 28 m allowed
  - MPM line tension of 18.09 MN out of the 24.52 MN allowed

ALS – Level ice (with a broken)

- 2.69 m thick ice moving at 0.5 m/s but without wind and current
- 2.04 m thick ice moving at 1.5 m/s with a broken line but without wind and current
  - The broken line case always results in lower ice conditions despite the much lower safety factors for the line tension because the broken line lowers the stiffness of the system which means that at the maximum offset of 28 meters the MGRF will be lower.
- 2.45 m thick ice moving at 0.5 m/s
- 1.83 m thick ice moving at 1.5 m/s with wind (40 m/s) and current (1.3 m/s)

ALS – Waves (with a broken)

- Johnswap spectrum, H_s = 15 m, T_0 = 15.3 s and with wind (40 m/s) and current (1.3 m/s) results in:
  - MPM offset of 21.93 m out of the 28 m allowed.
  - MPM line tension of 12.95 MN out of the 24.52 MN allowed (lower than ULS due to the much lower safety factors).

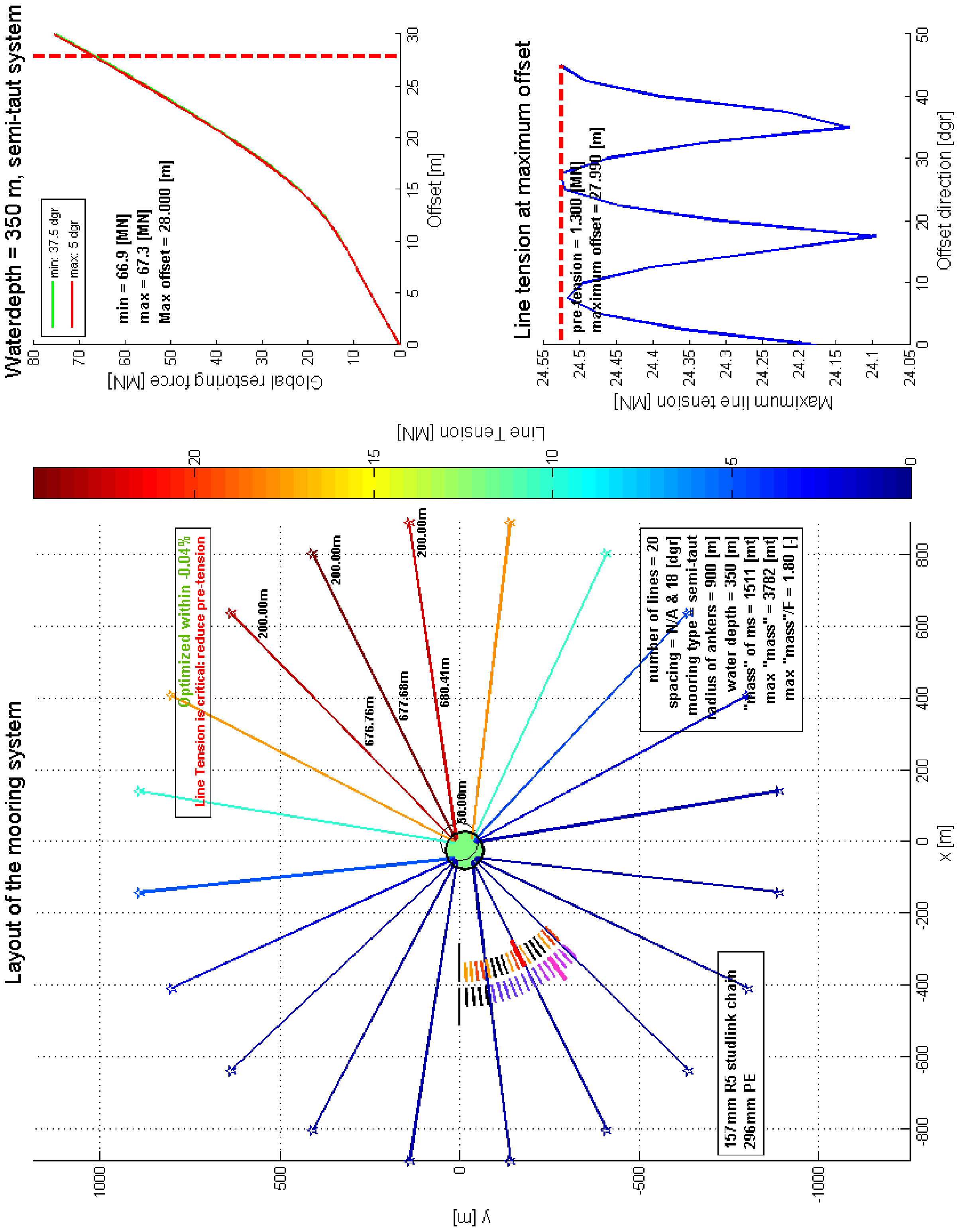

Figure 4-10: The global restoring force curve and the other properties of the final design. The initial stiffness of the system is 1.26 MN/m and the stiffness at large offsets is 3.76 MN/m.

Polyester clearance was checked for all ice conditions shown above and there was around 10 – 20 meters of chain left before the polyester would touch the seabed.

The natural periods of the system are:

- Mass = 277620000 kg
- $k_1 = 1.26\ MN/m$
- $k_2 = 3.76\ MN/m$

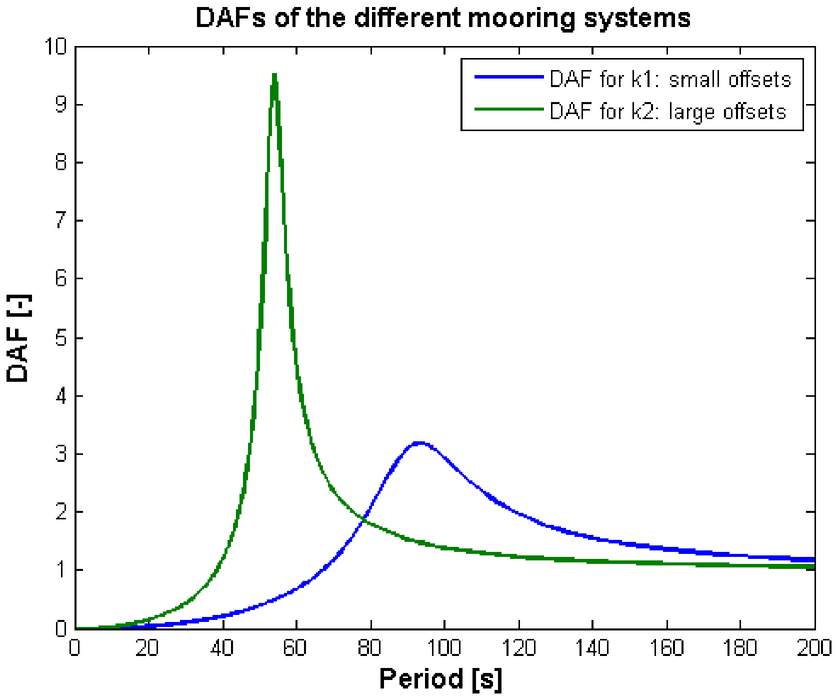

Figure 4-11: 1DOF approximation of the DAFs for the final design at different offsets. Not too much value should be attached to the height of the peaks because of the 1DOF approximation and linearized damping.

The vessel shows no signs of instability for ice thicknesses up to 4m thick. Beyond this thickness no investigations were done. See the next section for a more detailed explanation.

Comparison with the mooring system from the static report

The mooring system designed in this chapter has the following advantages over the original mooring system from the static mooring report:

- A restoring force nearly independent of the direction of the loading
- Being able to handle the same ice conditions despite the loading being higher due to the dynamics
- The static MGRF is 29% higher.
- For the broken line scenario a MGRF which is 67 % higher (51 MN versus 31.2 MN).

4.5 INSTABILITY

Due to the relation between the ice force and the trim angle (see Figure 4-12) instability of the vessel might occur. When the trim angle starts to deviate a bit from its mean position it can get into the region where it interacts with the orange section. Not only will this increase the horizontal loading this will also increase the moment around the y-axis, the exact moment which is cause the trim angle in the first place. This could in turn cause the vessel to vibrate around the y-axis. If resonance would occur this would increase the trim angle again and push the interaction into the red section causing even larger vibrations.

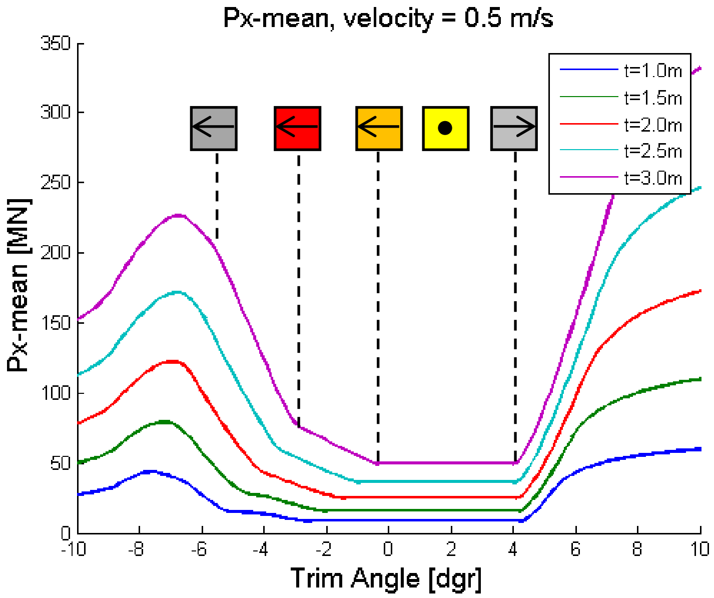

Figure 4-12: The relation between the trim angle and the horizontal ice load.

During preliminary, incorrect, models this type of behavior was seen when the ice thickness was increased beyond three meters and resulted in trim angles of up to 10 degrees. However after several correction had been made to the dynamic model this type of instability was not seen again.

To be safe a check was done with the final design of the mooring system were the ice thickness slowly increased to four meters and no instability was seen during this simulation.

4.6 CONCLUSION

Using the Matlab software a mooring system was design which is optimized for interaction with ice of about 3 meters thick.

- Uniformly distributed mooring lines should be used whenever possible to get a directionally independent restoring force.
- Optimization of a mooring system for a certain ice conditions can be done by using the corresponding ratio between the mean and fluctuating part of the ice loading in combination with their safety factors.
- Large gains can be achieved by using an optimized pretension.
- A detailed study should be done with broken ice so the impact of ice management can be evaluated.

5 CONCLUSION AND RECOMMENDATIONS

This section contains all the conclusions that were drawn during this thesis and recommendations for future work to further improve the quality of the work done or further increase the understanding of the vessel – ice interaction.

5.1 CONCLUSIONS

Model tests

For level ice at the operational draft the following summary can be made for the failure mechanic. An important thing to note is that all are due to limit stress:

- The most common failure mechanic is downward bending;
- The second most common failure mechanic is buckling, due to rubble and the geometry of the vessel axial forces can build up resulting in buckling. The main reason for this is the jump in impact angle and the force required to push through the rubble.
- Crushing occurs situational; it is highly dependent on the trim angle and the ice thickness.

General observations:

- The ice action becomes more simultaneous as the ice becomes thicker (larger ice action size);
- The velocity has a negligible impact on the vessel-ice interaction phenomenon observed;

Ice model

- The transition between failing in bending and failing in crushing is dependent on the section of the hull the ice is interacting with because each section has a different impact angle (angle between the ice and the hull). Which section of the hull the ice is interacting with in turn depends on the trim angle of the vessel, the ice thickness and the heave motion of the vessel.
- The fluctuating component of the horizontal force starts at maximum amplitude almost directly at the start of the interaction between the ice and the vessel. This component is caused by the failure of the ice sheet. The mean component of the horizontal force grows linearly from zero to its maximum value during the transient phase. The transient phase last anywhere from 300 to 500 seconds and is caused by the buildup of rubble in front of the vessel.
- No clear frequencies can be seen in the spectrums of the ice loading data. The ice fails at many different frequencies and no correlation in frequencies can be seen between the different tests.
- The spectrums created from the model test data could not be used in the ice model as their chaotic and random properties made interpolation between them impossible.
- A white noise or flat spectrums offered the best solution in modeling the fluctuating load.

Vessel's behavior

- During all the time-domain simulations done the trim angle never became high enough for crushing to occur. This is because even though the moment causing the trim angle is increasing as the ice thickness increases, so do the restoring forces caused by the mooring system. This means that the height of the yellow section of the hull (the part that is 45 degree downward sloping) has a sufficient height.

- No instability or resonance of the vessel was observed.
- After this initial contact between the ice sheet and the vessel the two never lose contact if the ice has a constant velocity.

Mooring system

- By optimizing the pretension of a mooring system so that both offset and line tension design criteria are fully utilized large gains in the maximum global restoring force can be achieved.
- It is possible to further increase the capabilities of the 20 lines system by changing the anchor radius but this will quickly increase the cost and weight of the system.
- A 16 line mooring system is possible but this will reduce the possible ice conditions and greatly reduce the maximum global restoring force in case of a broken line.
- The maximum breaking load of the final design is limited by the diameter of polyester that is currently available on the market. Currently a chain diameter of only 157 mm is used while they are available up to 177 mm, leaving a room of improvement of 20%. If the diameter of polyester can be increased then this can greatly increase the capabilities of the mooring system however at increased costs and weight.
- A full taut mooring system performed worse than the semi-taut system.
- Due the overshoot in the transient phase (see section 3.2.1.4) the natural period of the moored vessel cannot be higher than the build time of the transient phase. A safe upper-limit is 250 seconds.

Operational limits

With the final design of the mooring system it is possible to handle the following ice conditions:

- It is possible to operate in areas with level ice up to 3.1 meters thick at 0.5 m/s or 2.4 meters thick at 1.5 m/s.
- It is possible to operate in areas with ridges for level ice up to 1.79 meters thick depending on the relative size of the ridge compared to the nearby level ice. It is important to note that this value is a very crude estimate.
- In case of a broken line the maximum allowable ice conditions decrease by 14 to 17 %.
- The environmental loads in the survival conditions in open water are not a problem even with a broken line.

Operations in the arctic

5.2 RECOMMENDATIONS

5.2.1 RECOMMENDATIONS FOR FUTURE MODEL TESTS

Hydrodynamic properties

- More detailed calculations or model tests should be done to determine the added mass of the JBF Arctic when it is surrounded by ice. This way a better understanding of the impact of the adjacent ice sheet and rubble on the added mass can be obtained.
- Calculations or model tests should be done in order to determine the radiation damping caused by the propagation of waves through the ice sheet.

Ice model tests

- Do tests at high velocity and thick ice. This way it can be check if the high velocity indeed increases the probability of crushing.
- Do test at very slow velocities (around 0.1 m/s) with thick ice at relatively warm temperatures to investigate creep as this can lead to very high loads which have thus far been neglected.
- The data of Pz was very poor. More attention should be paid to the other components next time model tests are done.
- More tests should be done to allow for higher order interpolations and better quality models. Especially for the trim angle dependency it would have been very useful to have one or two more tests between 2.5° and 5.0° to get a better understanding of the transition from failure in bending to crushing.
- Do repeated tests or longer tests (the same for stationary ergodic vessel-ice interactions) to get more reliable spectrums. This way the assumed flat spectrum can be verified or replaced with an improved model that can interpolate between the spectrums associated with the different parameters of the ice.
- Do tests were other parameters are varied, such as the ice temperature and salinity in order to test their impact on the loading.
- Quite a few peculiarities were found in the data received from KSRI. Next time the possibility of using a different ice model test facility should be investigated. Below is a list of observation based on my experience of working with KSRI's data:
    - The measurements of Pz data are very poor up to the point where they are not usable anymore.
    - The statistical properties of all the time histories received differ from the statistics written down in the report.
    - Spectrums should be included in the data package.
    - The underwater footage was of very poor quality.
    - There is no description of what they did regarding the scaling / size effect and other post processing like filtering of the signals.
    - No information is available on the terms used in the regression model.

5.2.2 RECOMMENDATIONS TO IMPROVE THE DESIGN OF THE MOORING SYSTEM

- Do a fatigue analysis of the mooring lines.
- Do an economic analysis of the mooring system so the most cost efficient design can be chosen.
- Whoever is in charge of the mooring system during operations should pay stricter attention to the offset limit states of the mooring system as the safety on it is much lower than on the line tension.
- Contact manufacturers of polyester mooring lines to see if it is possible for them to increase the maximum diameter that they can deliver.
- A study should be done to determine what kind of anchor is required to handle the loads.

5.2.3 RECOMMENDATIONS FOR FOLLOW-UP RESEARCH FOR THE JBF ARCTIC

Due to the limited capabilities of the JBF Arctic to handle ice ridges a study should be done on ice management and in particular ice breakers. The basis for this study will be to split the operational window into three seasons: ice free season (waves), mild ice conditions and severe ice conditions where the mild ice conditions can still be handled without an ice breaker present. This study will then comprise of two phases:

Phase 1: Unmanaged operations

It should be determined for what kind of duration the vessel can remain operational without the presence of an ice breaker or ice management. This will included the ice free season for obvious reasons and initial period of the ice season. Depending on the area the vessel is located in it should be determined for how long the ice and ridges will remain thin enough for the vessel to handle them on its own. This phase will be limited by ridges and the current ice model can provide an estimate for the maximum allowable ice conditions. Information is needed on the probability of occurrence of a certain thickness of a ridge given a certain thickness of level ice so the desired level of safety can be guaranteed. Once this is no longer possible ice breakers assistance can commence.

Phase 2: Ice management

Phase 2 of the study will focus on designing an ice management system and the interaction with broken ice and requires the following steps:

- A new series of model tests is required specific for interactions with broken ice of varies sizes. The sizes and shapes should follow from a study performed beforehand to determine the distribution of the dimensions of the broken ice pieces after level ice or a ridge of a certain thickness (variable) has been crushed by a certain type of ice crusher (variable).
- Another ice model can be then be created based on the model test data which can predict the loads for broken ice. This model can be used to do time-domain simulation and investigate the vessel-ice interaction for this kind of ice feature.
- A study should be done to determine what kind of mooring system is required and if it is possible to use DP instead of a mooring system.
- Finally a study should be done on the logistical aspect of ice management. The detection range should be determined so an adequate level of safety can be guaranteed under all circumstances. Key parameters influencing this are: statistics on the ice velocity, thickness and ridges, the time required to break a certain ice feature and the required level of safety.

A tradeoff has to be made between using a brute-force approach where a very strong mooring system is used and the duration of phase 1 can be extended. Only in the winter months would ice breakers be required and due to the strong mooring system a lower amount and small class of ice breakers will suffice. For areas with milder ice conditions an extreme mooring system could be used so ice breakers might no longer be needed but this might require larger diameter polyester to be available.

The alternative is to use a weaker mooring system or even a dynamic positioning and relying heavily on ice breakers / ice management for nearly the whole ice season to tone down the ice loads. The economic aspect will probably be one of the key deciding factors when deciding between the two options.

6 REFERENCES

BDA. (2011). *Mooring Analysis - Time Domain.*

Brown, M. O. (sd). FORMATION, BEHAVIOUR AND CHARACTERISTICS OF ICE.

Cold Region Reseach. (sd). Opgehaald van http://coldregionsresearch.tpub.com/CR97_06/CR97_060016.htm.

Coulomb, L. (2003). *Most probable maximum- an explanation.* Bluewater.

DNV. (Oct 2008). *DNV-OS-E301 Position Mooring.* DNV.

Holthuijsen, L. H. (2007). *Waves in Oceanic and Coastal Waters.* Cambridge: Cambridge University Press.

http://coldregionsresearch.tpub.com/CR97_06/CR97_060016.htm. (sd).

IVR. (08-04-2011). *"S:\Projects\Year-2010\A10-50000 JBF Arctic Vessel Design\00 General\A10-50000-00130-02 RevA Mooring System - Static Analysis.pdf".*

Liferob, P. (2004). *Ice rubble behaviour and strength: Part II. Modelling.* Trondheim.

Loset. (2006). *Actions from ice on arctice offshore and coastal structures.*

Metrikine, A. (2006). *Dynamics, Slender Structures and an Introduction to Continuum Mechanics.* Delft: TUDelft press.

Ochi. (1998). *Ocean Waves: The Stochastic Approach.* Cambridge University Press.

Ramnas Offshore Safety. (sd). Opgehaald van http://www.ramnas.com/atlas/file.php?id=822

Rodrigues, O. (sd). *Wikipedia: Rodrigues' rotation formula*. Opgehaald van Wikipedia: http://en.wikipedia.org/wiki/Rodrigues'_rotation_formula

Schulson, E. M. (1997). The brittle failure of ice under compression.

Serway, R. A. (1999). *Physics for Scientists and Engineers.*

APPENDIX A OVERVIEW OF THE MODEL TEST SETUP

This appendix gives an overview of the setup used during the model tests at KSRI.

A.1 THE BASIN

The model tests were conducted in KSRI's ice model basin in St. Petersburg. The basin has the following properties:

- Maximum ice length of 35 m;
- Ice width of 6 m;
- Water depth of 1.75 m;
- A towing carriage of 186 kN which can provide a pulling force of up to 5000 N in a velocity range of 0.15 – 2.0 m/s and a pulling force of up 20000 N in a velocity range of 0.0005 – 0.2 m/s. Velocity measurement error is 0.22 %.

The test facility has the capability to generate two types of ice: fine grain ice or columnar ice. For this test fine grain ice was used for the tests.

A.2 THE MODEL OF THE JBF ARTIC

The construction of the JBF Artic model was part of the contract and as such was done by KSRI. When determining the model scale they considered the following aspect:

- Relations between dimensions of the ice field working sections and overall model dimensions;
- Geometry and strength parameters of the simulated ice formations;
- The tasks set by Huisman.

Based on these criteria a model scale of 1:58 was chosen.

When building the model the exterior surface was coating with epoxy paint and finished with pentaphtol coating. The final surface was treated to provide an ice/model dynamic friction coefficient of 0.15 [-] as described by Huisman. In Figure A-1 the final model can be seen as well as the different drafts.

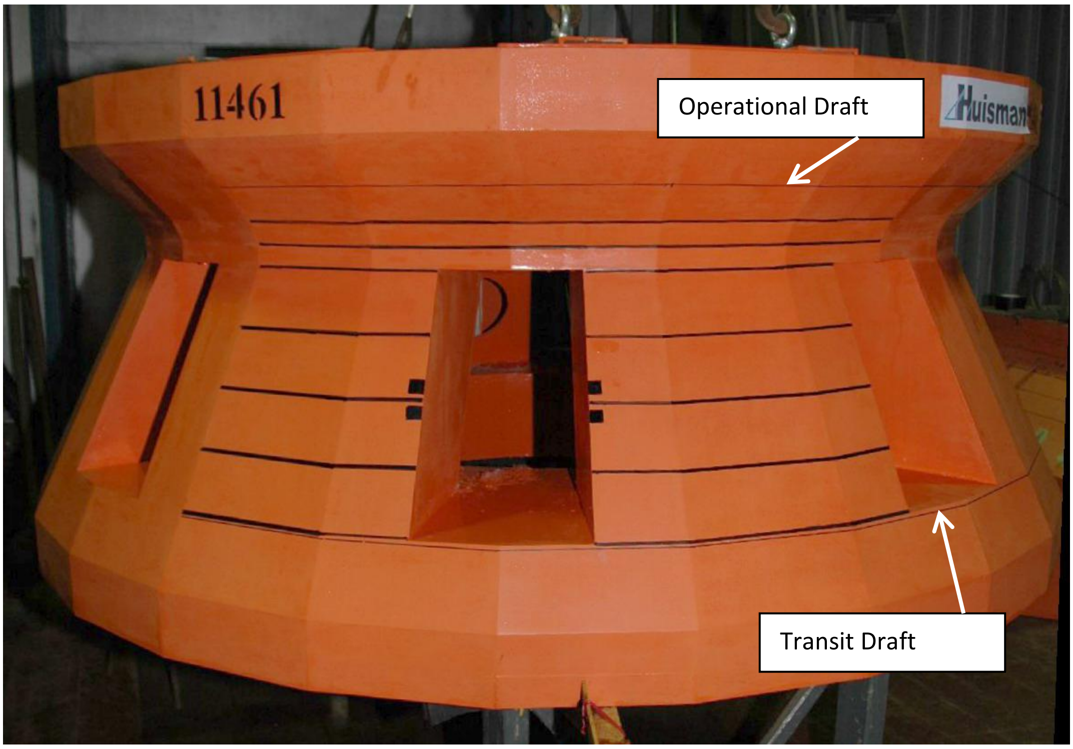

Figure A-1: The final model.

A.3 THE ICE

In total 6 different sheets of ice were grown with which all the tests were performed. Each ice sheet was used for several tests which each used up a part of the ice sheet. After each test the carriage was stopped and moved back a bit and then measurement and movement was restarted for the next test.

The following ice conditions were tested:

- Level ice of 1.0 m, 1.5 m, 2.0 m and 3.0 m thickness;
- A channel of 40 m width in 1.0 m level ice that is made by an icebreaker;
- A channel of 80 m width in 2.0 m level ice that is made by one or two icebreakers;
- Broken ice fields with a floe size of 30 m x 30 m and 100 m x 100 m and a concentration of 8~9/10;
- Two hummocks (3.0m consolidated layer, 10m and 18m keel depth) with a 40 wide channel made by an icebreaker;

The modeled ice was of the fine-grain type and was prepared as per Kvaerner MasaYaards technology and had a flexural strength of 500 kPa for all tests. Channels in the ice to simulate icebreakers were made with a cutting tool were the edges of the channel are made uneven to imitate an icebreaker’s run. Broken ice was cut from level ice to the appropriate flow size and then distributed across the water surface to get the required ice concentration. The hummocks were prepared in accordance with the technology used in the Krylov’s ice basin.

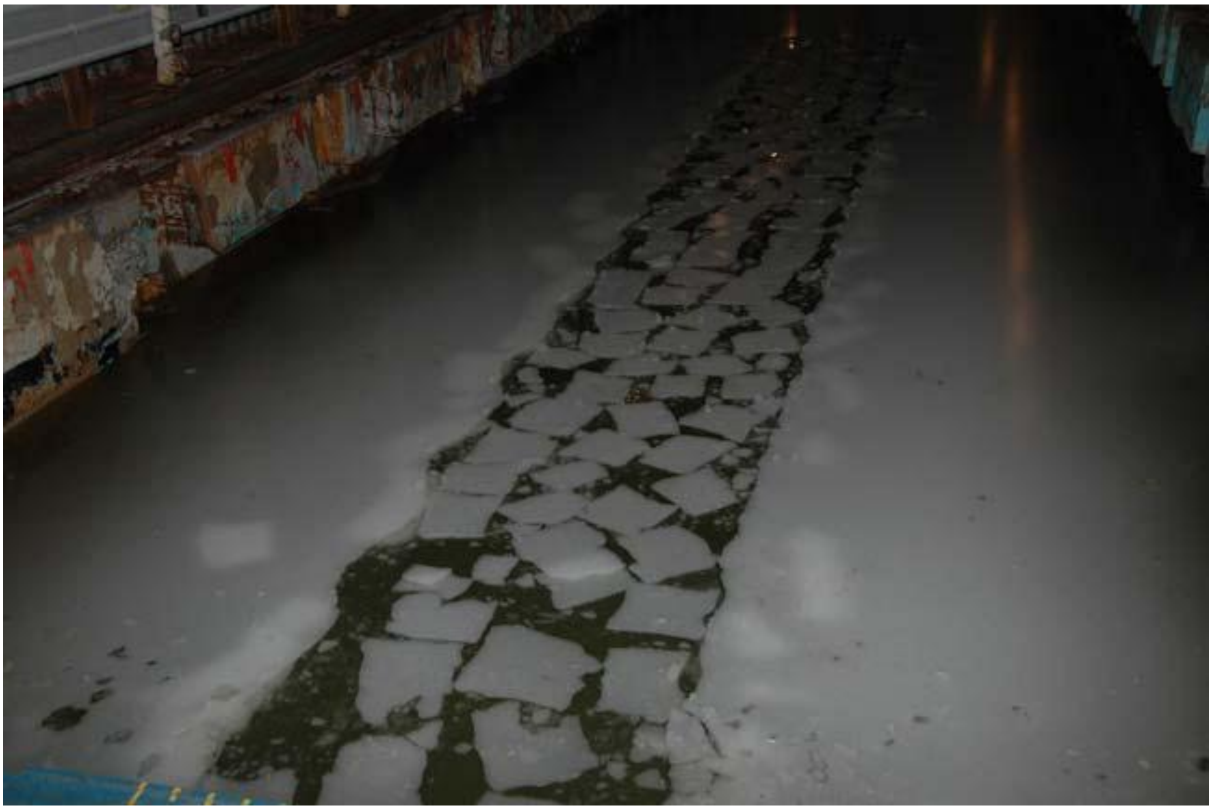

Figure A-2: A channel in level ice.

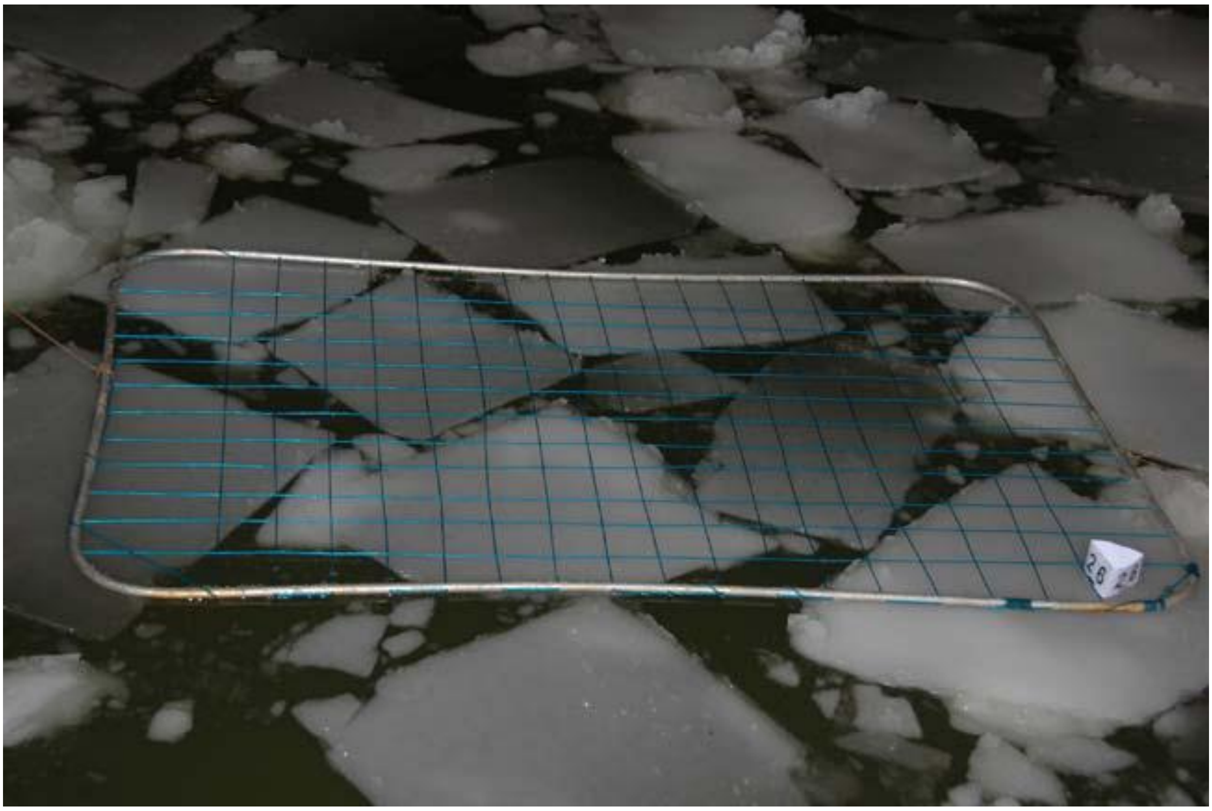

Figure A-3: Broken ice with dimensions of 30 m x 30 m and a concentration of 8/10.

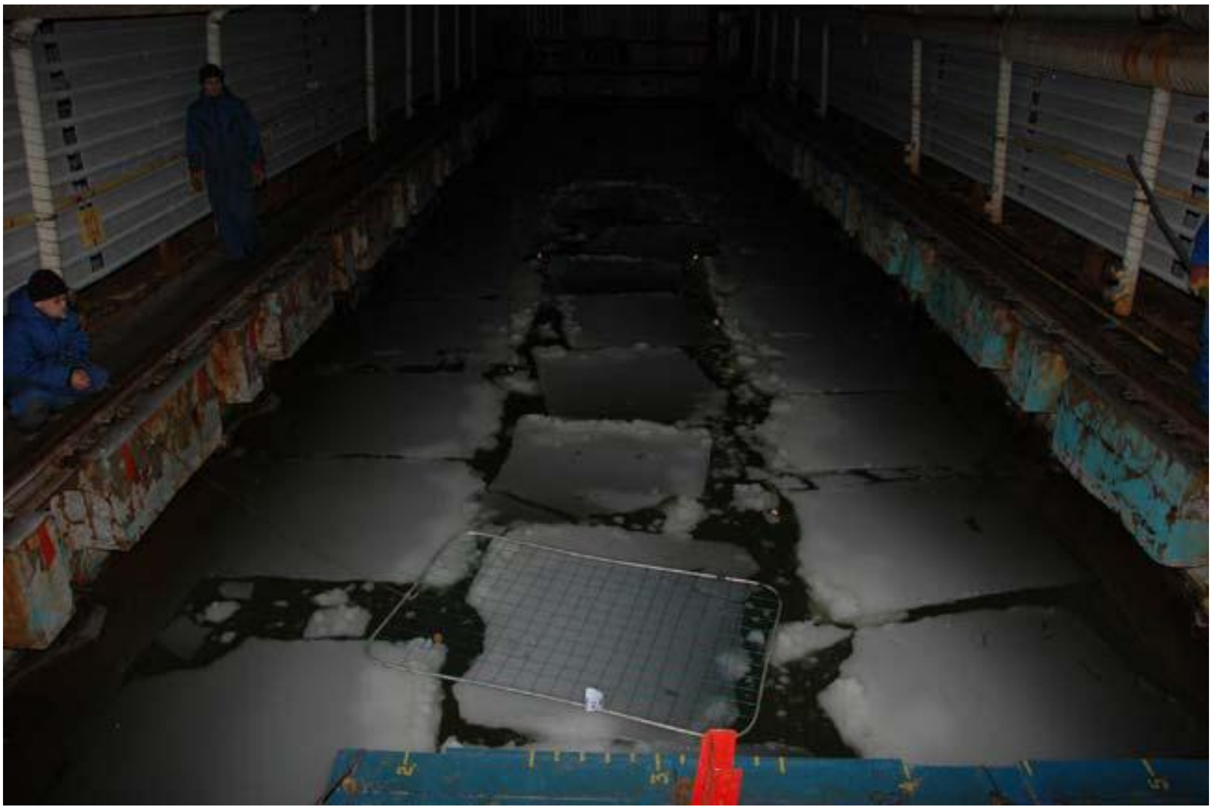

Figure A-4: Broken ice with dimensions of 100 m x 100 m and a concentration of 8/10.

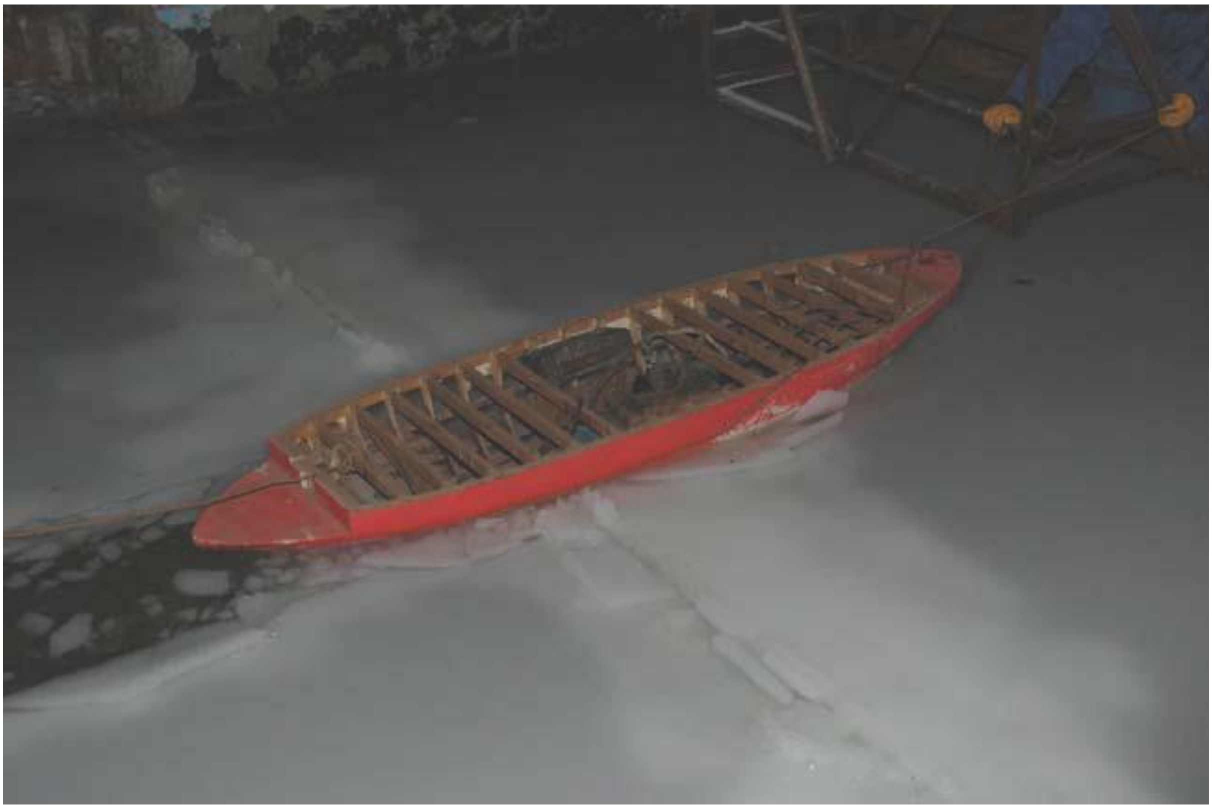

Figure A-5: A channel being created in a hummock using an icebreaker model.

A.4 MEASUREMENT OF PHYSICAL PROPERTIES

During the tests varies parameters were recorded. The following list gives a brief overview of the measurements done and the techniques involved.

- The forces and moments exerted by the ice on the vessel were measured using a 6 DOF dynamometer at a sampling frequency of 150 Hz per channel. The time histories of the load components were digitally filtered with a cut-off frequency of 2 Hz in order to reduce the amplitudes at frequencies close to the model's natural frequencies. The model's natural frequency was about 4 Hz at transit draft and about 3 Hz in operational draft.
- The thickness of level ice and the consolidated layer of the hummock were measured at the edge of the channel made in the ice by the model. The measurements were taken using a measuring rule.
- The ice bending strength was found by breaking a floating cantilever beam in situ before commencing the tests. The bending strength was found from the following formula:

  $$\sigma_f = \frac{6Pl}{bh^2}$$

  where P [N] is equal to the maximum force applied to the free end of the cantilever which causes bending failure at the root section; l [m] is equal to the beam length (the distance between the force application point and the section were failure occurred); b [m] is equal to the beam root width and h [m] is equal to the beam thickness.

  The ice bending strength was assumed to be equal to the mean value of several tests.

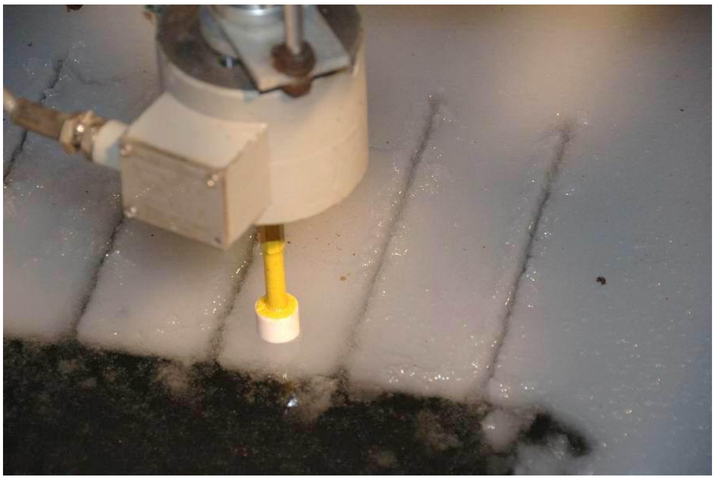

Figure A-6: Ice bending strength measurements being performed

- The profile of the hummock was measured in either one or two cross-sections of the hummock using a measuring staff and an instrumentation prod. The mean value of the maximum depths obtained for each section was assumed as the hummock's keel depth.

  In Krylov's ice basin the keel properties of model hummocks, cohesion and angle of internal friction, were determined on a basis of a punch tests (vertical punch through the keel) and a direct shear tests (horizontal shear of consolidated layer block along the upper surface of the keel). These experiments require significant free areas of the surface of the modeled hummock, and it was impossible to provide them in the performed tests due to the large dimensions of the model. Using the results of investigations that were carried out in the ice basin previously, the cohesion was assumed to be equal 8-10 kPa (full scale value) and the angle of internal friction was assumed to be equal to 30°-36°. The hummock keel porosity was 18-25%.

- The factor of dynamic ice friction against the model's surface was found by dragging an ice specimen over a surface identical to that of the test model and measuring the applied horizontal force (Figure A-7). Based on the obtained data the dynamic ice/platform surface friction factor could be assumed as 0.15.

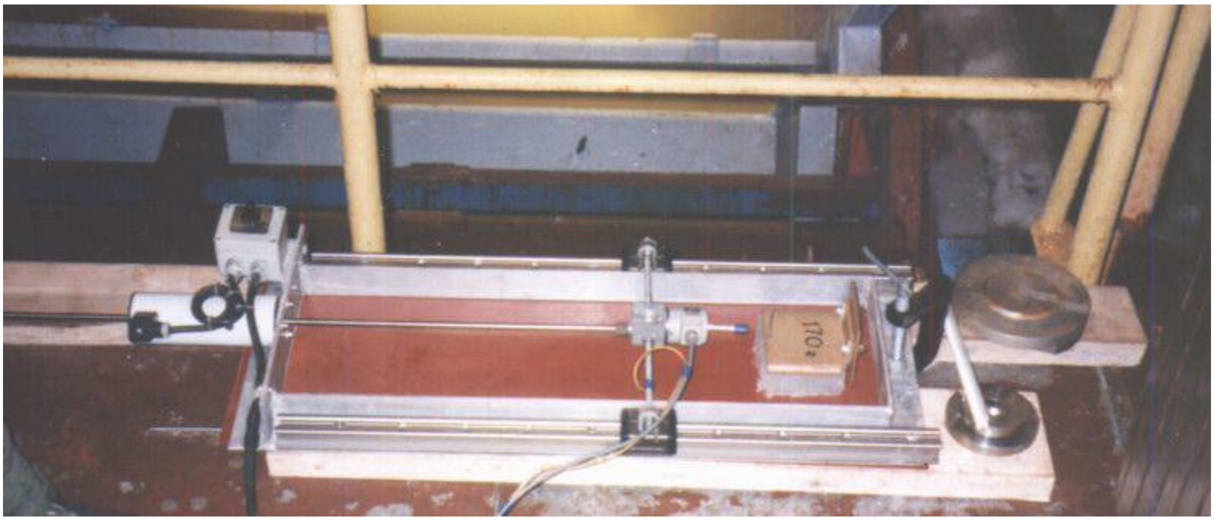

Figure A-7: Measuring the dynamic friction factor

- The ice density is determined using a technique that is recommended by the ITTC Ice Committee. The average model's ice density is 920 kg/m^3.
- Video en photographs were taken during the tests from varies angles.

A.5 ACCURACY OF INSTRUMENTATION

The measuring accuracy of the instrumentation used is given in the following table.

Instrument	Measuring range	Accuracy
Dynamometer	Px ±2000 N Py ±2000 N Pz ±3000 N Mx ±600 N My ±600 N Mz ±600 N	Px ±10 N Py ±5 N Pz ±20 N Mx ±2 N My ±2 N Mz ±2 N Non-linearity within 0.3%
Towing carriage velocity sensor	0.02 - 1.00 m/s	Reduced error ±(0.046+100/N), where N - number of measured pulses

Measuring facility with force transducer	0 - 100 N	Reduced error less than ±0.4% Non-linearity within 0.01%
Instrument for measuring displacements	0 - 4 mm	Limits of reduced error ±0.2% Non-linearity within 0.9%

Table 12: Accuracy of measuring instrumentation

A.6 EXPERIMENT LAYOUT

The model tests were done by towing the model through the immovable ice sheet. The model was fixed to the towing carriage through a six-component dynamometer. The six components can be seen in Figure A-8. The model was orientated in such a way that the model faces the ice with one of its legs rather than with one of the gaps between the legs.

The duration of each test was chosen such that a stationary situation was reached.

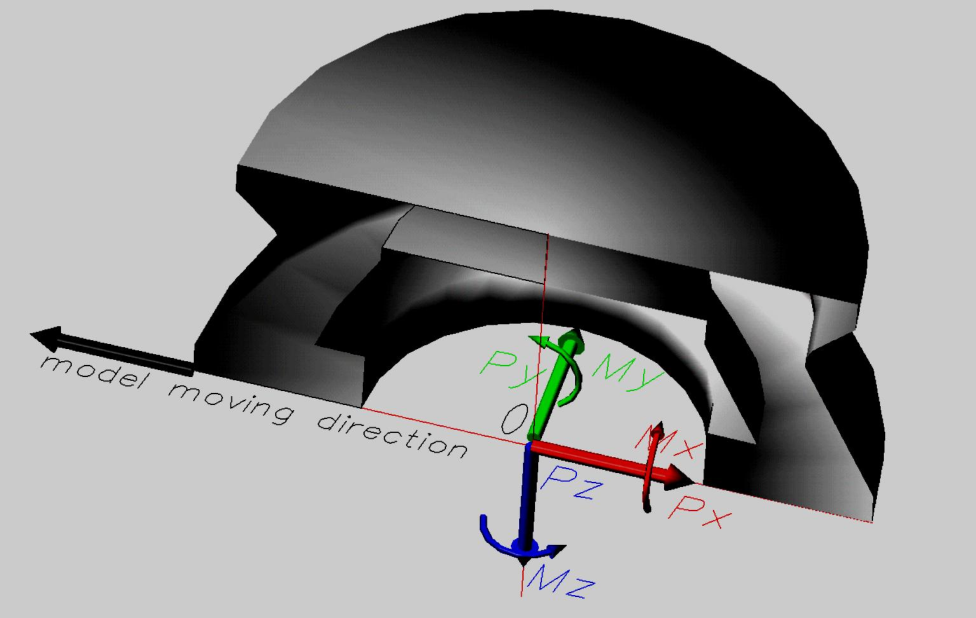

Figure A-8: The coordinate system used during the tests

A.7 THE TEST PROGRAM

The tests were performed on a total of 6 different ice sheets. Each ice sheet was used for 3 to 8 different tests. During the whole test program a total of 34 tests were performed, 14 in transit draft and 20 in operational draft.

Between the different tests several parameter were used as variable: the ice thickness (1 m, 1.5 m, 2 m and 3 m), the ice features (level ice, 40 m wide channel, 80 m wide channel, 30 m broken ice, 100 m broken ice and hummocks), the ice velocity (0.5 m/s, 0.75 m/s, 1 m/s and 1.5 m/s) and finally the trim angle (0°, 2.5° and 5°).

The wide range of variables allow for a prediction of the ice-forces in a wide variety of ice and vessel conditions.

In Table 12 the entire test program is listed.

		Run#	Ice conditions	Ice thickness [m]	Ice drift velocity [m/s]	Trim angle, degree
day #1	Transit draft	1_1	Channel 40m	1.0	1.50	0.0
		1_2	Channel 40m	1.0	0.75	0.0
		1_4	Level ice	1.0	1.50	0.0
		1_5	Level ice	1.0	0.75	0.0
		1_6	Managed 100m	1.0	1.50	0.0
		1_7	Managed 100m	1.0	0.75	0.0
		1_8	Managed 30m	1.0	1.50	0.0
		1_9	Managed 30m	1.0	0.75	0.0
day #2	Transit draft	2_1	Channel 80m	2.0	1.50	0.0
		2_2	Channel 80m	2.0	0.75	0.0
		2_4	Managed 100m	2.0	1.50	0.0
		2_5	Managed 100m	2.0	0.75	0.0
		2_6	Managed 30m	2.0	1.50	0.0
		2_7	Managed 30m	2.0	0.75	0.0
day #3	Operational draft	3_1	Level ice	1.5	0.50	0.0
		3_2	Level ice	1.5	1.50	0.0
		3_3	Level ice	1.5	1.00	0.0
		3_4	Managed 100m	1.5	0.50	0.0
		3_5	Level ice	1.5	0.50	5.0
		3_6	Level ice	1.5	0.50	2.5
day #4	Operational draft	4_1	Level ice	2.0	0.50	2.5
		4_2	Level ice	2.0	0.50	5.0
		4_3	Level ice	2.0	1.50	0.0
		4_4	Level ice	2.0	1.00	0.0
		4_5	Level ice	2.0	0.50	0.0
		4_6	Managed 100m	2.0	0.50	0.0

day #5	Operational draft	5_2	Hummock, keel depth 10 m	3 m (consolidated layer)	0.50	0.0
		5_3	Hummock, keel depth 18 m		0.50	0.0
day #6	Operational draft	6_1	Level ice	3.0	0.50	0.0
		6_2	Level ice	3.0	1.50	0.0
		6_3	Level ice	3.0	1.00	0.0
		6_4	Level ice	3.0	0.50	2.5
		6_5	Level ice	3.0	0.50	5.0
		6_6	Managed 100m	3.0	0.50	0.0

Table 13: The test program

A.8 SCALING FROM MODEL TO FULL-SCALE CONDITIONS

The scaling of the model test's results to full-scale was done by KSRI. It was done in accordance with the guidelines applied in the ice towing tank of KSRI. The guidelines are based on principles of simulating physical processes that ensure compliance with criteria of geometry, kinematic and dynamic similarity.

KSRI also made a regression model based on the model test results, creating multi-factor regress-dependencies between measured load components and experiment parameters. If generation of the regress-models is not possible, corrections for measured load component values are introduced based on expert estimations. After this, recalculation of the load components to full-scale conditions is carried out according to the simulation principles (see Table 14).

Linear dimensions (geometrical parameters of the vessel and of ice features)	$L_f = L_m * \lambda$ $h_f = h_m * \lambda$
Strength (bending, compression)	$\sigma_f = \sigma_m * \lambda$
Elasticity modulus	$E_f = E_m * \lambda$
Velocity	$V_f = V_m * \sqrt{\lambda}$
Frequency	$H_f = H_m / \sqrt{\lambda}$
Force	$F_f = F_m * \lambda^3$
Volume	$v_f = \mathrm{v}_m * \lambda^3$
Moment	$M_f = M_m * \lambda^4$
Friction coefficient	$f_f = f_m$

Table 14: Model to full-scale extrapolation rules.
Where: λ is the scale factor and equal to 58
index m applies to model and f to full-scale

In order to separate the ice loads from the water resistance loads open water test runs were performed to measure the water resistance load. These were then deducted from the measured total loads to get the ice load.

This concludes the summary of the model test setup.

APPENDIX B DIVISION OF THE PROJECTED VESSEL-ICE INTERFACE AREA

In this appendix the projected vessel-ice interface area is divided in different section each with a different impact angle. The total area is divided into three sections: “yellow”, “orange” and “red”. For each section an equation is derived that calculates the percentage of the total area that is taken up by each of the section. The same approach was used for the “grey” and “deck box” sections to accommodate extreme trim angles.

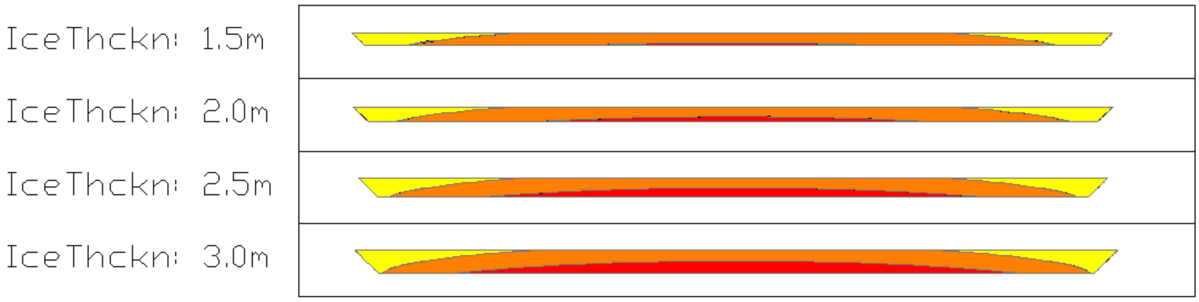

Figure B-1: One equation that calculates the percentage each colored areas takes up is coming right up!

B.1 GEOMETRY

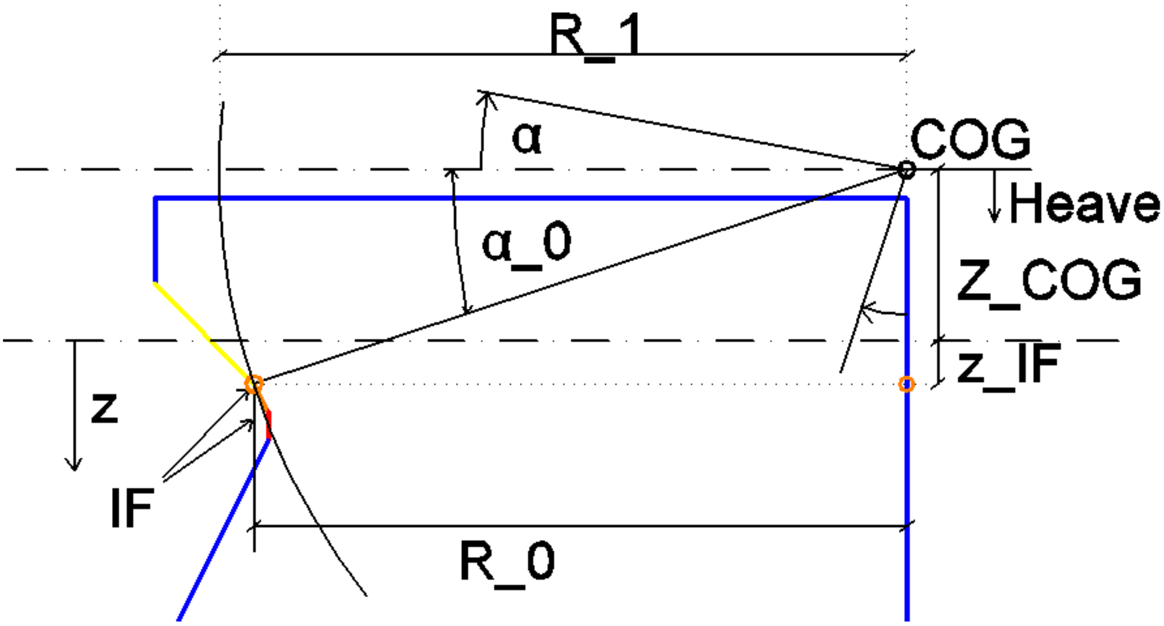

Figure B-2: Geometry in side plane. Note that the actual COG is located below the mean water line, but this does not influence the derivation.

Definitions in Figure B-2:

- α [°] Trim angle of the vessel (VARIABLE)
- α_0 [°] Initial offset of trim angle at the center line due to distance between COG and Z_{IF} (FIXED)

COG	name	Center of gravity (= center of rotation) (FIXED)
IF	name	Interface we are interested in (FIXED, in this example it is the orange dot)
R_0	[m]	Initial horizontal distance between COG and IF (FIXED, 49 m for yellow, 46 m for orange and 45 m for red) (FIXED)
R_1	[m]	Initial distance between COG and IF (radius of the circle) (FIXED)
Heave	[m]	Heave motion of the vessel (VARIABLE)
z	[m]	Definition of positive depth (z) coordinate
Z_{COG}	[m]	Vertical coordinate of the COG (FIXED)
Z_{IF}	[m]	Vertical coordinate of the interface (FIXED)

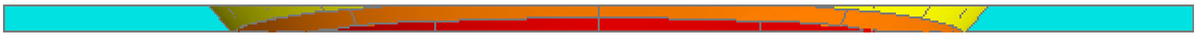

Figure B-3: The vessel-ice interaction area as seen from the ice.

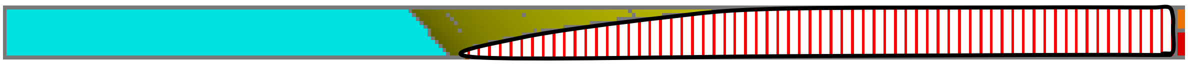

Figure B-4: Half of the vessel-ice interaction area and the same colors are applied as used below. The red vertical dashed area is the same as the red dashed area below and the black outline (but then unprojected, so 3D rather than 2D) is also the same below.

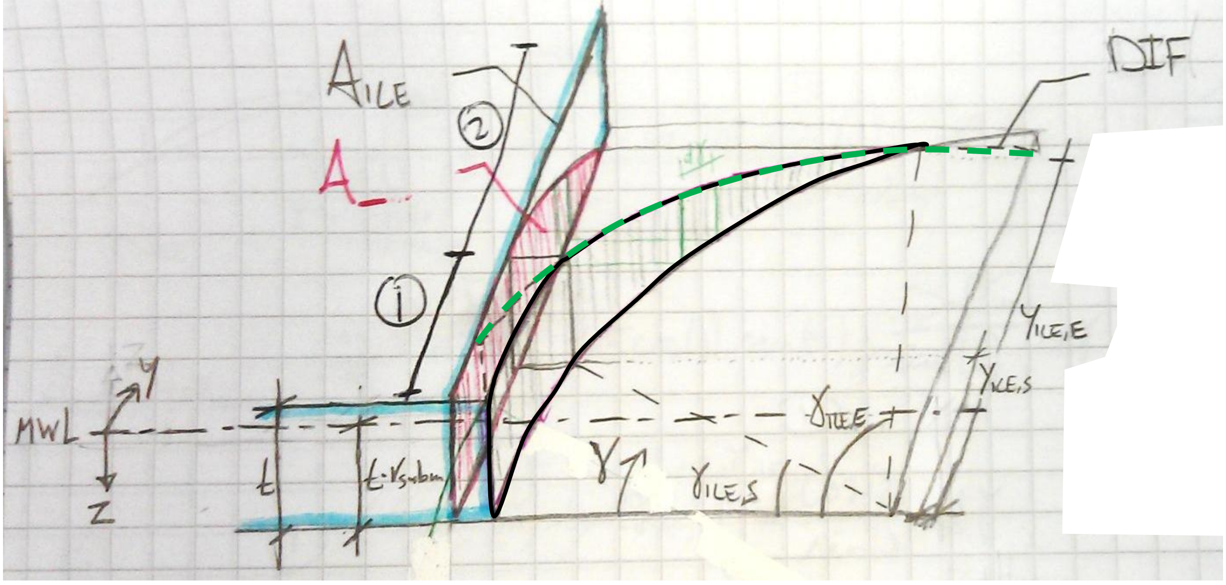

Figure B-5: Geometry in top-down isometric special view. The blue rectangle in the YZ-plane is the projected ice interaction area and the red part inside it is interacting with the part of the hull being considered (yellow, orange, red, etc.). The green dashed line shows the depth of the interface (DIF) and the black shape is the un-projected area of the ice that is interaction with the part of the hull being considered.

Definitions in Figure B-5:

A_...	[m^2]	The projected area interacting with a specific section of the hull: the yellow, orange or red section (TO BE CALCULATED)
A_{ice}	[m^2]	The total projected area of ice interacting with the vessel (TO BE CALCULATED)

DIF	func	Depth of the interface between two areas; orange and red for instance. Everything below the interface will be interacting with the red section and everything above the interface will be interacting with the orange section (TO BE CALCULATED)
t	[m]	Ice thickness (VARIABLE)
r_{subm}	[-]	Ratio of ice below the water. With an ice density of 920 kg/m^3 (calculated during the tests) and a sea water density of 1025 kg/m^3, r_{subm} is equal to 0.8975609756 [-] (FIXED)
y	[m]	Definition of positive Y-coordinate
γ	[°]	Definition of positive circumferential (γ) coordinate
$\gamma_{ICE,S}$	[°]	Start of the sloping part of the ice's projected area (TO BE CALCULATED)
$\gamma_{ICE,E}$	[°]	End of the sloping part of the ice's projected area (TO BE CALCULATED)
$y_{ICE,S}$	[m]	Start of the sloping part of the ice's projected area (TO BE CALCULATED)
$y_{ICE,E}$	[m]	End of the sloping part of the ice's projected area (TO BE CALCULATED)

B.2 STEP 1: THE DEPTH OF THE INTERFACE

Only in hindsight did it become apparent that the shape of vessel was assumed to be fully circular instead of a 24-sided polygon. However when looking at Figure B-6 one can see that the differences are very small so this assumption does have a significant influence on the results. Also an external circle was used so the projected side frontal views of the vessel are actually slight smaller then calculated below, thus making the approach slightly conservative.

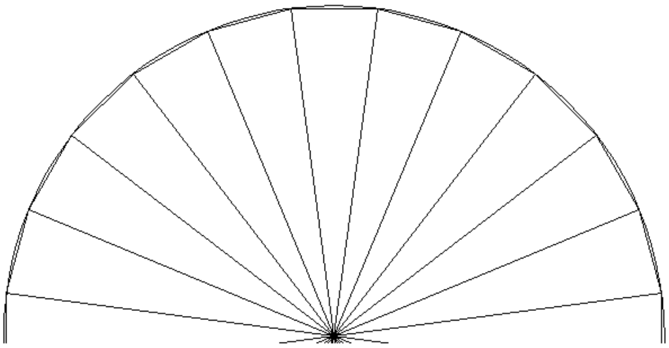

Figure B-6: External circular and 24-sided polygon. Not that when looking at the vessel from the top, the vessel is slightly thinner than the external circle.

The first step is to determine the depth of IF for all trim angles and for all circumferential angles. Because IF is not on the same vertical level as the COG, a correction is needed in order to translate rotation of the vessel around to COG to translations of the interface. For ease the point on the center line will be considered first (the line starting from the center of the vessel and then going radially outwards):

$$\alpha_0 = \operatorname{atan}\left(\frac{z_{COG} + z_{IF}}{R_0}\right)$$

$$R_1 = R_0/\cos(\alpha_0)$$

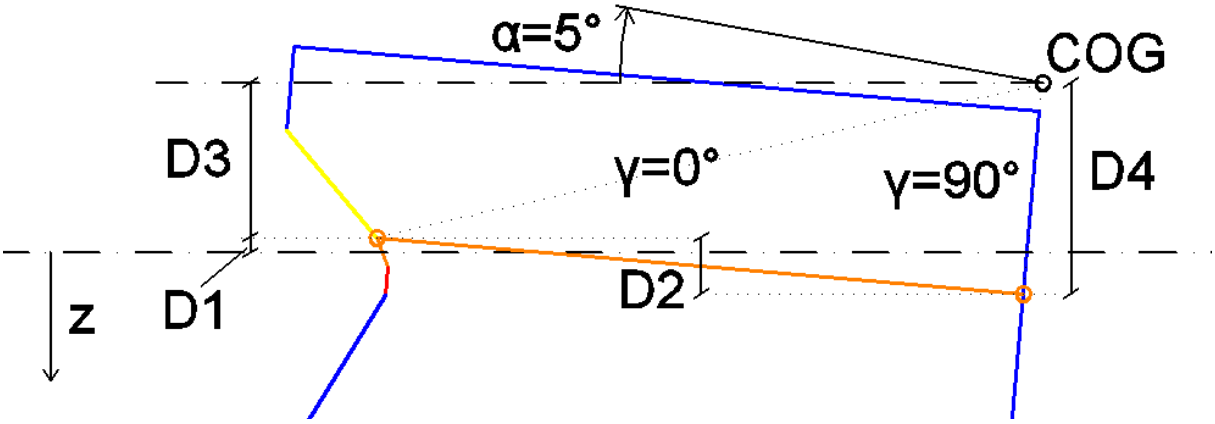

The depth of the point of the interface on the center line is given by:

$$D1 = -R_1 * \sin(\alpha - \alpha_0) + z_{COG} + Heave$$

Next the dependency on the circumferential angle will be added. Because of the circular shape a non-linear interpolation has to take place in order to correct for the circumferential angle. The vertical distance over which has to be interpolated is D2. D2 is defined as follows:

$$D2 = D4 - D3 = [(Z_{IF} - Z_{COG}) * \cos(\alpha)] - [-R_1 * \sin(\alpha - \alpha_0)]$$

The interpolation depends on the horizontal distance between the two circles. The horizontal distance as a function of the circumferential angle is defined as:

$$\frac{R_1 * \cos(\gamma)}{R_1} = \cos(\gamma)$$

Because D1 is needed and not (D2-D1), $1 - \cos(\gamma)$ has to be taken. This also gives the final equation for the depth of the interface:

$$DIF = -R_1 * \sin(\alpha - \alpha_0) + z_{COG} + Heave + ([(Z_{IF} - Z_{COG}) * \cos(\alpha)] - [-R_1 * \sin(\alpha - \alpha_0)]) * (1 - \cos\gamma)$$

B.3 STEP 2: FINDING THE BOUNDARIES

Next the intersection depth with the ice has to be found. The vertical coordinate of the top of the ice is given by:

$$-t(1 - r_{subm})$$

The bottom by:

$$t * r_{subm}$$

This gives two equations for the bounds:

$$DIF = -t(1 - r_{subm})$$

$$DIF = t * r_{subm}$$

Solving these bounds gives the bounds in terms of γ:

$$\gamma_{ICE,S} = \operatorname{acos}\left(1 - \frac{-t(1 - r_{subm}) + R_1 * \sin(\alpha - \alpha_0) - z_{COG} - Heave}{R_1 * \sin(\alpha - \alpha_0) + (Z_{IF} - Z_{COG}) * \cos(\alpha)}\right)$$

$$\gamma_{ICE,E} = \operatorname{acos}\left(1 - \frac{t * r_{subm} + R_1 * \sin(\alpha - \alpha_0) - z_{COG} - Heave}{R_1 * \sin(\alpha - \alpha_0) + (Z_{IF} - Z_{COG}) * \cos(\alpha)}\right)$$

B.4 STEP 3: PROJECTING THE 3D SHAPE TO 2D

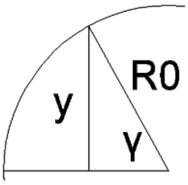

In the current state with circumferential coordinates the sections of the hull which are almost perpendicular to the ice flow direction would have a large influence on the overall ratios between the three colors. In order to solve this problem the 3D shape is projected to 2D, where the x-component is removed. The way this is done is by simplifying the circumferential coordinate to merely its y-component. This is done as follows:

$$\sin(\gamma) = \frac{y}{R_0}$$

From this it follows that:

$$y = R_0 * \sin(\gamma)$$

$$\gamma = \operatorname{asin}\left(\frac{y}{R_0}\right)$$

Applying this to the boundaries:

$$y_{ICE,S} = R_0 * \sin\left(acos\left(1 - \frac{-t(1 - r_{subm}) + R_1 * sin(\alpha - \alpha_0) - z_{COG} - Heave}{R_1 * sin(\alpha - \alpha_0) + (Z_{IF} - Z_{COG}) * cos(\alpha)}\right)\right)$$

$$y_{ICE,E} = R_0 * \sin\left(acos\left(1 - \frac{t * r_{subm} + R_1 * sin(\alpha - \alpha_0) - z_{COG} - Heave}{R_1 * sin(\alpha - \alpha_0) + (Z_{IF} - Z_{COG}) * cos(\alpha)}\right)\right)$$

B.5 STEP 4: THE INTEGRAL

Due to symmetry only half of the hull has to be integrated. The integral works as follows; first it calculates the area between the dotted lines in Figure B-7, then it subtracts the area above the curved line. The result is the area below the curved line.

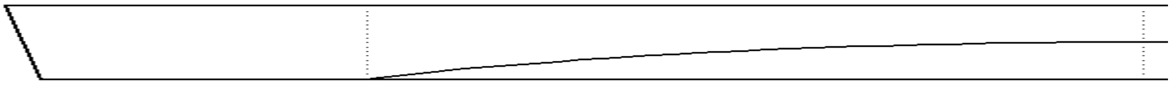

Figure B-7: Integral. Note that the figures aspect ratio is not 1:1.

$$\begin{aligned}\%COLOUR = \frac{1}{A_{ice}} \int_0^{y_{ICE,E}} t\, dy \\ - \int_{y_{ICE,S}}^{y_{ICE,E}} t(1 - r_{subm}) - R_1 * \sin(\alpha - \alpha_0) + z_{COG} + Heave \\ + ([(Z_{IF} - Z_{COG}) * \cos(\alpha)] - [-R_1 * \sin(\alpha - \alpha_0)]) * \left(1 - \cos\left(\operatorname{asin}\left(\frac{y}{R_0}\right)\right)\right) dy\end{aligned}$$

$$A_{ICE} = (R_0 + z_{IF} - (r_{subm} - 0.5)t)t$$

By solving the integral the final solution is obtained:

$$\%COLOUR = \frac{1}{A_{ice}}\left(t * y_{ICE,E} - \left[\left(y_{ICE,E} - y_{ICE,S}\right) * \left(t\left(1 - r_{subm}\right) - R_1 * \sin(\alpha - \alpha_0) + z_{COG} + Heave\right) + \left(R_1 * \sin(\alpha - \alpha_0) + \left(Z_{IF} - Z_{COG}\right)\cos(\alpha)\right) * \left(\left(y_{ICE,E} - y_{ICE,S}\right) - \frac{1}{2}\left(\left(y_{ICE,E}\sqrt{1 - \frac{y_{ICE,E}^2}{R_0^2}} + R_0 * \text{asin}\left(\frac{y_{ICE,E}}{R_0}\right) \right) - \left(y_{ICE,S}\sqrt{1 - \frac{y_{ICE,S}^2}{R_0^2}} + R_0 * \text{asin}\left(\frac{y_{ICE,S}}{R_0}\right) \right) \right) \right) \right] \right)$$

B.6 STEP 5: RESULTS

The results are 3 plots:

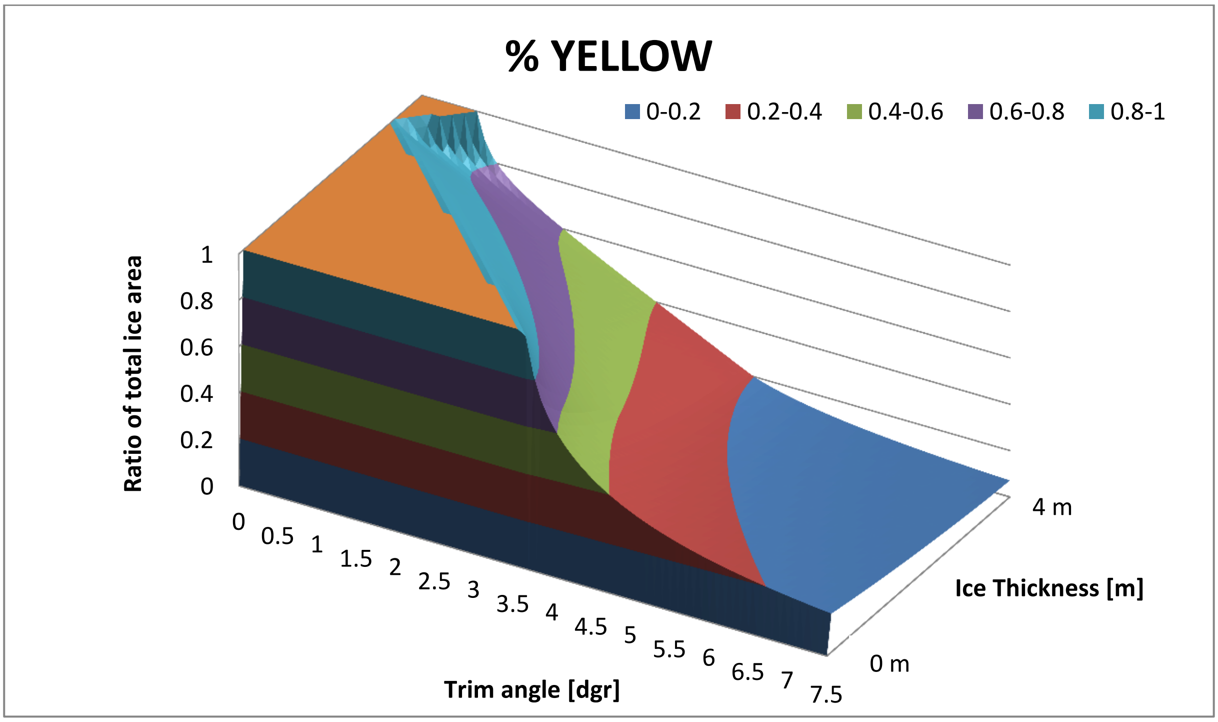

Figure B-8: %YELLOW. Ice thickness varies from 0 to 4.0 m.

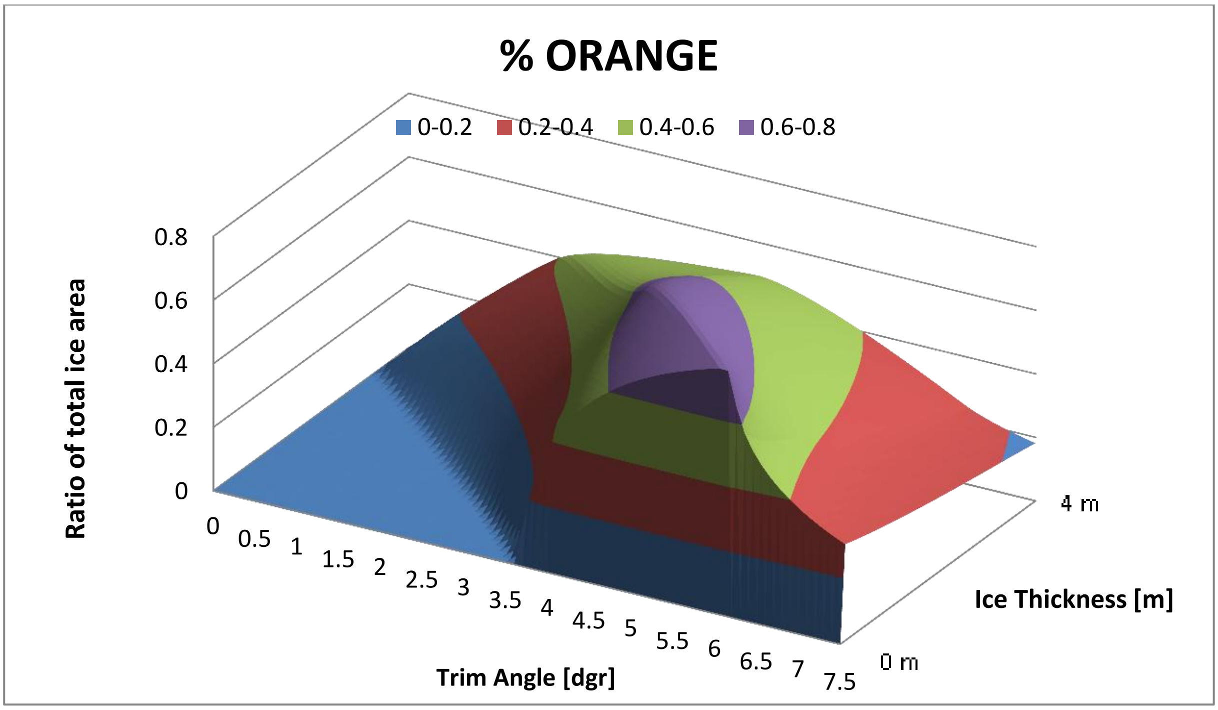

Figure B-9: %ORANGE. Ice thickness varies from 0 to 4.0 m.

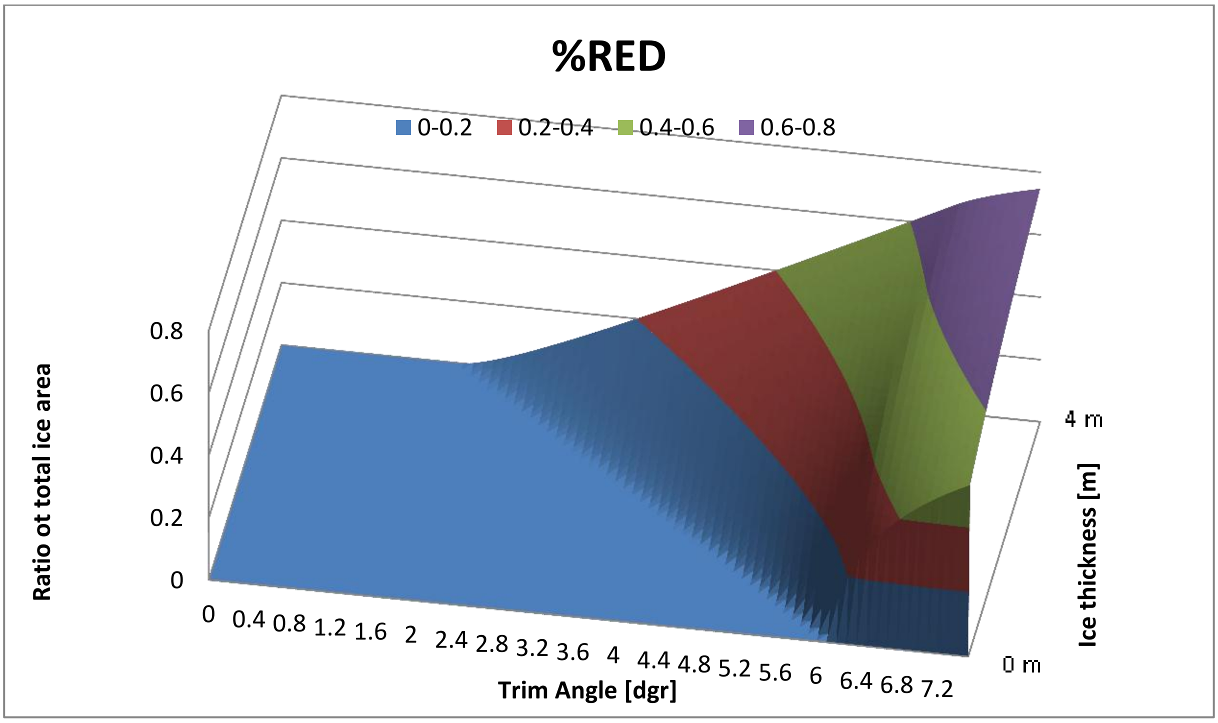

Figure B-10: %RED. Ice thickness varies from 0 to 4.0 m.

B.7 STEP 6: VERIFICATION

Since there is about a 103.4% chance to make mistakes during a derivation like this, the equation is compared with AutoCAD in order to check if the results are correct.

Data used to compare %RED to AutoCAD:

- $Z_{IF} = 5\ m$
- $Z_{COG} = 0\ m$
- $Heave = \ 0\ m$
- $R_0 = 45\ m$
- $r_{subm} = 0.898\ [-]$

Data used to compare %ORANGE to AutoCAD:

- $Z_{IF} = 3\ m$
- $Z_{COG} = 0\ m$
- $Heave = \ 0\ m$
- $R_0 = 46\ m$
- $r_{subm} = 0.898\ [-]$

%YELLOW is then calculated as follows:

$$\%YELLOW = 1 - \%ORANGE - \%RED$$

Next up are a few comparison of values. On the left is the AutoCAD value and on the right the equation's value for % yellow:

$t = 1.5\ m\ and\ \alpha = 3.0\ dgr$	
.7584	0.758
$t = 3\ m\ and\ \alpha = 5.0\ dgr$	
.1738	.173
$t = 2.5\ m\ and\ \alpha = 1.5\ dgr$	
.9067	.907

For the AutoCAD model the Z_COG was 0 m, thus the COG was on the mean water level. As this certainly will not always be the case in reality, another AutoCAD model was made were the COG was not at MWL in order to make sure the equation also gives the correct results for this case. After setting up the model and comparing the results, they also vary less than 0.1%.

APPENDIX C DERIVATION OF THE COMPLEX MOORING SYSTEM

The basis for the complex mooring system is the quasi-static mooring system response calculated by AQWA-DRIFT. The forces are given as a function of the in line horizontal and vertical distance from the anchor point.

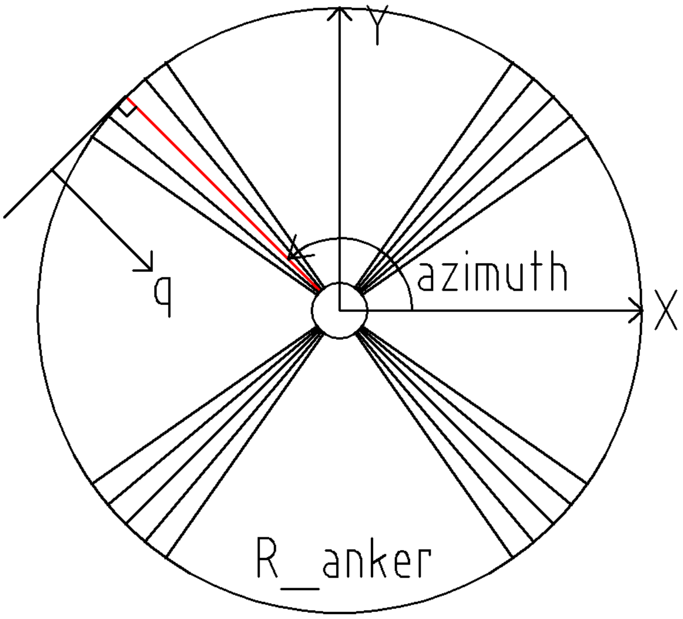

Figure C-1: The coordinate system of the vessel used in the rest of the report, (x,y), and the coordinate system used for the mooring lines, (q,d). Note that the q-axis is defined differently for every mooring line, as the axis is always parallel to the mooring line when viewed from the top. The starting point for the q-axis is always at the anchor point. The azimuth angle is defined as above and is 135 degrees for the red mooring line.

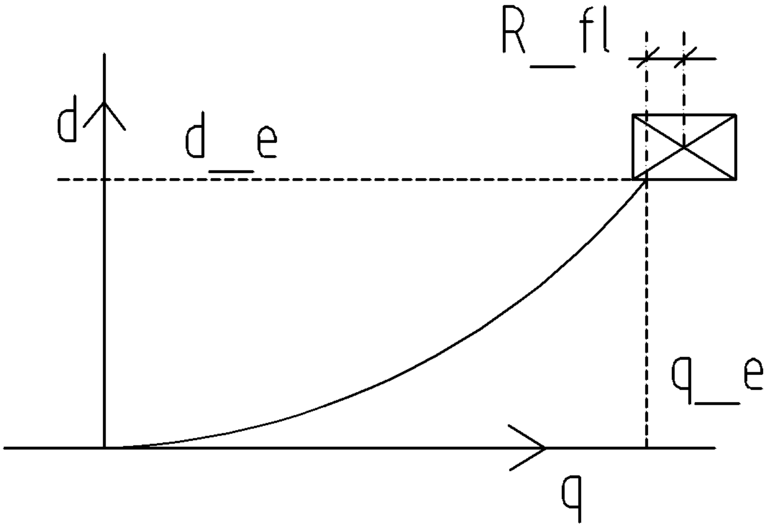

Figure C-2: Coordinate system used for the mooring system. The origin is at the anchor point. The ending points is located at (q_e, d_e). By looking up this location in the table from AQWA the quasi-static forces for this line can be determined.

C.1 INDIVIDUAL MOORING LINES

The first goal is too lookup up the mooring forces in the table from AQWA for every single mooring line. The input for this is the current vessel location and rotations as this determines the end point at the fairlead of each mooring line.

As the anchor points are all on the same circle with radius R_{anker} (see Figure C-1) their location in the global coordinate system (x,y,z) is given by:

$$Anker_x = R_{anker} * \cos(azimuth)$$

$$Anker_y = R_{anker} * \sin(azimuth)$$

The fairleads (points where the mooring lines enter the vessel) are also all on the same circle with radius R_{fl} (see Figure C-2). Their location in the global coordinate system (x,y,z) is given by:

$$fl_x = R_{fl} * \cos(azimuth)$$

$$fl_y = R_{fl} * \sin(azimuth)$$

$$fl_z = z_{cog} - z_{keel-fl}$$

Here z_{cog} is the vertical distance between the keel and the COG of the vessel. $z_{keel-fl}$ is the vertical distance between the keel and the fairleads (they all have the same vertical coordinate). The three distance fl_x, fl_y and fl_z effectively give the distance between the COG (= center of rotation) and the fairleads.

Next the fairlead positions need to be changed so they will account for the motions of the vessel. First the locations are translated in order to account for all three vessel rotations. This is done by using Ismail Hameduddin Matlab code of Rodrigues' rotation formula (Rodrigues). This gives the translated coordinates of the fairleads: $fl_{x,rot}, fl_{y,rot}$ and $fl_{z,rot}$. After this the x-, y-, and z-offset of the vessel are added to fl_x, fl_y and fl_z.

Now the start and ending coordinates of the mooring lines are known in the global coordinate system (x,y,z) and can now be calculated in the mooring system' coordinate system (q,d):

$$q_e = \sqrt{\left(anker_x - \left(fl_{x,rot} + x\right)\right)^2 + \left(anker_y - \left(fl_{y,rot} + y\right)\right)^2}$$

$$d_e = waterdepth - \left(fl_{z,rot} + \left(39 - z_{cog}\right)\right)$$

The last term in the d_e calculation is the distance between the vertical origin and the COG of the vessel. Added to fl_z it gives the depth of the fairleads in the (x,y,z) coordinate system. This depth is subtracted from the water depth as this is how the AQWA table is defined.

Now that the coordinates in the mooring coordinate system are known (q_e, d_e) the AQWA-LINE table comes into play. The table does not follow a regular Cartesian axis system, but has a diamond shape. This is because each entry of "d" (vertical mooring coordinate) has its own set of "q's" (horizontal mooring coordinates).

So the lookup process is done as follows. First the two values between which the vertical position (d_e) is located are found and then the two values between which the horizontal position falls (q_e). Now a very important check is done due to the diamond shape of the grid.

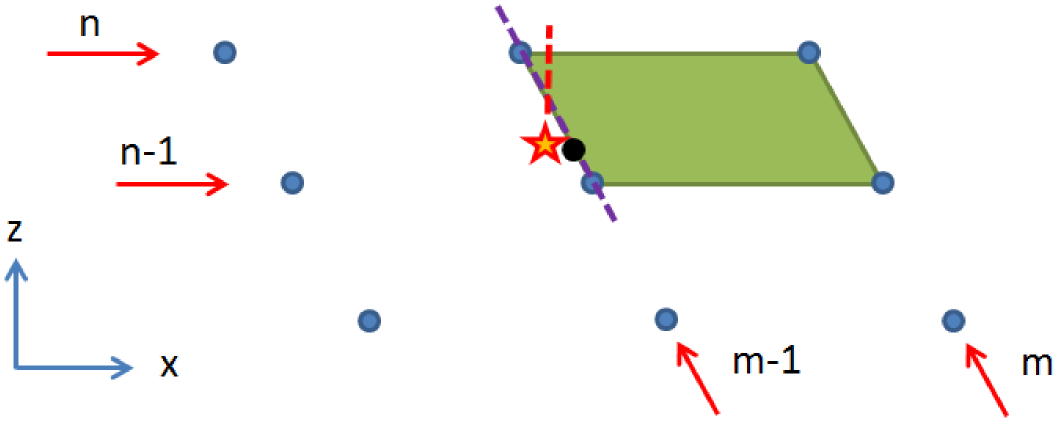

Figure C-3: Checking if the correct area if used or not.

Let us say the location (q_e, d_e) you are trying to find is represented by the star in the table. First the Z-value is checked. The Z-coordinates all have a regular spacing which makes it easy to see that the Z-coordinate of the star falls between rows "n" and "n-1". Next the two columns between which the X-coordinates of the star falls have to be found. The check is done in row "n", so when following the dashed red line upwards to row "n" we can see the Z-coordinate of the star is between the two blue dots of columns "m" and "m-1".

Now it would be easy to assume that the location of the star is inside the area with coordinates we just found (most of the time it is), this is the green diamond. However when looking at the location of the star it is not located inside the area! For this reason a check has to be done to determine on which side of the purple dashed line the star is located. The way this is done is by interpolating between points (n,m-1) and (n-1,m-1) to get the purple line. The X-coordinate of the purple line can now be calculated at the same Z-coordinate as the star, giving the black dot. If the X-coordinate of the star is smaller than the X-coordinate (to the left) of the black dot the area to the left of the green diamond should be used, thus 1 should be subtracted from the value of “m” calculated initially. If the X-coordinate of the star is bigger than the X-coordinate (to the right) of the black dot the green area is the correct area and also the initially value calculated for “m” is correct.

Now that the correct green area is known, the value at the location of the star can be calculated by using interpolation, see Figure C-4. First interpolating between the four blue points is done, to get the values at the correct Z-coordinates (the red dots). Then interpolation between the red points is done to get the value at the correct X-coordinate. This gives the final interpolated value at the purple dot.

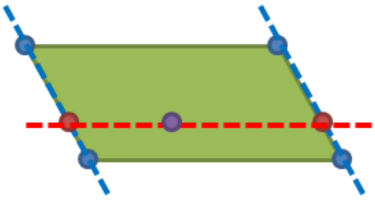

Figure C-4: Interpolating within the green area.

This interpolation process can be done twice to get the interpolated value of the horizontal F_h and vertical inline forces F_v of each individual line.

C.2 THE COMBINED EFFECT OF ALL THE MOORING LINES

Transferring between coordinate systems

Next all the inline forces need to be transferred to the global coordinate system (x,y,z). The z-force is the same in both coordinate systems so that one does not require any transformation. However the horizontal inline force needs to be decomposed into an x and y-component. This requires the azimuth angle of each mooring line after all the rotations of the vessel. For instance, in Figure C-5, it can be seen that a yaw-angle will results in a change in the azimuth angle. Similar (although smaller) effects occur due to the pitch and roll rotations.

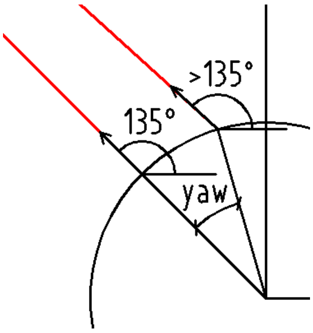

Figure C-5: A yaw-angle resulting in a different azimuth angle. The red line represents the mooring line.

The new azimuth angle is calculated as follows (written as Matlab code):

$$azimuth_{new} = atan2\left((anker_y - fl_y), (anker_x - fl_x)\right)$$

Atan2 is used because this gives angles from -π to π, unlike the normal atan which is limited to -π/2 to π/2.

Combining the restoring forces from of all the lines

Finally the combined effect of the N decomposed forces can be calculated. This then gives the global forces and moments acting on the vessel. This results in the following six equations:

$$F_x = \sum_{i=1}^{N} F_{h,i} * \cos\left(azimuth_{new,i}\right)$$

$$F_y = \sum_{i=1}^{N} F_{h,i} * \sin\left(azimuth_{new,i}\right)$$

$$F_z = \sum_{i=1}^{N} F_{v,i}$$

$$F_{mx} = \left(\sum_{i=1}^{N} -fl_{z,i} * F_{h,i} * \sin\left(azimuth_{new,i}\right)\right) + \left(\sum_{i=1}^{N} fl_{y,i} * F_{v,i}\right)$$

$$F_{my} = \sum_{i=1}^{N} fl_{z,i} * F_{h,i} * \cos\left(azimuth_{new,i}\right) + \sum_{i=1}^{N} -fl_{x,i} * F_{v,i}$$

$$F_{mz} = \sum_{i=1}^{N} -fl_{y,i} * F_{h,i} * \cos\left(azimuth_{new,i}\right) + \sum_{i=1}^{N} fl_{x,i} * F_{h,i} * \sin\left(azimuth_{new,i}\right)$$

Implementation in the ice-model

At each time-step the vessel's coordinates and rotations are send to the complex mooring force model. It then returns the three forces and moments which are then used to calculate the displacement for the next time step.

C.3 VERIFICATION

The complex mooring system model was checked in three different ways:

- Checking the interpolation code
- Checking the geometrical part
- Checking the answers

Checking the interpolation code

The lookup code could very easily be checked by seeing if the interpolated values fall within the bounds of the interpolation and after that by doing a few hand calculations to see if the code was doing the correct interpolation. After this it was checked if the code returned a smooth line for a constant increasing offset.

Checking the geometrical part

The translation of the fairleads due to the rotations of the vessel was quite a tricky part to set up correctly. The code was checked by creating a AutoCAD model with the same geometry as the vessel and then given it some (x,y,z) offset and rotating it in all three dimension. The values measured for (q_e, d_e) in AutoCAD were then compared against the value calculated by the code.

Checking the answers

First the final answers for the forces and moments were checked using common sense:

- When the vessel is located at the origin all the forces and moment should be zero
    - Only the z-component was not zero, resembling the mass of the lines.
- Given the vessel a certain horizontal offset (+40m), the vessel should be pulled down a bit (+0.17m) by the mooring lines and should get a slight negative rotation (-0.3 degree). The negative angle is correct because the horizontal mooring forces at the bottom of the vessel are pulling in negative x-direction and are thus creating a negative moment and thus a negative rotation.

The second check was to compare the calculated restoring force as a function of offset versus the same graph from the static mooring line report.

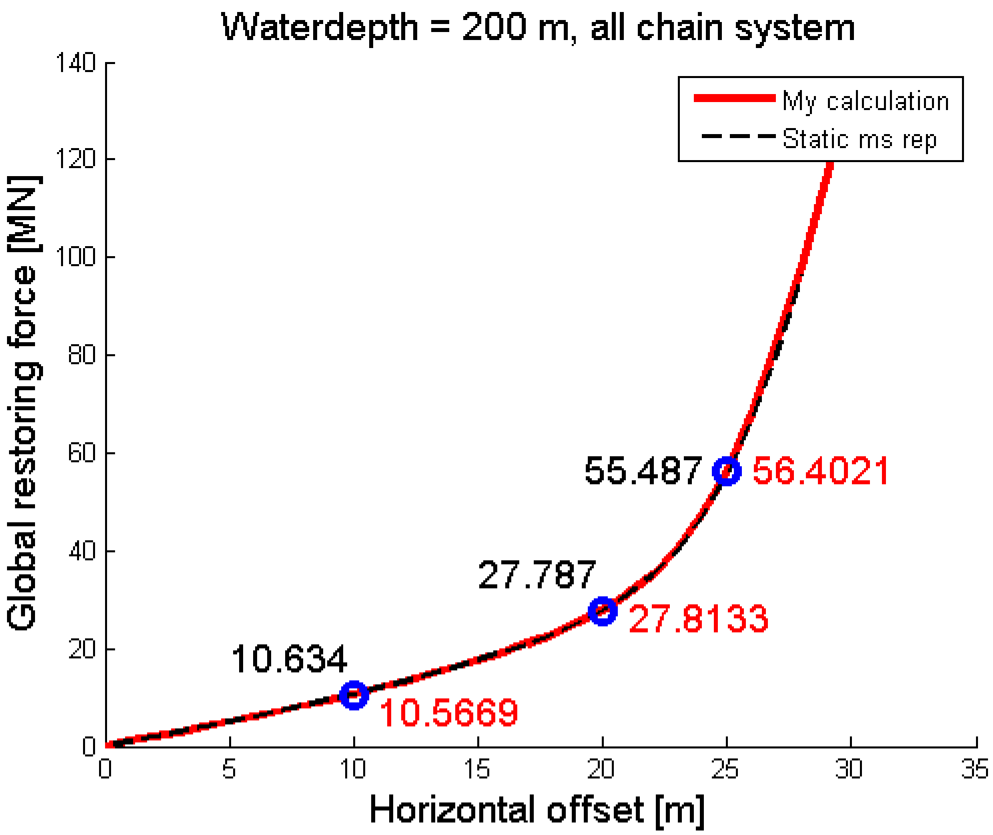

Figure C-6: Comparison between the implementation explained in this appendix and the original data from the static mooring line report.

When comparing the value they are very close indeed. At an offset of 10 meters the implementation explained here underestimates the original value by -0.7%. At 20 meters it is -0.3%. At 25 meters it is +1.65% and at the maximum offset of 28 meters it is 2.00%.

Conclusion

The performance of the complex mooring system is nearly exactly the same as the original calculation from the static mooring analysis.

APPENDIX D ALLOWING THE ICE TO COME FROM ALL DIRECTIONS

Because the mooring system is not radially symmetrical the response of the vessel is not the same for all direction of the ice. For this reason functionality is added that allows the ice to come from all directions and calculate all the loads accordingly.

In order to add this functionality several aspects have to be changed when switching from operating in a single direction to operating in a 2D plane. The things to be changed are:

- Relative velocity
- Ice force and moments
- Incorporation of the moments
- Trim angle

Next the changes to each of these aspects will be discussed.

D.1 RELATIVE VELOCITY

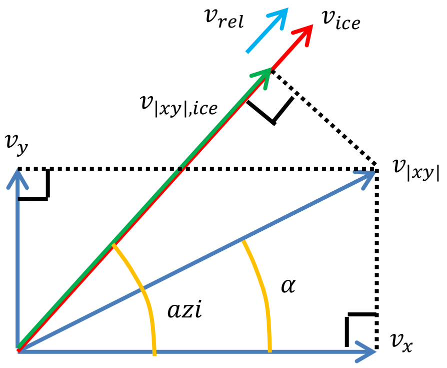

Using vectors the relative velocity is graphically derived as above. “azi” is the azimuth angle the ice makes with the positive X-direction and α is the azimuth angle the vessel’s velocity makes with the positive X-direction. v_x, v_y and $v_{|xy|}$ are the velocities of the vessel. Using equations the relative velocity can be calculated as follows:

$$v_{|xy|} = \sqrt{v_x^2 + v_y^2}$$

$$\alpha = atan2(v_y, v_x)$$

$$v_{|xy|,ice} = v_{|xy|} * \cos(\alpha - azi)$$

$$v_{rel} = v_{ice} - v_{|xy|,ice}$$

D.2 ICE FORCE AND MOMENTS

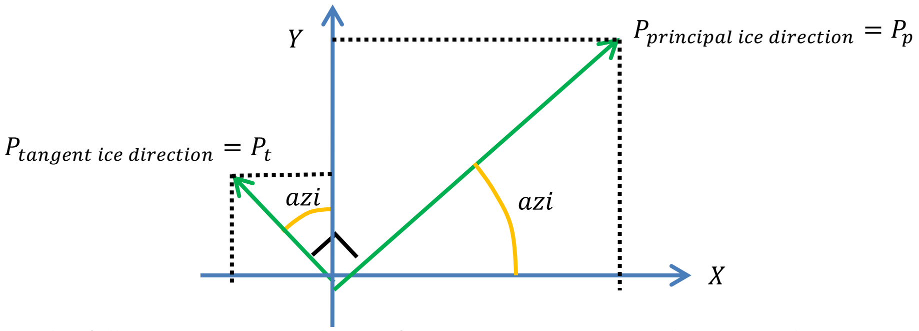
Y
$P_{principal\ ice\ direction} = P_p$
$P_{tangent\ ice\ direction} = P_t$
azi
azi
X

Using the following equations the ice forces and moments in the principal and tangent ice directions can be transformed into loads in the X and Y direction:

$$P_x = P_p * \cos(azi) - P_t * \sin(azi)$$

$$P_y = P_p * \sin(azi) + P_t * \cos(azi)$$

$$M_x = M_p * \cos(azi) - M_t * \sin(azi)$$

$$M_y = M_p * \sin(azi) + M_t * \cos(azi)$$

In matrix form, where c is cosine and s is sine:

$$\begin{bmatrix} \mathrm{c}(azi) & -\mathrm{s}(azi) & 0 & 0 & 0 & 0 \\ \mathrm{s}(azi) & \mathrm{c}(azi) & 0 & 0 & 0 & 0 \\ 0 & 0 & 1 & 0 & 0 & 0 \\ 0 & 0 & 0 & \mathrm{c}(azi) & -s(azi) & 0 \\ 0 & 0 & 0 & \mathrm{s}(azi) & \mathrm{c}(azi) & 0 \\ 0 & 0 & 0 & 0 & 0 & 1 \end{bmatrix} * \begin{bmatrix} P_p \\ P_t \\ P_z \\ M_p \\ M_t \\ M_z \end{bmatrix} = \begin{bmatrix} P_x \\ P_y \\ P_z \\ M_x \\ M_y \\ M_z \end{bmatrix}$$

D.3 INCORPORATION OF THE MOMENTS

In section 3.2.7 the arms for My where determined. Now that the ice can come from different directions this still has to results in the same motions. This means that the roll Mx needs to have the same arms as Mx. In matrix form it looks like:

$$\begin{bmatrix} 1 & 0 & 0 & 0 & 0 & 0 \\ 0 & 1 & 0 & 0 & 0 & 0 \\ 0 & 0 & 1 & 0 & 0 & 0 \\ 0 & 18.29 & -6.36 & 1 & 0 & 0 \\ -18.29 & 0 & 6.36 & 0 & 1 & 0 \\ 0 & 0 & 0 & 0 & 0 & 1 \end{bmatrix} * \begin{bmatrix} P_x \\ P_y \\ P_z \\ M_x \\ M_y \\ M_z \end{bmatrix} = \begin{bmatrix} P_x \\ P_y \\ P_z \\ M_x \\ M_y \\ M_z \end{bmatrix}_{correct}$$

First the calculation in section D.2 is done. The resulting forces and moments are multiplied with the matrix in this section.

D.4 TRIM ANGLE

Before when the ice was always moving in the positive X-direction the trim angles was always equal to the pitch angle (shown in Figure D-1). However now that the ice can come from any direction the trim angle has to be calculated in the direction of the ice (shown in Figure D-2).

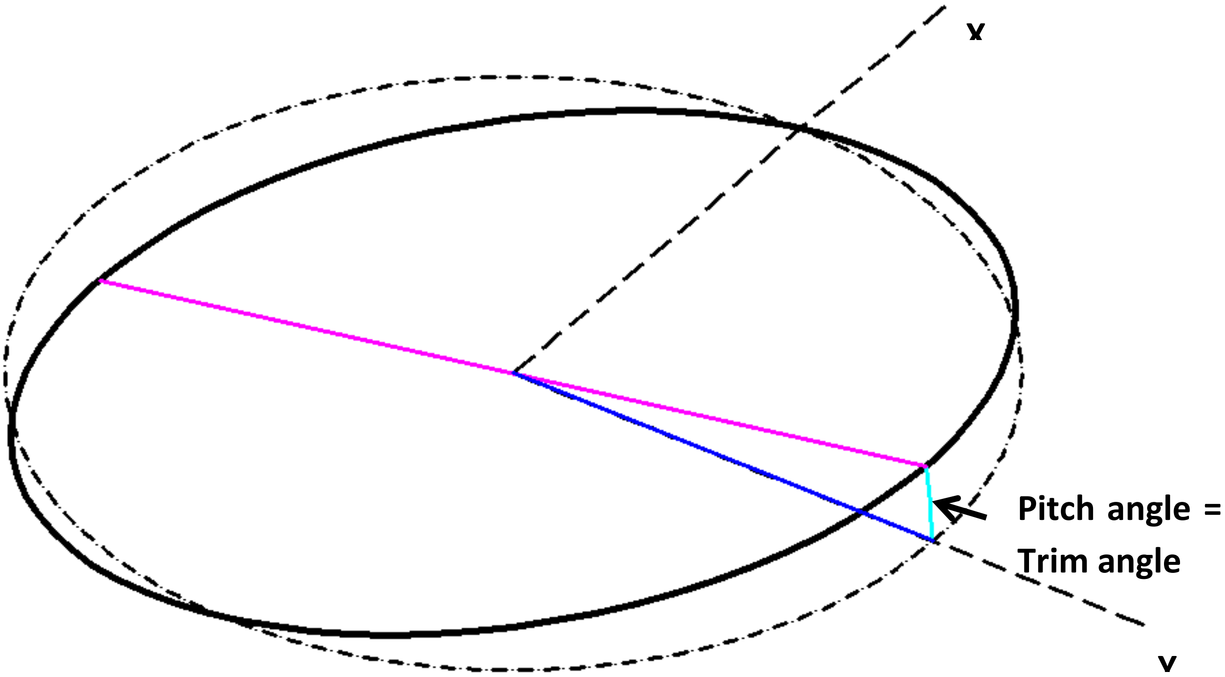

Figure D-1: Original situation where the pitch angle equals the trim angle.

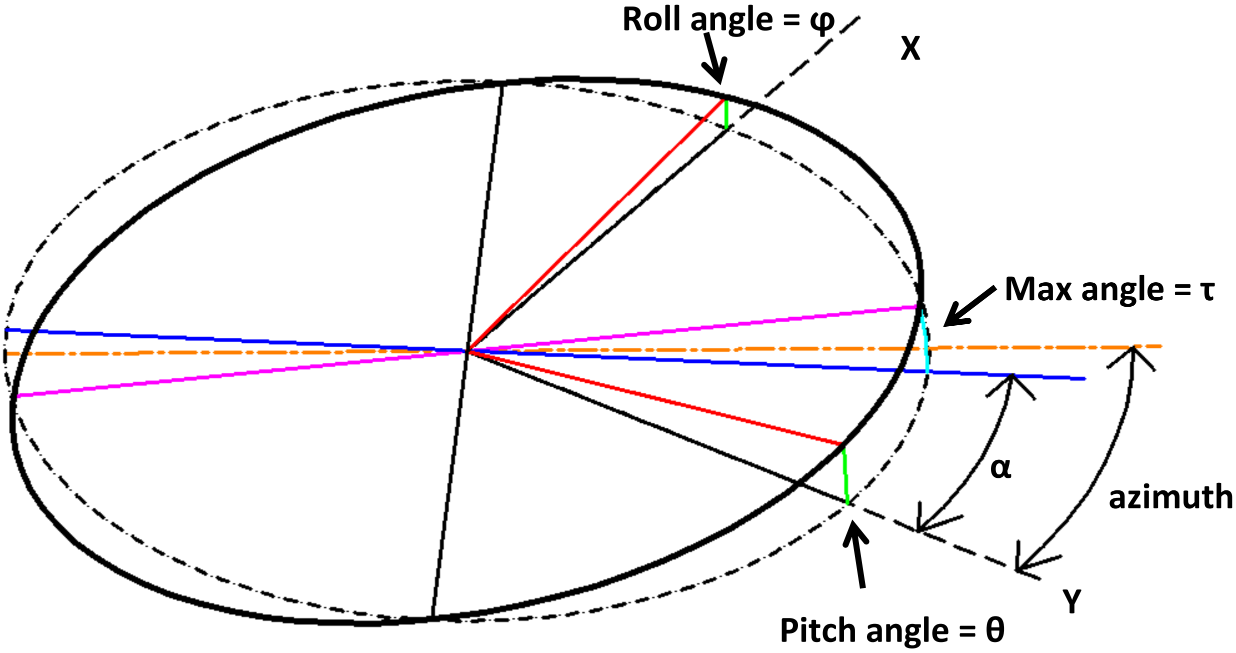

Figure D-2: The new situation where the ice can come from any direction. Note that the ice direction (azimuth) does not have to coincide with omega, which is the maximum trim angle.

The height of the end point of the purple line is, where τ is the maximum angle:

$$h = R * \tan(\tau)$$

The height on any point of the circle is then as a function of alpha:

$$h(\alpha) = R * \tan(\tau) * \cos(\alpha)$$

The roll and pitch angle are known since there are calculated at each time step. So by setting the equation above equal to the known angles we get two equations:

$$\tan(\varphi) = \frac{h(90-\alpha)}{R} = \frac{R * \tan(\tau) * \cos(90-\alpha)}{R} = \tan(\tau) * \cos(90-\alpha) = \tan(\tau) * \sin(\alpha)$$

$$\tan(\theta) = \frac{h(\alpha)}{R} = \frac{R * \tan(\tau) * \cos(\alpha)}{R} = \tan(\tau) * \cos(\alpha)$$

Now alpha can be found:

$$\frac{\tan(\varphi)}{\sin(\alpha)} = \frac{\tan(\theta)}{\cos(\alpha)} \rightarrow \frac{\sin(\alpha)}{\cos(\alpha)} = \frac{\tan(\varphi)}{\tan(\theta)} \rightarrow \tan(\alpha) = \frac{\tan(\varphi)}{\tan(\theta)} \rightarrow \alpha = \operatorname{atan}\left(\frac{tan(\varphi)}{tan(\theta)}\right)$$

Now the trim angle can be calculated by substituting the alpha in one of the equation above:

$$\tan(\varphi) = \tan(\tau) * \sin(\alpha) \rightarrow \tau = \operatorname{atan}\left(\frac{tan(\varphi)}{sin\left(atan\left(\frac{tan(\varphi)}{tan(\theta)}\right)\right)}\right)$$

Now the trim angle in the direction of the ice can be calculated as follows:

$$\tan(trim\ angle) = \operatorname{atan}(\tau) * \cos(azimuth - \alpha)$$

$$trim\ angle = \operatorname{atan}\left[tan\left(atan\left(\frac{tan(\varphi)}{sin\left(atan\left(\frac{tan(\varphi)}{tan(\theta)}\right)\right)}\right)\right) * cos\left(azimuth - atan\left(\frac{tan(\varphi)}{tan(\theta)}\right)\right)\right]$$

By simplifying the final equation for the trim angle is:

$$trim\ angle = \operatorname{atan}\left[\frac{tan(\varphi)}{sin\left(atan\left(\frac{tan(\varphi)}{tan(\theta)}\right)\right)} * cos\left(azimuth - atan\left(\frac{tan(\varphi)}{tan(\theta)}\right)\right)\right]$$

The equation above was verified by using AutoCAD.

APPENDIX E SOLVING THE EQUATION OF MOTION

In this section the steps taken to arrive at the final dynamic model are described.

E.1 ANALYTICAL SOLUTION

The equation of motion derived in section 3.1.7 is simplified in order to allow for an analytical solution. What was done was to linearize the quadratic drag term and the global horizontal restoring force curve. For the 1DOF system the equation of motion now reduces to the following:

$$(m + a_{11})\ddot{x} + c\dot{x} + k_{ms,11}x = F_{ice,x}$$

Where m and a_{11} were taken from data as described in section 3.1, for c the added damping term was taken at the wave frequency equal to the natural frequency, for k a linearized spring term was derived from the mooring system's restoring force table and $F_{ice,x}$ was changed as needed.

Analytical solution

Next the differential equation has to be solved. The analytical solution has the following form (Metrikine, 2006):

$$x(t) = \exp(-nt)\left(x_0\cos(\omega_1 t) + \left(\frac{v_0}{\omega_1} + \frac{nx_0}{\omega_1}\right)\sin(\omega_1 t)\right) + \frac{1}{\omega_1}\int_0^t f(t')\exp\left(-n(t-t')\right)\sin\left(\omega_1(t-t')\right)dt'$$

Where:

$$n = \frac{c}{2m}, \qquad \omega_n^2 = \frac{k}{m}, \qquad f(t) = \frac{F(t)}{m}, \qquad x(0) = x_0, \qquad \dot{x}(0) = v_0$$

In order to solve the Duhamel integral a numerical approach was used due to the discrete form of the load function. The trapezoidal rule was chosen for its simplicity and velocity since a higher order of accuracy was not needed at this point as the equation would only be used for testing more advanced solutions.

Verification

The model was verified in this following ways:

- Check that when entering a constant load of F=5*k the vessel stabilizes at an offset of 5 meter
    - OK
- Check whether the motion of the vessel decays
    - OK
- Check whether the period of the motion corresponds with natural period calculated by hand
    - OK

E.2 NUMERICAL SOLUTION USING SIMULINK – 1DOF

The next step was to find a way to solve the equation of motion but now including the drag term. The answer came in the form of Simulink, an add-on to Matlab which allow the user to solve equations by simply connecting boxes.

After setting up the Simulink model it soon became apparent that the trapezoidal rule was much slower than using Simulink. Because of this everything was quickly transferred to Simulink to take advantage of the extra speed. Simulink is also capable of handling matrices and vector and therefore can be changed to represent a 3DOF system with only minimal effort involved, making it very future proof.

Replicating the analytical solution

The initial step was to create a model in Simulink that could replicate the results on the analytical solution to allow verification of the new Simulink model. Since this old version with linear damping was altered afterwards to include the quadratic drag term, no plots are available anymore. However the Simulink model was tweaked and fixed until it gave the exact same results as the analytical solution (apart from a small difference caused by numerical rounding, probably due to the usage of the trapezoidal rule).

Including drag & non-linear mooring forces

The next step was to add quadratic damping in the form of the drag force and to replace the linearized mooring force by its non-linear lookup table. The resulting Simulink model is briefly discussed as it forms the basis for all future models.

The 1DOF Simulink model consists of several sections as can be seen in Figure E-1. The principal behind the model is that it start with force, this is then divided by the mass to get acceleration. The acceleration is then integrated to give the velocities. Damping forces are then calculated based on this velocity and the velocity is then integrated to give displacement. The displacements are used to calculate the mooring force. All calculated forces are than added together to provide input for the next time step.

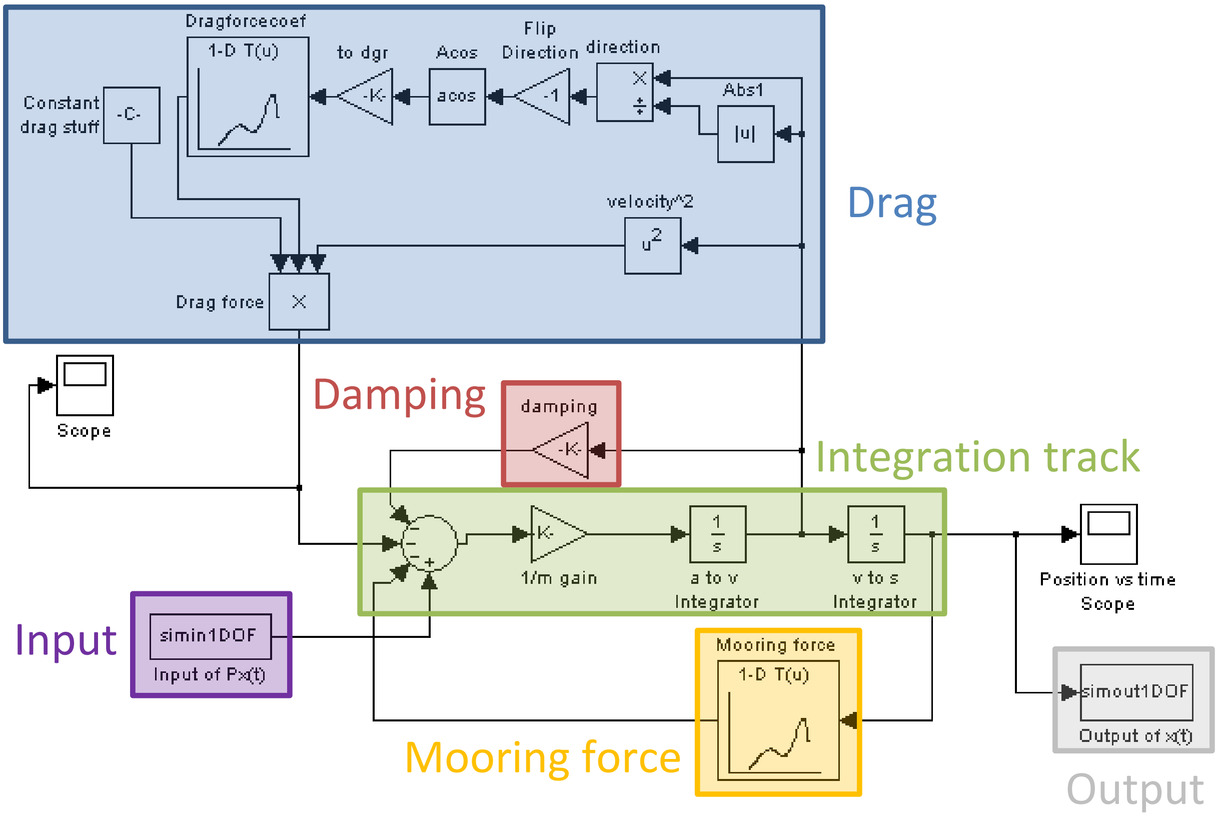
Dragforcecoef
1-D T(u)
to dgr
-K-
Acos
acos
Flip
Direction
-1
direction
Abs1
|u|
Constant
drag stuff
-C-
velocity^2
u^2
Drag force
Drag
Scope
Damping
damping
-K-
Integration track
-K-
1/m gain
1/s
a to v
Integrator
1/s
v to s
Integrator
Position vs time
Scope
Input
simin1DOF
Input of Px(t)
Mooring force
1-D T(u)
Mooring force
simout1DOF
Output of x(t)
Output

Figure E-1: 1DOF Simulink model.

Next a detailed explanation of each of the units that make up the total model will be given. Although the description is given for the 1DOF model, the 3DOF and 6DOF models works in a very similar way.

- **Integration track**: the first block in the integration track is the summation block, called the force pool from now on. In this block the input of the horizontal component of the force from the ice model arrives together with all the other horizontal components of the force from within the system. Next the force is divided by the mass in order to get the acceleration. This is then integrated to get the velocities and integrated again the get the displacements. The displacements are then sent back to Matlab.
- **Mooring force**: the simple mooring force is calculated using a lookup-table. It uses a table taken from the static mooring line calculation. The table contains the global restoring force as a function of the displacement of the vessel. The displacement enters the lookup-table. Based on cubic-spline interpolation the restoring force is calculated and then added to the force pool.
- **Damping**: the velocity branches off into two parts. The red damping part is actually not used for the 1DOF system as the linear viscous damping only has components in the Z, pitch and roll direction.
- **Drag**: the other branch of the velocity is used to calculate the drag force. The velocity input is used twice; the bottom path is used to calculate the velocity squared which is used in the drag force calculation itself and the upper path is used to select the correct drag coefficient, which is based on the direction in which the vessel is moving. For the 1DOF model, it can only move in two directions: positive X and negative X. The direction is determined by dividing the velocity by the absolute value. This step then returns 1 (moving towards positive X) or -1 (moving towards negative X).

  Because the coefficients used come from a calculation for the drag force caused by the current, the direction has to the changed 180 degrees. The reason for this is that when the vessel is moving the positive X-direction, it effectively experiences a current coming from the negative X-direction. For the 1DOF system, 180 degrees can simply be added by multiplying by -1. Next the arccosine is taken to revert back to degrees, which is used in the lookup-table.

  Finally all the components are multiplied and the drag force is returned to the force pool.
- **Input**: a vector is send from the Matlab environment to the Simulink model containing the force at each time step.
- **Output**: the calculated motions are sent back to Matlab at each time step.

Verification

Due to the addition of the drag and non-linear mooring force some checks were in order:

- Check that when entering a constant load taken from the mooring force table results in the corresponding offset
  - OK
- Check whether decay of the vessel's motions shows a quadratic relation
  - OK
- Check whether the period of the motion corresponds with natural period calculated by hand
  - OK

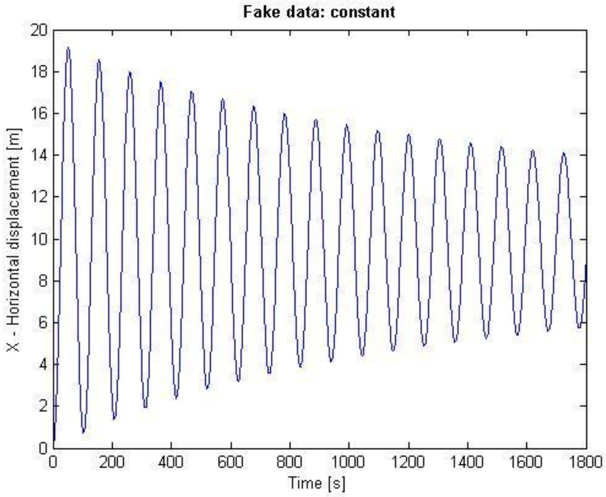

Figure E-2: Decay in the peaks of the motions. Also somewhat visible is that the vessel will stabilize at an offset of 10 meters, given the correct offset as the force corresponding to 10 meter was entered. The natural frequency is 108 second, exactly like the period between the peaks.

E.3 NUMERICAL SOLUTION USING SIMULINK – 6DOF

The Simulink model shown above is only 1DOF and is still missing several key components. Consecutive models which increase the “realism”, functionality and accuracy of the dynamic model where all rigorously tested. In general the following steps the following steps were used; however simpler addition skipped a few steps:

- Build the new module in an isolated environment so it can be tested on its own. This removes most of the obvious bugs having to do with the calculations themselves.
- Integrate the module in the model and test if all the interfaces with other modules work properly. This removes most bugs having to do with communication between individual modules
- Finally run the model and test the results against common sense and previous version of the model. The following hierarchy was used for testing:
    - AQWA -> Simulink 6DOF -> Simulink 3DOF -> Simulink 1DOF -> Analytical solution

  Where possible the model was also tested against other sources of data to provide further verification.

The main level of the final Simulink model is shown below.

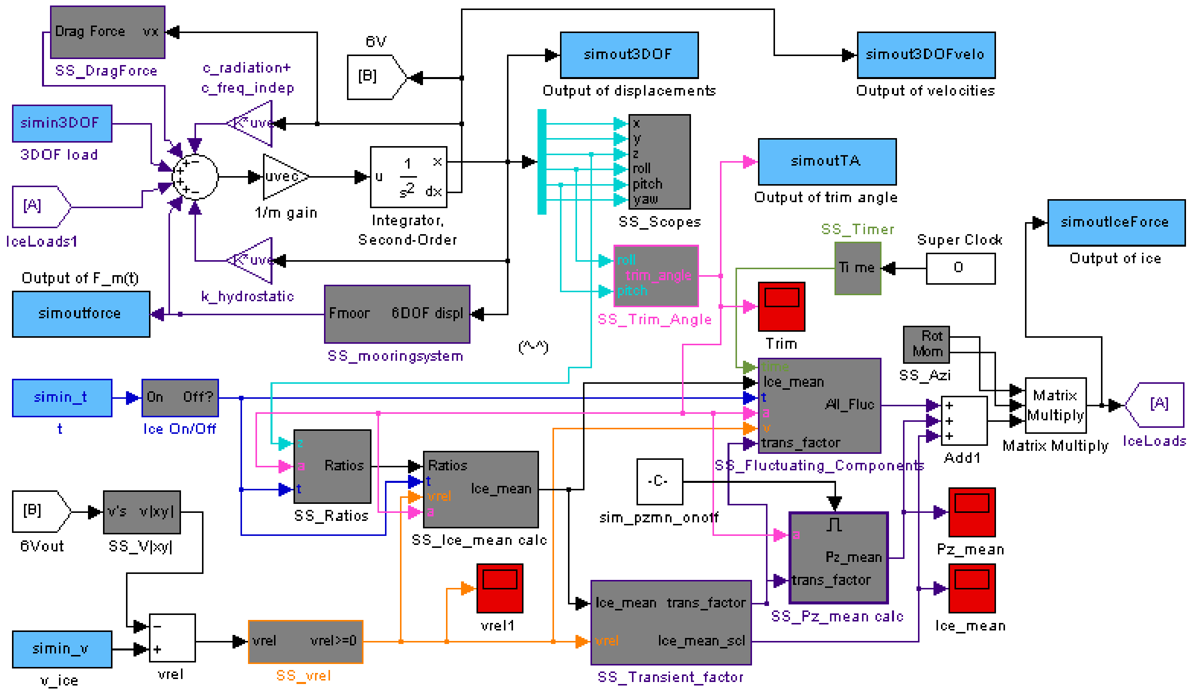
Drag Force vx
SS_DragForce
c_radiation+
c_freq_indep
6V
[B]
simout3DOF
Output of displacements
simout3DOFvelo
Output of velocities
simin3DOF
3DOF load
[A]
IceLoads1
K*uvec
uvec
1/m gain
1
s2
u
x
dx
Integrator,
Second-Order
x
y
z
roll
pitch
yaw
SS_Scopes
simoutTA
Output of trim angle
SS_Timer
Time
Super Clock
0
simoutIceForce
Output of ice
Output of F_m(t)
simoutforce
K*uvec
k_hydrostatic
Fmoor 6DOF displ
SS_mooringsystem
(^-^)
roll
trim_angle
pitch
SS_Trim_Angle
Trim
Rot Mom
SS_Azi
simin_t
t
On Off?
Ice On/Off
Ice_mean
All_Fluc
t
a
v
trans_factor
SS_Fluctuating_Components
Add1
Matrix Multiply
Matrix Multiply
[A]
IceLoads
z
a
t
Ratios
SS_Ratios
Ratios
t
vrel
a
Ice_mean
SS_Ice_mean calc
-C-
sim_pzmn_onoff
a
Pz_mean
trans_factor
SS_Pz_mean calc
Pz_mean
Ice_mean
[B]
6Vout
v's v|xy|
SS_V|xy|
vrel1
simin_v
v_ice
vrel
vrel vrel>=0
SS_vrel
Ice_mean trans_factor
vrel Ice_mean_scl
SS_Transient_factor

Figure E-3: This main level of the final Simulink model. Grey boxes are subsystem, blue boxes are interfaces with Matlab and red boxes are used to show the output of the connection line.

APPENDIX F SIGNAL CREATION

In this appendix two methods to create statistically identical signals from measured data are discussed. First the use of spectrums is discussed and after that autoregressive models.

F.1 SPECTRUMS

When analyzing frequencies contained within a signal an obvious thing to try is to create a spectrum. In this section the process of creating a spectrum from the model test data is described. All the steps and their impact on the spectrums are discussed. Finally a conclusion is given on the usage of spectrums for generation of ice loads.

F.1.1 BACKGROUND INFORMATION

When discussed during class making a spectrum was made out to be very easy thing, however when actually trying to create a spectrum it turned out to be much more difficult. The problem becomes even greater because some means of interpolation between the spectrums is also needed. Due to the large task ahead, it is helpful to first sketch an ideal situation which would results in a perfect spectrum and then come back to the model test data to investigate in which ways the current signals are lacking.

The information below comes from (Holthuijsen, 2007) and in particular Appendix C – Spectral analysis and was covered in his class Ocean Waves (a great class).

The definition of the spectrum is given as follows:

$$E(f) = \lim_{\Delta f \to 0} \frac{1}{\Delta f} E\left\{\frac{1}{2} \underline{a_i^2}\right\}, \quad with\ \Delta f = \frac{1}{D}$$

Where E(..) is the expected value, Δf is a frequency band, a is the amplitude of a harmonic component and D is the duration of the time history.

In order to be able to calculate the perfect spectrum several things are needed:

- In order to calculate the limit, an infinitely long time history is needed in order to get infinitely small frequency bands (and thus an infinitely high spectral resolution).
- In order to calculate the expected value for each of the amplitudes squared, an infinite number of tests are required.
- The sample rate at which the sensor acquires data has to be infinitely short to get a continuous signal.

Just by reading the requirements it quickly becomes apparent that any spectrum created from the model tests will be far from perfect. The shortcomings of the available data have certain consequences:

- The load time histories are not infinitely long. This means that Δf will not be infinitely small. The implication of this shortcoming is that instead of having a value at every infinitely small distance (which results in a near-continuous series of dots) the spectrum only has values at a fixed interval. This results in a series of discrete set of dots as can be seen in Figure F-1. So what happens as the duration of the time history decreases is that the spectral resolution is reduced.

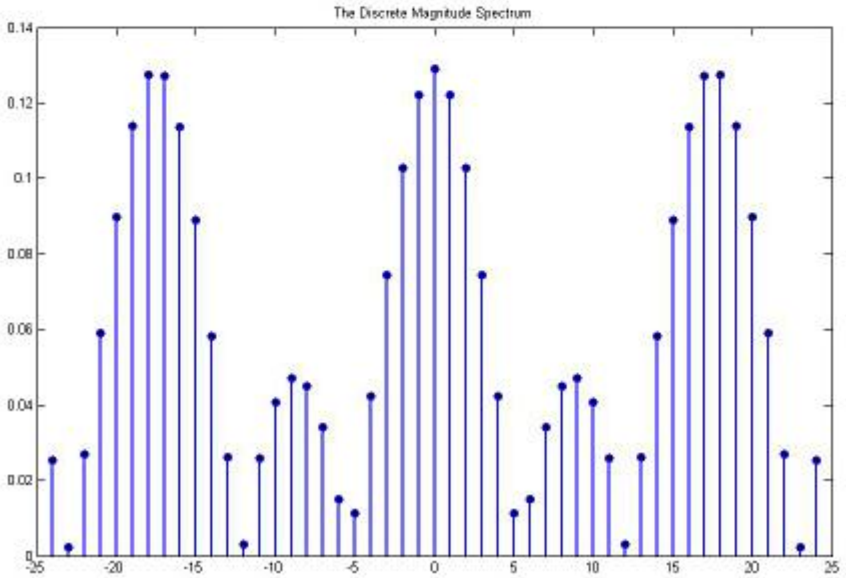

Figure F-1: An example of a discrete spectrum (from Wikipedia).

- The next shortcoming is that each test was only repeated once. This means that when calculating the expected value, an average is calculated with a sample size of only one! The result of this that the calculated spectrum looks very spiky, see Figure F-2. What this basically means is that there is a large error for each of the values in the spectrum. This simplest way to reduce this error is to cut the original time history into several smaller ones. By then calculating the spectrum of each of those smaller time histories and averaging the spectrums, a more reliable estimate of the actual spectrum is obtained. The big downside to this is that it comes at a loss of spectral resolution because the lengths of time histories are much shorter.

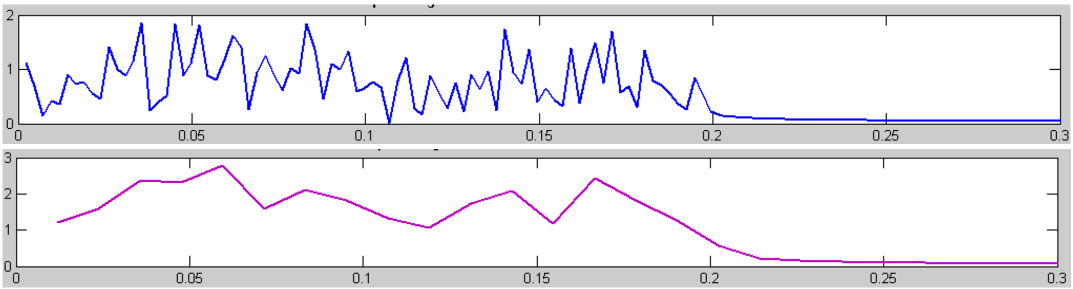

Figure F-2: Two spectrum of the same time history. The top one has a large error but a high spectral resolution. The bottom one has a smaller error but this came at a loss in spectral resolution.

- The third shortcoming is that the time history is discrete because it was sampled at a fixed time interval. However as the sampling rate was high enough for these tests, 150 Hz at model scale or about 20 Hz at full scale, this does not create any problems as the frequency of the ice action is in the order of about 0.1-0.2 Hz, thus given enough detail in the time history in order for the FFT algorithm to be able to distinguish individual waves and avoid aliasing.

In order to generate a signal a spectrum will have to be created regardless of all the shortcomings described above. The process to create these spectrums is described next.

F.1.2 Original data

After the model tests KSRI post-processed the data and selected segments from the full time histories. They choose segments which they thought represented a stationary situation that was free of weird anomalies such as large random spikes. These were then used to calculate things like the mean and max and then ended up in their report.

The problem with KSRI's pre-selected data is that in general they only choose a very small duration of the total available time history. As discussed in the previous section; the shorter the time history used, the poorer the resulting spectrum. Despite this problem several spectrum were created and indeed their spectral resolution was very poor and in general the spectrums were very spiky. Since the time histories were already very short, splitting them so the resulting spectrums can be averaged in order to reduce the error did not seem like a good idea.

Beating

In addition there was another problem. When generating a signal using the spectrums the length of the generated signals was exactly equal to the length of the original signal, or basically beating starting to happen, see Figure F-3. This is directly related to the beating of two sin waves:

$$\sin(2\pi f_1 t) + \sin(2\pi f_2 t) = 2\cos\left(2\pi \frac{f_1 - f_2}{2} t\right) \sin\left(2\pi \frac{f_1 + f_2}{2} t\right)$$

The carrier wave takes on the frequency of the frequency difference between the two waves $f_{carrier\ wave} = f_1 - f_2$. The same thing happens when superimposing several sinuses, e.g. when recreating a signal from a spectrum. The carrier will again take on the frequency of the smallest frequency difference between any of the waves present in the spectrum. As the frequency step size of the spectrum was defined as $\Delta f = \frac{1}{D}$, the smallest frequency difference possible for any spectrum is the width of its frequency step size. Therefore the lowest frequency the carrier waves can take is exactly Δf. The resulting beating-period is then $\frac{1}{\Delta f} = D$, which is the exact length of the original signal. This explains why the signal generated from any spectrum has the same length as the original signal.

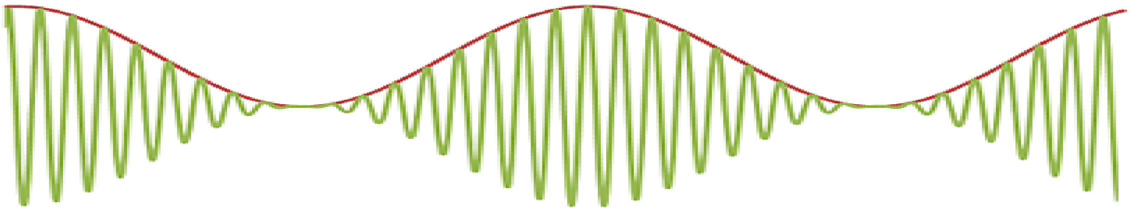

Figure F-3: Two sin waves superimposed result in beating. The red wave is the carrier wave and its frequency is equal to the beating frequency and thus to length of the signal that can be generated.

F.1.3 LONG DATA

In order to improve to quality of the spectrum longer time histories were needed and luckily these were available. Included in the package of files received from KSRI were the full length time histories from most of the test. In Figure F-4 the original data and the data selected can be seen.

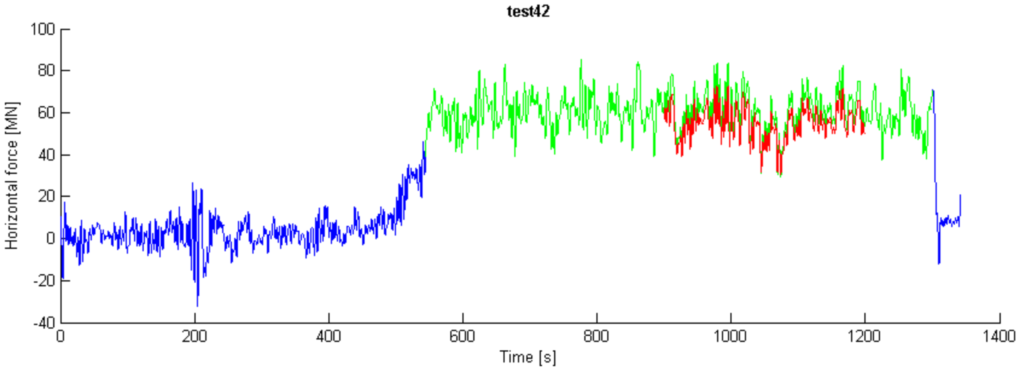

Figure F-4: Blue: original signal. Green: the segment selected by the algorithm. Red: the segment selected by KSRI. Note that this figure shows one of the better improvements in term of length, not all of the tests improved this much.

The selection was made using an algorithm that was created that calculates the moving average and then checks how much it deviates from the mean value of the segment selected by KSRI. By doing this several times, new starting and ending location are calculated. The segment selected by the algorithm is shown in green in Figure F-4.

When looking at Figure F-4 one can note that the red segment is lower than the green segment (or blue which is directly behind the green). This reason for this is that KSRI did some post-processing on the signal which results in a different mean value. But as the green segment will only be used to model the fluctuating part of the force, which is the same for the red or green, this does not matter.

Next there is one more problem with the green data, and that is that it has spikes in it. KSRI chose the segment they did because they are free of spikes. Therefore ideally the spikes have to be removed from the green segment in order to create a more reliable spectrum. This time consuming process was postponed for now and the not-so-perfect spectrum will be used for now.

F.1.4 WINDOW FUNCTIONS

In signal processing it is common to use windows on the originals signals. The windows scale the original signal so that the part of the signal that falls outside the window is equal to zero. Within the window the original signal is multiplied by the window function. Each window has a different shape. The different shapes result in different shapes of the spectrums generated. The general goal of a window is to reduce the impact of the discontinuity at the beginning and end of the signal on the resulting spectrum. Below are some examples of common windows.

Rectangular windows

The simplest shape is a rectangular window. Quoting from Wikipedia:

"The rectangular window is sometimes known as a Dirichlet window. It is the simplest window, equivalent to replacing all but N values of a data sequence by zeros, making it appear as though the waveform suddenly turns on and off. Other windows are designed to moderate the sudden changes because discontinuities have undesirable effects on the discrete-time Fourier transform (DTFT)"

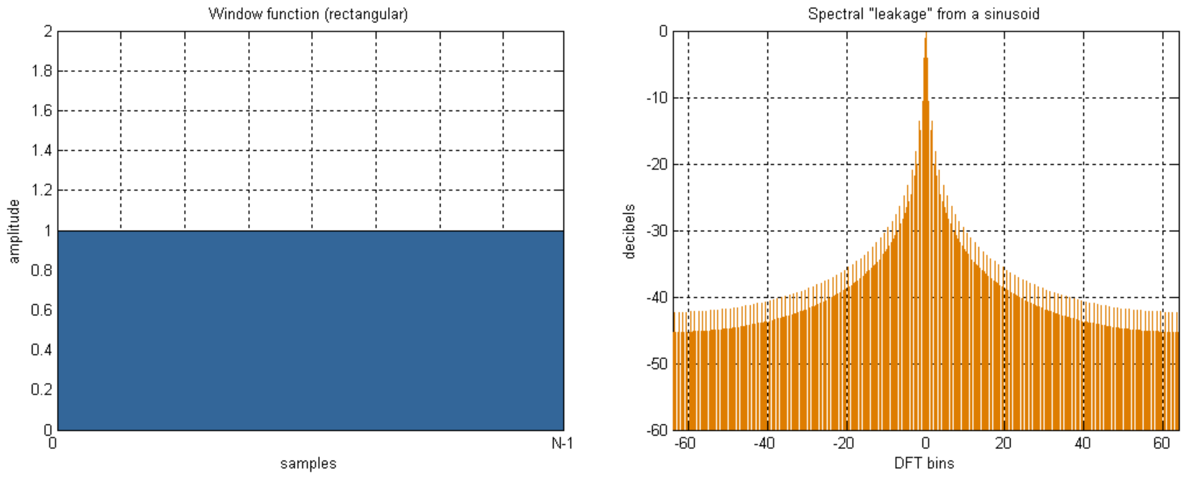

Figure F-5: The rectangular window and its spectrum (from Wikipedia).

Hanning window

The Hanning window is a very common window to use. According to the internet: "The Hanning window is a general purpose window for the analysis of continuous signals and should be used in most cases, because it has the best overall filter characteristic. The Hanning window may also be used for system analysis (frequency response measurements) - for both excitation and response signal when a random excitation signal is used."

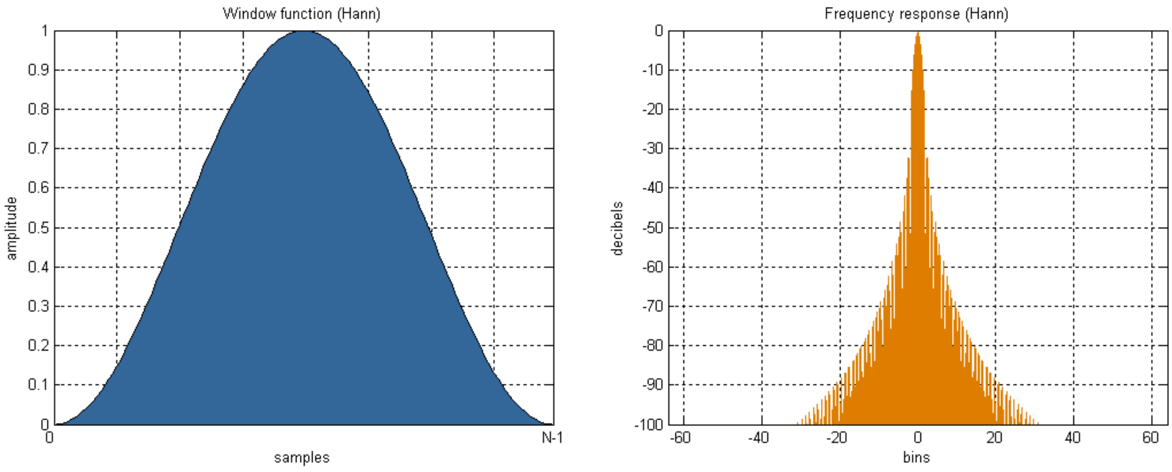

Figure F-6: The Hamming window and its spectrum (from Wikipedia).

Using the window

Now the influence of the different windows on the spectrums is tested by creating a spectrum from the model test data, see Figure F-7.

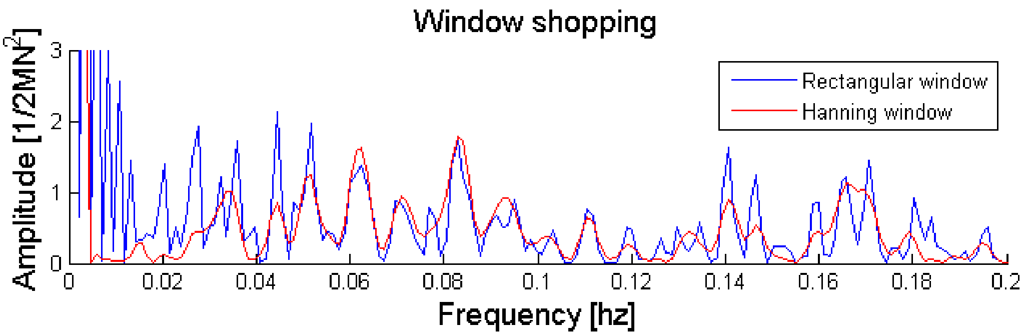

Figure F-7: Comparing the spectrums created when using different windows. Data is from Test 31, Px. 1.5 m, 0.5 m/s. 0 degree.

The difference between the two windows is quite significant. The windowed spectrum has less large peaks in the low frequency ranges. When checking other kinds of window functions to make sure this results is not unique to the Hanning window they also show a similar result.

However if we look at a different test the impact is even more significant:

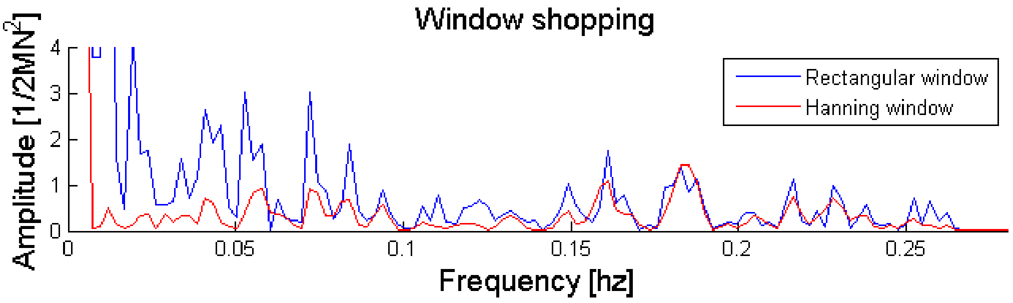

Figure F-8: Window comparison for test 32, Px. 1.5 m, 1.5 m/s. 0 dgr.

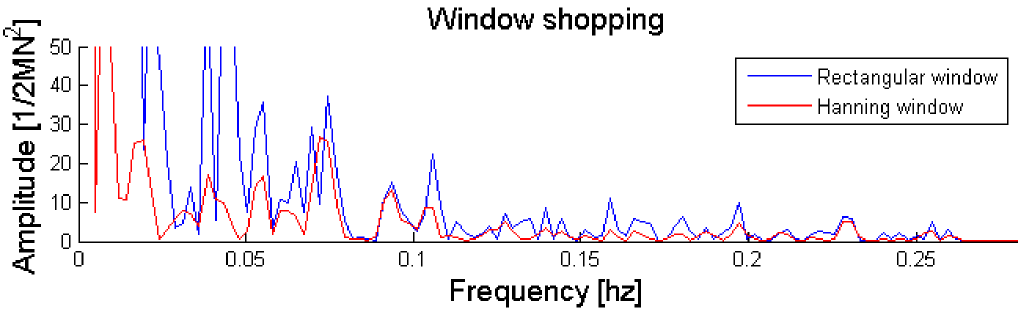

Figure F-9: Window comparison for test 65, Px. 3.0 m, 0.5 m/s. 5 degree.

Again using the Hanning window resulted in a significant reduction at the lower frequencies. At this point it is unknown whether the windows are making things more realistic or not. The very low frequencies (<0.01 Hz) should not be there as they were not observed during to video footage and would hopefully become less when using a window. However the vibrations with frequencies around 0.05 Hz were seen in the tests and thus should not disappear so much.

At this point it is hard to say whether or not a window should be used.

F.1.5 AUTOCORRELATION

Another option is to first calculate the autocorrelation of the data prior to applying an FFT. The autocorrelation is calculated as follows:

$$R(\tau) = \frac{E[(X_t - \mu)(X_{t+\tau} - \mu)]}{\sigma^2}$$

The autocorrelation function above calculates the autocorrelation of a function with a time-shifted version of itself. Next an FFT can be taken from the calculated equation.

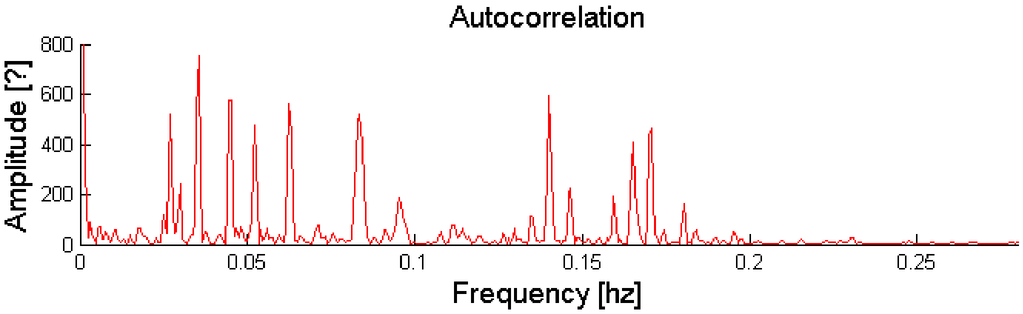

Figure F-10: Spectrum from the autocorrelation.

The spectrums generated in this way are all very spiky and the unit is unknown. They do look very similar to the spectrums calculated before.

Also it is interesting to note that technically there should not be any different between first calculating the autocorrelation function and then taken the spectrum. A common technique for calculating the autocorrelation function actually involves the FFT and IFFT.

F.1.6 INTERPOLATING THE DATA

Let us for a second assume that the calculated spectrums using a Hanning window are good and can be used for the next step which is interpolation. In Figure F-11 all the spectrums are shown. The figure shows how the spectrums changes when one of the variable is increased.

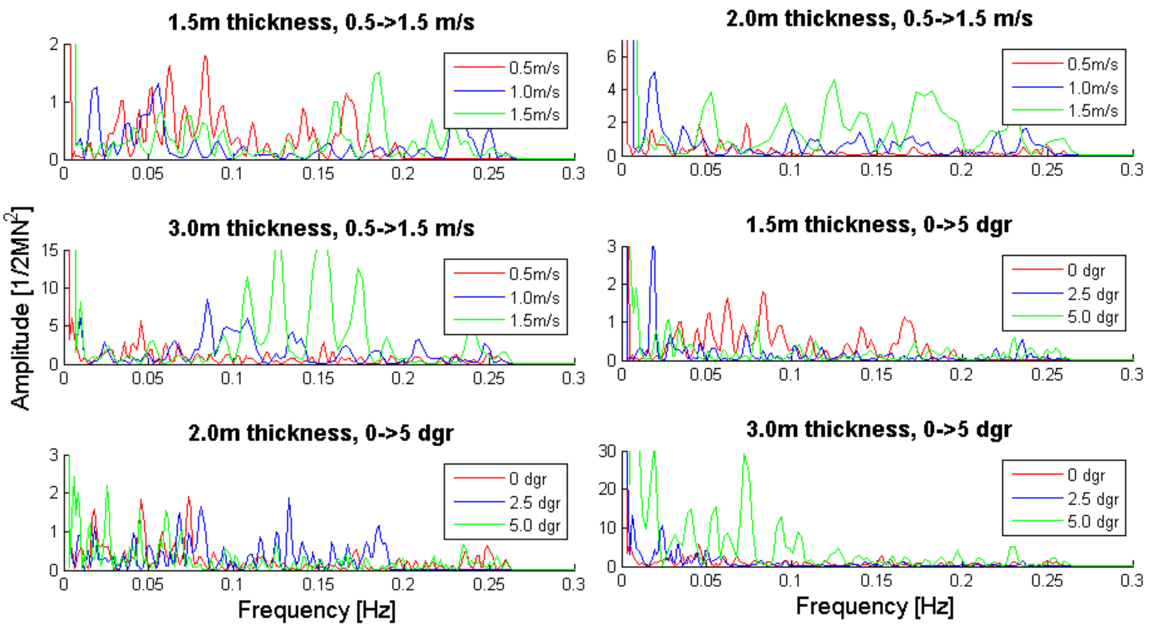

Figure F-11: Although some groups of spectrums show some relation, most are very different.

Interpolating between the spectrums based on the three variables appears to be an impossible task. Normal interpolation method will not work here.

One option could be to simply scale between the different spectrums. When the trim angle is 2.5 degrees, the corresponding spectrum is used. The spectrum is then multiplied with a factor that goes from 1 to 0 when moving from 2.5 to 5.0 degrees. The 5.0 degrees spectrum then has to opposite multiplication factor, so it goes from 0 to 1 when moving from 2.5 to 5.0 degrees. However this still creates problem when there is a combined trim angle and ice velocity as no tests were done for the combined occurrence.

F.1.7 CONCLUSIONS

All in all it is turning out to be quite hard to make a set of spectrums and using them to model Px_fluc. A summary of the reasons why:

- The length of the time histories varies between all the tests. This means that the resulting spectrums have different spectral resolutions and errors.
- The statistical properties of the full length data differ from the values in KSRI report and cannot be rescaled properly to give it the same values as in the report.
- There is no correction for the scaling of the bending stiffness, which results in inaccurate frequencies in the spectrums.
- The impact of the windows is unclear and it is not clear which one is the most appropriate one to use.
- Interpolating between the different spectrums proved to be impossible since their shapes are very irregular and chaotic.

This concludes the section on spectrum.

F.2 AUTOREGRESSIVE MODELS

After having a meeting with Richard Hendriks from the Signal and information processing group at the EWI faculty at the TUDelft he suggested to use an AR model to create a synthetic signal. AR stands for autoregressive model. It is based on a group of linear prediction formula to predict the output of a system based on previous outputs. It uses the following equation:

$$X_t = \sum_{i=1}^{p} a_i X_{t-i} + wn_t$$

Where p is the order of the method, a_i are the parameters of the model and wn_t is white noise with a certain variance. The model basically works by taken white noise as an input and then altering it in consecutive steps based on the parameters in order to add correlation between the subsequent entries.

A better description of the method would have been given if it was not for the fact that it actually does not really work for ice.

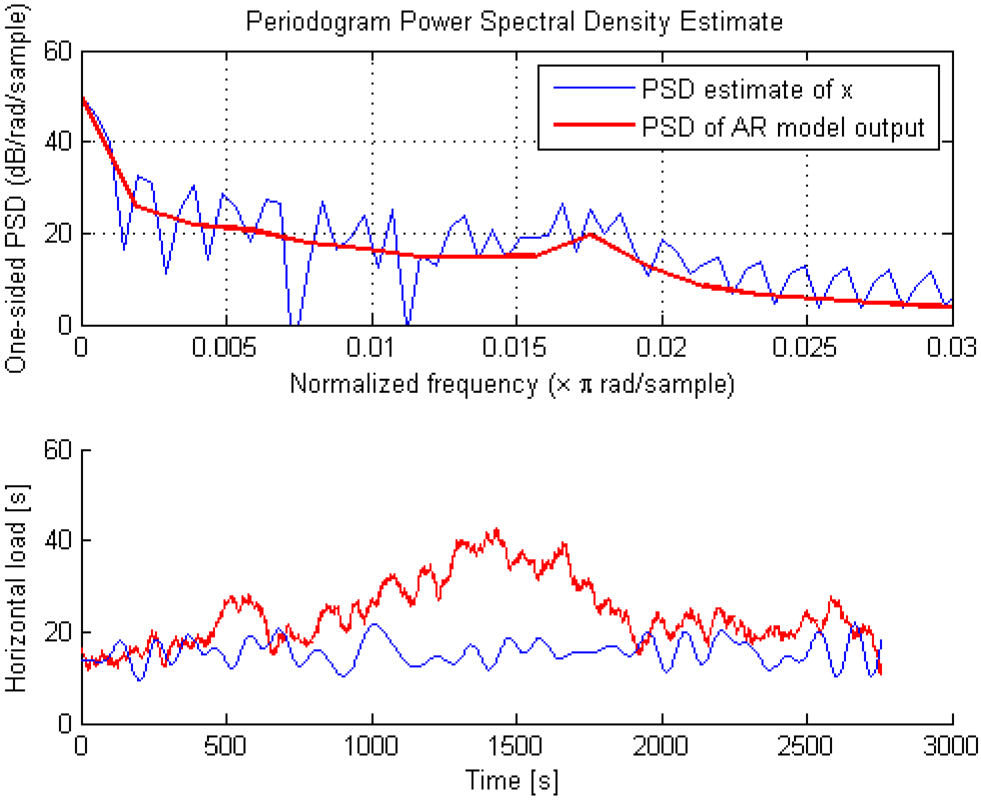

Figure F-12: Blue: original signal and periodogram. Red: AR model's prediction (use Yule-Walker)

When looking at Figure F-12 the general trend of the red line seems to be fairly similar to the blue one. There is a problem and this is that the AR model adds high frequency vibrations to the signal. This is not a really big deal as a moving average could be calculated to remove them again.

Another problem that occurs is the signal generated by the AR model is not stable. The reason for this is that the first estimated parameter is always smaller than -1 no matter which test or order of the model is used. When the absolute value of one the parameters is larger than 1, the synthetic signal will be unstable.

The next problem is that generated signal is not based on sinuses so the shape of the synthetic signal is not similar to that of the original signal.

All in all, AR models are not suited for recreating these kinds of signals.

APPENDIX G PRELIMINARY ANALYSES OF THE MOORING SYSTEM

In this section the impact of several items will be checked:

- Cable dynamics
- Wind and current loading
- Assumption of the flat spectrum
- Dynamics versus static approach

As including cable dynamic is more realistic and required by DNV, cable dynamics are included in all tests unless otherwise stated.

The line tension plots shown in this appendix were created by first calculating the mean of all 20 mooring lines during a test. The statistics (mean, standard deviation, etc.) of the line with the highest mean were then used for the plots and the calculations.

G.1 CABLE DYNAMICS

AQWA allows calculation of the dynamics of the individual mooring cable during the time domain simulation. When CD (cable dynamics) is turned off AQWA uses a pre-calculated lookup table which contains the quasi-static response of the moorings lines for a certain position of the fairlead. This method was also used for the dynamic model which was used during this thesis and is further explained in Derivation of the complex mooring system.

From the AQWA manual: *"When the dynamics of a cable are included in the analysis of cable motion, the effects of the cable mass and drag forces are considered, and tensions are no longer quasi static, i.e. forces on the cable are time varying and have 'memory'. The cable will, in general, respond in a non-linear manner. The solution during a time history and the solution in the frequency domain are fully coupled, i.e. the cable tensions and motions of the vessel are considered to be mutually interactive where cables affect vessel motion and vice versa."*

In Figure G-1 the effects of CD are shown for a semi-taut mooring system. The effects of the CD on the offset are very minor.

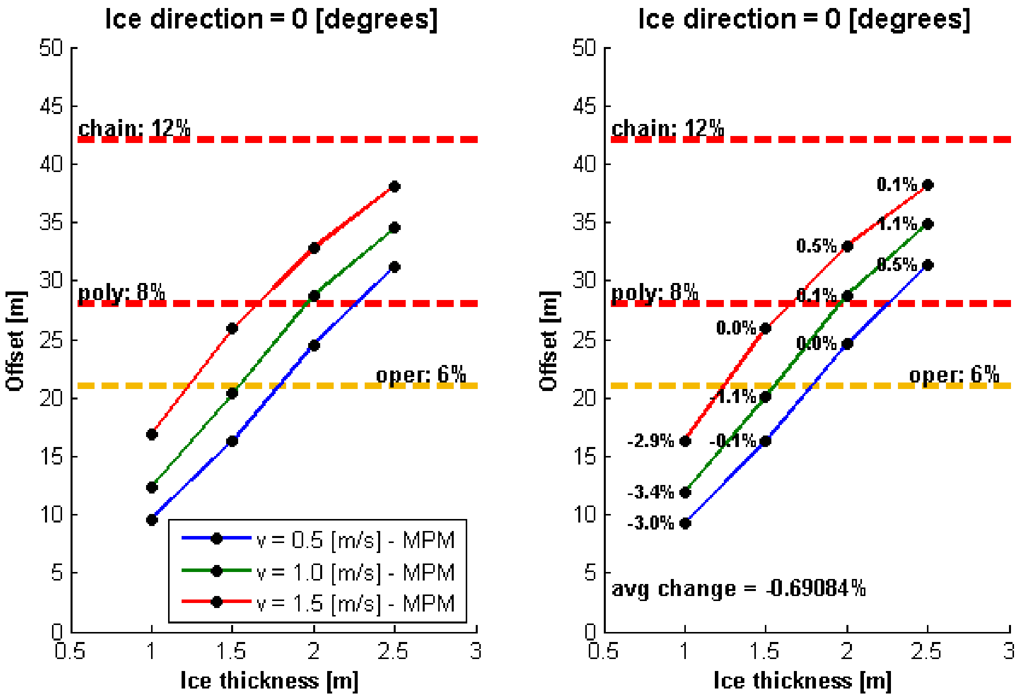

Figure G-1: MS3 (350m, semi-taut). The MPM offset of the vessel. The left graph has CD off, the right one on. The percentages in the figure show the changes between the two cases.

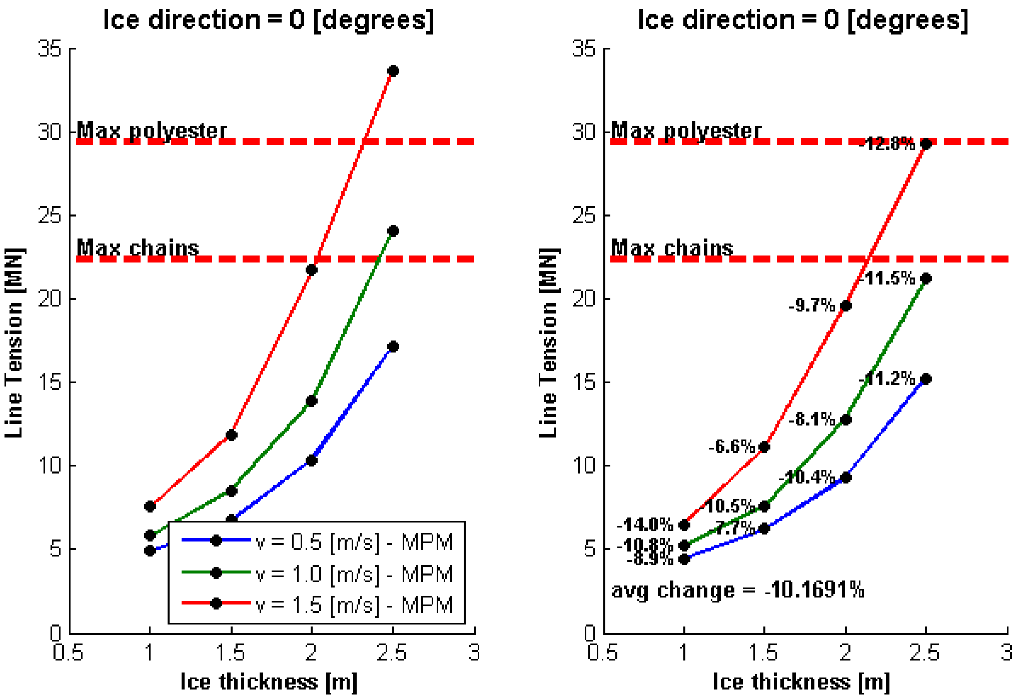

Figure G-2: MS3 (350m, semi-taut). The MPM line tension of the vessel. The left graph has CD off, the right on.

The effects on the line tension are more significant. On average the CD reduces the line tension by 5%.

The above was for a semi-taut system. Next a catenary system is investigated to see if there are any differences. The effects on the offset are of the same order of magnitude as the semi-taut system. The effect on the line tension is also similar to the semi-taut system.

Conclusion

As cable dynamics brings the calculation a step closer to reality it will used as the default case from now on (since its effects are not negligible, otherwise it could be turned off to saved computation time as using CD almost doubles it), however it is still interesting to note the impact it has on the calculation:

- Vessel offsets are barely influenced by cable dynamics; it is only reduced by about 1-3%.
- Cable dynamics reduces the line tensions by about 5%.
- Cable dynamics has the same impact on both semi-taut and catenary mooring system.

G.2 WIND AND CURRENT LOADING

According to ISO19906, ice and waves do not occur simultaneous when the concentration of the ice is above 80 percent. As this thesis focuses on level ice, which has a concentration of around 100%, waves do not have to be taken into account as an environmental load. However wind and currents can still occur simultaneous with the ice and therefore it is interesting to check the impact of these two loads on the overall loading.

The wind and current were modeled after the maximum environmental conditions in the Barents and Kara Sea. The wind velocity was taken as 40 m/s and the current velocity was taken as 1.3 m/s. The direction of both loads was taken the same as the ice's direction. Because the wind and current loading is constant for all the different tests, the relevance of the loads will decrease as the ice load increases.

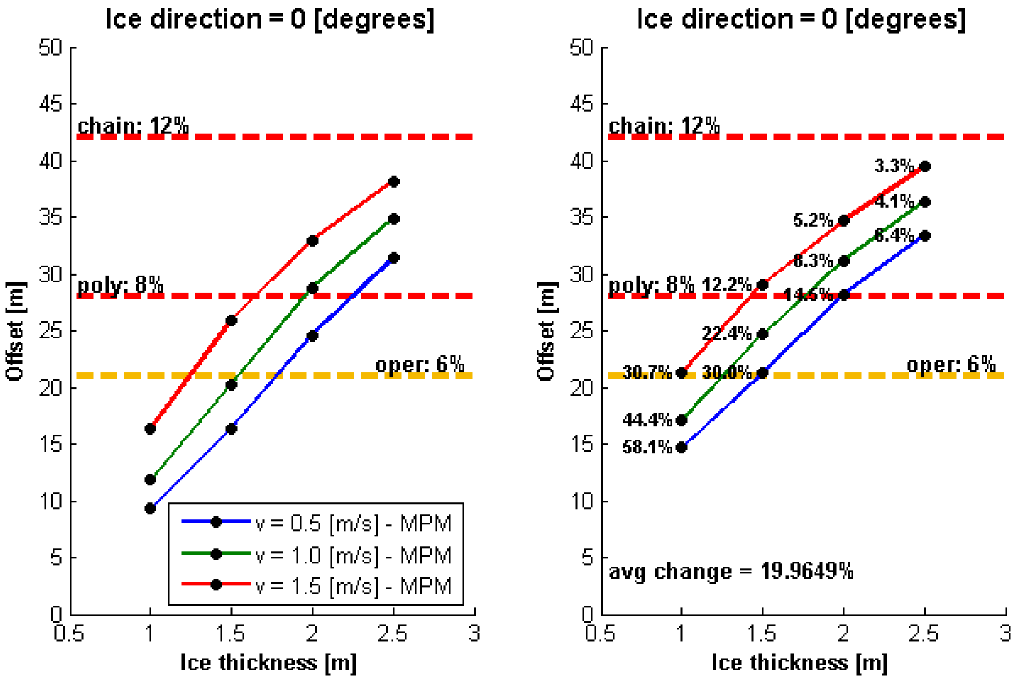

Figure G-3: MS3 (350m, semi-taut). The mpm offset of the vessel. The percentages in the figure show the changes between the default case and the test case.

Figure G-3 shows the increase in offset due to the wind and current and as expected there is a significant increase when the ice loading is low, but the impact decreases as the ice loading increases.

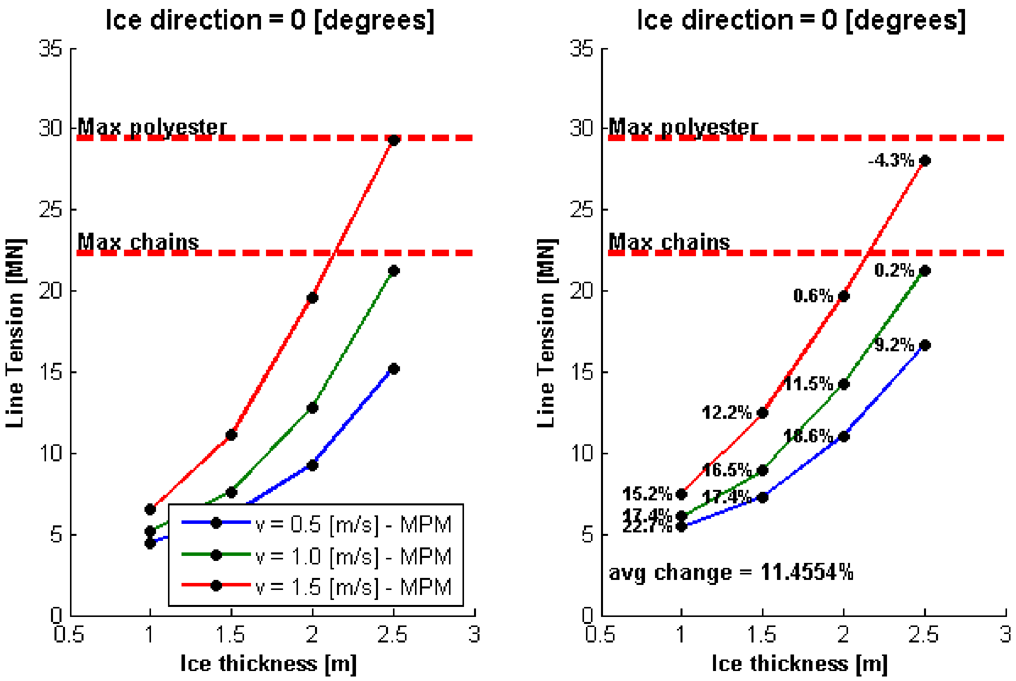

Figure G-4: MS3 (350m, semi-taut). The MPM line tension.

For the line tension the same results can be seen.

Conclusion

- The impact on the offset is quite small for the extreme ice cases and only results in an increase of about 3-5%.
- For the more modest ice cases the increase due to the wind and current is much more significant (increased by 10 to 60 %). However it should be noted that the values taken for the wind and current were the extreme values and thus under normal circumstances the loads would be less. But even then there will still be a significant impact on operability (orange dashed line).
- The impact of the wind and current on the fatigue limit state will probably be fairly significant and definitely should not be neglected.

G.3 ASSUMPTION OF THE FLAT SPECTRUM

A big assumption that was made in section 3.2.2 was the shape of the spectrums. Due to the irregular shapes and the lack of patterns between related spectrums it was necessary to assume a shape for the spectrums. As no dominant shape was found amongst all the spectrums, the spectrums were assumed to be a realization of a white noise spectrum. As this assumption is quite an important one made during this thesis it is important to check what the impact of this assumption is on the mooring system and the vessel’s response.

A good way to change to shape of the ice spectrums is to, well, actually change their shapes. But as the original spectrums did not provide a good source of inspiration of shapes to try, a slightly different approach was used. Instead of changing the shape of the spectrums it is easier to just increasing the energy contained within the spectrum by increasing the standard deviation which determines the “height” of a spectrum. So rather than redistributing the energy between different frequencies by changing the shape of the spectrum, this approach increases the energy across the board by changing the standard deviations (which makes the spectrum “higher”).

Recall the following equation which was used to turn a spectrum back into a vibrating signal using a superposition of sinuses:

$$Fluctuating\ ice\ load = \sum_{i=1}^{N} \sqrt{2 * Var * Ratio_i} * \sin\left(\frac{i-0.5}{N} * f_{max} * t * 2\pi + \varphi_i\right)$$

By multiplying the standard deviation with a factor the following changes:

$$Fluctuating\ ice\ load = \sum_{i=1}^{N} \sqrt{2 * \left(SD_{factor}\ * SD\right)^2 * Ratio_i} * \sin\left(\frac{i-0.5}{N} * f_{max} * t * 2\pi + \varphi_i\right)$$

$$Fluctuating\ ice\ load = SD_{factor} * \sum_{i=1}^{N} \sqrt{2 * SD^2 * Ratio_i} * \sin\left(\frac{i-0.5}{N} * f_{max} * t * 2\pi + \varphi_i\right)$$

So effectively the entire load signal is multiplied by the factor.

G.3.1 IMPACT ON THE OFFSET OF THE VESSEL

Below are the AQWA results from simulations where the standard deviation was increased.

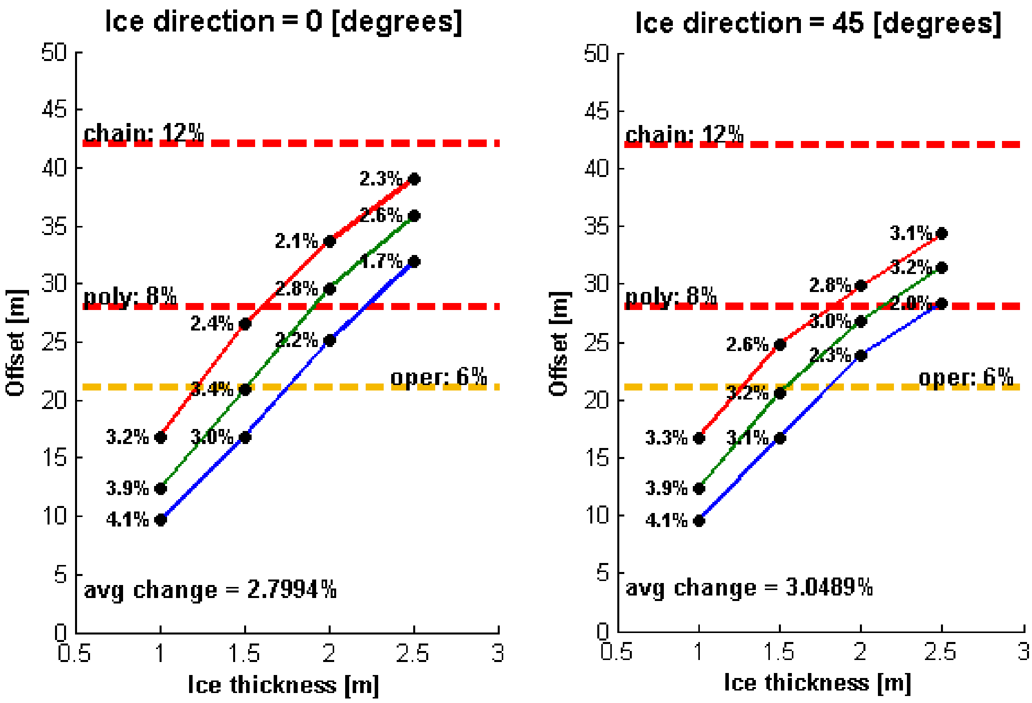

Figure G-5: MS3 (350m, semi-taut). The MPM offset and line tension of the vessel. The standard deviations are multiplied by 1.25 [-]. The percentages in the figure show the changes between the default case and the test case.

In Figure G-5 the results are shown for the case when the standard deviations are multiplied by a factor of **1.25 [-]**. On average the **offset** is increased by about **2.8 %.** For the lower ice loads it starts out at about 4 % but drops down to around 2.0 % as the ice load increases. For the 45 degree ice direction case the impact is slightly larger, on average **3.05 %**.

	SD-Factor [-]	Ice direction [°]	Increase at low ice loads	Average increase	Increase at high ice loads
Offset	1.25	0	4.00%	2.80%	2.50%
		45	4.00%	3.05%	3.00%
	1.5	0	7.70%	5.52%	4.80%
		45	7.70%	6.04%	6.30%

Table 15: The impact of the increased standard deviation on the offset.

There appears to be a linear relation between the SD-factor and the average increase. The ratio between an increase in the SD-factor and the resulting increases in offset is fairly low. For the offset from the 0 degree case it is 0.11 [%/%], so an increase in the SD-factor by 100 % would increase the offset by 11 % (at an ice direction of 0 degrees):

- Offset at 0 degrees:	0.11 [%/%]	(on average)
- Offset at 45 degrees:	0.12 [%/%]	(on average)

So the average impact of the standard deviation is fairly low. This fairly low correlation between the standard deviation and the offset is off course very good but what is the reason behind it?

The most important thing to note is that on average the fluctuating component only accounts for about 17 % of the total offset at low ice loads and for about 11 % of the total offset at high ice loads. This means that the impact of any increase in the fluctuating part of the offset is significantly reduced when looking at the total offset. If we look at **only** the fluctuating part of the offset, it scales about 1:1 (**0.92 [-]**) with an increase in SD.

If we go back to the original equation, an expression can be made for the impact of the SD-factor on the offset of the vessel:

$$Pxfluc = SD_{factor} * \sum_{i=1}^{N} \sqrt{2 * SD^2 * Ratio_i} * \sin\left(\frac{i-0.5}{N} * f_{max} * t * 2\pi + \varphi_i\right)$$

$$Offset = mean_{offset} + \mathbf{0.92} * SD_{factor} * fluc\_offset$$

This means that the fluctuating part of the offset scales almost linearly with the standard deviation but because the fluctuating component of the offset is relatively small compared to the total offset, any increase the fluctuating component only has a minor increase on the overall offset.

G.3.2 IMPACT ON THE LINE TENSION

The effect on the line tension is a bit larger than the effect on the offset, see Table 16. This is due to the larger safety factor of 2.1 [-] by which the fluctuating part is multiplied.

	SD-Factor [-]	Ice direction [°]	Increase at low ice loads	Average increase	Increase at high ice loads
Line Tension	1.25	0	4.00%	5.62%	8.00%
		45	3.00%	4.83%	7.50%
	1.5	0	7.00%	10.81%	15.50%
		45	6.00%	9.51%	15.00%

Table 16: The impact of the increased standard deviation on the line tension.

The ratio between an increase in the standard deviation and the resulting increase in the fluctuating component in the line tension is **0.76 [-]**. This is 0.15 [-] lower than for the offset.

G.3.3 CONCLUSION

- When increasing the SD of the ice load the resulting increase in the SD of the fluctuating components was checked. The ratio between an increase in the SD of the load and an increase in the SD of the **offset** is **0.92 [-]** and **0.76 [-]** for the **line tension**.
- Because the fluctuating component of the offset is only a relatively small part of the total offset (fluctuating + mean), any increase in the fluctuating component of the offset only has a minor increase in the overall offset. This same applies to the line tension.

G.4 DYNAMIC VERSUS STATIC APPROACH

Before comparing the results from the static and the dynamic approach, the results from AQWA are checked first to make sure that the mean of the dynamic calculations are the same as in the static mooring analysis. Figure G-6 show the results from the static case. It is interesting to note that all five mooring systems have almost the same maximum load which is around 50 MN. This corresponds to 3 m thick ice moving at 0.5 m/s or 2.3 m thick ice moving at 1.5 m/s.

Another very important thing about the static report is that only one ice direction was used. In the direction used the mooring system is actually the stiffest and this results in the highest MGRF (around 50 MN, as seen below). However in the weakest direction the mooring systems can only handle 37.2 MN. In section 4.4.1 this strange choice is analyzed more closely. For the comparison in this section the original results from the static mooring report will be used.

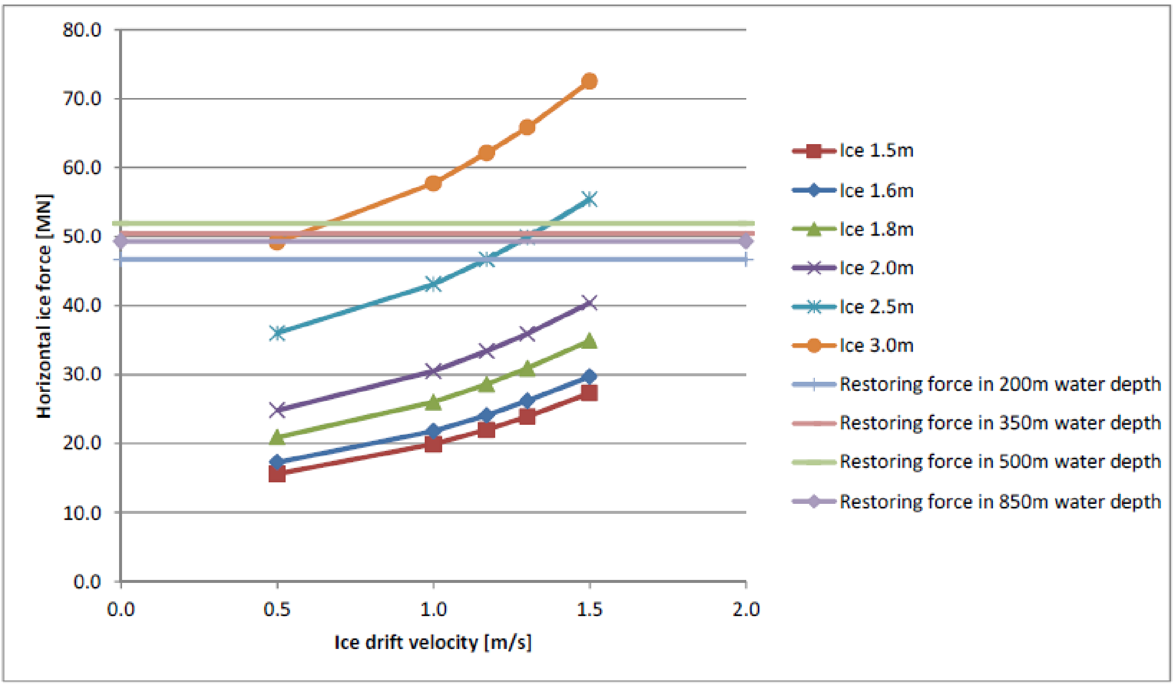

Figure G-6: The results from the static case. Mooring systems for other water depths are also shown, however only the 350 m water depth one will be used further on.

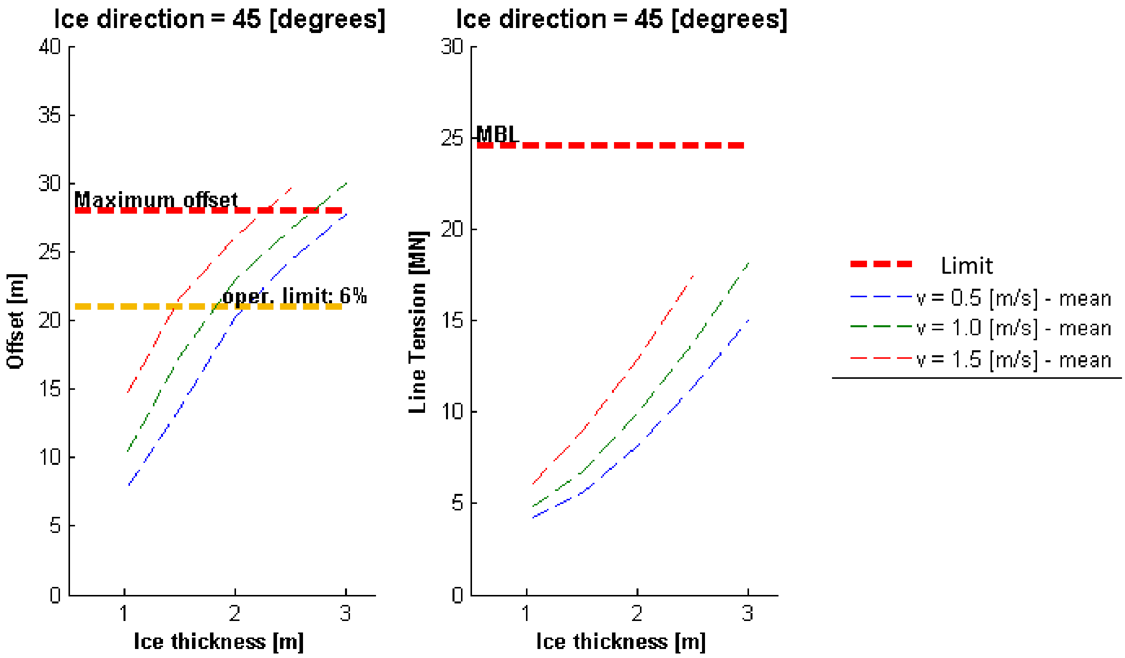

Figure G-7: MS3 (350m, semi-taut). The mean of each test is plotted so they can be compared with the static case to validate the AQWA calculations. The left figure shows the offset and the right figure shows the line tension.

When looking at Figure G-7 the maximum ice conditions due to the dynamic load can be found. At an ice velocity of 0.5 m/s it can handle an ice thickness of about 3.1 m. At 1.5 m/s it can handle about 2.3 m thick ice. These results are the same as in the static report so this is a good verification of the calculation with AQWA.

G.4.1 COMPARISON WITH THE STATIC CASE

Now that the AQWA results have been validated to some extend it is time to look at what kind of maximum ice condition both methods predict. The table on the next page shows the results.

Comparison between the maximum allowable ice conditions for the static and dynamic calculations

Mooring system	Static				Dynamic						Static - Dynamic Ratio *		% of line tension used**	
	0 degree case		45 degree case		0 degree case			45 degree case			0 dgr case	45 dgr case	0 dgr case	45 dgr case
	velocity [m/s]	thickness [m]	velocity [m/s]	thickness [m]	velocity [m/s]	thickness [m] Offset	thickness [m] LineTen	velocity [m/s]	thickness [m] Offset	thickness [m] LineTen	[%]	[%]	[%]	[%]
MS1 - Chain	0.5	N/A	0.5	2.91	0.5	2	2.69	0.5	2.31	2.85	-	-21%	49%	68%
	1	N/A	1	2.64	1	1.76	2.31	1	1.98	2.5	-	-25%	55%	64%
	1.5	N/A	1.5	2.22	1.5	1.45	1.91	1.5	1.66	2.17	-	-25%	56%	65%
MS2 was dropped as it was always performing worse than MS3 (both are for 350 m water depth).														
MS3 - Semi-taut	0.5	N/A	0.5	3.04	0.5	2.25	2.97	0.5	2.53	3+	-	-17%	55%	73%
	1	N/A	1	2.76	1	1.95	2.56	1	2.22	2.64	-	-20%	55%	74%
	1.5	N/A	1.5	2.34	1.5	1.65	2.14	1.5	1.9	2.34	-	-19%	61%	73%
MS4 - Semi-taut	0.5	N/A	0.5	3.09	0.5	2.49	3+	0.5	2.72	3+	-	-12%	65%	76%
	1	N/A	1	2.81	1	2.2	2.65	1	2.36	2.78	-	-16%	69%	75%
	1.5	N/A	1.5	2.39	1.5	1.87	2.19	1.5	2.01	2.46	-	-16%	74%	74%
MS5 - Semi-taut	0.5	N/A	0.5	3.01	0.5	2.52	3+	0.5	2.75	3+	-	-9%	57%	75%
	1	N/A	1	2.72	1	2.24	2.87	1	2.42	2.85	-	-11%	61%	75%
	1.5	N/A	1.5	2.3	1.5	1.88	2.42	1.5	2.06	2.52	-	-10%	64%	74%

Table 17: This table shows all the results for the five mooring systems from the static report. A detailed description can be found on the next page.

The table was produced as follows. A certain ice velocity was taken and then the maximum allowable ice thickness was found so that one of the limit states was completely exhausted. This gave two maximum ice thicknesses, one for each limit state. This was done for both the static case and the dynamic case and for an ice direction of 0 degrees and 45 degrees. As the mooring system is not optimized the maximum allowable ice thickness is not the same for both criteria.

* The static - dynamic ratio shows the reduction in maximum allowable ice thickness due to the dynamics of the ice load.

** The last two columns show the % of the maximum breaking load (MBL) that has been used at the maximum allowable offset.

General differences

When directly comparing the maximum allowable ice thicknesses for the static and the dynamic case the dynamic case falls short be about 10 to 25 %.

Notes for the optimization

After this an optimization will be done of the layout of the mooring system. There are two points of weakness in the mooring system designs from the static report which will be improved upon during the optimization:

- The most important result is that for all cases the maximum ice conditions are limited by the offset of the vessel. In general only 65-75% of the maximum allowable line tension is used when the offset has already reached the full 100% that is available (the last two columns in the table). During the optimization one of the main goals will be to rebalance the distribution between the two design criteria so that they will both be utilized around 100%.
- The second most important result is that, with the mooring system from the static report, the mooring system can handle higher ice conditions in the 45 degree direction than in the 0 degree direction. On average the maximum allowable ice thickness in the 0 degree direction is 10-15% lower than in the 45 degree direction. As the JBF Arctic has to operate in many different areas it is very unlikely that all of these areas will have ice coming from one particular direction at all times. During the optimization the second goal will be to minimize the difference in strength between the different directions.

APPENDIX H MOST PROBABLE MAXIMUM

The motions of the vessel are dynamic because of the fluctuating component of the loading. The random element is the phase angles of the sinuses making up the fluctuating component. This means that any time-domain simulation can be seen as a single realization of a stochastic process. The maximum offset obtained during a time-domain simulation of some duration is only one realization of this stochastic process and therefore some calculations are needed in order to get the expected maximum offset based on some exceedance probability rather than proceed based on a single realization.

First the offset of the vessel will be investigated and after that the line tension.

H.1 STATIONARY GAUSSIAN PROCESS

The first step is to look at what kind of distribution the offset of the vessel has at any given moment in time. Since the offset of the vessel is dependent on many variables, by the central limit theory one would expect it to have a Gaussian distribution.

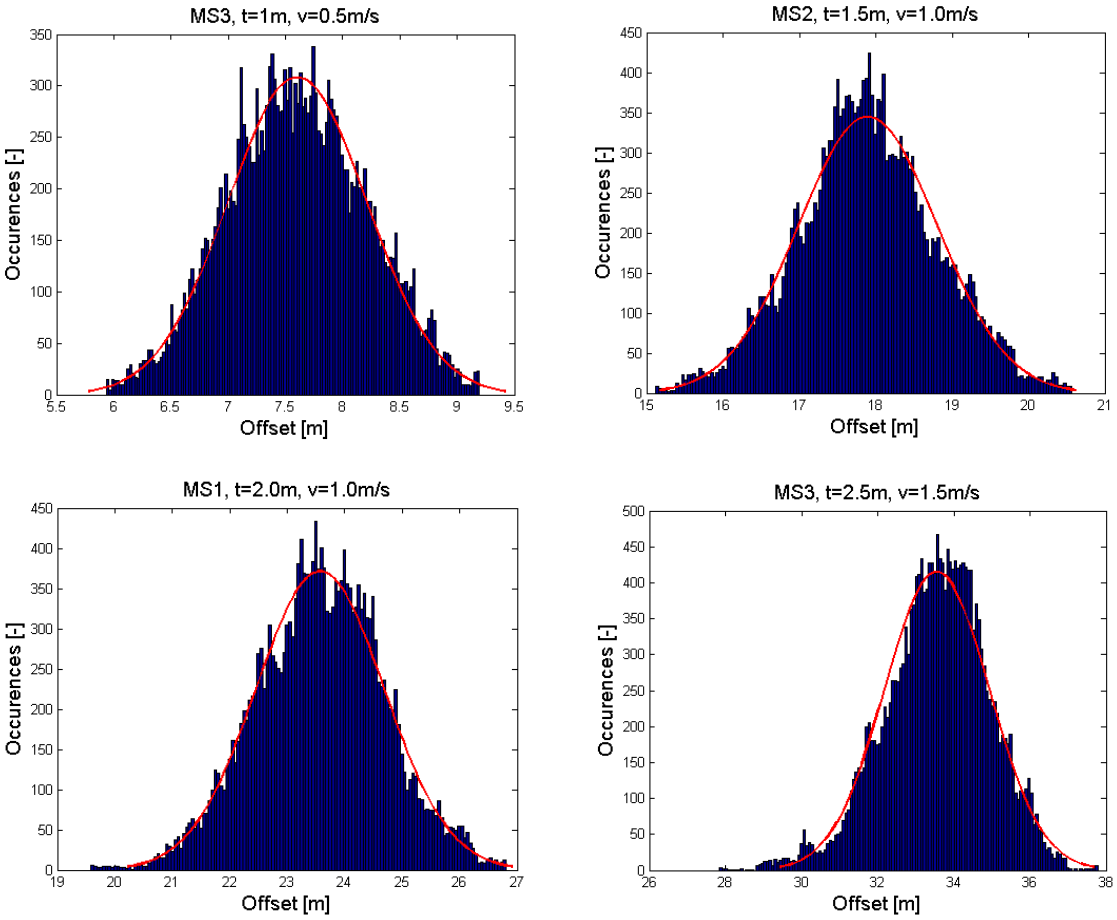

Figure H-1: For the four different simulations above a normal shape seems to give a very good fit for the data. All data is for an ice direction of zero degrees (moving towards the positive x-axis). Each graph contain almost 3 hours of data.

Figure H-1 support the idea that the offset at an arbitrary moment is Gaussian distributed. When looking at other simulations with other mooring systems and ice parameters they all have a Gaussian distribution, except a few tests. Several tests where the ice loading was very high (high thickness in combination with a high velocity) the distribution was not Gaussian. Due to the high load the vessel was operating in the non-linear part of the mooring system.

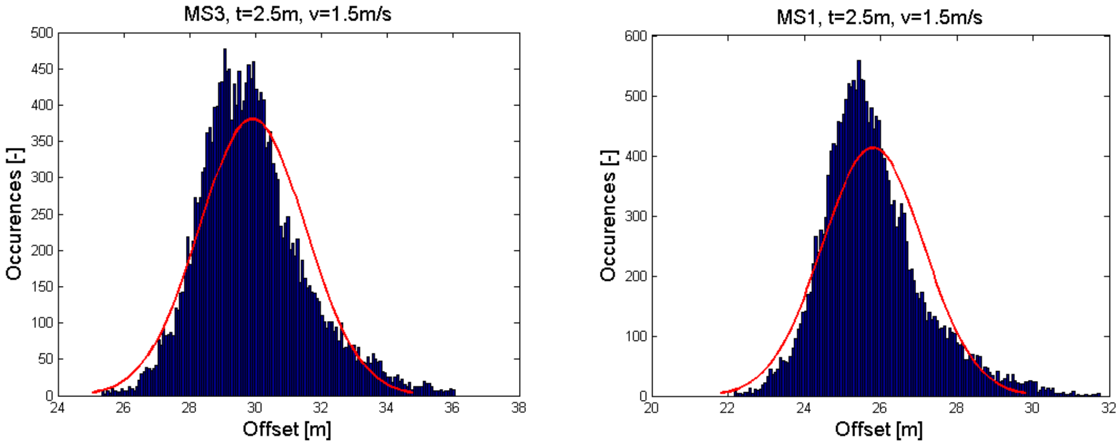

Figure H-2: A non-Gaussian distribution occurs when the ice is operating in the non-linear range of the mooring system.

H.2 EXTREME VALUE STATISTICS

The approach used here is based on a similar approach used for ocean waves. Under the assumption that the motions of the vessel are a stationary Gaussian process the Rayleigh distribution method provides a direct calculation based on the spectral moments of the data.

The derivation and use of spectral moments to fit the Rayleigh distribution is described in detail in (Ochi, 1998). Ochi shows that, under the Gaussian assumption, the most probable maximum occurring in storm with duration T is given by:

$$mpm = \mu + \sigma\sqrt{2\ln(n)}$$

Next Ochi also derives the following equation which calculates the extreme value with an exceedance probability α:

$$mpm = \mu + \sigma\sqrt{2\ln\left(-\frac{n}{ln(1-\alpha)}\right)}$$

From this equation it can be derived that the exceedance probability of the MPM is equal to $1 - 1/e = 0.6321\ [-]$

The parameter n is defined as follows:

$$n = \frac{T_0}{D}, \qquad where\ T_0 = mean\ zero\ crossing\ period \qquad and\ D = storm\ duration$$

There are several ways to calculate T_0. One method is based on the variance density spectrum of the response:

$$T_0 = \sqrt{\frac{m_0}{m_2}}, \qquad where\ m_i = i^{th}\ order\ moment\ of\ the\ spectrum$$

The problem with this method is that it requires the calculation of the variance density spectrum. In order to calculate the second order moment of the spectrum, the estimate for the spectrum has to be very good as all errors are enhanced when taking the second order moment. For this reason another approach was used, which is to directly calculate the mean zero-crossing period from the time series themselves.

H.3 STORM DURATION

Everything that is required to calculated the most probably maximum is now known expect for the duration. Because a very similar approach is used for equation for H_s and H_{max} for a certain sea-state, it is helpful to first make a quick comparison between ice and waves.

When dealing with ocean wave the assumptions is that the surface elevation is a stationary Gaussian process. This is a reasonable assumption for the duration of a wave record (typically 15-30 min) but sometimes it is also assumed for the duration of a storm (typically 6-12 h).

If we go back to ice, although the response of the vessel might be a stationary Gaussian process, which allows for easy estimation of the most probably maximum, this is only valid if the ice thickness and velocity remain constant for a specific duration. For ocean waves the spectrum contain all the statistical properties of a sea state and can be represented with a H_s and T_0. During the specified duration (generally 3 hours) these two parameters are assumed to be constant.

If the ice thickness would vary only very slowly over time and space and would be fairly smooth than a similar approach could be used where the ice thickness is represented as a spectrum, which can be decomposed into a “signal” again using a superposition of harmonic vibrations. In reality the thickness of level can vary quite significantly over even short distances and contains other ice features such as ridges. For this reason we cannot simply speak of a significant ice thickness when dealing with ice because the spatial correlation is also very important. For the ice velocity this approach would be more applicable as changes in the velocity of the ice are related to the mass, which is quite significant and thus changes in the velocity will be relatively slow, especially when compared to the changes in the ice thickness.

During this thesis work is done with completely level ice of constant speed so the stationary Gaussian assumption is valid. Since some duration has to be specified otherwise the most probably maximum cannot be calculated it is decided to use the duration recommended by DNV for environmental loads which is three hours.

H.4 MOORING LINE TENSION

Next the mooring line tension will be checked to see what kind of distribution it has. The same method as for the vessel offset will be used to derive the most probable maximum for the line tension.

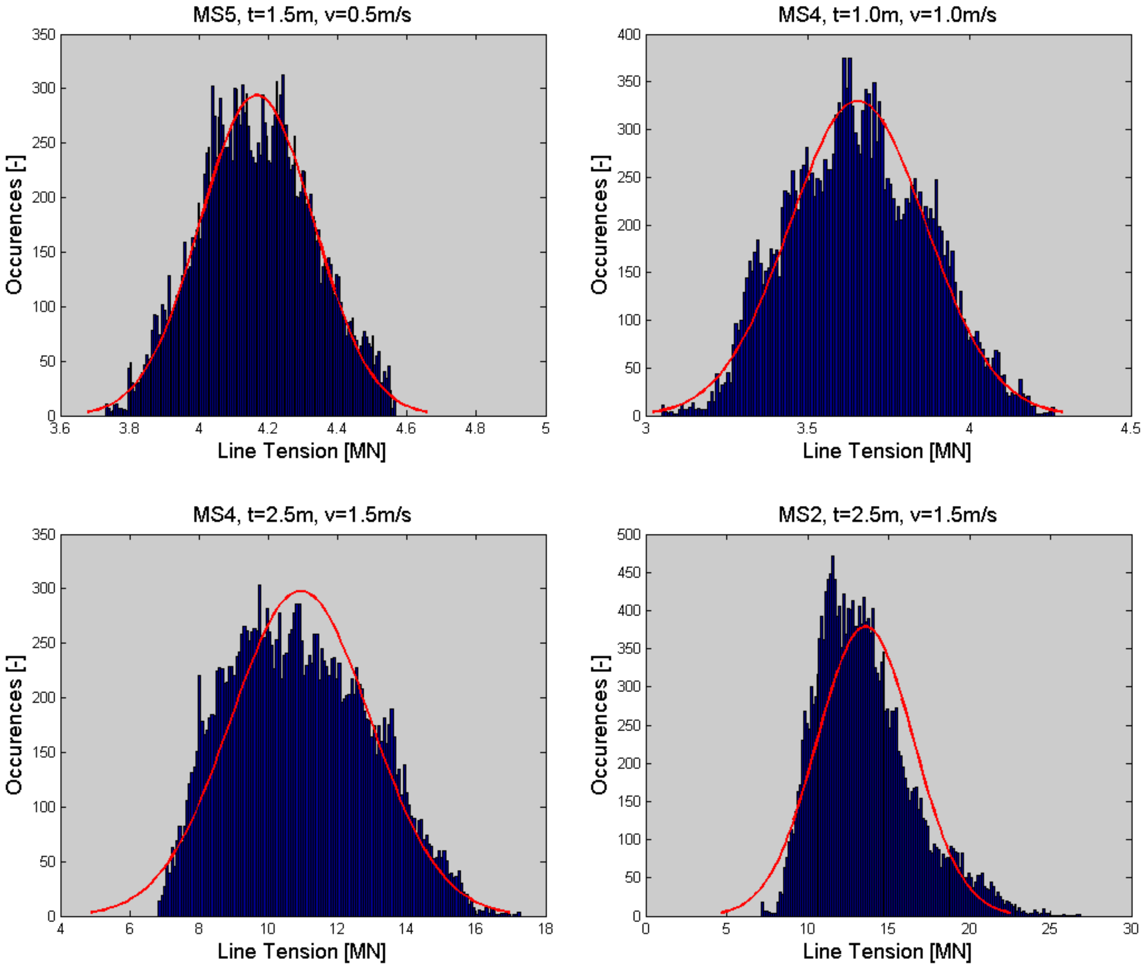

Figure H-3: A series of histograms for the line tension. Each graph contain almost 3 hours of data.

In general the line tension at any giving moment has a Gaussian distribution. But again once the ice force becomes large the shape is somewhat distorted, as shown in the bottom left picture in Figure H-3. For the mooring systems which use a catenary chain system (MS1 and MS2, the bottom right picture in Figure H-3), the Gaussian shape is distorted even further as higher loads occur more frequently in these systems.

For simplicity it is assumed that the mooring line tension also has a Gaussian shape so the same formula can be used for the most probably maximum.

This concludes the analysis on the most probably maximum for the unrealistic situation where the ice is assumed to have a constant thickness and velocity for an extended period of time.

No polar bears or penguins were harmed during the creation of this thesis.

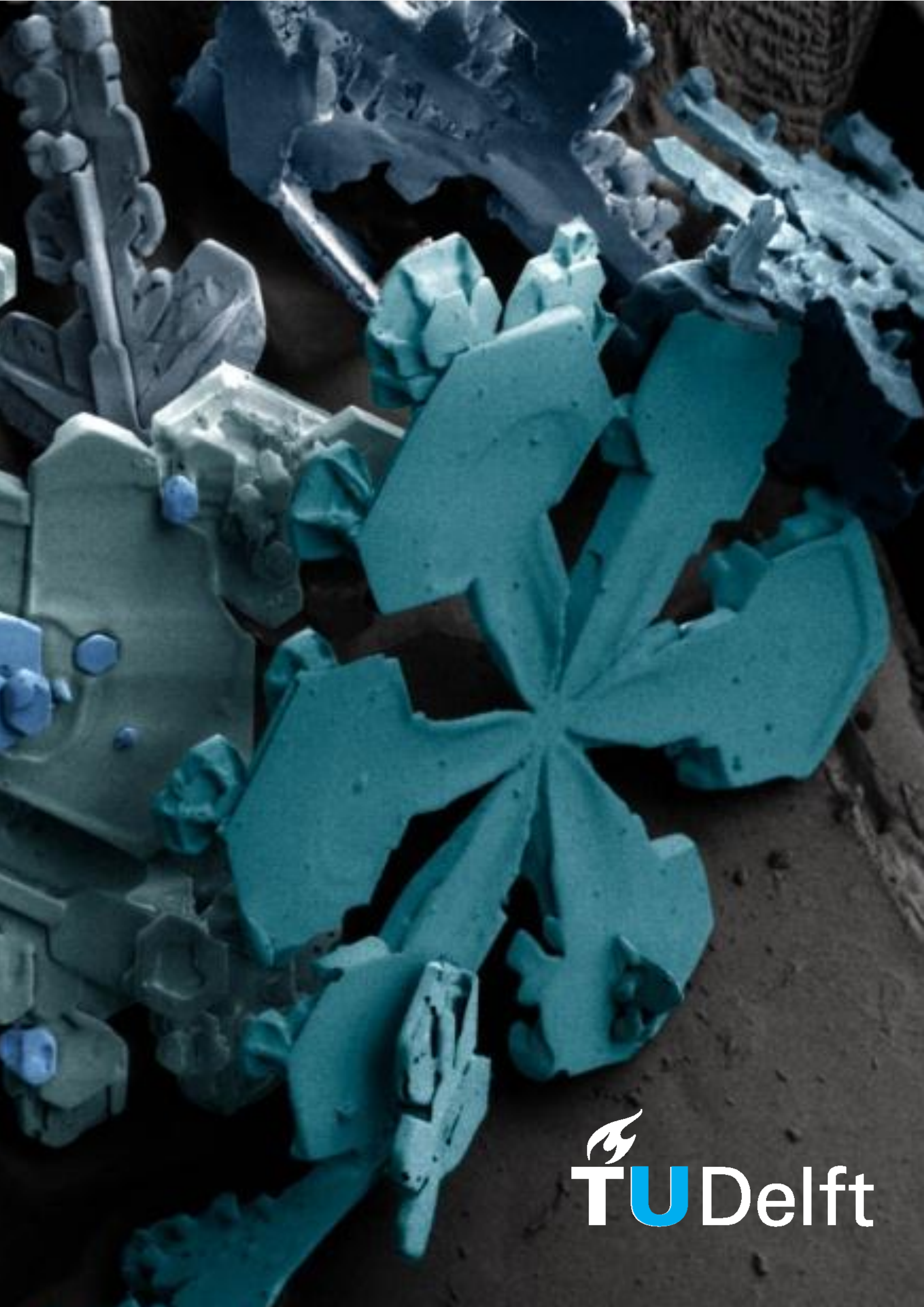
TU Delft